12-2001

Pedogenic Relationships in a Texas Vertisol Climosequence Defined by Geochemical Mass Balance of Whole Soil and Chemistry of Iron-Manganese Nodules

Cynthia A. Stiles
University of Tennessee, Knoxville

To the Graduate Council:

I am submitting herewith a dissertation written by Cynthia A. Stiles entitled "Pedogenic Relationships in a Texas Vertisol Climosequence Defined by Geochemical Mass Balance of Whole Soil and Chemistry of Iron-Manganese Nodules." I have examined the final electronic copy of this dissertation for form and content and recommend that it be accepted in partial fulfillment of the requirements for the degree of Doctor of Philosophy, with a major in Geology.

Steven G. Driese, Claudia I. Mora, Major Professor

We have read this dissertation and recommend its acceptance:

Larry D. McKay, Sally P. Horn

Accepted for the Council:

Carolyn R. Hodges

Vice Provost and Dean of the Graduate School

(Original signatures are on file with official student records.)

To the Graduate Council:

We are submitting herewith a dissertation written by Cynthia A. Stiles entitled "Pedogenic Relationships in a Texas Vertisol Climosequence defined by Geochemical Mass Balance of Whole Soil and Chemistry of Iron-Manganese Nodules." We have examined the final copy of this dissertation for form and content and recommend that it be accepted in partial fulfillment of the requirements for the degree of Doctor of Philosophy, with a major in Geology.

Steven G. Driese, Major Professor

Claudia I. Mora, Major Professor

We have read this dissertation
and recommend its acceptance:

Larry D. McKay, Associate Professor

Sally P. Horn, Professor

Accepted for the Council:

Vice Provost and Dean of Graduate Studies

PEDOGENIC RELATIONSHIPS IN A TEXAS VERTISOL CLIMOSEQUENCE DEFINED BY GEOCHEMICAL MASS BALANCE OF WHOLE SOIL AND CHEMISTRY OF IRON-MANGANESE NODULES

A Dissertation
Presented for the
Doctor of Philosophy
Degree
The University of Tennessee, Knoxville

Cynthia A. Stiles
December 2001

Acknowledgments

I thank my two co-advisors, Steven Driese and Claudia Mora, for their unflagging support and exemplary professional attitude towards me throughout my residence in Geological Sciences. I could always rely on helpful and insightful advice from them in all aspects of this research effort. The money for the majority of the work was provided by a grant from the National Science Foundation (EAR-9814607 to Driese and Mora), with additional funding provided by the Southeastern Branch of the Geological Society of America. For this support and the opportunity it provided, I am indebted.

I thank the members of the cooperative team who worked on this project: Warren Lynn and Doug Wysocki, USDA-NRCS Soil Survey Center; Larry Wilding, Texas A & M University; Lee Nordt, Baylor University; Jon Wiedenfeld, Wes Miller, and Rick Lambert, USDA-NRCS Soil Survey; and fellow graduate students Amy Robinson and Dana Miller for their help in the field and laboratory. I thank my committee members, Dr. Larry McKay and Dr. Sally Horn, for their patience and helpful input, and finally the entire UT Geological Sciences Department, who have accepted and supported a non-traditional student.

Finally, I thank my husband, Harry, who has never questioned my abilities or decisions and who has solidly and quietly supported this effort. Without this stalwart backing, I never would have made it this far, nor would I look so brightly to the future.

Abstract

Climosequence Vertisol profiles derived from the Upper Beaumont Formation in the Gulf Coastal Prairie physiographic province of Texas were examined for geochemical trends ascribed to different precipitation regimes. Mass-balance relationships were utilized for the comparisons. Compositional differences in zirconium (Zr) content between the solum and lower sub-soil precluded it use an immobile strain (volumetric change) indicator. This difference was correlated to sand weight percent ($r^2 = 0.65$**). Titanium (Ti) content did not shift correlatively with depth, thus making Ti the preferred strain index element for mass-balance calculations. Depths at which the Zr compositions shifted were not directly related to mean annual precipitation (MAP) regime and are considered to be functional boundaries between open-system pedogenesis and more closed system hydrogeochemical weathering.

Mass-balance relationships of ten elements examined within the climosequence showed trends ascribed to precipitation intensity. Mass-balance relationships varied not only between locations but also between microtopographic positions within each Vertisol pedon. Basic mass-balance trends with depth in the climosequence profiles fall into four broad categories depending on the relative mobility and geochemical reactivity of the individual elements: 1) framework, 2) clay interaction, 3) leachable/biocycle, and 4) climatic/redox-sensitive. Net mass flux percentages indicate a relative steady-state of around -16% (±3%) in climosequence Vertisol pedons with MAP > 900 mm.

The total Fe (Fe_{TOT}) content of pedogenic iron-manganese (Fe-Mn) nodules from Vertisol profiles correlates with mean annual precipitation (MAP, $r^2 = 0.92$***). No significant trend of Fe_{TOT} with depth was noted in profiles. Using the regression developed from modern Vertisol data, Fe_{TOT} contents of Paleozoic paleo-Vertisol Fe-Mn nodules yielded MAP regimes comparable to previously inferred paleoenvironmental interpretations. Paleoprecipitation estimates derived from Fe-Mn nodules for an uneroded, Late Mississippian paleo-Vertisol are very close to estimates made from a depth to pedogenic carbonate horizon (DCH) proxy determined from the modern Vertisol climosequence. Because the Fe-Mn nodule proxy is independent of depth, consistent paleoprecipitation estimates can be made even in eroded paleo-Vertisols and, in combination with the DCH, may be useful in determining original paleosol thickness.

Table of Contents

Chapter 1. Introduction 1

1.1. Soils and Paleosols as Environmental Indicators 1

1.2. Geologic Context of Paleo-Vertisols and Their Modern Counterparts 2

1.3. Modern Soil Geochemistry 6

1.4. Modern Analog Setting - The Texas Gulf Coastal Prairie 16

1.5. Goals, Hypotheses, and Objectives 32

Chapter 2. Evaluating Strain Indicators and Pedogenic Thresholds in Vertisols from the Upper Beaumont Formation, Gulf Coastal Plain, Texas. 35

2.1. Abstract 35

2.2. Introduction 36

2.3. Materials and Methods 43

2.4. Results 45

2.5. Discussion 63

2.6. Conclusions 71

Chapter 3. Mass-Balance Relationships in Vertisol Climosequence Profiles Derived from the Upper Beaumont Formation, Gulf Coastal Plain, Texas. 75

3.1. Abstract 75

3.2. Introduction 76

3.3. Materials and Methods 86

3.4. Results and Discussion 87

3.5. Conclusions 117

Chapter 4. Pedogenic Iron-Manganese Nodules in Vertisols: A New Proxy for Paleoprecipitation? 119

4.1. Abstract 119

4.2. Introduction 119

4.3. Materials and Methods 124

4.4. Results and Discussion 127

4.5. Conclusions 135

Chapter 5. Overall Conclusions and Future Research 136

5.1. Modern Climosequence Vertisols - What Do They Tell Us? 136

5.2. Future Research 137

References 144

Appendices 161

Appendix 1: Data for Chapter 1 162

Appendix 2: Data and Statistical Tables for Chapter 2 203

Appendix 3: Data and Statistical Tables for Chapter 3 236

Appendix 4: Data and Statistical Tables for Chapter 4 257

Vita 264

List of Tables

1-1 Soil taxonomic, geographic, and climatic data for pedons used in this study . . . 20

2-1 Climosequence functional boundary depths, Ti/Zr volumetric contents, percent differences, and statistical information for the upper and lower units in microlow profiles. 48

2-2 Pedon alluvium source lithologies and relative Ti:Zr in upper and lower units. . 51

2-3 Surface feature characteristics assessed in SEM survey of individual very fine sand-sized rutile and zircon grains 58

2-4 Least significant difference profile groupings based on SEM survey characteristics differences between the upper and lower units. 61

2-5 Least significant difference profile groupings based on SEM survey characteristic contrasts between upper units of adjacent pedons 62

3-1 Mean whole soil compositions for pedon deep (parent material) samples 89

3-2 Correlation matrix for all elemental translocations in microlow and microhigh profiles (excluding pedon LAW 239) 113

3-3 Elemental mass fluxes for climosequence profile samples 115

4-1 Paleosol outcrop features and paleoclimatic interpretation. 130

A1-1 Pedon field descriptions 163

A1-2 Mean monthly ambient temperatures for pedon locations 199

A1-3 Mean monthly precipitation (MMP), potential evapotranspiration (ET_p), and estimated moisture deficits for pedon locations 201

A2-1 X-ray fluorescence (XRF) raw data for Ti and Zr 204

A2-2 Carbonate correction factors (as determined using procedure in Chapter 2) . . . 208

A2-3 Carbonate-corrected XRF element wt % (as determined using procedure in Chapter 2) 210

A2-4 Dry clod bulk density (BD) values 214

A2-5 Volumetric elemental content 219

A2-6 Particle size distribution data 223

A2-7 Mean separations between upper and lower unit Ti and Zr contents 227

A2-8 Mean separations in Ti or Zr contents between laterally adjacent profiles 228

A2-9 SEM survey results 231

A2-10 Mean separations between zircon and rutile SEM features in upper and lower units 233

A2-11 Mean separations between zircon and rutile SEM features in upper units of adjacent pedons 234

A2-12 Mean strain values for all profiles 235

A3-1 Whole soil XRF data, uncorrected element oxide data 238

A3-2 Whole soil carbonate-corrected element oxide data 247

A4-1 Elemental contents of bulk iron-manganese nodules isolated from modern Vertisols 258

A4-2 Descriptive statistics for iron and manganese in nodules isolated from modern Vertisols 262

A4-3 Elemental contents of bulk iron-manganese nodules isolated from paleo-Vertisols 263

List of Figures

1-1. Modern Vertisol climosequence sampling locations designated by series and NRCS pedon number 17

1-2 Composite daily temperature trends for all pedon locations. 22

1-3 Monthly precipitation trends for soil series and pedons 24

1-4 Monthly estimated soil moisture deficits for soil series and pedons.calculated as mean monthly precipitation [0 - Thornthwaite evapotranspiration index (ET_p)] . 27

1-5 Monthly precipitation trends estimated for pedon LAW 239 (Jackson County, TX) based on data from proxy locations with respect to coastline proximity 29

2-1 Identification of the functional boundary depth in microlow pedons indicated by shifts in Ti:Zr 46

2-2 Element (volumetric content) comparisons of Ti and Zr from different soil series 49

2-3 Particle size distribution and textural classification of climosequence microlow profile horizons. 52

2-4 Photomicrographs of textural contrasts contrasts across the functional boundary in two pedons 54

2-5 Separated regression analyses of sand content versus volumetric Zr content by soil series. 55

2-6 Linear regression relationship between sand content and volumetric Ti and Zr content in microlow pedons, undifferentiated by series 56

2-7 Photomicrographs of characteristic very fine sand-sized rutile and zircon grains.59

2-8 Identification of the functional boundary depth in microhigh profiles indicated by shifts in Ti:Zr. 65

2-9 Conceptual climosequence Vertisol pedogenesis model based on depth to functional boundary as a function of MAP. 68

2-10 Linear regression of ϵ_{Ti} and ϵ_{Zr} calculated from mean depth interval values for all profiles. 72

3-1 Residual enrichment for all profiles 90

3-2 Titanium-based strain for all profiles. 92

3-3 Mean Ti- and Zr-strain values. 93

3-4 Translocations of Al in profiles 95

3-5 Translocations of Si in profiles 97

3-6 Particle size modal percentages 98

3-7 Translocations of Ca in profiles 100

3-8 Translocations of Mg in profiles 101

3-9 Translocations of Sr in profiles 102

3-10 Translocations of K in profiles 105

3-11 Translocations of Rb in profiles 106

3-12 Translocations of Fe in profiles 107

3-13 Translocations of Mn in profiles 109

3-14 Translocations of P in profiles 111

3-15 Mass flux as a function of MAP 116

4-1 Thin section views of pedogenic Fe-Mn nodules 122

4-2 Paleosol sampling locations 126

4-3 Data and regression from modern Vertisol Fe-Mn nodules: A) Mean total Fe and Mn (modern Vertisols) versus MAP; B) Regression relationship between modern Vertisol Fe_{TOT} and MAP 128

4-4 Mean annual precipitation as a function of DCH in modern Vertisol microtopographic positions 131

4-5 Paleoprecipitation estimates for Penington Formation paleosol 2 based on nodules Fe_{TOT} and DCH from modern Vertisols 134

Chapter 1

Introduction

1.1 Soils and paleosols as environmental indicators

Soils are direct integrations of environmental effects on their geologic parent material over time. As such, they may provide interpretive tools in understanding their environment of formation (Jenny, 1941a, 1980; Birkeland, 1999). Authigenic mineral formation, morphological characteristics, and geochemical changes all attest to the evolution of a soil through time in response to direct environmental influences. Most pedogenic processes require 10^2 - 10^4 years before a clear environmental signature is defined (Yaalon, 1971) This is a virtual geologic "eye blink" in many paleosol (ancient lithified soil)-bearing sedimentary sequences, which may record millions of years of environmental change. Paleosols have been used to interpret the paleoenvironments in which they formed (McSweeney and Fastovsky, 1987; Cerling et al., 1989; Nordt et al., 1994; Mora et al., 1996; McCarthy et al., 1999). The interpretive power of paleosols is greatly enhanced by the examination of modern soil and environmental analogs, where pedogenic processes and conditions can be monitored and quantified. For paleoenvironmental reconstructions, useful paleosols are those which:1) experienced minimal post-pedogenic alteration, 2) remained cohesive during the burial process, and 3) have experienced a minimal amount of diagenetic fluid-rock interaction, preserving both physical and chemical pedogenetic evidence. It is also desirable that these paleosols are both easily identifiable with modern analog soils and geographically widespread.

Paleosols analogous to several modern soil types have been identified in the rock record (Mack et al., 1993). Clay-rich soils, or Vertisols, and their ancient analogs meet the requirements suggested above. Vertisols have been identified in many modern geographic regions, forming on a wide range of parent materials and maturing to have remarkably similar physical/geochemical characteristics within a geologically brief period of time (from 1000 - 4000 yr; Wilding and Coulombe, 1996; Robinson, 2001). Lithified Vertisols (paleo-Vertisols) have been identified in many geologic successions, particularly Paleozoic-age successions in the Appalachian Foreland Basin of eastern North America (Driese et al., 1992; Driese and Mora, 1993; Mora and Driese, 1999). These paleosols clearly show field characteristics fitting modern taxonomic criteria for Vertisols, often despite deep burial and post-pedogenic alterations (Caudill et al., 1996). Geochemical and petrographic analyses of paleo-Vertisols show trends remarkably similar to modern Vertisols, suggesting that the interpretive power of these paleosols may be extensive (Driese et al., 2000).

1.2 Geologic Context of Vertisols and Their Ancient Counterparts (Paleo-Vertisols)

1.2.1 Vertisols in Present Day Conditions

According to U.S. Soil Taxonomy, Vertisols are soils that have: 1) a layer (>25 cm thick) of slickensides or wedge-shaped peds with long axes tilted 10-60° from horizontal, 2) >30 wt % clay, and 3) cracks which open periodically (Soil Survey Staff, 1998). Vertisols form relatively rapidly on flat-lying, fine-grained, base-rich parent materials across a broad

range of climatic regions with periodic soil-moisture deficits (Ahmad, 1983; Coulombe et al., 1996a). These soils attain comparable mineralogic assemblages over time, regardless of parent material, with mineral percentages and micromorphologic expressions differing across climatic gradients (Millot, 1982).

Clay minerals make up 30 to 95% of the particle size fractions of Vertisols. Most clay minerals are 2:1 phyllosilicates, usually in the smectite group (montmorillonite and/or beidellite), although micaceous intergrades and kaolinite have been reported (Dixon, 1982; Coulombe et al., 1996a). Smectites are particularly surface-reactive and often participate in hydrochemical reactions involving water-soluble organic compounds and ionic species. These clays also hold relatively large percentages of water under high potentiometric conditions (>1500 kPa, the functional wilting point beyond which plants can no longer effectively remove water from the soil). This behavior dictates Vertisol geochemistry and hydrogeochemical behavior. Accessory silicate, oxide and hydroxyoxide minerals are also found and may be used to elucidate the provenance and continuity of soil parent material, in addition to providing clues to redox conditions (Stephen, 1953; Wang et al., 1993). Coulombe et al. (1996a) proposed that mineralogic assemblages in Vertisols may have been underinterpreted in the past and that there are still clues to pedogenesis and environment of formation to be gained from closer examination of the relationships therein. Dudal and Eswaran (1988) claim that this is supported by Vertisol morphologies having complicated internal hydrochemical and physiological systems rather than the simplistic overturn model suggested by earlier pedologists (Templin et al., 1956).

The physical morphology of Vertisols, induced primarily by the influence of differential moisture stress on the clay-rich matrix, includes gilgai and slickensides (Wilding and Tessier, 1988). Slickensides are planar features, occasionally striated parallel to dip and occurring at a critical depth within the profile, along which rhombohedral masses of soil matrix are dislocated (Yaalon and Kalmar, 1978). Gilgai, or "little water bowls" (aboriginal Australian term), are bimodal microtopographic expressions of subterranean plastic deformation along slickenside planes that occur during wetting. As the wetting front descends, large volumes of soil matrix are forced upward, creating small anticlines or "microhighs" (Hallsworth et al., 1955). Poorly-drained basins ("microlows") form in the synclinal areas adjacent to the microhighs, tending to accumulate more organic matter, whereas in the microhighs, water is conducted upward along the slickenside planes aided by evapotranspiration (Newman, 1986). Microtopographic domains persist across time and disturbance episodes, their development and preservation aided by the very nature of the physico-chemical environment they generate. This distinctive topography essentially creates a pedogenic continuum within the formational environment, with morphologic expression sensitive to changes in vegetative cover and precipitation seasonality. Geochemical differences are noted between the microtopographic domains, with the microlows acting as more closed hydrogeochemical systems, whereas the microhighs tend to be "drier" open systems influenced by dynamic physical actions (Driese et al., 2000).

1.2.2 Pre-Quaternary Paleo-Vertisols

Clay-rich paleosols showing analogous morphology to modern Vertisols have been

identified in several Paleozoic age sequences of the Appalachian Foreland Basin (Mora and Driese, 1999). These paleo-Vertisols tend to be well-preserved and may even be over-represented in geologic successions compared to modern day occurrences, due to either cohesion and resistance to erosion, lack of physical compaction (Caudill et al., 1997) or simply because these types of soils were more prevalent in the past (Driese and Foreman, 1991, 1992; Gustavson, 1991; Caudill et al., 1996, 1997). Basic geochemical trends of paleo-Vertisols have been found to match those of modern counterparts, suggesting a relatively closed-system chemical environment during burial diagenesis, even to the extent that microtopographic differentiation of chemical trends may still be discerned (Driese et al., 2000).

Preserved gilgai microtopography, along with slickensided aggregates, are the most notable characteristics identifying paleo-Vertisols (Caudill et al., 1996). The pedogenically altered clay-rich matrix does not allow for significant compaction, unlike typical subaqueous clay deposition (Caudill et al., 1997). Significant geochemical differences found between microtopographic positions in modern Vertisols may be expressed similarly in the paleo-Vertisols. Driese et al. (2000), upon noting large differences in geochemical composition between pedons from adjacent microtopographic positions, suggested that interpretation of paleo-Vertisol compositions without full knowledge of the microtopographic positions may be misleading. Microlows tend to preserve a better signature of hydrodynamic conditions, as they act as more closed systems. It is imperative in studies of Vertisol genesis to include comparisons between the

microtopographic positions in order to assess the differential ranges of geochemical signatures attributable to genetic factors.

1.3 Modern Soil Geochemistry

Studies of modern soil geochemistry has largely focused on the agricultural aspects of mineral alteration, aqueous dynamics, and translocations (*sensu* Lindsay, 1979). Geochemical maturation of natural soil bodies in response to environmental factors has been studied using various techniques. Early pedologists, having classical geology backgrounds (Harrassowitz, 1926; Marbut, 1935), were inclined to utilize elemental composition ratios to determining loss or gain within weathering profiles. It was also discerned that combinations of elements, behaving in similar or contrasting modes, were especially effective in differentiating patterns of weathering (Birkeland, 1999). Chadwick et al. (1990) broadened the interpretive powers of elemental compositional variations by using ratio categories in combination with mass-balance relationships. Langley-Turnbaugh and Bockheim (1998) successfully utilized mass-balance relationships with traditional soil extraction methods to determine alterations and add interpretive power to a marine terrace chronosequence in Oregon.

1.3.1 Mass-Balance Overview

Systematic mass-balance equations used to determine weathering intensity in residual profiles were initially defined by Brimhall et al. (1985) to study residual enrichment in supergene ore deposits. These relationships allow for meaningful comparisons of

elemental translocations by essentially accounting for volumetric changes, residual enrichment, and open system transport of material in soil (Brimhall et al., 1985; Brimhall and Dietrich, 1987). Relatively closed system alterations are quantified through *strain* (ϵ) based on the concentration of an immobile element and bulk density measurements (Eq. 1):

$$\epsilon_{i,w} = (\rho_p C_{i,p}/\rho_w C_{i,w}) - 1 \quad (1)$$

Where ϵ is strain, ρ is bulk density, p is unweathered parent material, w is weathered material, and C is concentration of immobile element i. Strain indicator elements, such as zirconium (Zr) and titanium (Ti), in theory, are residually enriched relative to elements translocated from leached zones, and depleted relative to elements accumulated in secondary phases. The magnitude of open- system transport of an element ($\tau_{i,w}$) is determined by incorporating the strain index into a volumetric correction equation similar to Eq. 1:

$$\tau_{i,w} = [(\rho_w C_{i,w}/\rho_p C_{i,p})(\epsilon_{i,w}+ 1)]-1 \quad (2)$$

These equations have been used with relative success in many pedogenic settings (Chadwick et al., 1990; Merrits, et al., 1991; Nieuwenhuyse and van Breeman, 1997; Langely-Turnbaugh and Bockheim, 1998; Mason and Jacobs, 1998; Driese et al., 2000). Chadwick et al. (1990) pointed out that there were some shortcomings inherent in the calculations, specifically the lack of accounting for differences in parent material (particularly superjacent accumulations) and the difficulties of accurately assessing bulk densities in coarse-textured soils. Brimhall et al. (1991a, 1993) recognized the major shortcomings were the pre-suppositions that: 1) parent material remains consistent

throughout the entire depth of the profile, and 2) strain indicator elements remain geochemically "fixed" in the weathering profile. Subsequent studies have attempted to address solutions to this problem, either through examination of minerals containing immobile elements within profiles for evidence of differential transport and dissolution (Brimhall et al., 1993) or by defining the most conservative elements in weathering monolithic systems (Hill et al, 1999; Kurtz et al., 2000). Despite the cautionary observations, mass-balance relationships present a promising approach to comparing modern pedogenic settings with ancient analogous environments.

1.3.2 Determining Soil Strain

In mass-balance relationships, strain is quantified using a relatively immobile element, one that behaves conservatively under weathering conditions. Brimhall and Dietrich (1987) suggested the use of Ti or Zr as immobile strain indicators based on Australian bauxite data from Sadleir and Gilkes (1976). These elements are components of relatively stable minerals in most geologic materials, particularly rutile (TiO_2), ilmenite ($FeTiO_3$), and zircon ($ZrSiO_4$). However, there are legitimate questions about the "immobility" of these elements, as mineral phases in soils degrade during pedogenesis and small mineral grains from outside sources may be added and then transported downward in the solum. Within lateritic profiles, the residual soils developed under long-term intense weathering conditions from which the original mass-balance equations were derived, the provenance of these relatively inert minerals has been called into question (Brimhall et al., 1991a & b, 1993; Colin et al., 1993). Degradation of Ti- and Zr-bearing minerals, which is limited

but not implausible, occurs under different weathering conditions, depending upon hydrogeochemical factors such as the presence of soluble organics (Ti; Correns,1978), or ionic strength fluxes (Zr; Speer, 1978).

Most soils do not develop under the relatively closed-system model of a monolithic, fixed-composition parent material throughout the entire weathering duration. Soil mantles are dominantly polygenetic, in the sense that geologic or biologic material is constantly being added to the solum. The most dramatic cases of this are loess sequences and accumulated alluvial deposits (Birkeland, 1999). Such soils, termed "cumulative" by Nikiforoff (1949), can be compared to underlying unweathered parent materials through mass-balance calculations only by factoring out the influence of fresh overburden (Brimhall et al., 1993). Alluvially-derived soils have complex depositional architectures (noted most frequently as particle-size distribution shifts; Aslan and Autin, 1998) to complicate long-term models of pedogenesis. However, the assumption can be made that a stream derives its parent sediment from a source basin, which in most cases does not significantly shift its lithologic composition over time (Van Andel and Poole, 1960). Thus, there should not be major compositional shift within the basin during active down-cutting and mass-balance relationships are still valid. Comparing soils from between basins requires that strain be calculated from the estimated intrabasinal parent material of each alluvial deposit. Once this is done, the relative translocations are easily compared between pedons derived from different parent alluvium.

1.3.3 Soil - Paleosol Comparisons

Most elements behave in a predictable fashion in mineral soils, being lost through primary mineral degradation and leaching and accumulating through secondary mineral precipitation. Chadwick and Chorover (2001) suggest that soils progress through a series of pedogenic thresholds dictated by weathering regime and geological setting. Paleosol/modern analog soil comparisons are based on the uniformitarian hypothesis that the essential thermodynamics of soil-forming processes have not changed through geologic time, such that if a notable trend occurs in a (Phanerozoic) paleosol, a comparable trend can be described in modern analogs of that paleosol. There are some exceptions, particularly past ambient conditions that cannot be found on present day Earth except under experimental control, such as paleoatmospheric compositions with elevated pCO_2 and pO_2, warmer temperature regimes, and Bryophyte megaflora communities (Retallack, 1990). Soils formed under these types of conditions have no modern analogs and paleopedogenesis can only be estimated (Mack and James, 1994). The most limiting aspect of paleosol/modern analog soil comparisons is the paucity of well-preserved paleosols. Most paleosol profiles are only partially preserved, as the most erodible surface horizons are partially or entirely removed prior to burial. How well a particular soil type can be preserved in the geologic record determines the efficacy of modern analog studies of this type.

Dreise et al. (2000) found that modern Vertisol mass-balance characteristics were translatable to ancient Vertisols. The clay-rich matrix characteristic of Vertisols not only

dictates their geochemistry, but also preserves some of the imprinted geochemical signature emplaced by pedogenic processes. When directly compared, the bulk composition of many elements, such as aluminum (Al), potassium (K), and silicon (Si) were notably different between modern and ancient soil, most likely due to changes induced by burial diagenesis. But when mass-balance relationships were employed, comparisons of pedogenic signatures are more readily accomplished. For example, the general translocation patterns for Ca, magnesium (Mg), and phosphorus (P) were very similar between modern Vertisols and their ancient counterparts. These encouraging findings suggest an expanded role for paleo-Vertisols in paleoenvironmental reconstructions — as a sub-aerial proxy for long-term climate changes induced by regional tectonism and Milankovitch cycles. The analog comparison studies open new doors to cooperative investigations between pedologists and geologists searching for finer-resolution paleoclimate correlatives for existing stratigraphic and paleontologic records.

1.3.4 Pedogenic Climate Indicators

Several soil characteristics expressed in modern soils are preserved in geologic successions. The most notable preserved paleosol characteristics are: carbonate nodules/ rhizocretions/calcretes, evaporite pseudomorphs, dessication cracks, ped structure, root traces, and redox-induced depletions/concentrations/glaebules (Retallack, 1990). Occasionally plant traces are noted and even some preserved organic material, but this is rare, particularly in oxidized paleosols. Several of these characteristics are indirectly

induced by climatic conditions and are fairly well-preserved in paleo-Vertisols, most particularly carbonate and redox features (Mora and Driese, 1999). Some features are less useful, as they may be easily overprinted or induced by more than one soil-forming condition (ped structure, crack morphology).

1.3.4.1 Depth to Carbonate Enriched Horizons

Most Vertisols are enriched in pedogenic calcium carbonate (calcite-$CaCO_3$), as they selectively form on base-rich parent materials in areas where there are distinct periods of drying. The hydrodynamic nature of smectitic clay matrices also induces carbonate precipitation at higher relative moisture contents than coarser-textured soils, as hydrophilic smectites effectively reduce free-water content, enriching soil-solution bicarbonate (HCO_3^-) beyond saturation with respect to calcite or mixed composition carbonates (Doner and Lynn, 1989). Depth to carbonate-enriched zones (Bk horizons) has been utilized as a proxy for climatic conditions (Jenny and Leonard, 1934; Jenny, 1941b; Arkley, 1963), as the carbonate leaches to just below effective meteoric infiltration. Retallack (1992) utilized this relationship in paleosol sequences to fortify evidence of climatic change across the Eocene-Oligocene boundary. Caudill et al. (1996) utilized an equation derived from Retallack (1994) to estimate precipitation in a Mississippian-age paleo-Vertisol. The method is not without problems, however, as variable hydraulic conductivities and mixed phase mineral stabilities precluder consistent or simple correlation in most cases. Royer (1999) found a weak relationship between a large data set of depths to top of carbonate horizon derived from the United States

Department of Agriculture - Natural Resource Conservation Service (NRCS) database and mean annual precipitation (MAP; $r^2 = 0.31$; $P < 0.001$). Royer (1999) suggested that more robust correlations may be obtained if there is stricter control on edaphic conditions within modeled climoseries, such as vegetation type, hydraulic conductivies, and precipitation patterns. Certainly paleo-Vertisol paleoprecipitation interpretation should be based on well-controlled analog model derivations.

1.3.4.2 Pedogenic Iron-Manganese Nodules

Another indicator of redox status in soils is the presence of pedogenic iron-manganese (Fe-Mn) concentrations or glaebules. Iron and Mn minerals are the most abundant metallic oxides in soils (McKenzie, 1989; Schwertmann and Taylor, 1989). Often associated with soil color, Fe and Mn mineral phases can coalesce into stable authigenic glaebules, or nodules, in soils with alternating wet and dry hydrologic conditions. The pedogenic Fe and Mn mineral phases which form the nodules are responsive to changes in Eh/pH and ionic strength of soil solution along with free-water availability. Because vadose hydrochemistry is controlled by meteoric supplies, formation of pedogenic Fe-Mn nodules in Vertisols is largely dictated by rainfall trends.

The mechanics of nodule development differ between marine and pedogenic settings, as does the resulting minor mineral content. In marine settings, nodules form at the sediment-ocean interface where oxidizing water reacts with diffusive supplies of reduced Fe and Mn from the sediments (White and Dixon, 1996). Microbial processes mediate

sediment reduction in low-influx settings, and as oxygenated sea water is not limited, marine nodules can often grow quite large and contain relatively pure-phase mineral assemblages. Pedogenic nodules, however, are more responsive to immediate changes in the sub-aerial environment, initially coalescing as hydrous-phase assemblages in micropores, and accreting outward in concentric fashion. These nodules grow displacively and incorporate resistant mineral grains, such as quartz and zircon, into their matrix, unlike their marine counterparts (Cescas et al., 1970).

The intimate relationship of Fe and Mn in marine and pedogenic nodules has been widely studied (Lundgren and Dean, 1979; Postma, 1985; Golden et al., 1993) and the presence of Mn seems to be required for Fe-enrichment. The major similarity between the two nodule-forming environments is a redox gradient necessary for mineral dissolution/precipitation (Ehrlich, 1981). It is believed that Mn oxides containing structural Mn(IV) initially precipitate (Senyaki et al., 1989) and subsequent oxidation of Fe^{2+} by Mn(IV) reduction to Mn(II) induces Fe(III) mineral phases to precipitate (Golden et al., 1988). In pedogenic nodules, an additional driving mechanism is vadose hydrology, dictated by seasonal wetting and drying cycles. Hydrous Fe and Mn mineral phases (ferrihydrite, birnessite) form in hydrochemically favorable micropores, and as water becomes limiting, establish more stable crystalline lattices (goethite, lepidocrocite, hollandite) that are resistant to later post-pedogenic alterations.

Most common modern occurrences of pedogenic Fe-Mn nodules are in fine-textured (silt-

or clay-rich) soils with poor or imperfect drainage in moderately warm to tropical regimes. In many cooler climates, most Fe and Mn phases are amorphously associated with, or chelated by, humic substances (soil organic matter or SOM). Significant volumetric nodule contents are usually not found in sandy or well-drained soils, where high hydraulic conductivities and well-oxygenated conditions are inconsistent with the Eh/pH range and variability required for nodule initiation. Lack of SOM in these settings also discourages Fe-Mn concentration, inasmuch as microbially-mediated amorphous phases are often precursors to later mineral accretions (Schwertmann and Taylor, 1989)

Pedogenic Fe-Mn nodules have been found in numerous clay-rich paleo-Vertisols (Carboniferous - Joeckel, 1995; Caudill et al., 1996; Cretaceous - McSweeney and Fastovsky, 1987; McCarthy et al., 1999; Tertiary - Smith et al., 1994). Two findings suggest little post-pedogenic alteration of Fe-Mn nodules in clay-rich paleosols: 1) Clay-accumulation (argillic or Bt) horizons, within which most Fe-Mn nodules are found, experience minimal compaction during burial (Caudill et al., 1997); 2) Thin-section morphology shows ancient Fe-Mn nodules to be very similar to their modern counterparts, including the accretionary growth patterns. Post-pedogenic transformations of goethite (FeOOH) to hematite (Fe_2O_3) occur during diagenetic, but for the most part, Fe is conserved. As they occur widely in modern clay-rich soils (i.e., Vertisols), where edaphic effects can easily be measured, it is reasonable to assume that comparison of ancient and modern Fe-Mn nodule geochemistry and morphology could provide insight about ancient environmental conditions.

1.4 Modern Analog Setting - The Texas Gulf Coastal Prairie

1.4.1 Geological Setting

When developing models of pedogenesis, the influence of soil-forming factors needs to be accounted for in a systematic way, in settings where all but one factor is held relatively constant. Such studies have been carried out in the past on chronosequences (time variable; Harden, 1988; Langely-Turnbaugh and Bockheim, 1998) found in many climatic zones. Climosequences (precipitation regime variable) are relatively rare, requiring a stable topographic position on a single parent material unit deposited contemporaneously across a significant area (Chadwick et al., 1994). A Vertisol climosequence exists on the Gulf Coastal Prairie of Texas, where the exposed Pleistocene-age (35 ka) Beaumont Formation provides a large expanse of Vertisols across a precipitation gradient of 600 to 1600 mm MAP. Topography, time, and parent material can thus be considered "fixed". Compared to other soil types, biotic factors are not strongly implicated in developing characteristic features of Vertisols. The dominant factor is climate, which limits the range and variability of flora and fauna.

The Beaumont Formation is a fluvio-deltaic complex derived from coalescing alluvial plains of several rivers flowing into the Gulf of Mexico (Fig.1-1). It is the youngest Pleistocene unit of several coast-parallel depositional sequences that occur along the Texas coast, formed during Pleistocene glacio-eustatic sea-level changes (Doering, 1956). Each of the Pleistocene sequences (Willis, Lissie and Beaumont) is bounded on top with an oxidized soil and older surfaces occur updip of more recent deposition, creating on

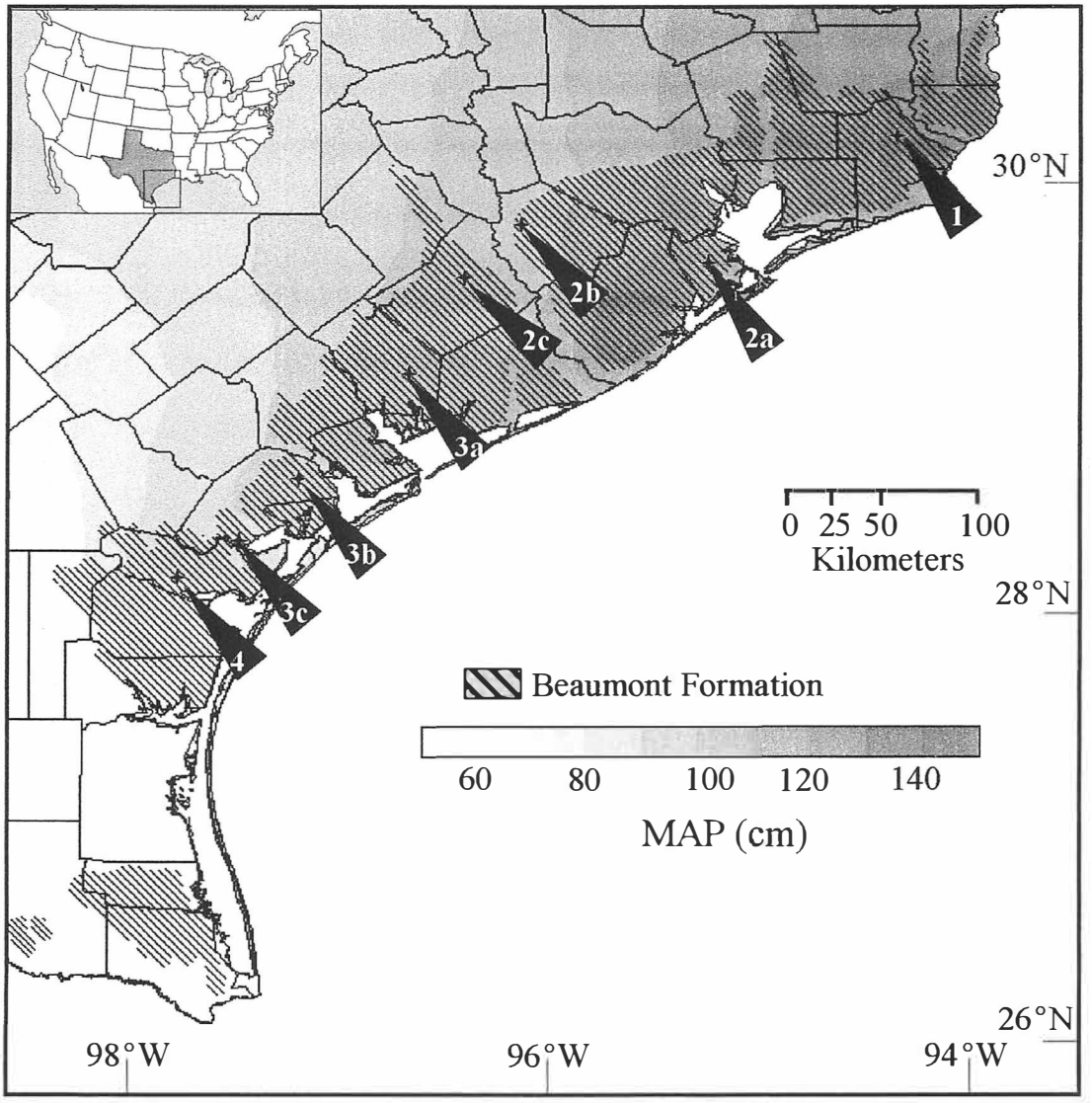

Figure 1-1. Modern Vertisol climosequence sampling locations designated by series and NRCS pedon number: 1 = League 245A; 2 = Lake Charles / a = 201, b = 157, c = 481; 3 = Laewest / a = 239, b = 469, c = 391; 4 = Victoria 409.

onlapping series of buried surfaces (Bernard and LeBlanc, 1965). Blum and Price (1994) stated that within the Beaumont, numerous cross-cutting and/or superimposed valley fills occur within each broad alluvial realm, complicating stratigraphic continuity. Thus, the Beaumont is comprised of relatively older, stable interfluve terraces with multiple channel meanderbelts associated with each river, and pedologic age is dictated by the position relative to these features. Because they are distal depositional areas, meandering river bed loads mainly consists of silt- and clay-sized particles (<62.5 μm and <4 μm, respectively), with occasional incursions of sands during storm events. The general age of the stable Beaumont deposits is around 35 ka (Birdseye and Aronow, 1991), this time representing the end of the last interstadial (highstand) prior to the most recent glacial (Shackleton, 1988).

The Texas Coastal Prairie is dominated by Vertisols. These soils dictate agricultural and construction practices by their physical properties, as the high clay contents tend to limit infiltration and disrupt building foundations and road surfaces with seasonal shrinking and swelling. Texas Vertisols are among the most well-studied soils in the world because they are agriculturally productive and they also underlie one of the United States largest cities, Houston (Newman, 1986). The USDA-Natural Resource Conservation Service (NRCS) has extensively mapped these Vertisols, classifying them into standard orders using Soil Taxonomy (Soil Survey Staff, 1998), a system which categorizes soil types by field characteristics and climatic setting. High-resolution soils maps (1:24,000 scale) based on geologic maps, aerial photography, and soil sampling data have been published and

updated by NRCS.

1.4.2 Climosequence Soil Series

The Texas Vertisol climosequence is comprised of several named soil series, the highest level of U.S. Soil Taxonomy differentiation, which change characteristics with climate. Four soil series are of particular interest for determining climate impact on Vertisol pedogenesis in this study, as they straddle an important MAP boundary which has long been associated with a major shift in ecosystem and pedogenic characteristics. This series transition extends from humid regions in the east, across moist and dry sub-humid regions in the coastal bend into the semi-arid region to the south, crossing a classical, though somewhat outdated, pedogenic mapping boundary between "pedalfers" (forest soils with Fe-enriched horizons) and "pedocals" (prairie soils with carbonate-enriched horizons; Marbut, 1935; Jenny, 1941b). Series names are (from wettest to driest): League, Lake Charles, Laewest, and Victoria (Table 1-1). Each soil series has characteristic morphological and geochemical characteristics which are the result of long-term external natural factors. Because each series tends to be found within a relatively narrow range of these pedogenic factors, with climate being the only significant variable in this case, series are good regional indicators of climatic inputs.

This study utilizes internal and NRCS-generated code names for sampled climosequence pedons. Because these codes are used extensively throughout the study, Table 1-1 gives specific locations and other pertinent information for each pedon. Figure 1-1 also shows

Table 1-1. Soil taxonomic, geographic, and climatic data for pedons used in this study[a].

Series name and U.S. Soil Taxonomy description	Profile designation	Geographic Location	Ambient temperature (°C)			Precipitation (mm)	
			MAT[b]	High[c]	Low[c]	MAP	Annual deficit[d]
League fine, smectitic, hyperthermic Oxyaquic Hapluderts	LEG 245A	30°02′22″N 94°11′36″W	20.1	25.5	14.7	1437	604
Lake Charles fine, smectitic, hyperthermic Typic Hapluderts	LAC 201	29°35′40″N 95°04′14″W	20.6	25.8	15.4	1321	774
	LAC 157	29°24′12″N 95°43′42″W	20.6	26.3	14.8	1170	866
	LAC 481	29°22′21″N 96°04′22″W	21.0	25.2	16.8	1124	1019
Laewest fine, smectitic, hyperthermic Typic Hapluderts	LAW 239	28°52′48″N 96°24′11″W	21.0	25.2	16.8	1066	1149
	LAW 469	28°43′12″N 96°45′23″W	21.2	26.7	15.8	1000	1381
	LAW 391	28°28′27″N 97°07′00″W	21.8	27.4	16.1	924	1402
Victoria fine, smectitic, hyperthermic Calcic Haplusterts	VIC 409	28°06′45″N 97°20′55″W	21.8	27.4	16.1	844	1482

[a] All climate information derived from 100 yr of daily temperature and precipitation data from nearest Class 1 meteorological recording station to sampling locations; National Climate Data Center, Asheville, NC

[b] Mean annual temperature

[c] Mean values

[d] Shown as 0 - (MAP-ET_p) so that deficits are positive values

locations and climatic context. Detailed descriptions for each pedon included in this study are given in Table A1-1, along with NRCS pedon code number allowing access to more information within the NRCS database maintained on their internet website:www.statlab.iastate.edu/soils/. Generalized descriptions of the soil series are also available at that web site.

1.4.3. Climatic Setting

1.4.3.1 Air and Soil Temperature

The present day Texas Gulf Coastal Prairie climate is largely influenced by the interaction of the dominating warm, moist convective maritime tropical air masses of the Gulf of Mexico with incursions of continental air masses (Bomar, 1995). Seasonal temperatures are relatively moderate, with daily highs ranging from 16.9-18.5°C in January to 32.4-34.7°C in August (Table A1-2; all climate information derived from 100 years of daily temperature and precipitation data from nearest Class 1 meteorological recording station to sampling locations; National Climate Data Center, Asheville, NC). There is moderate diurnal variation between daily highs and lows (8-12°C) and mean annual temperatures (MAT) range from 20.1-21.8°C, warming to the south. Figure 1-2 shows seasonal temperature variations. Most years remain relatively frost-free, with only 15-40 days of frost occurring in the most extreme of years (Bomar, 1995). Soil temperature is a direct function of ambient air temperature, as radiant heat is translated into soil profiles through direct conduction. The thermal diffusivity properties of most soils limits penetration of heat to 10 cm for diurnal temperature variations and 1.5 m for annual forcing (Hartmann,

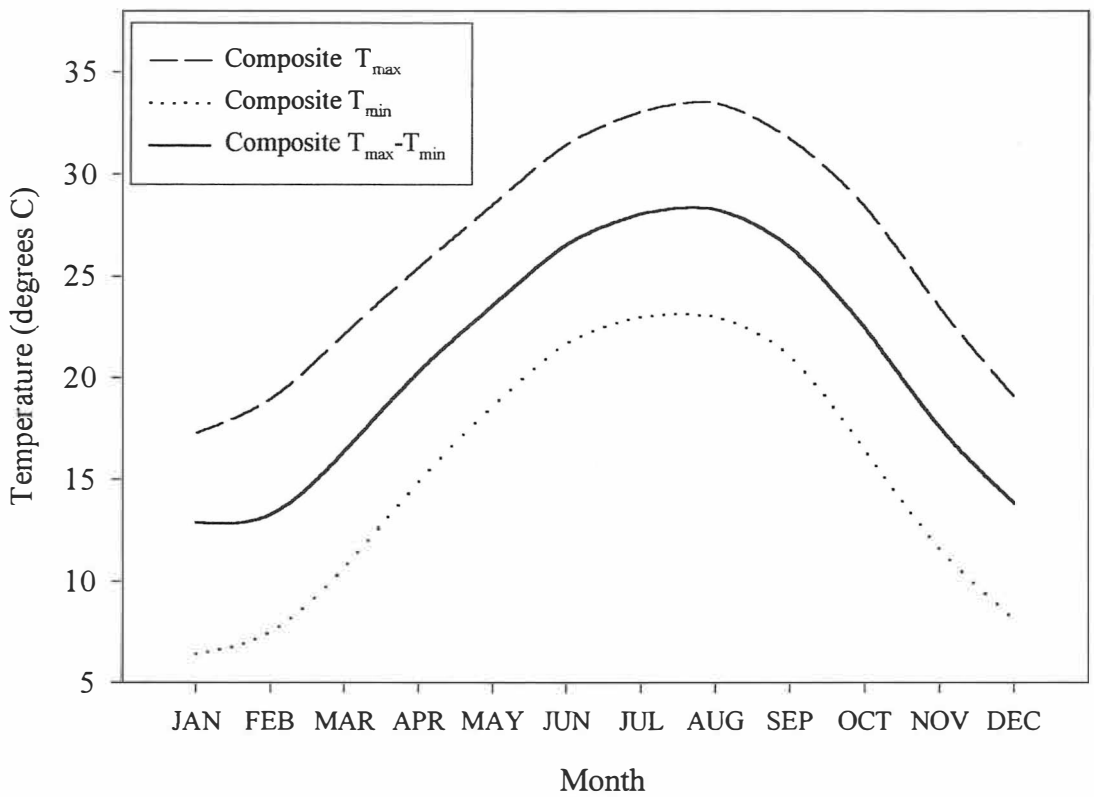

Figure 1-2. Composite daily temperature trends for all pedon locations.

1994). Effective heat transfer is also dictated by profile hydraulic saturation, as the addition of water modifies the heat capacity. Wet soils heat more slowly, as radiant heat is utilized to evaporate soil water during the warming process. Thus, dry Vertisols receive and disperse heat somewhat differently than wet Vertisols, which amplifies physical and geochemical differences.

1.4.3.2 Precipitation

Rainfall trends are the most important variable in the Texas Vertisol climosequence setting. The climosequence precipitation gradient within this study ranges from >1400 mm in its northeastern extent to <900 mm in the south (Fig. 1-1), and pedon locations effectively span that range. The rainfall patterns are strongly and consistently bimodal (Fig. 1-3, Table A1-3), reflecting the influence of drier continental air masses in spring and autumn. This seasonality is ameliorated in the easternmost areas of the climosequence, with the nearly constant onshore flow of tropical maritime air. Seasonality is most pronounced in the southern portion, where onshore flow is limited by the prevailing south-to-north air currents carrying dry air from Mexico. This predominantly meridional pattern is only overridden by strong fronts in the spring and tropical storms in late summer/early autumn (Bomar, 1995).

Because of the high clay content of Vertisols, meteoric moisture uptake and retention are highly variable. There are changes in structural and hydraulic characteristics related to pore size distribution through which a Vertisol proceeds as it wets and dries (Yule and

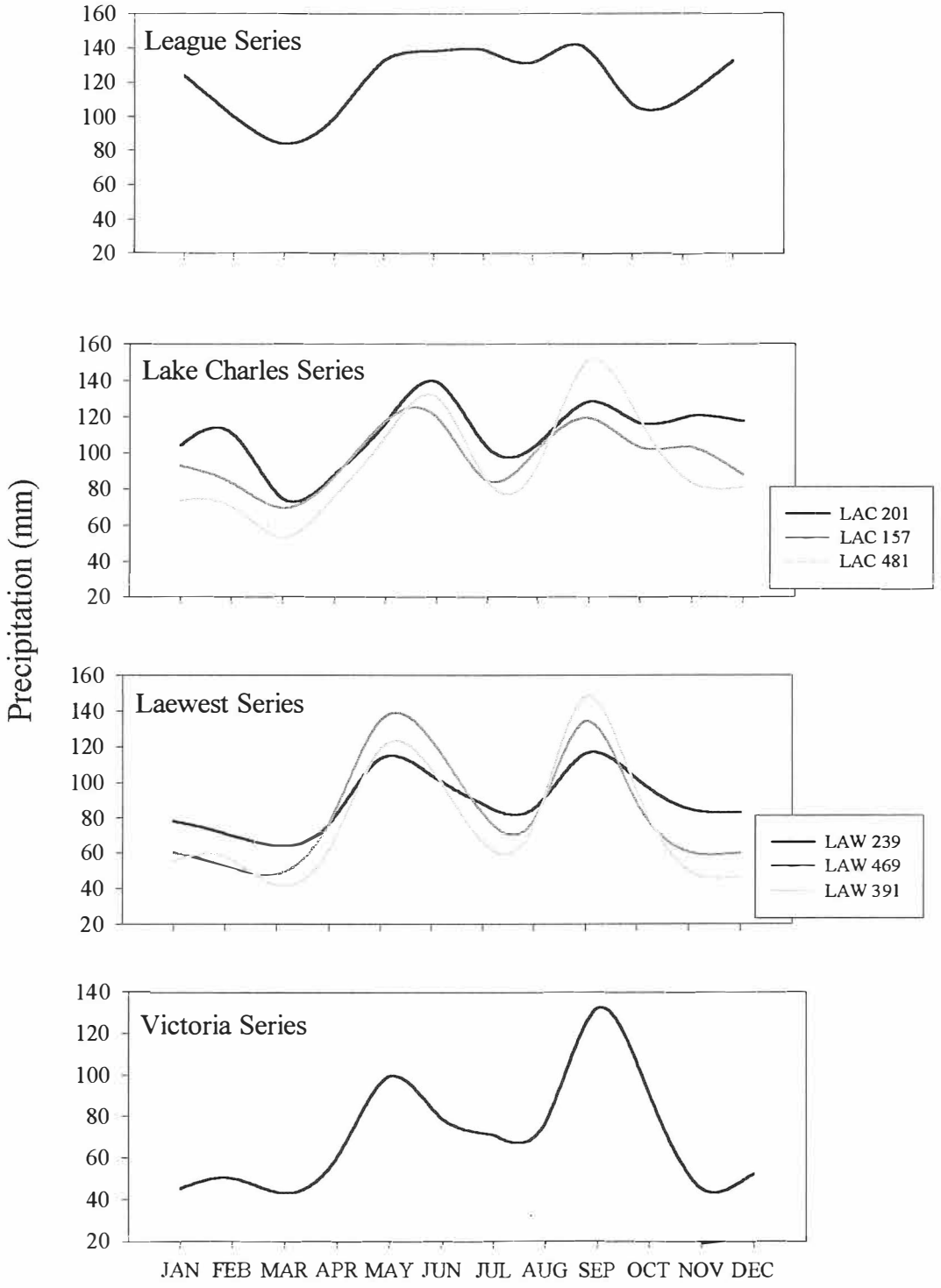

Figure 1-3. Monthly precipitation trends for soil series and pedons.

Ritchie, 1980). Initially, large cracks (macropores) formed during dry periods (especially in summer, when evapotranspiration is greatest) serve as conduits to meteoric water as it initially infiltrates the profile until the clays associated with the macropore swell sufficiently to block the opening. Smaller pores close off more rapidly than large cracks, channeling water into the macropores. Once all macropores are effectively sealed by clay swelling, capillary action takes over and water infiltrates the clay matrix itself. This understandably takes longer, as unsaturated hydraulic conductivities can be as low as 10^{-8} cm min^{-1} in Ca-saturated, confined Vertisols at 0.2 g g^{-1} water content (Kutílek, 1973). Infiltration is retarded by macropore closure, meteoric water ponds on the soil surface, particularly in the microlow microtopographic positions, and is shed off of the microhighs. Thus, a Vertisol formed within a given MAP zone tends to behave as a soil in either a lower or higher MAP zone, depending on microtopographic position. Relative comparisons between climosequence Vertisol pedons have greater power if they are done on similar microtopographic positions.

Seasonal moisture deficits have the most pronounced effect on the climosequence Vertisols, dictating the formation of authigenic mineral phases and morphological features (Dudal and Eswaran, 1988). Measurements of moisture deficits usually involve estimations of radiant heat influx (based on daylength and solar incidence) and generalized advective loss through foliar transpiration. The Thornthwaite annual Potential Evapotranspiration (P-E) index (Thornthwaite and Mather, 1955) is widely used for determining a baseline estimate of the seasonal soil-moisture status and is usually included

in the NRCS database entries for soil series. Long-term trends are more easily tracked within Thornthwaite indices than other estimators, because temperature and evapotranspiration (ET_p) are both functions of net radiation and as such are autocorrelated (Rosenberg et al., 1983). The P-E index is based on MAP minus estimated Et_p, calculated as:

$$ET_p = 1.6\left(\frac{l_t}{12}\right)\left(\frac{N}{30}\right)\left(\frac{10T_a}{I}\right)^{a1} \quad (3)$$

where l_t = actual day length (h), N = number of days in a month, T_a = mean monthly air temperature (C°), and a^1 is defined as:

$$a^1 = 6.75 \times 10^{-7} I^3 - 7.71 \times 10^{-5} I^2 + 1.79 \times 10^{-2} I + 0.49 \quad (4)$$

where I is a heat index derived from 12 monthly index values, i, obtained from:

$$i = \left(\frac{T_a}{5}\right)^{1.514} \quad (5)$$

Each location has a Thornthwaite index value based on local climatological data. Seasonal moisture deficits for each pedon are estimated by subtracting calculated ET_p from mean monthly precipitation (MMP; Table A1-3). Deficits are converted to positive value by subtracting the Thornthwaite index from zero, for ease of depiction. Figure 1-4 shows the annual deficit patterns for the climosequence series. Obviously the deficits increase in magnitude from northeastern to southern locations along the coast. This climatic index can be used with geochemical data to constrain Vertisol response to climatic forcing, and to provide additional climatologic insight in paleoenvironmental conditions expressed in paleo-Vertisol geochemistry.

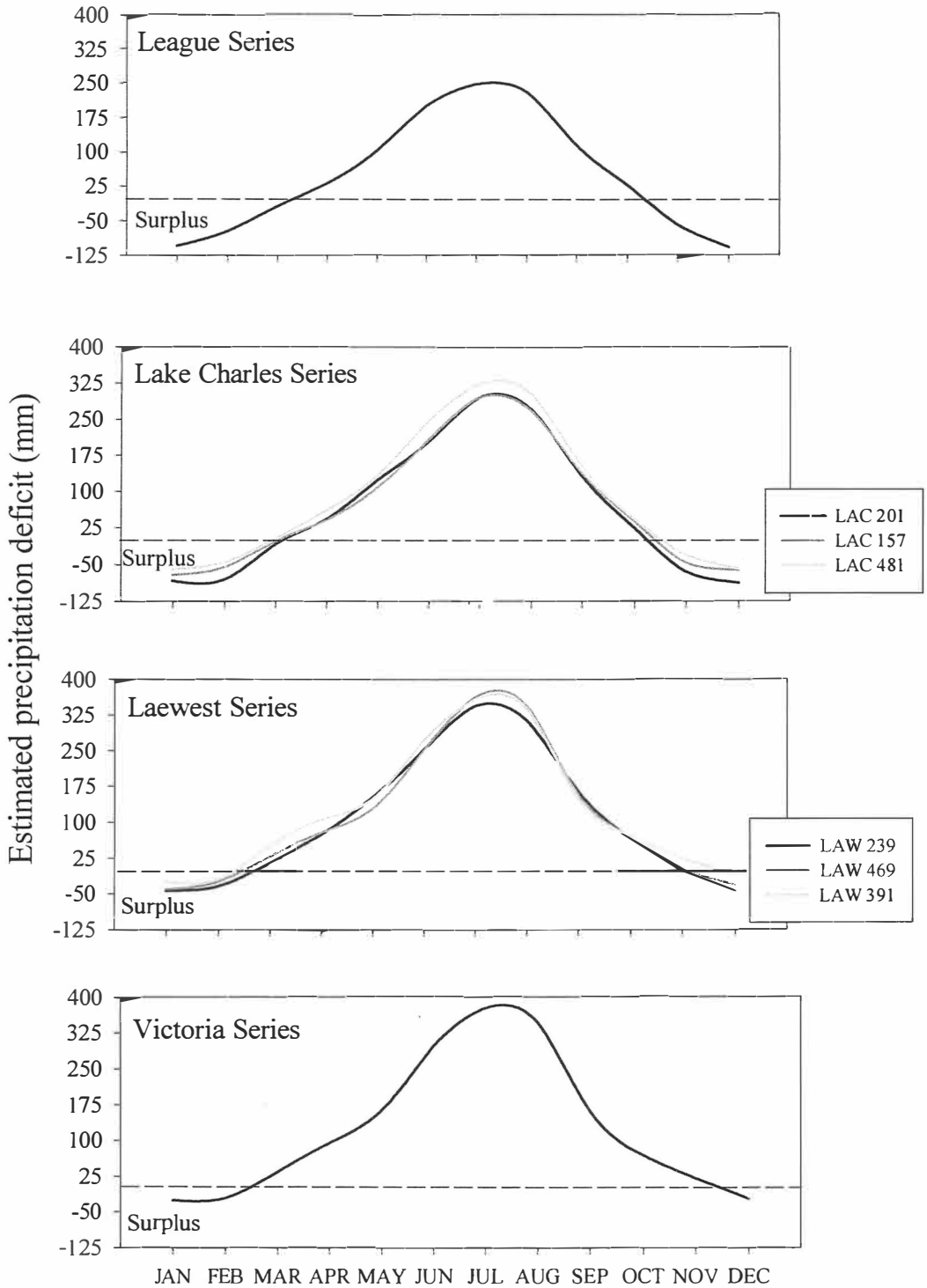

Figure 1-4. Monthly estimated soil moisture deficits for soil series and pedons, calculated as 0-[mean monthly precipitation - Thornthwaite evapotranspiration index (ET*p*)]. Deficits are depicted as positive values.

Another large-scale climatic consideration to incorporate into the discussion is the effect of glacio-eustatic sea-level changes over the past full-glacial/interglacial cycle. The pedons used in this study are all now within the influence of tropical maritime air masses originating from the Gulf of Mexico. But most Quaternary paleoenvironmental reconstructions suggest a sea level lowering of as much as 122 m during the greatest extent of Laurentide glacial advance (Fairbanks, 1989). This would cause the Gulf of Mexico coastline to recede nearly 80 km from present positions along most of the Texas coast. The influence of maritime air masses would thus be marginalized and a more continental type of climate would dominate the locations of the climosequence pedons during the full-glacial event (ca.18 - 20 ka). These air masses would be cooler and drier and would induce vegetation changes as well as affect pedogenesis, as was noted in isotopic vegetation/climate proxies (Miller, 2000). Also, late glacial pulses of meltwater into the Gulf of Mexico maintained the continental domination even as sea level was rising (Kennett and Shackleton, 1974; Fairbanks, 1989), such that the present-day climatic patterns were not established until well after meltback (Nordt et al., 1994).

Because the rainfall patterns are an important concept in determining the effect of climate on Vertisol pedogenesis, it is of interest to investigate these trends through modern proxy locations. Precipitation curves for one location, LAW 239, are shown in Figure 1-5. The proxy curves were derived from precipitation from two stations assigned by coastal displacement vectors: 1) the sea-level regression proxy location was determined from GCMs illustrated in COHMAP (1988) and assuming a 75 km displacement eastward

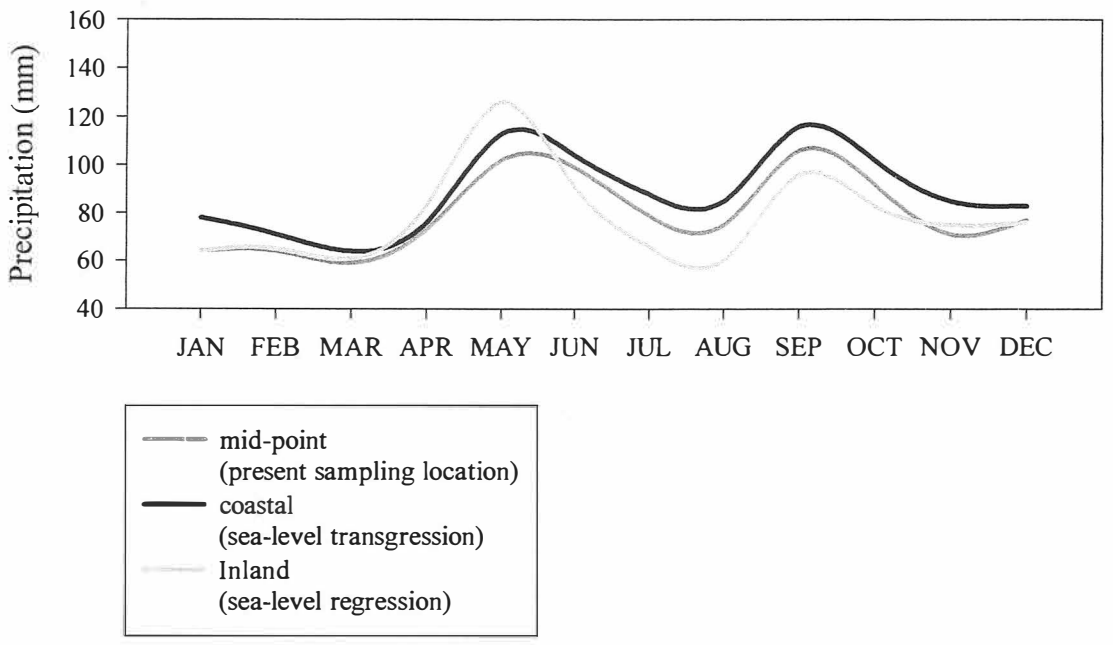

Figure 1-5. Monthly precipitation trends estimated for pedon LAW 239 (Jackson County, TX) based on data from proxy locations with respect to coastline proximity.

during the full-glacial; 2) the sea-level transgressive proxy location was the recording station closest to LAW 239 directly on the coastline. Differences in seasonal distribution is indicated but overall, the statistical differences in monthly rainfall amounts is not significant ($P < 0.65$). Thus, as soil-formation is an integrative process, it is assumed that the climosequence pedons will all contain a mutual signature of the sea-level regression, but it will not be significantly expressed in the gross morphology or inorganic geochemical trends. Drier conditions were induced by continental airmasses and induced dry-Vertisol type morphology and geochemistry during that earlier sea level regression, and evidence of these climate changes are preserved in some pedogenic features (i.e., pedogenic carbonate nodules; Miller, 2000). Although its usefulness may be limited in the paleo-Vertisol interpretations, this climate shift may provide some additional insight into finer-scale pedogenic geochemical shifts with depth.

1.4.4 Topography and Biota

Topography and floral/faunal communities exert some consideration in this study, although they are less influential than the other soil-forming factors already mentioned. The Beaumont Formation is a flat (0-1% slope) landform dissected by several steeply embanked rivers. None of the locations sampled in the study had more than 1% slope. Thus, in geomorphic terms, this is a cumulative landscape where sediment accumulation rates far exceed erosional removal (i.e., it is transport limited). This type of landscape promotes a soil system that has only minor geochemical denudation and dominantly closed-system, or diffusionally-controlled, dynamics (Stallard, 1995). This reinforces the

hypothesis that inherent properties of the Texas climosequence Vertisols are more directly controlled by climate, particularly meteoric inputs (i.e., precipitation and dust), rather than by other soil-forming factors.

The predominant physical processes affecting Vertisols tend to regulate biotic communities. Seasonal shrink-swell phenomena displace large volumes of soil along slickenside planes, hindering large root growth and permanent burrowing complexes. Seasonal moisture deficits requires biotic communities to be drought-tolerant (Dudal and Eswaran, 1988). Vertisol plant communities all along the Texas climosequence transect are dominated by grasses, deciduous forbs and shrubs with diffuse rooting patterns that often penetrate into the solum along slickensides planes. The microtopographic differences in water status creates vegetational micro-communities, with microhighs usually having more drought-tolerant forbs and microlows containing more grasses and deeper-rooted moisture preferring forbs (Mermut et al., 1996). This difference was noted throughout the climosequence and may be partially responsible for organic matter enrichment in microlow profiles, particularly in the mid-MAP Vertisols (Wilding et al., 1990).

Faunal communities in Vertisols are also affected by the physical processes which dominate pedogenic processes in these soils. In the wettest Texas climosequence Vertisols (MAP <1200 mm), crayfish (*Fallicambarus devastator*) krotovina (burrows) are particularly evident in the microlows. The influence of these vertically-oriented burrows,

typically 1.5 to 2.5 m in depth and 3-5 cm diameter, has not been well-documented in Vertisols, but it is obvious that they do impact the geochemical signature, bringing up reduced sediments from deeper in the profile and redistributing this material at the surface. Krotovina distribution ranged from 1-2 to >10 burrows m^{-2}, increasing with higher MAP. In moderate MAP areas, ants are the most prevalent agent of bioturbation, with fire ants (*Solenopsis invicta, Solenopsis germinata*) tending to build nests up to 0.5 m deep on the microhighs and transporting several dm^3 of material to the surface annually (Weber, 1966). Land snails (*Helix* spp.) are commonly found in the low MAP soil profiles, particularly in seasonal vertical cracks, but do not effectively disturb the solum.

1.5 Goals, Hypotheses, and Objectives

The principal goal of this study is primarily to develop a set of climate-sensitive geochemical parameters from the modern Vertisols climosequence that have the potential to be preserved in the geologic record and may be applicable to paleoclimatic studies of paleo-Vertisols such as those occurring in the Appalachian Foreland Basin. In this study, comparative systems for modern and paleo-Vertisols will involve only techniques that can translate faithfully between the two entities. Although pedological methods provide strong tools for understanding modern soil genesis, not all of these procedures can be used on lithified paleosols. The results of this dissertation is presented in three chapters summarized below:

Chapter 2 exams strain indicator elements to assess the validity of comparisons made

between Vertisols formed on alluvial sequences. This assessment must be made to: 1) determine a suitably consistent strain index element and 2) determine if discontinuities indicated by volumetric Zr contents represent a significant shift in parent material, or are expressions of pedogenic domains. This study examines both whole soil Ti and Zr geochemical data and separated rutile and zircon grain morphology from climosequence profiles, above and below identified discontinuities.

Chapter 3 presents construction of mass-balance relationship trends from whole-soil geochemistry and comparison with precipitation regimes. Depth functions, correlative relationships, and regression models are presented. Ten elements are assessed: Al, Ca, Fe, K, Mg, Mn, P, rubidium (Rb), Si, and Sr (strontium), each with some significant role and behavior in Vertisol pedogenesis. Assessment includes examination of geochemical losses and accumulations with depth, amplitude of those patterns, and variability between microtopographic positions. Determining if a meaningful depth-to-carbonate relationship can be derived from the climosequence Vertisols is a critical aspect of this portion of the study.

Chapter 4 presents an examination of Fe-Mn nodule geochemistry to determine if a proxy paleoprecipitation model can be derived from elemental composition. Nodules from modern climosequence Vertisols are used to define a correlative relationship from which a predictive equation can be derived. Paleoprecipitation estimates for the paelsols are made based on paleosol Fe-Mn nodule elemental content and the derived equation.

Paleoprecipitation estimates for the Pennington Formation upper paleosol, a relatively uneroded sequence (Caudill et al., 1996) are determined using both Fe-Mn nodule composition and depth to pedogenic carbonate curve from the modern setting. This comparison proves the applicability and validity of geochemical trend models derived from modern analog Vertisols to the paleo-Vertisol record.

Manuscripts derived from the chapters are in submission to or have been accepted by the following journals:

Chapter two: Evaluating Strain Indicators and Pedogenic Thresholds in Vertisols from the Upper Beaumont Formation, Gulf Coastal Plain, Texas - to be submitted to Geoderma.

Chapter three: Mass Balance Relationships in Vertisol Climosequence Profiles Derived from the Upper Beaumont Formation, Gulf Coastal Plain, Texas - to be submitted to Geoderma.

Chapter four: Pedogenic Iron-Manganese Nodules in Vertisols: A New Proxy for Paleoprecipitation? - accepted by Geology, to be published October, 2001.

Chapter 2

Evaluating Strain Indicators and Pedogenic Thresholds in Vertisols from the Upper Beaumont Formation, Gulf Coastal Plain, Texas

2.1 Abstract

Eight Vertisols pedons formed in a climosequence on the Upper Beaumont Formation of the Texas Gulf Coastal Plain show compositional differences (lithologic discontinuities) at 80-260 cm depth based on significant shifts in volumetric zirconium (Zr) content. Titanium (Ti) contents do not shift correlatively across discontinuities, suggesting that different processes dictate Ti and Zr content and distribution in these Vertisols. The depths of the discontinuities are not directly related to the mean annual precipitation (MAP) regime, but are a complex function of original sediment composition and physico-chemical processes. The discontinuities are considered to be functional boundaries (i.e., pedogenic thresholds) between open-system pedogenesis and more closed-system hydrogeochemical weathering. Zirconium contents are positively correlated to sand weight percent (r^2 = 0.65**), whereas Ti is not correlated to any particular size fraction. Scanning electron microscopy of individual very-fine sand-sized (vfs, 125 - 62.5 μm) zircon and rutile grains shows that zircons have been physically damaged by extensive transport, whereas rutile grains were hydrochemically weathered. Individual grains are slightly more weathered at shallow depths, but no statistical difference in overall grain morphology can be discerned across the discontinuity, suggesting uniform sedimentation processes. Significant morphological differences between grain populations from contrasting MAP regimes can be attributed to both sediment sources and weathering

intensity. Profile volume loss/gain (i.e., soil strain, ϵ), calculated assuming either Zr or Ti immobile, are correlative ($r^2 = 0.83$***), with ϵ_{Zr} nearly four times greater than ϵ_{Ti}. Within individual horizons, mean ϵ_{Zr} values are relatively extreme considering the comparable nature of clay-rich Vertisols and their parent alluvial sediment. This is due primarily to enrichment of volumetric Zr and sand contents above the functional boundary. Despite the hydrogeochemical stability of zircon, its physical mobility and association with sand incursions in Vertisols precludes its use as an immobile strain indicator in these soils. Titanium, despite evidence of primary mineral degradation, is conserved within weathering clay-rich profiles and is better-suited as a closed-system strain indicator in determining mobile elemental translocation.

2.2 Introduction

Soils record the environmental conditions in which they form as the result of physico-chemical alterations that are facilitated by pedogenic fluxes over time. Similarly, paleosols (i.e., fossil soils) contain geochemical signatures of their past formational environments. These signatures can be discerned by comparison with modern analog soils (Driese et al., 2000) using chemical mass-balance relationships (Brimhall et al., 1985; Brimhall and Dietrich, 1987; Brimhall et al., 1988, 1991a & b). Mass-balance calculations determine the open-system geochemical behavior of a mobile element (translocation, τ; Eq. 1) by assessing loss or gain of that element at a depth relative to parent material content. The translocation equation includes a term for closed-system volume loss/gain or strain (ϵ; Eq. 2). Strain is determined by using an "immobile" strain indicator element that behaves

conservatively within a weathering profile, usually titanium (Ti) or zirconium (Zr). The pertinent equations are:

$$\tau_{i,w} = [(\rho_w C_{i,w}/\rho_p C_{i,p})(\epsilon_{i,w} + 1)]\text{-}1 \quad (1)$$

$$\epsilon_{i,w} = (\rho_p C_{i,p}/\rho_w C_{i,w}) - 1 \quad (2)$$

where $\tau_{i,w}$ is the translocation index, ρ is bulk density in *p* (unweathered parent material) or *w* (weathered material), C is the concentration of element *i*, and $\epsilon_{i,w}$ is strain in terms of immobile element *i*.

Estimation of strain in weathered material is fairly straightforward in any system where initial parent composition is known (i.e., from relatively unweathered regolith). Mass-balance studies of chrono/climosequences derived from volcanic lava flows (Vitousek et al., 1997; Kurtz et al., 2000), marine terraces (Merrits et al., 1991), and loess-sequences (Langley-Turnbaugh and Bockheim, 1998; Mason and Jacobs, 1998) have satisfactorily demonstrated the relationship between the intensity of various soil-forming factors and translocation. Nieuenhuyse and van Breeman (1997) pointed out that these monolithic conditions are rarely satisfied, as most weathering surfaces are composed of complex and heterogeneous deposits that become welded and obscured through pedogenesis (*sensu* Ruhe and Olson, 1980). In heterogenous parent materials, Ti and Zr compositions may also be a tool to decipher lateral lithologic differences as well as weathering intensity (Sommer et al., 2000). Weathering of alluvium, where complex sedimentation patterns produces great spatial variability (Aslan and Autin, 1998), introduces additional problems, including resolving the parent material geochemistry and the most appropriate choice of

strain indicator. Many pre-Quaternary paleosols have been identified in fluvio-deltaic successions comprised of complex sediment accumulations, emphasizing the need for clarification of the behavior of "immobile" elements in modern analog profiles.

2.2.1 The "Immobile" Elements

The relatively insoluble nature of primary minerals that concentrate strain indicator elements, such as zircon ($ZrSiO_4$) and rutile/anatase (TiO_2; Marshall and Haseman, 1942; Jackson and Sherman, 1953), dictates their use as indicators of profile development. These minerals are, in theory, residually enriched relative to translocated elements released from soluble mineral phases in leached zones in the profiles, and depleted relative to secondary accumulation phases. However, "insoluble" is not synonymous with "immobile". In alluvial settings, resistant minerals have often gone through several periods of transport, reducing grain size and increasing their effective physical transportability from source rocks within drainage basins (Marshall, 1967), and their occurrence and abundance are typically less a function of weathering than of differential deposition. Brimhall et al. (1993) examined individual zircon grains from a lateritic residuum and found distinct morphological and geochemical populations arising from both detrital and exotic sources. Euhedral grains were derived from local gneiss, whereas rounded grains were derived from much older, downwind sources, possibly as far away as the Asian continent. Most transported grains were determined to be robust single crystals, possibly recycled through numerous weathering and transport cycles. Colin et al. (1993) found that zircons are highly mobile in the rooting zone of lateritic soils in coastal Gabon,

Africa. Here, as in Brimhall et al. (1993), two grain morphologies were identified from scanning electron microscopy (SEM) examination: euhedral (local source) and rounded, degraded (transported and reworked). Smeck and Wilding (1980) described similar morphologies in glacial deposits in Ohio and suggested that a careful preliminary micromorphological examination of zircons should be carried out prior to interpretations of profile polygenesis.

2.2.2 Defining Functional Boundaries in Deep Soil Profiles

The actual depth of pedogenic influence is a contentious issue (Richter and Markewitz, 1995) and has important implications for understanding pedogenesis using mass-balance relationships. The USDA-Natural Resource Conservation Service (NRCS) typically uses only the top meter of a soil as the control section for taxonomic purposes, limiting differentiation of soil types to processes that occur within the shallow, active portion of a weathering profile (Soil Survey Staff, 1998). Thus, a great deal of information exists about pedogenesis to this depth, but there tends to be a dearth of information about subjacent strata between the bottom of the control section and the unweathered bedrock (Cremeens et al., 1994). The influence of weathering and pedogenesis may be so great that the resulting soil mantle scarcely resembles the parent lithology (e.g. Vertisols derived from basalt; Eswaran and Bin, 1978). The textural composition and mineralogy of soils change as they age, even if they are derived from relatively uniform parent material. The term "lithologic discontinuity" is used by field pedologists to describe a distinct change in particle-size distribution, grain morphology, lithologic composition, and/or color, but no

firm criteria have been established, other than there is some obvious difference between super- and subjacent horizons (Soil Survey Staff, 1998). As more information becomes available about regolith and saprolite geochemical composition, it is not certain if this term describes an actual difference in lithology (i.e., mantled soils) rather than a difference in gross processes.

As rock weathers and loses volume, resistant mineral grains such as zircon remain behind and are witness to pedogenic processing. Compositional differences in Zr and Ti are often used to differentiate strata in soils, particularly in cumulative systems such as loess sequences (Ruhe, 1984). However, bulk contents of these elements can be confounded by penecontemporaneous weathering and accumulation. A lateritic bauxite (Jarrahdale, Western Australia) initially interpreted to contain a sedimentologic discontinuity was reinterpreted by Brimhall et al. (1991a), based on zircon grain morphology as a single biomechanical unit subdivided into two functional layers. The upper layer was dominated by bioturbation and downward translocation of authigenic and exotic materials, whereas low permeability in the lower layer limits invasive translocation. The transition zone (translocation crossover or "TCO"; Brimhall et al., 1991a) in these "old" soils (>1 Ma) occurs at around 3.5 m depth, predictably shallowing in younger soils. Thus, within the upper (superactive) zone, exotic additions and physical relocations of mineral grains are the rule rather than the exception. Any mineral carried onto, and eventually *into* a profile, will enrich the relative constituent geochemistry of that zone. The subactive zone, dominated by volume loss, closed-system geochemistry, and pronounced slowing of

mineral degradation, is still affected by pedogenesis, but is much less likely to experience gross alterations, retaining a geochemical signature relatively close to that of parent sediments. In this paper, the term "functional boundary" is used to denote compositional differences due to multiple processes in the weathering profiles. This allows for greater interpretive latitude with regards to the essential nature of this boundary, be it pedogenic or an actual sedimentologic difference.

In a transport limited system, such as the Texas Vertisol climosequence, where low relief limits erosion and chemical denudation, functional boundary depths are expected to be in equilibrium with long-term climatic influences (precipitation patterns) and matrix physical characteristics, primarily dictated by texture. Because strain indicator elements reside within detrital minerals in a soil column subject to physical and chemical processes, the assignment of immobile strain element must take into consideration the physico-chemical nature of the matrix. Because Zr is found almost exclusively in zircon, small additions of zircon to a clay-rich soil column can drastically change total Zr weight percentage (Brooks, 1969) and can significantly skew weight percentages of that element within depleted matrices. Titanium-bearing minerals, on the other hand, may experience chemical degradation and secondary mineral phase incorporation (for review, see Milnes and Fitzpatrick, 1989). Titanium is commonly found replacing iron (Fe) in hydrous Fe oxyhydroxide phases, particularly in finer-textured soils, leading to the "leucoxene"-weathering phase assemblage (Stage 13) described by Jackson and Sherman (1953). Thus, the choice of an "immobile" element in a weathering profile must be approached

with caution and consideration for the nature of the matrix and environmental setting.

2.2.3 Objectives and Applications to Paleo-Vertisols

Paleozoic age paleo-Vertisols found in the Appalachian foreland basin usually display a "stacked", polygenetic nature, where multiple generations of Vertisols have formed from fluvio-deltaic alluvial sequences (Mora and Driese, 1999). Mass-balance relations derived from geochemical data from the paleo-Vertisols have used Ti as the strain indicator element of choice, based on observations that this element tends to act most conservatively in the clay-texture profiles (Driese et al., 2000). Within the paleo-Vertisols, there is a suspicion that Zr may over-represent volume loss in Vertisol systems which are, in fact, fairly resistant to overburden compaction compared to non-pedogenic shales (Caudill et al., 1997). Using the Texas Vertisol climosequence as the modern analog for passive margin Paleozoic paleo-Vertisols, clarification of the behavior of Ti and Zr will contribute to better understanding and justification of comparative mass-balance trends.

With this in mind, the primary objectives of this study are to: 1) delineate Ti and Zr compositional differences with depth; 2) determine FB depths in the pedons, and 3) assess if the compositional and textural differences between the superactive, or upper, unit and subactive, or lower unit are due to the intensity of processes experienced by the soils or actual lithologic differences within profiles. Morphological surveys and statistical comparison of particle size and compositional trends are used to develop an interpretive

Vertisol pedogenesis model based on functional boundary characteristics and to augment considerations for choice of strain indicator for mass-balance relationships in fine-textured soils.

2.3 Materials and Methods

2.3.1 Geographic Setting and Sampling

The setting for this investigation was described in Chapter 1 (Fig.1-1). Samples for this investigation were recovered from large soil pits (2m wide, 3-5m long) excavated at each site, transecting microtopographic features peculiar to Vertisols (Lynn and Williams, 1992), herein referred to as microhighs and microlows. Bulk soil samples from microtopographic pairs were collected at 10 cm intervals from the surface to the base of each pit for geochemical analysis, and from each pedogenic horizon for bulk density measurement.

2.3.2 Analytical Methods

Whole soil samples were oven-dried at 60°C, ground in a shatterbox, and pelleted for bulk geochemical analysis using X-ray fluorescence (EG&G ORTEC TEFA III, Singer and Janitsky, 1986; data in Table A2-1). Precision for TiO_2 and Zr is 0.01 wt % and 23 ppm, respectively. Bulk density was determined by the paraffin-coated air-dried clod method (Blake and Hartge, 1986). Because significant carbonate content can lower the composite sample weight, elemental weight percentages were corrected for carbonate content dilution prior to mass-balance calculations (modified from Soil Survey Staff, 1995).

Carbonate correction factors (CCF; Table A2-2) were determined by the following stepwise calculation:

1) Background CaO wt % was determined in microlow positions as an average of CaO wt % in intervals within the depth of effective leaching. This value was then subtracted from CaO wt % for each depth interval of all profiles. Any difference <0 was assumed to have a CCF of 1.00.

2) CaO wt % was converted to Ca wt % by multiplying by 0.71, and if the depth interval contained any sulfur (S), S wt % was subtracted from Ca wt % to account for gypsum. The Ca wt % difference was converted to carbonate equivalent wt % by multiplying by 1.50.

3) The final CCF is determined as (100% + carbonate wt %)/100%. All elements are then multiplied by CCF for the corrected elemental values (Table A2-3). Multiplying the wt % by bulk density (Table A2-4) allows for direct volumetric comparisons as the first step in strain calculation (Table A2-5). Particle size analysis was carried out at the National Soil Survey Laboratory in Lincoln, Nebraska, using the pipet method (Gee and Bauder, 1986; Table A2-6). NRCS data for these soils are available to the public at the National Soils Laboratory website at www.iastate.statlab/soils under the NRCS field pedon code listed with each profile in Table A1-1. Thin sections were prepared from oriented clods using resin impregnation and described using terminology of Brewer (1964) and Bullock et al. (1985).

Heavy mineral grains were separated from very fine sand fractions (125 - 62.5 μm) above

and below the functional boundary in all microlow profiles using sodium metatungstate (SOMETU-USA, Sherman Oaks, CA). Zircon and rutile grains were initially separated from heavy mineral populations using relative relief under the binocular scope, and then from each other using difference in refractive index (zircon: 1.92-1.96, rutile: 2.61; Refractive Index Oil at 2.11, Cargille, Inc., West Chester, PA). At least twenty-five grains from each sample were mounted and examined using a Hitachi S-3500 N scanning electron microscope to produce digital images of each grain. Digital images were then visually surveyed for various surface features, as described by Darmody (1985) and Tejan-Kella *et al*. (1991).

2.4 Results

2.4.1 Bulk Geochemical Analysis

2.4.1.1 Boundary Delineation

Initial bulk geochemical analyses revealed notable changes in the relative volumetric composition of Ti and Zr (shown as the Ti:Zr ratio in Fig. 2-1) at depth. Trends in Microlow profiles (Fig. 2-1) show inflections in the ratios at depths between 160 - 260 cm depth, with minor inflections in some profiles at 80-100 cm, which appear to represent FB. The depths of inflection cannot be strictly ascribed to climate, as the shallowest inflections occur within soils formed in the intermediate precipitation range (1000-1200 mm MAP) of the climosequence. Above the boundary, Ti:Zr ratios are predominantly invariant with depth and ratios have no clear relationship with MAP. Tukey's *w* procedure using Studentized range and pairwise comparisons of the Ti:Zr values was used to statistically

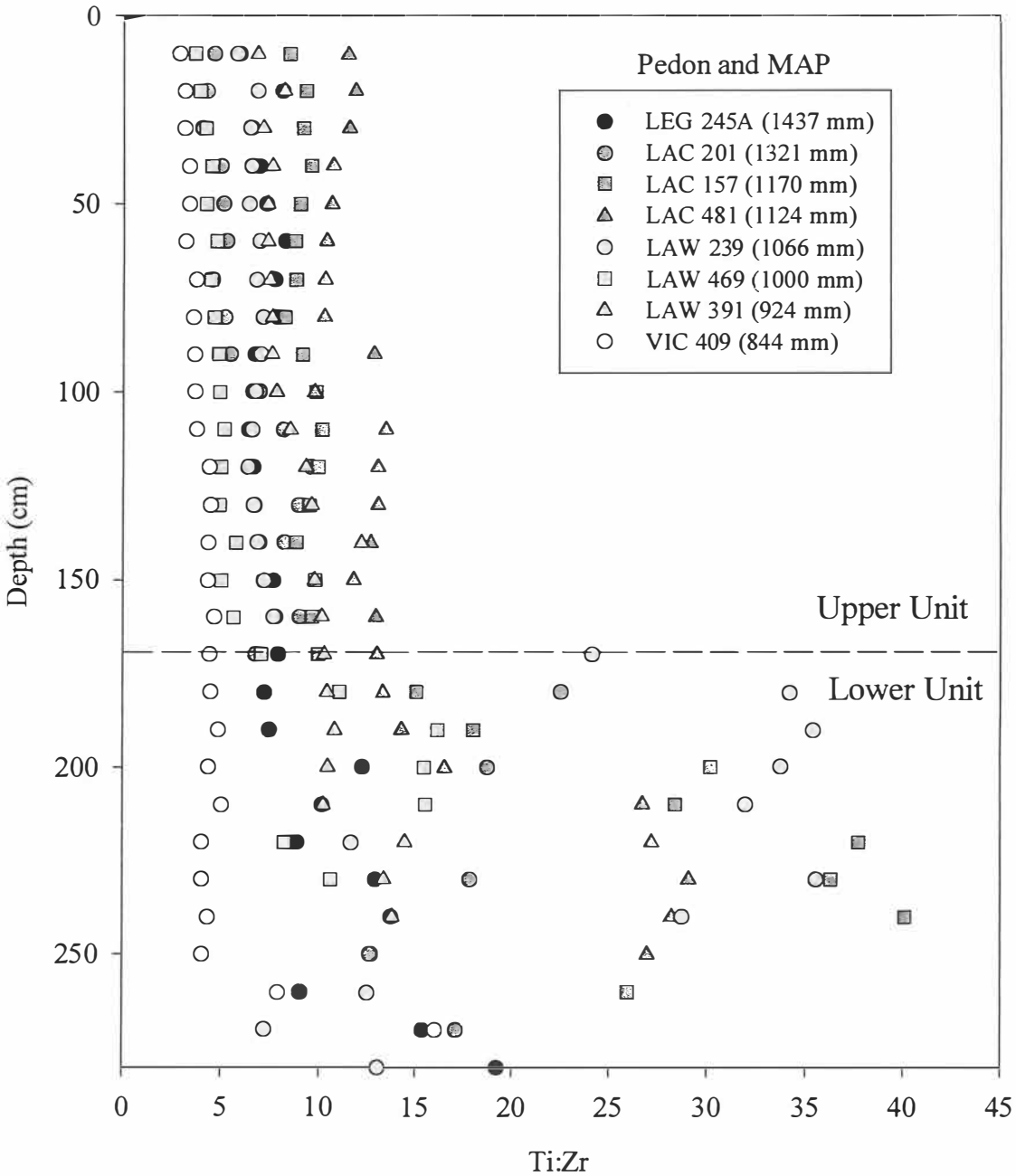

Figure 2-1. Identification of the functional boundary depth in microlow pedons indicated by shifts in Ti:Zr. Series abbreviations: League = LEG, Lake Charles = LAC, Laewest = LAW, and Victoria = VIC.

determine the functional boundary depth between the upper and lower units (Table 2-1 and Table A2-6). Mean volumetric contents of the two elements show that Ti contents do not vary greatly between upper and lower units (-4.7 to -31.6%), confirmed by the mean separation and least significant difference (LSD) values shown in Table 2-1. Only the wettest Laewest profile (LAW 239) showed significance at $P \leq 0.025$, possibly due to proximity to the Colorado River terrace sequences and susceptibility to fresh parent material accumulations. However, Zr differences vary from -75.5 to -239.3% between the upper and lower units and are all statistically significant at $P < 0.001$ (Table 2-1). This pervasive difference could be caused either by: 1) a regional sedimentological discontinuity, or 2) differences in pedogenic regime, whereby the upper portion of the profile is more intensely influenced by open-system physico-chemical dynamics, and the lower portion is more influenced by closed-system hydrogeochemical fluxes, similar to the model presented in Brimhall et al. (1991a).

2.4.1.2 Ratio Trends

Ratio-element trends for Ti and Zr (Fig. 2-2) show that Zr is the more influential element within the pairing. Titanium (Fig. 2-2, A-D) is relatively insensitive to increases in the Ti:Zr ratio, even across the functional boundary, although pedon differences in overall elemental content have discrete groupings, particularly in the Laewest series. Systematic increases in Zr with increasing Zr:Ti in all series (Fig. 2-2, E-H) indicate that the behavior of Zr largely determines variability. Volumetric Zr content in the lower unit is less than that of the upper unit.

Table 2-1. Climosequence functional boundary depths, Ti/Zr volumetric contents, percent differences, and statistical information for the upper and lower units in microlow profiles.

Element	Property	Pedon							
		LEG 245A	LAC 201	LAC 157	LAC 481	LAW 239	LAW 469	LAW 391	VIC 409
	FB[a] depth (cm)	200	190	170	200[b]	160	170	220	260
Ti	UU[c] composition (mg cm^{-3})	10.47 (0.21)[d]	9.04 (0.31)	9.48 (0.21)	9.55 (0.21)	9.37 (0.11)	7.87 (0.17)	7.22 (0.10)	6.13 (0.14)
	LU composition (mg cm^{-3})	9.60 (0.78)	8.39 (0.44)	8.49 (0.37)	7.86 (0.21)	7.12 (0.27)	7.52 (0.39)	6.56 (0.07)	5.48 (0.26)
	% Difference	-9.1	-7.7	-11.7	-21.5	-31.6	-4.7	-9.9	-12.0
	Mean separation	0.88 (2.55)[e]	0.65 (2.44)	0.99 (2.29)	1.69 (2.10)	2.25 (1.62)	0.35 (2.12)	0.65 (1.74)	0.65 (1.36)
	Significance	ns[f]	ns	ns	ns	**	ns	ns	ns
Zr	UU composition (mg cm^{-3})	1.45 (0.05)	1.46 (0.19)	0.99 (0.06)	0.79 (0.05)	1.38 (0.05)	1.63 (0.098)	0.83 (0.05)	1.59 (0.13)
	LU composition (mg cm^{-3})	0.74 (0.14)	0.45 (0.09)	0.26 (0.06)	0.26 (0.01)	0.34 (0.14)	0.55 (0.10)	0.47 (0.02)	0.51 (0.32)
	% Difference	-82.7	-220.1	-239.3	-179.4	-254.9	-167.3	-75.5	-210.7
	Mean separation	0.66 (0.32)	1.03 (0.37)	0.70 (0.15)	0.51 (0.15)	1.00 (0.20)	1.03 (0.30)	0.36 (0.23)	1.08 (0.44)
	Significance	***	***	***	***	***	***	***	***

[a] Functional boundary
[b] Irregular FB depth at 100 cm
[c] UU = upper unit, LU = lower unit
[d] Parenthetical value in compositional field is the 95% confidence interval for the individual profile data set
[e] Parenthetical value in mean separation field is the 95% least significant difference for the individual profile data set
[f] ns = not significant, * significant at $P \geq 95\%$, ** significant at $P \geq 97.5\%$, *** significant at $P \geq 99\%$

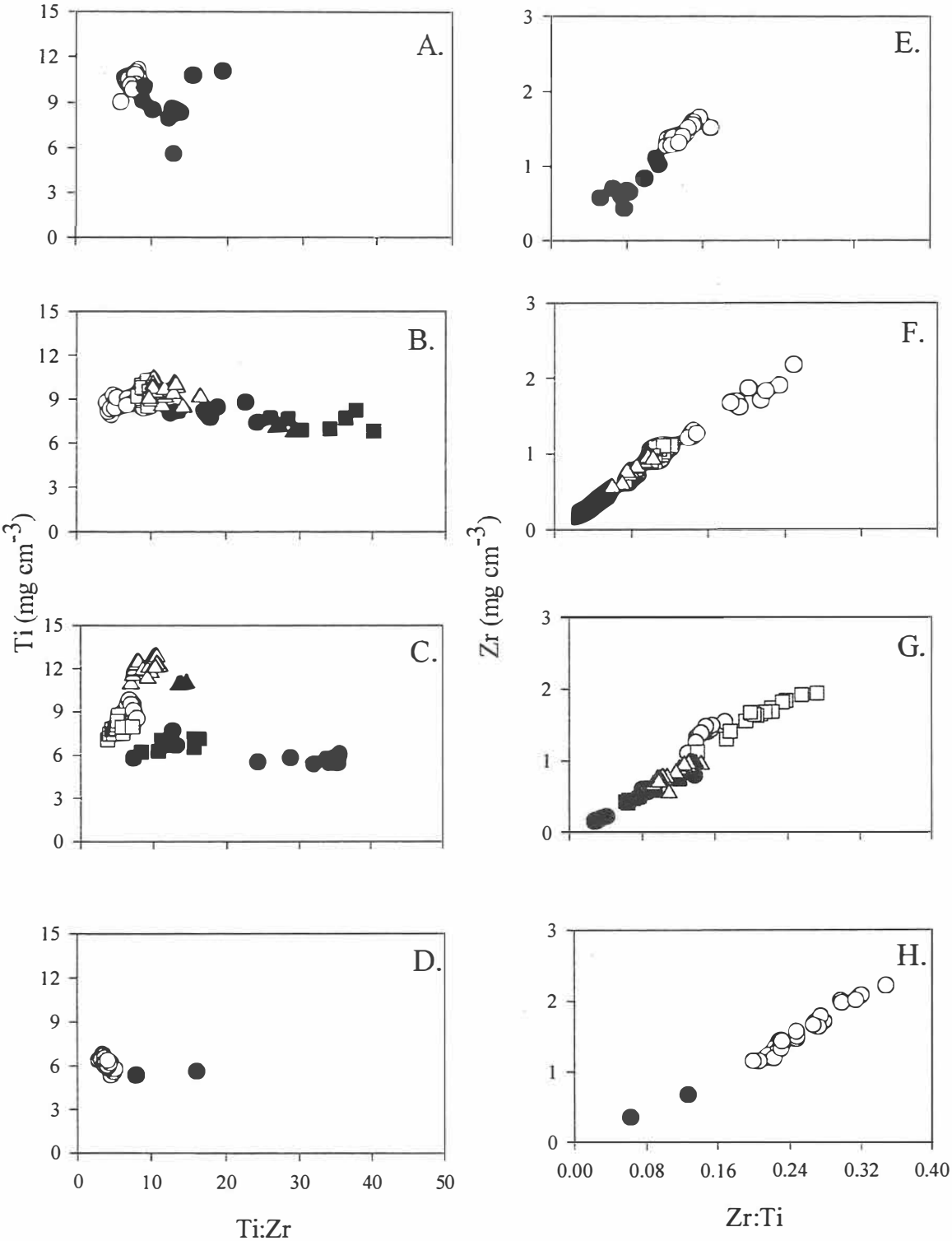

Figure 2-2. Element (volumetric content) to ratio comparisons of Ti and Zr from different soil series. League (A&E), Lake Charles (B&F), Laewest (C&G), and Victoria (D & H). Light symbols represent upper unit values, dark symbols represent lower unit values, different symbols represent pedons within each series.

Differences in Ti and Zr contents are noted between as well as within profiles (Table 2-1, Tables A2-7&8). These differences are most likely due to slightly varying sediment sources in the individual river basins which transect the climosequence. Differences in heavy mineral compositions of Texas Gulf Coast river sediments are actually diverse enough to have been used in Gulf of Mexico sand provenance studies (*sensu* Van Andel and Poole, 1960). Table 2-2 lists rivers in the vicinity of sampling sites, upstream source lithology in respective drainage basins, and a relative of the Ti:Zr ratio above and below the functional boundary. Pedons in the transitional semi-arid precipitation zone (MAP 1000-1100 mm) have relative Ti:Zr ratios that are always lower in pedogenic units above the functional boundary than units below it (Table 2-2). These pedons are more likely to have experienced episodic aeolian accumulations during drought periods. Pedons in drier areas (LAW 391 and VIC 409) have experienced continuous dust inputs and lower weathering rates, and thus show attenuated variations in Zr with depth. Pedons in the wetter regimes (League and Lake Charles profiles) have weathering rates that exceed the rate of aeolian influx and will show similar attenuated variation in Zr content.

2.4.2 Particle Size Distribution and Component Comparisons

The sand component of these fine-textured soils is an important contributor to the observed functional trends. Climosequence Vertisol pedons are fine-textured, with clay contents of 35.8 - 72.6 weight % (Fig. 2-3). Sand contents are highest in the Victoria and drier Laewest pedons. In the profiles, soil textures tend to coarsen upward and are significantly finer below the functional boundary (Fig. 2-3, filled symbols).

Table 2-2. Pedon alluvium source lithologies and relative Ti:Zr in upper and lower units.

River	Pedons influenced	Source lithology	Relative Ti:Zr in soils	
			UU[a]	LU
Neches	LEG 245A	Paleogene marine sedimentary	Medium	Medium
Trinity	LAC 201	Paleogene marine / Neogene continental sedimentary	Medium	Medium
Brazos	LAC 157, 481	Cretaceous / Paleogene marine sedimentary	High	High
Colorado	LAW 239	Paleogene / Ordovician marine sedimentary Precambrian metavolcanics	Medium	High
Guadalupe	LAW 469	Cretaceous / Paleogene marine sedimentary	Low	Medium
Aransas	LAW 391	Cretaceous / Paleogene / Neogene marine sedimentary	Medium	Medium
Nueches	VIC 409	Cretaceous / Paleogene marine sedimentary Paleogene volcanics	Very Low	Very Low

[a] UU = upper unit, LU = lower unit

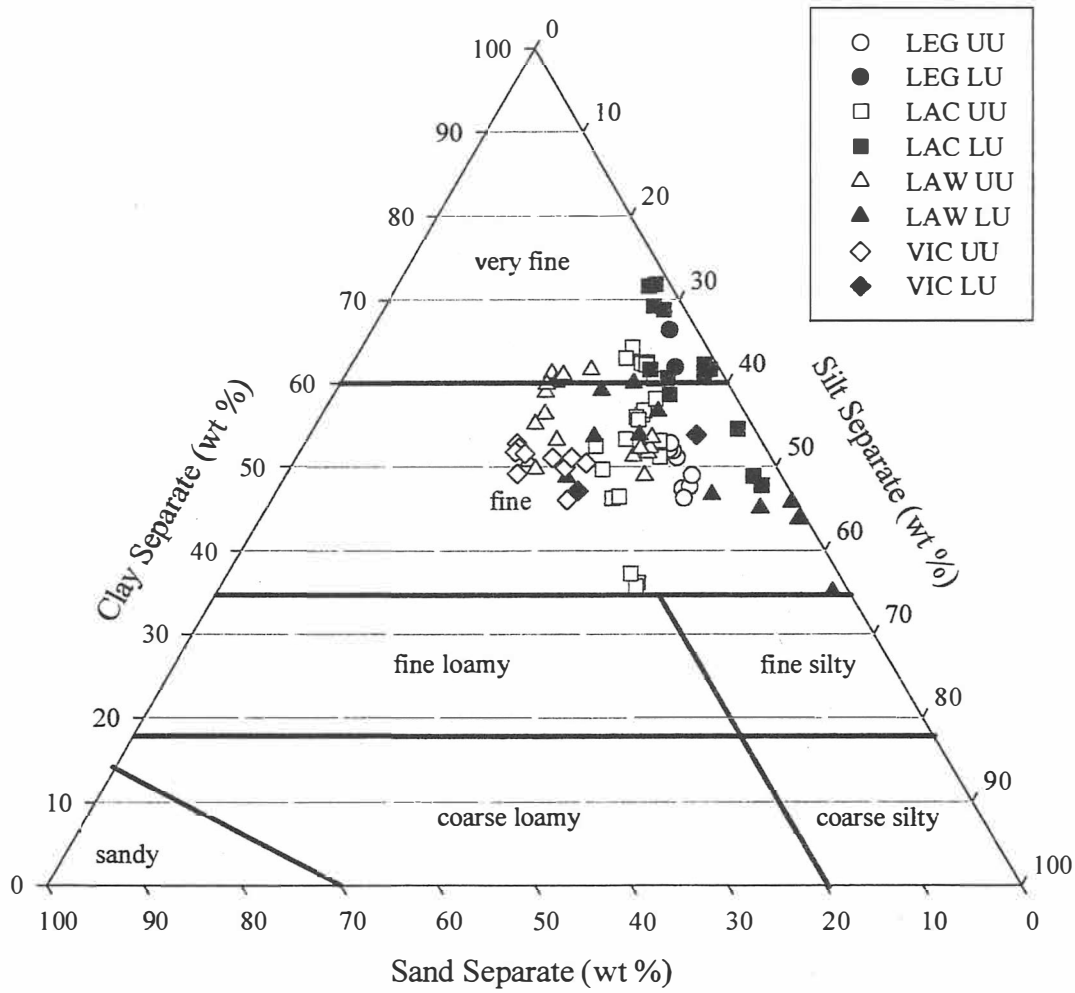

Figure 2-3. Particle size distribution and textural classification of climosequence microlow pedon horizons. Open symbols represent textures prevalent above the functional boundary, closed symbols represent textures below the functional boundary. Soil series abbreviations are defined in Fig. 2-1.

Micromorphologic differences across the boundary are pronounced between the upper and lower units (Fig. 2-4). Quartz sand grains above the boundary in both pedons have similar morphology and abundance (Fig. 2-4, A & C). Similarly, there are significantly fewer large grains in lower units of both pedons (Fig. 2-4, B & D).

Volumetric Zr contents are plotted against sand content in Fig. 2-5, and show significant correlation in all profiles. Regression analysis of series show positively correlated relationships with r^2 values from 0.56 - 0.82 ($P < 0.001$). The slopes of series regressions are steepest at the MAP extremes (i.e. League and Victoria series), indicating a significant increase of Zr, most likely present in zircon, with little additional sand. Thus, the primary compositions of sand fractions in the Lake Charles and Laewest series may be more silica-rich than sands found within League and Victoria, indicating some inter-series sediment source variability within the Texas climosequence.

When Ti is plotted against sand content in the microlow pedons, undifferentiated by series (Fig. 2-6), although there is a weakly negative correlation. The correlation coefficient ($r^2 = 0.18$, $P < 0.001$) is not significant in this regression. The overall regression of Zr with sand, however, has a significant correlation of $r^2 = 0.65$ ($P = 0.023$), with the relationship defined by the following regression equation: volumetric Zr content = 0.3468 + 0.0560 sand separate wt %. This suggests that there is a minor Zr component (0.3468 mg cm^{-3}) in the fine-earth components (silt and clay) and that approximately 0.11 wt% of the sand component is zircon. As most sand occurs in the upper portion of the profile, this

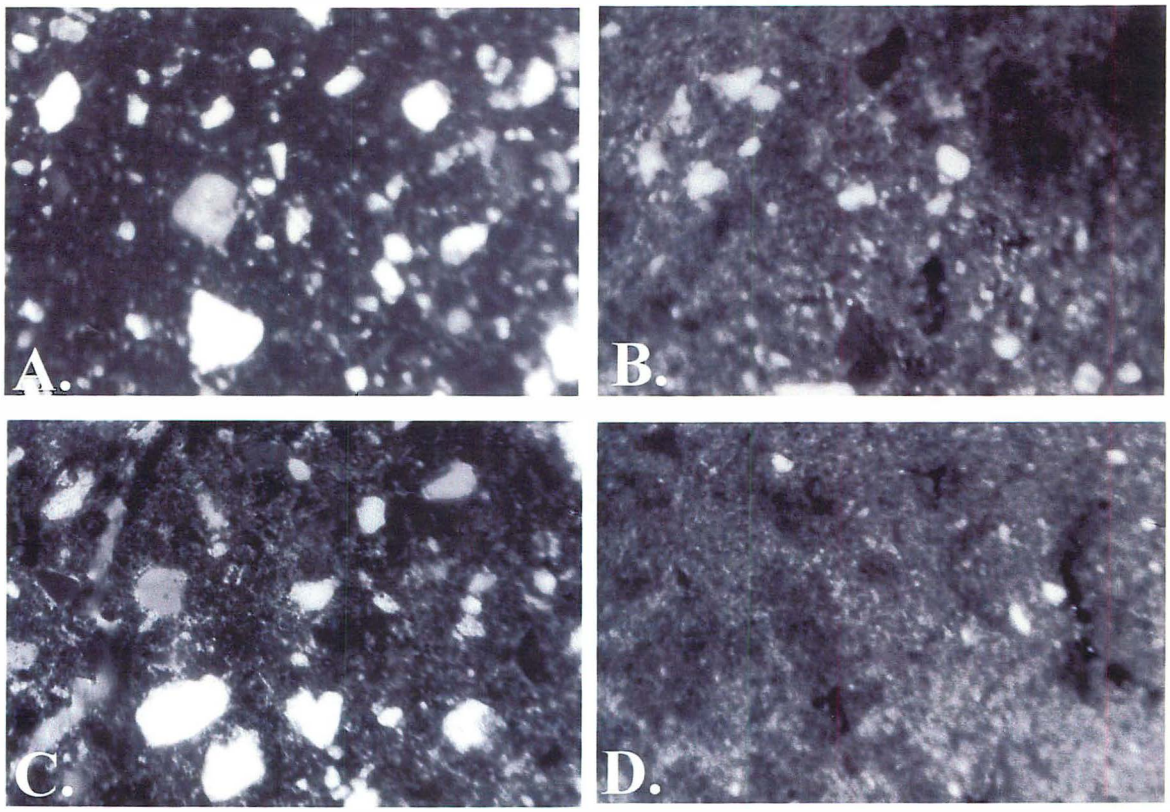

Figure 2-4. Photomicrographs of textural contrasts across the functional boundaries in two pedons. A: Lake Charles 201 Bss2 (43-72 cm depth); B: Lake Charles 201 B′ss3 (245-265 cm depth); C: Laewest 469 Bss3 (74-118 cm depth); D: Laewest 469 B′kss2 (252-275 cm depth). All views 100x, cross-polarized light.

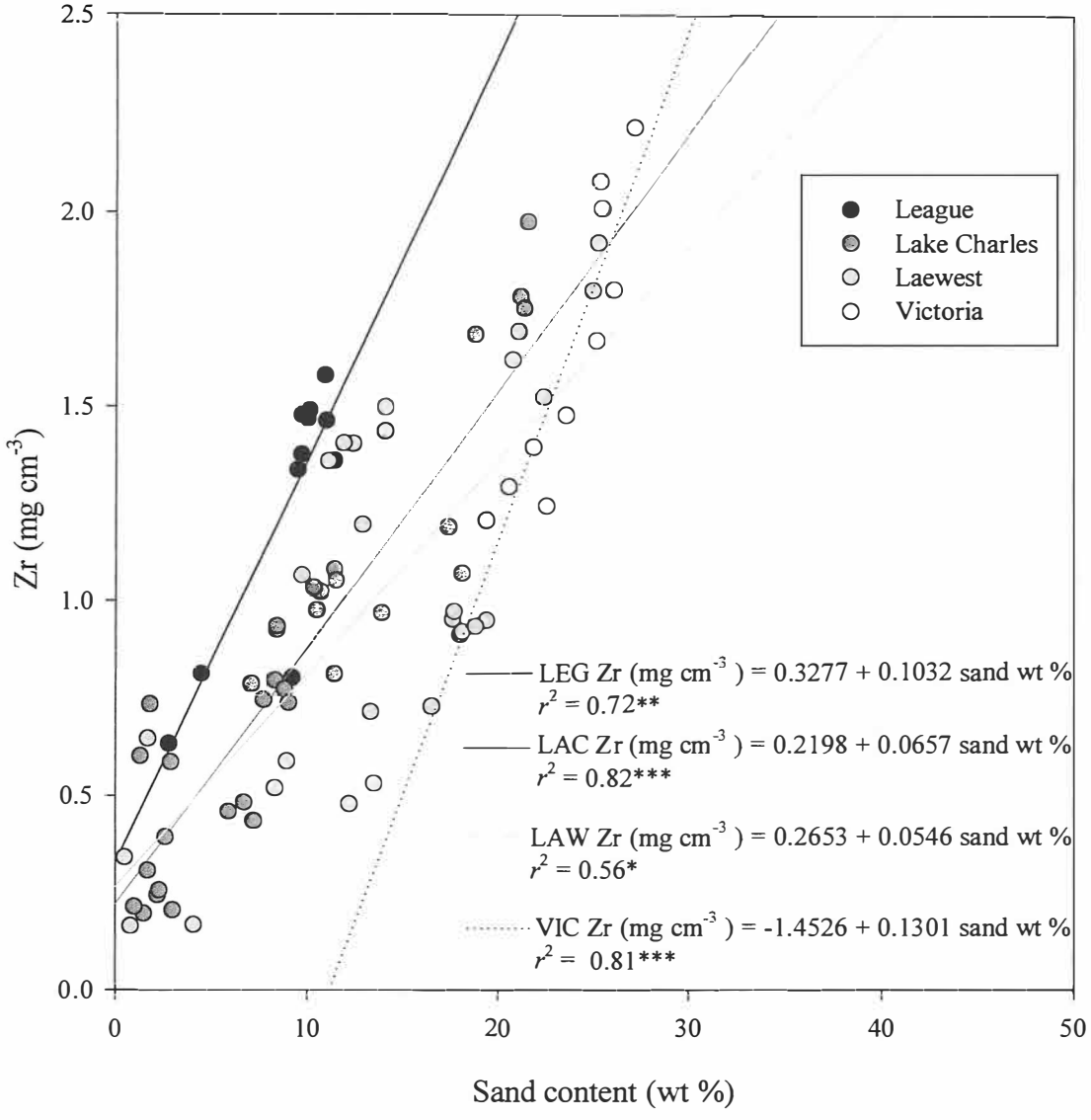

Figure 2-5. Separated regression analyses of sand content versus volumetric Zr content by soil series. Significance designated as: * $P \geq 95\%$, ** $P \geq 97.5\%$, and *** $P \geq 99\%$.

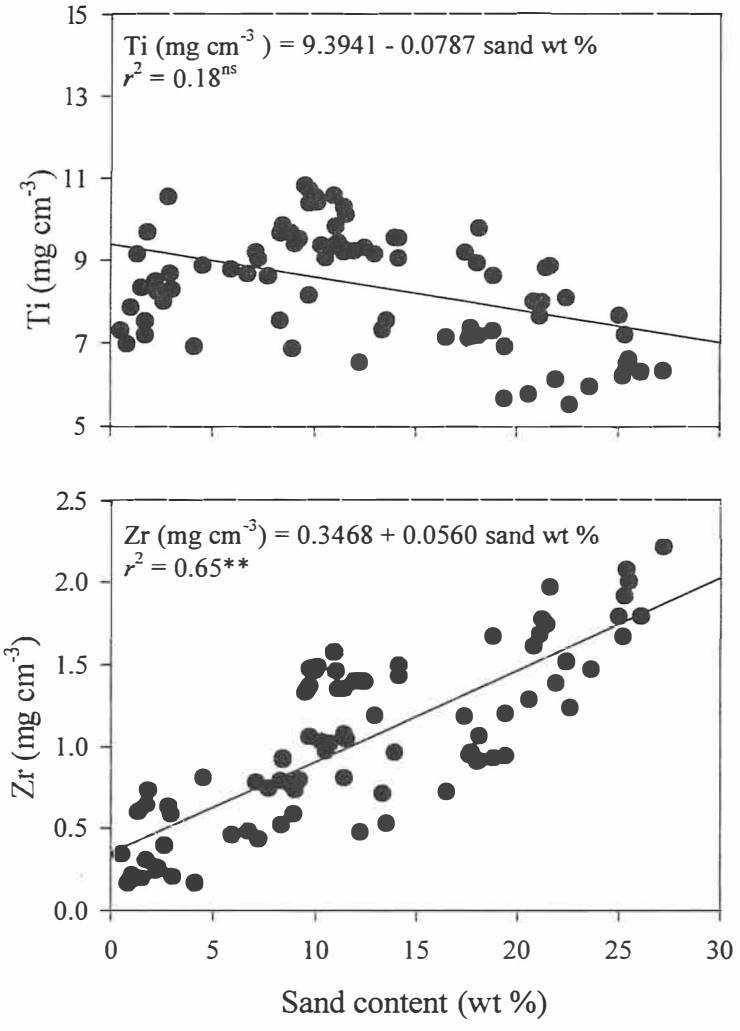

Figure 2-6. Linear regression relationship between sand content and volumetric Ti and Zr content in microlow pedons, undifferentiated by series. Significance designated as: ns = not significant and ** $P \geq 97.5\%$.

strongly suggests that sand-sized zircon is significant in the upper portion of the weathering profiles in the climosequence. The weak, but negative, correlation between Ti content and sand indicates that Ti does not commonly occur in the sand-sized fraction, or may have been preferentially removed. The high value of the y-intercept coefficient in the Ti regression equation relative to mean profile Ti compositions (9.3941 compared to 5.4759-10.4727 mg cm^{-3}; Table 2-1) indicates that most of the Ti occurs in finer texture components.

2.4.3 Qualitative Analysis of Surface Microfeatures

Surface features of rutile and zircon grains were assessed by SEM. The features were categorized as either being influenced by: 1) physical processing suggestive of transport, or 2) weathering / hydrogeochemical degradation (Table 2-3, Table A2-9). Rutiles showed more evidence of hydrogeochemical alteration (82-98% in the upper unit, 58 - 95% in the lower unit; Fig.2-7: B, F; Table 2-4) and zircons were physically damaged by transport reworking (58 - 83% in the upper unit, 57 - 73% in the lower unit; Figure 2-7:A,C; Table 2-4). Grain-frosting and rounding, which attest to long-term aeolian transport, are evident in the driest profiles (Victoria and dry Laewest series, Fig. 2-7: C, D), again particularly in the upper unit, although differences in transport features are not as great as those suggesting hydrogeochemical weathering (Fig. 2-7: B, F). The presence of occasional euhedral zircons in the upper unit of non-volcanic source basin pedons, such as in Lake Charles 481 (Fig. 2-7:E), strongly suggests external additions from volcanigenic lithologies to the south-southwest (Table 2-2).

Table 2-3. Surface feature characteristics assessed in SEM survey of individual very fine sand-sized rutile and zircon grains.

Hydrogeochemical alteration	Physical transport and reworking
Dissolution and chemical edge attrition	Conchoidal fracture/breakage blocks/ v-shaped pits (percussion marks)
Surface roughness or scaling	Hairline cracks
Oriented or random etch pits	Rounded grains, subdued edges, and frosting

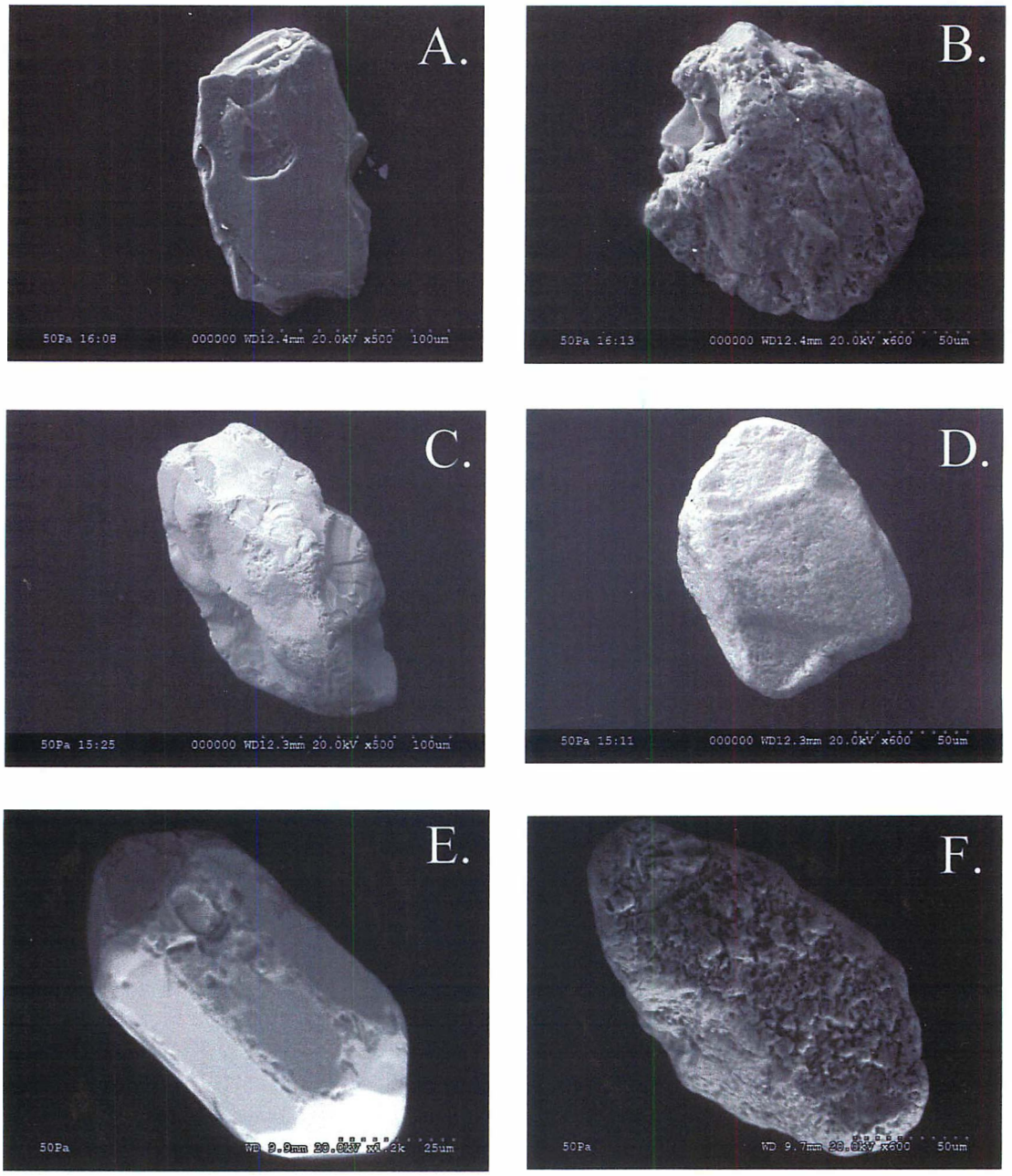

Figure 2-7. Photomicrographs of characteristic very fine sand-sized rutile and zircon grains. A: zircon, League 230 cm depth; B: rutile, League 230 cm depth; C: zircon Victoria 30 cm depth; D: rutile, Victoria 30 cm depth; E: zircon, Lake Charles 481 30 cm depth; F: rutile, Lake Charles 481 30 cm depth. Scale shown in lower right hand corner of each frame.

Statistical analyses and mean separation categorization for differences in percent of grains having a particular morphology between upper and lower units (Tables 2-4 and A2-10) and between laterally "adjacent" pedons (Tables 2-5 and A2-11) allows for three-dimensional interpretive comparisons across the climosequence. Alphabetical Duncan's least significant difference (LSD) categories were set at $P < 0.001$ for maximum comparative power and letters indicate differences between vertical units or adjacent pedons were higher than the 99% variance allowance, and therefore can be considered to be separate pedofunctional groups. The Student's *t*-test probabilities indicate that overall differences between the upper unit and lower unit for both minerals and functional categories were not significant (Table 2-4), although the separations by category (i.e., hydrochemical or physical) and overall means of morphological expression suggest that more hydrogeochemical alteration occurs in the upper unit of each profile, particularly in profiles from wet settings (League and Lake Charles series). Differences in the grain morphology expressed laterally (i.e., across pedons) in the upper unit (Table 2-5) are more complicated than variations noted within the pedons themselves, reflecting the influence of parent material depositional history, in addition to pedogenic effects. However, the number of significant separation categories suggest that processes expressed by both rutile and zircon have fundamental differences. Rutile grains have four divisions resulting from hydrogeochemical alteration that correspond well with MAP regime (a:>1300 mm, b:1300-1000 mm, c:1000-900 mm, d: <900 mm). Zircons also show this trend, but the divisions are at relatively shallower depth, attributed to their higher weathering resistance. Lateral (between pedon) morphological differences related to physical transport in both

Table 2-4. Least significant difference profile groupings based on SEM survey characteristics differences between the upper and lower units.

	Hydrogeochemical		Physical transport	
Pedon	Rutiles	Zircons	Rutiles	Zircons
LEG 245A	a[a]	a	a	a
LAC 201	a	a	b	b
LAC 481	a	b	b	c
LAW 469	a	b	b	c
LAW 391	a	b	b	c
VIC 409	b	b	c	d
Overall means (% - UU[b] / LU)	91.4 / 84.7	22.3 / 17.8	52.9 / 52.1	70.5 / 65.4
Student's *t* probability	0.78 ns[c]	0.31 ns	0.30 ns	0.41 ns

[a] Letters designate statistically separate categories at $P \leq 0.001$ determined by Duncan's lsd

[b] UU = Upper unit, LU = Lower unit

[c] Difference not significant, with larger probability indicating greater similarity between overall unit means

Table 2-5. Least significant difference profile groupings based on SEM survey characteristic contrasts between upper units of adjacent pedons.

	Hydrogeochemical		Physical transport	
Pedon	Rutiles	Zircons	Rutiles	Zircons
LEG 245A	a[a]	a	a	a
LAC 201	a	b	b	ab
LAC 481	b	b	c	b
LAW 469	b	b	cd	c
LAW 391	c	c	d	d
VIC 409	d	d	e	e

[a] Letters designate statistically separate categories at $P \leq 0.001$ determined by Duncan's lsd

rutile and zircon fall into similar statistical categories, which may reflect lateral contiguity of parent sediment deposition. Both rutiles and zircons have one category overlap occurrence that does not match with the other, LAW 469 and LAC 201, respectively. Both of these locations are in MAP "boundary" settings, LAW 469 at 1000 mm MAP and LAC at 1321 mm MAP, which may account for their marginal behavior and dual classifications.

2.5 Discussion

What is causing the pronounced shifts in Ti and Zr content with depth? There is an obvious difference in morphological and micromorphological characteristics between the material occurring above and below the functional boundary. Does this difference indicate a lithologic discontinuity, a regional scale depositional event prior to pedogenesis of the upper unit, or does the functional boundary indicate a change in physicochemical pedogenic inputs? Zirconium content alone seems to be dictating shifts in the Ti:Zr ratio in all profiles and the SEM survey demonstrates contrasting pedogenic influences on rutile and zircon. Yet there is no statistically significant difference between features from the upper and lower units, which counter-indicates a depositional sequence variation. As the Gulf of Mexico Basin subsides under increasing sediment load, the marginal fluvio-deltaic deposits which comprise the Texas Gulf Coast may be depositing coarser material over the finer-textured (clayey) deposits within a complex glacio-eustatic retrogradational sequence. However, thicknesses of the upper unit in the Vertisol profiles (1.6 - 2.6m), the relatively advanced morphological maturity, and temporal limitations make a major

depositional change an unlikely scenario in this relatively low-energy depositional setting.

2.5.1 Discerning Pedogenic Processes

The climosequence Vertisols are exposed to different levels of physical and geochemical pedogenic processes and the Functional boundary acts as an indicator of relative influence and intensities of these processes. The upper and lower units are essentially parts of a whole, with the upper unit acting as an open-system, superactive domain, where pedogenesis is dominated by external inputs. The lower unit also responds to external influences, but in an attenuated fashion, moderated by microporosity and groundwater dynamics. Vertisols are remarkable for their expressions of physical processing, with characteristic slickensides and microtopographic differentiation generated and maintained by seasonal shrink-swell mechanisms (Lynn and Williams, 1992). Seasonal cracking, which occurs more frequently within microlows, tends to obliterate depth trends down to the depth of cracking (Wilding et al., 1990), creating a solum responsive to meteoric inputs. Microhighs tend to act not only as foci for upward physical material transport, but also as evaporative conduits for soluble phases (Newman, 1986). Although depth trends in the Ti:Zr ratio in the microhigh profiles shows greater variability and shallower inflections than corresponding microlows (compare Fig. 2-8 and Fig. 2-1), there is roughly parallel behavior along the climosequence in that pedons in MAP extremes have the deepest functional boundaries, while the shallowest functional boundaries are in moderate MAP pedons. The relatively higher relief of microhighs allows them to physically "shed" materials into the bowl-like depressions of the microlow, reaching maximum expression in

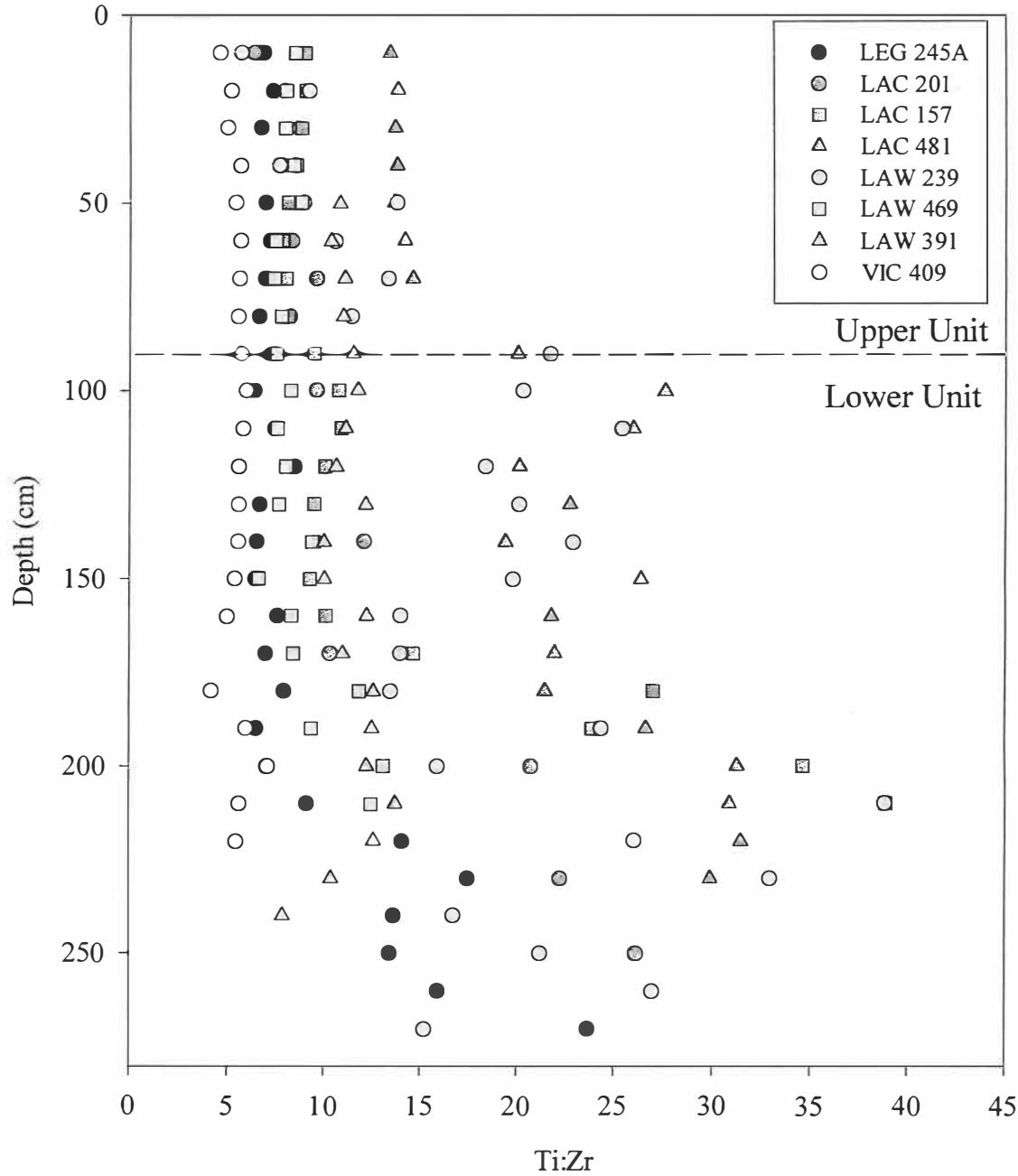

Figure 2-8. Identification of the functional boundary depth in microhigh profiles indicated by shifts in Ti:Zr.

climatic zones experiencing large seasonal soil-moisture deficits. This contrast is more subdued in both the wetter and drier ends of the climosequence, where microtopographic relief is much less.

In wet climates with lower seasonal moisture deficits, Vertisol pedogenesis is strongly influenced by relatively high biotic activity/productivity. High productivity enhances overall elemental cycling and bioturbation, ameliorating the strictly physical effects of seasonal shrink-swell processes. Eluviation of dissolved organic acids produced by organic matter decay enhances rates of mineral weathering, a phenomenon noted in the SEM survey, where both rutile and zircon grains were more hydrogeochemically altered in the upper unit and in higher MAP pedons. In the Texas study site, Vertisols with MAP >1300 mm have evidence of extensive bioturbation, particularly crayfish (*Fallicambarus devastator*) krotovina. Krotovina extended as deep as two meters in the profiles and accumulation of crayfish wastes at the surface was notable in microlows.

Vertisols formed in lower MAP climates with extended periods of soil moisture deficits show evidence of limited slickenside and microtopographic development simply because there is not enough available soil water, even in the wet season, to generate the necessary clay-swelling and associated physical forces (Wilding and Tessier, 1988). Cracks form and remain open for longer periods of time during dry periods, providing ample conduits for wind-borne dust into the profiles. Aeolian accumulations tend to form a blanket that thickens over time in most soils (Yaalon, 1987) and are effectively intercalated into

Vertisol cracks. Lower soil moisture also effectively retards mineral weathering, lessens active transport of coarse fragments, and contributes to sand preservation in the profile. This argument is supported by the relationship between the sand component and Zr content of the VIC profile (Fig. 2-5), which has relatively strong correlation and high slope.

2.5.2 Conceptual model

It is now possible to hypothesize that two primary processes are at work to influence the functional boundary depth in the climosequence profiles (Fig. 2-9): 1) at high MAP, pedogenic processes are dominated by hydrogeochemical action and lessivage (i.e., solutional movement of dissolved and suspended material), and 2) at low MAP, aeolian accumulation and physical processes dominate. The functional boundary depth of both microlow and microhigh profiles are shown in Fig. 2-9 and the two curves show remarkable similarity. Differences between the functional boundary depth curves show the contrasting intensity of pedogenic processes and expression within MAP zones. Low MAP Vertisols experience rates of physical inputs that exceed hydrogeochemical processing, high MAP Vertisols experience high rates of hydro/biogeochemical activity greatly exceeding physical processes, and the mid-MAP Vertisols are subject to a combination of both.

Pedogenesis differs with available water levels. In low MAP Vertisols, microlows act as catchment basins for material shed from microhighs or brought in by wind. Because these

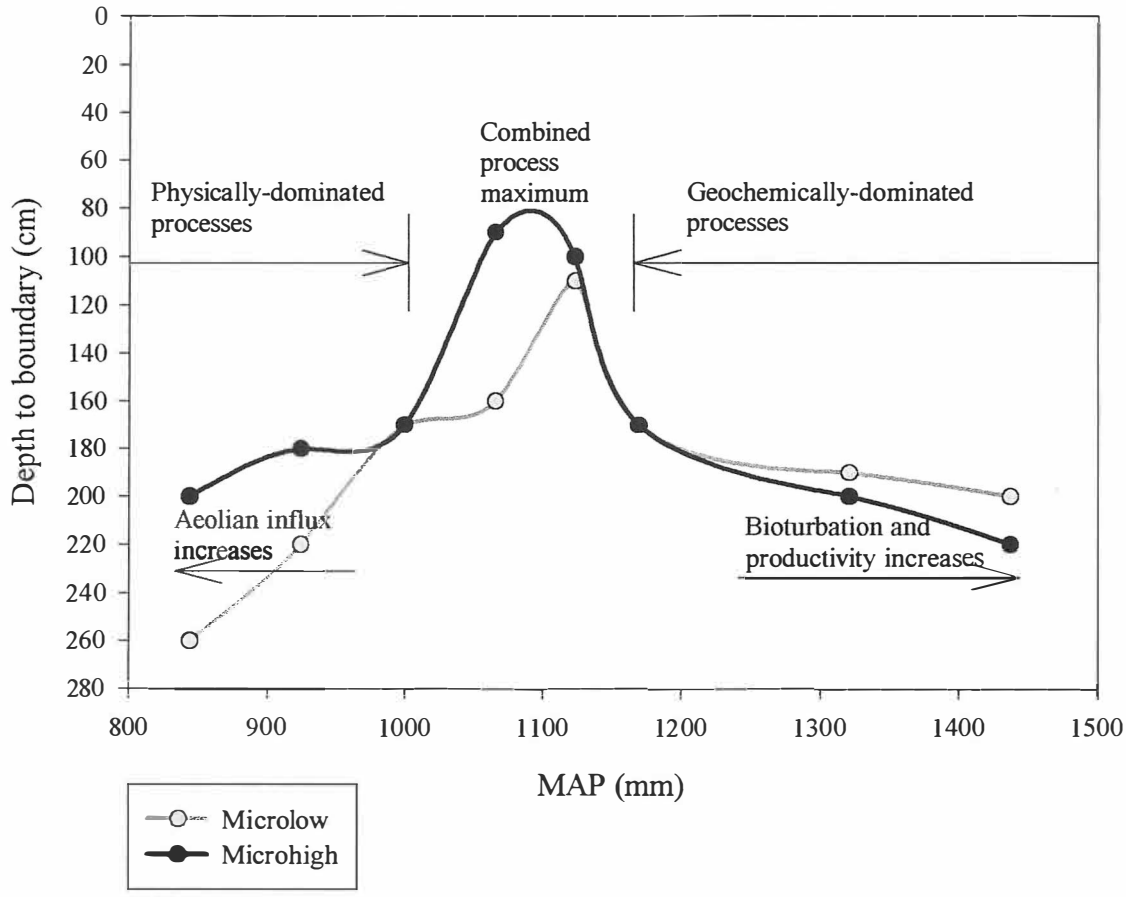

Figure 2-9. Conceptual climosequence Vertisol pedogenesis model based on depth to functional boundary as a function of MAP.

microlows more effectively capture the limited rainfall and are "wetter", they also are more deeply cracked during the dry season, inducing a deeper functional boundary than the microhigh. At the middle of the MAP scale, there is a zone influenced by combined processes, where both hydro/bio-geochemical cycling and maximized physical translocation (clay shrink-swell) are working on the soils to maximum effect, causing shallow and irregular functional boundary depths (Figs. 2-1 and 2-8). These profiles experience some aeolian input (Figure 2-7:E), but degradation /eluviation rates are equivalent to accumulation rates. In these profiles, packets of material occurring at 80-110 cm depths interpreted to be from greater depths were noted in morphologic characterizations, but were not statistically discerned, because the volumetric Ti and Zr contents fell within the 95% confidence interval for profile means. The offset in the microhigh Functional boundary depths is expected here, because these microtopographic features, dominated by physical processes and inorganic solute pumping, tend to be "drier" then their basinal microlow counterparts.

Within the high MAP Vertisols, water is not as limiting and Functional boundary depth increases in response to hydro/biogeochemical mechanisms. The presence of abundant dissolved and recalcitrant organic substances suppresses general aggregate stability, increases carbonate and salt solubility, and creates favorable conditions for lessivage. At the same time, bioproductivity increases, recycling material from deeper in the profile to the surface and producing more abundant OM to enhance lessivage. Microlows not only have higher OM contents (Coulombe et al., 1996), but also tend to be habitats for diverse

communities of soil-dwelling fauna. Physical transport of materials to the surface via meso- and macrofauna (particularly crayfish) tends to disrupt hydrogeochemical trends and attenuates strict downward weathering signatures. Thus, the functional boundary depth is shallower in the microlow than the microhigh, where crayfish accumulations are not subject to intense physical reworking and accumulation rates slightly exceed erosion.

2.5.3 Titanium as a Mass-Balance Strain Indicator in Clay-rich Soils

The principle objective for this work is to determine which "immobile" element is best to use for mass-balance analysis in the Texas Vertisol climosequence. This is a necessary foundation to allow for statistically confident comparisons between mass-balance trends in Appalachian paleo-Vertisols and their modern analogs. No element is truly immobile during intense pedogenesis, but is only *relatively* immobile due to retarded hydrogeochemical or physical processing. Thus, the choice of an immobile strain element is dependent upon the pedogenic setting. Elements associated with external influxes of material or fluids, such as the Zr-sand relationship, can only be used when such accumulations are dynamically balanced with other internal processes such that the influx is considered a component of pedogenesis. Such reasoning also holds true with elements found in minerals susceptible to hydrogeochemical alteration such as rutile-Ti. If the pedogenic conditions are such that the element is held in relative stasis by the mineral assemblage (i.e., Vertisol fine-earth fractions, Fig. 2-6), then that element becomes the strain indicator of choice in soils that are predominantly fine-textured. Another reason for using Ti is analytical: XRF-detectible Ti is always much more abundant than Zr in these

soils. Titanium contents are 3 - 40 times higher than Zr, with associated instrumental errors of 0.85-2.38% for TiO_2 and 1.85-25.00% for Zr. When used in Vertisol mass-balance relationships, Ti is the choice conservative element allowing for maximum depiction of pedogenic responses of an element of interest, rather than its relationship to the strain indicator itself.

In the climosequence Vertisols, mean strain (ϵ_i ; Eq. 1) for both Ti and Zr in all microlow/microhigh depth intervals is a strongly correlated ($r^2 = 0.83, P \leq 0.001$; Fig. 2-10), suggesting similarity in the pedogenic behavior of both elements. The regression line also shows that ϵ_{Zr} values are overall approximately four times greater than corresponding ϵ_{Ti}, due primarily to Zr accumulations in the upper unit of most of the pedons. Strain calculated from Ti shows the same trends as ϵ_{Zr}, but with lower magnitude suggesting more conservative behavior of Ti within the Vertisol profiles. Mean ϵ_{Zr} for depth intervals ranged from -0.6823 to +0.2036 (i.e., -68% to +20%) in microlows, and -0.6005 to +0.4739 in microhighs. By comparison, ϵ_{Ti} ranged from -0.1477 to +0.0513 in microlows, and -0.0942 to +0.1838 in microhighs, indicating markedly less pronounced volume loss/gain. The conservative nature of Ti in fine-textured Vertisols makes it a more suitable strain indicator than Zr, and an indicator that helps quantify pedogenic effects more reliably, both within and between Vertisol pedons.

2.6 Conclusions

Geochemical and physical evidence delineate a functional boundary in Vertisol pedons,

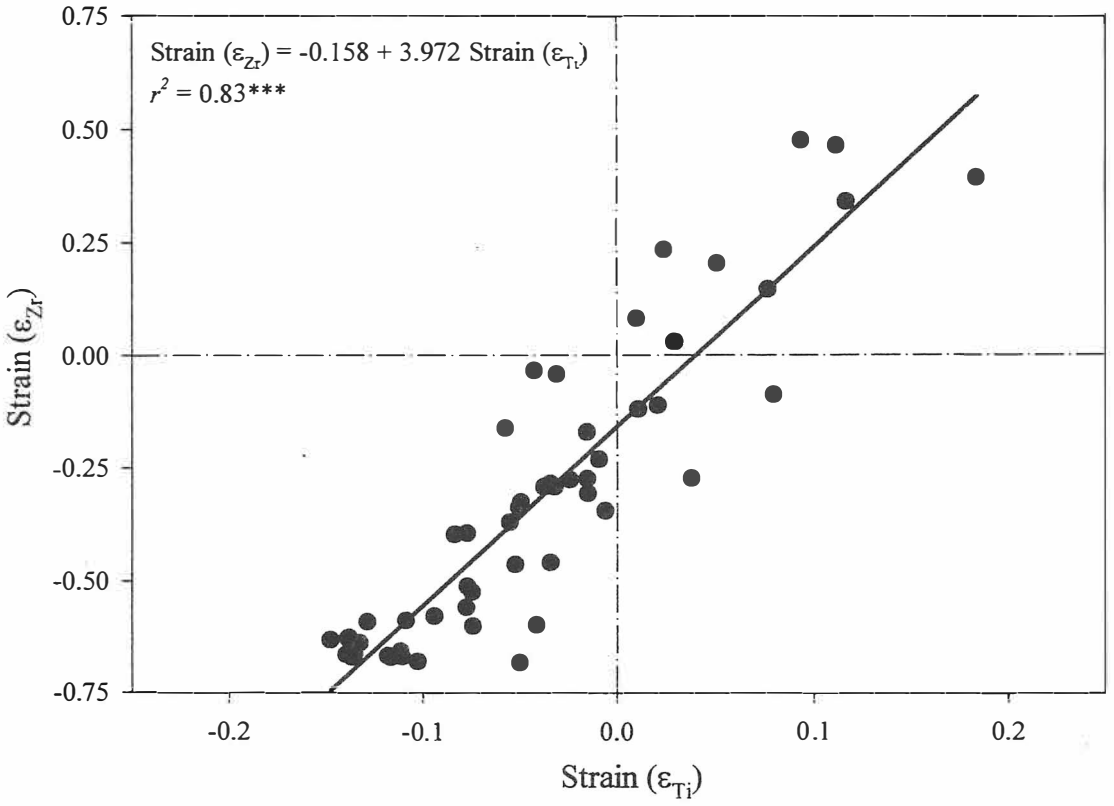

Figure 2-10. Linear regression of ε_{Ti} and ε_{Zr} calculated from mean depth interval values for all profiles. Significance designated as: *** $P \geq 99\%$.

which indicates a shift in primary pedogenic intensity. Depth to the functional boundary indicates the relative influence of contrasting pedogenic mechanisms (hydrogeochemical versus physical) across the climosequence. The functional boundary in the climosequence Vertisols defines the depth of the superactive pedogenesis domain, where external fluxes, in addition to maximum internal expressions of physico-chemical processes, create a dynamic open-system. Microscopic (SEM) survey of grain morphology revealed rutile grains were more hydrogeochemically weathered relative to zircon, wheras zircons always showed more physical grain damage indicative of extensive transport. This relationship was expressed throughout the Vertisol profiles, regardless of the functional boundary, although it was slightly more pronounced in zircon features as a function of MAP. Zirconium accumulations in the upper unit may be the result of weathering itself, that is, Zr the accumulation is due to loss of more mobile elements during pedogenesis, however, the strong correlation of Zr with the small, but significant sand component in these clay-rich soils, along with the SEM evidence that many very fine sand-sized zircon grains have been extensively transported from outside areas, argues that Zr is an indicator of physical processes rather than overall weathering during Vertisol pedogenesis. Also, despite evidence of primary mineral degradation, Ti is conserved within weathering clay-rich profiles and is better suited as a closed-system strain indicator to determinine mobile elemental translocation intensity using mass balance.

The concept of a "lithologic discontinuity" as it applies to U.S. Soil Taxonomy is not fully defined in terms of pedogenesis, although there are several criteria given by the Soil

Survey for its recognition (Soil Survey Staff, 1998). In some cases, there are true breaks in the lithologic composition of profiles, but in many cases, lithologic discontinuities may, in fact, be the translocation crossover described by Brimhall et al. (1991a) or the functional boundary described in this paper. Within the Vertisol climosequence, there is only a slight lithologic difference in the initial parent material in which soil begins to form, but over time, open-system dynamics create a complex lithology characteristic of the soil itself. The depth to the functional boundary becomes an interpretive tool for Vertisol pedogenesis using both Ti and Zr as indicators of contrasting pedogenic mechanisms. Within the Texas Gulf Coast climosequence, the interpretations gained from using this tool are:

1) All pedons experienced some level of aeolian input;

2) Hydro/biogeochemical and lessivage processes dominate wet Vertisols, subduing expression of shrink-swell phenomenon and slickenside development and microtopographic differences;

3) Physical processes dominate the pedogenesis of Vertisols formed in dry climates, where wind-borne material infiltrates into long-lived seasonal cracks and is only slowly weathered;

4) Mid-range MAP Vertisols show the maximum additive interaction between the physical and hydrogeochemical pedogenic processes.

Chapter 3

Mass-balance Relationships in Vertisol Climosequence Profiles Derived from the Upper Beaumont Formation, Gulf Coastal Plain, Texas.

3.1 Summary

A Vertisol climosequence on the Texas Gulf Coastal Prairie, spanning mean annual precipitation (MAP) regimes from 844 mm to 1437 mm, was examined using mass-balance relationships. The complex fluvio-deltaic sediments serving as parent material of the climosequence were similar enough to allow for meaningful geochemical mass-balance comparisons, on a whole-soil basis, across the entire MAP range. Only one pedon out of eight showed significant evidence of erosional truncation and the effects of polygenetic overprinting. Assessment of soil strain using two potential indicators showed that titanium (Ti) rather than zirconium (Zr) is the preferred immobile indicator in this clay-enriched setting, as Zr tends to be associated with a coarser grained fraction that may include aeolian additions to the upper portion of the soils. Mass-balance relationships of some of the ten elements examined within the climosequence showed trends ascribed to precipitation intensity. Mass-balance trends varied not only between locations but also between microtopographic (microhigh and microlow) positions within each Vertisol pedon. Mass-balance trends with depth in the profiles fall into four broad categories depending on the relative mobility and geochemical reactivity of the individual elements, including trends related to: 1) the coarse fraction, 2) the clay fraction, 3) leachable/ biocycled elements, and 4) climatic/redox-sensitive elements. Net mass flux percentages indicate a relative steady-state mass loss of around -16% (±3%) in climosequence pedons

with MAP > 900 mm. The driest Vertisol pedon had a net mass flux gain of around +3%, with particularly high gains of silicon, suggesting that accumulation of aeolian silt and sand is outstripping weathering and these soils are not forming within the same geochemical constraints as wetter Vertisol pedons.

3.2 Introduction

Weathering and soil formation involves the alteration of primary lithologic components through physico-chemical processes over time, resulting in a soil mantle in dynamic equilibrium with formation environment (Jenny, 1941a). The characteristic morphology and geochemistry of the upper portion (i.e., A & B horizons, solum or superactive domain) of a soil depends on the intensity of external (invasive) soil-forming factors such as precipitation/ temperature regime and biota (Richter and Markewitz, 1995). The lower portion of the weathering profile (regolith, saprolite, or subactive domain) behaves as a modified closed-system, where external biogeochemical fluxes originating in the superactive overburden are slowly translocated into parent lithology and equilibria kinetics are retarded by internal physical factors, such as permeability and mineral phase/solution exchange (Brimhall et al., 1991a). The depth of soil development is also dependent on a balance between production and erosion of the superactive domain (Heimsath et al., 1997). The superactive soil layer deepens in response to external environmental conditions and internal physico-chemical limitations to a steady-state depth, such that erosional removal is offset by deepening of the functional boundary at the expense of subactive saprolite. The subactive (C horizon) thickness can reach up to 50 m depth in

warm, humid settings (Eswaran and Bin, 1978). In areas of low relief and minimal overwash erosion, such as the regional setting of the Vertisol climosequence studied herein, the boundary depth between superactive and subactive domains is most sensitive to direct influences from climate-driven inputs.

Solum morphology and geochemistry are direct expressions of open-system dynamics and an excellent indicator of climatic influences. This is particularly true where all but one pedogenic formation factor is held relatively constant (e.g., chronosequences for time, climosequences for climate; Chadwick et al., 1990). Pedogenic trends are used to estimate geochemical denudation rates in studies of biogeochemical cycles, particularly where regional climate changes induce reservoir shifts of the cycling elements (Schwartzman and Volk, 1989; Stallard, 1995). Geochemical trends in soils can easily be assessed using mass-balance relationships, which account for volumetric changes as well as translocations relative to parent lithology. Mass-balance relationships are a consistent method of comparing weathering processes in various temporal and spatial scales (Chadwick et al., 1990; Brimhall et al., 1991).

3.2.1 Mass-Balance Overview

Brimhall et al. (1985) introduced mass-balance principles in studies of supergene ore bodies and later applied these same equations to soils (weathering profiles) as a measure of weathering intensity (Brimhall and Dietrich, 1987; Brimhall et al., 1991a & b). Pedologic "deformation", or volumetric change, is factored in by the strain indicator, ϵ, an

index based on the an immobile, relatively non-reactive tracer, as defined in equation 1:

$$\epsilon_{i,w} = (\rho_p C_{i,p}/\rho_w C_{i,w}) - 1 \quad (1)$$

Where $\epsilon_{i,w}$ is strain in weathered material w based on immobile element i, ρ is the soil bulk density, p is unweathered parent material interval, w is weathered material, and C is concentration of immobile element i in p or w. Movement of individual elements through open-system transport is determined by incorporating the strain index into a volumetric correction equation to determine translocation ($\tau_{i,w}$):

$$\tau_{i,w} = [(\rho_w C_{i,w}/\rho_p C_{i,p})(\epsilon_{i,w} + 1)]-1 \quad (2)$$

Chadwick et al. (1990) suggested that mass-balance relationships lend inherent consistency to and broadened their interpretive powers of soil-landscape comparisons. Mass flux is another useful application of these relationships, allowing chemical denudation rates to be determined by established material losses within the weathering profiles. This value is determined as the integration of all horizon translocations in terms of volumetric content of the original parent material composition, summed as weighted averages:

$$\text{Net mass flux } (m_{i,\,\text{flux}}) = (\rho_p C_{i,p}/100)\int_{Z=0}^{Z=D_{i,w}} \tau_{i,w(Z)}\,dZ \quad (3)$$

Where Z = depth, $D_{i,w}$ = depth of the weathered column, and other variables are described above (Brimhall et al., 1991a). The overall mass compositional flux percentage is the quotient of the summed mass flux values by total element oxide composition of the profile ($g\ cm^{-2}$) x 100%.

Several comprehensive pedogenesis studies of time, climate, and parent lithology have utilized mass-balance relationships. Work done on Pacific coastal chronosequences has successfully correlated the degree to which soil properties are differentiated to temporal exposure (Harden, 1988; Chadwick et al., 1990; Merrits et al., 1991; Nieuwenhuyse and van Breeman, 1997). In general, soil extractions based on agricultural applications are less useful for broad comparisons, because extraction efficiency is, in part, controlled by the particular soil components. Within well-controlled settings, however, chemical trends determined by soil-extraction methods may be more sensitive than whole soil compositions. Langley-Turnbaugh and Bockheim (1998) utilized mass-balance relationships with USDA - Natural Resource Conservation Service (NRCS) soil extraction methods to aid in interpreting pedogenic functions in a marine terrace chronosequence (Pliocene to modern) in Oregon. Their study showed clear relationships in mass fluxes between weathering indices quantified as oxalate- and citrate-dithionite extractable iron (Fe), aluminum (Al), and silicon (Si), pools which are strongly correlated to, and therefore indices of, weathering intensity (Soil Survey Staff, 1995). These trends may not have been detected in whole soil analysis, as the differences between the total Fe, Al, and Si in the chronosequence terraces was not significant. However, for broad comparisons across

time and locations, particularly in settings with extended weathering exposure, whole soil geochemistry may be more useful for mass-balance computations.

3.2.2 Use of Mass-Balance relationships in Soil-Paleosol Studies

One of the most promising applications of mass-balance relations is comparisons of paleosols and modern soil analogs. In this context, geochemical trends determined in a modern setting, where pedogenic factor inputs are well-constrained, can be translated, to some degree, to an analogous paleosol type to gain a better understanding of the paleoenvironment in which the paleosol developed (Driese et al., 2000). Although there are certain limitations in specific applications, particularly for elements which display diagenetic mobility, a judicious choice of soil type can minimize diagenetic overprinting. Amongst the most geochemically and physically stable paleosol type is the paleo-Vertisol, for which limited permeability and minimal post-burial compaction preserve not only gross morphological characteristics, but also geochemical trends (Mora and Driese, 1999; Caudill et al., 1996, 1997; Driese et al., 2000). Paleo-Vertisols occur throughout Paleozoic geologic successions in the Appalachian Foreland basin and provide an excellent opportunity for application of mass-balance interpretations developed in a study of their modern analogs. The Appalachian paleo-Vertisols have been extensively described and interpreted (for review, see Mora and Driese, 1999). Driese et al. (2000) were able to directly compare a modern Texas Vertisol (the Houston Black series) to a Mississippian age paleo-Vertisol (Pennington Formation) using mass-balance relationships. Relative mass balance trends in topographic microlow positions of both soil and paleosol indicate

similar translocation profiles for several elements, particularly those which are leached during active pedogenesis (Ca, magnesium - Mg, strontium - Sr, and phosphorus - P). The significant retention of whole soil/rock geochemical patterns in Vertisols/paleo-Vertisols strongly suggests that more detailed paleoenvironmental interpretations can be gained by further analog studies.

3.2.3 Elements of Interest

The choice of suitable elements for mass-balance assessments in Vertisols depends on their behavior both during and after weathering exposure. During active weathering, the intensity of surficial factors, such as climate and biotic productivity, dictates the removal of primary- and accumulation of secondary minerals within the Vertisols profiles in response to hydrogeochemical and internal thermodynamic conditions. Soils in moderately to well-drained conditions where rainfall is not limited behave as acid hydrosylate systems, where cations are replaced by meteorically- and organically-introduced protons (Chesworth, 1992). In seasonally to perennially moisture-deficient soils, such as the Texas Vertisols, high concentrations of electrolytes such as Ca^{2+}, Mg^{2+}, potassium (K^{+}), bicarbonate (HCO_3^{-}), and sulfate (SO_4^{2-}) reach supersaturated levels at depth and are precipitated out in secondary mineral phases (Wilding and Tessier, 1988), generating an "alkaline trend" soil, or a soil geochemistry dominated by salts (Spiers et al., 1984; Chesworth, 1992). Limited drainage, typical of fine-textured soils in low-relief topographic settings, induces locally variable Eh-pH conditions which greatly affect the behavior of redox-sensitive elements, such as Fe and manganese (Mn; Wang et al., 1993;

White and Dixon, 1996). The different drainage conditions associated with Vertisol microtopographic positions create contrasting trends within relatively close spatial associations (Wilding et al., 1990). Microlows retain moisture and therefore have weathering profiles more influenced by redox and acid-hydrolytic trends (mean profile pH values $\leq$ 7.0, USDA-Natural Resource Conservation Service Soil Survey Laboratory data accessible on the internet at www.iastate.edu/soils/ using pedon codes given in Table A1-1). Microhighs have to greater moisture-deficits due to elevated evaporation, tend to accumulate secondary minerals at shallower depths and behave as strictly alkaline-trend systems (mean profile pH values >7.0).

Elements are categorized by their general behavior in soils and paleosols (Chesworth, 1992). Then, relative loss during pedogenesis depends on bedrock composition and secondary mineral formation. Generally, the accepted kinetic order in chemical denudation studies has been: Ca > Mg > K > Si > Fe > Al (Harden, 1988), with some exceptions for extreme conditions. Elements such as Al and Si are abundant in continental lithologic (andesite/dacite/ rhyolite) compositions and provide structural frameworks for most primary and secondary minerals. Because these elements are not easily removed from the weathering profiles and are also conservatively retained within paleosols, they can be considered structural component elements (White and Brantley, 1995).

Alkaline earth elements (Ca, Mg, Sr) are associated with hydrolyzed primary minerals (pyroxenes and amphiboles) in weathering profiles and are released as cations into

solution. Aqueous phase cations can interact with clays in the soil matrix and are held in relatively low-energy associations with smectite exchange sites induced by isomorphic substitution (Wilding et al., 1990). These elements can also readily precipitate at depth in secondary minerals (carbonates and sulfates) in alkaline-trend profiles (soils dominated by salt dissolution/precipitation), where accumulations then serve as indicators of effective leaching depth (McFadden et al., 1991). Thus, Ca, Mg, and Sr are leaching/exchange sensitive components.

Potassium and rubidium (Rb) are commonly enriched in paleosols, emplaced by metasomatic processes during diagenesis (Nesbitt and Young, 1984). The role of K in modern soils is complicated by mica/feldspar weathering, plant uptake and recycling, and clay mineral exchange, but K is rarely lost to < 20% of its original content under natural conditions (Huang, 1989). Rubidium most likely behaves similarly to K due to its comparable atomic radius and charge, however, Rb forms relatively stronger bonds in silicates and the K:Rb ratio continually decreases with advanced soil maturity (Franz and Carlson, 1987).

The behavior of the two major redox-sensitive elements, Fe and Mn, has been reviewed in many studies (Schwertmann and Taylor, 1989). Loss and gain of these elements is due primarily to variable hydrochemical conditions (Eh-pE) within profiles, particularly in periodically poorly-drained settings. Complex hydrated oxides typically occur in soils (Bernal et al., 1959). Geochemical behavior of Fe and Mn can often be correlated directly

with color changes in profiles (Torrent et al., 1983), however, these elements may experience post-pedogenic compositional changes as soils become paleosols, particularly as the result of interaction with dysoxic and/or acidic diagenetic fluids. Paleo-Vertisols are commonly depleted in Mn and somewhat enriched in Fe, and all Fe is in well-crystalline oxide (hematite) form, as oxyhydroxides are dehydrated during burial diagenesis (Schwertmann and Taylor, 1989). Appalachian Basin paleo-Vertisols have a characteristic red color in outcrop due to the relatively high hematite content. In their comparison of a Mississippian age Pennington Formation paleo-Vertisol with a modern Houston Black Vertisol, Driese et al. (2000) found that total Fe was 75% greater overall in the paleo-Vertisol and total Mn was depleted by 75% relative to the modern analog. Manganese is soluble under redox conditions typical of burial diagenetic environments, thus, Mn-containing minerals will dissolve and Mn will be removed by fluid-rock interaction. Driese and Mora (1993) noted through cathodoluminescence microscope examination of paleosol carbonate cements that Fe remained fixed in the paleosol matrix but cements formed through secondary precipitation were enriched with Mn. Iron and Mn are grouped into redox-sensitive category in soils, with Mn being more mobile and variable, Fe conserved and even accumulated in Vertisol profiles.

Phosphorus does not fit into any one of the previous categories and thus is considered alone in climosequence profile comparisons. Phosphorus is a necessary macronutrient in most living organisms. It is susceptible to biocycling, fixed with Ca as hydroxyapatite in calcic horizons, or with Fe in secondary Fe mineral phases such as strengite ($FePO_4 \cdot 2H_2O$)

or vivianite [$Fe_3(PO_4)_2 \cdot 8H_2O$; Lindsay et al., 1989]; thus, P falls into several functional categories in soils and serves as an ancillary pedogenic indicator for other, more restrictive, categories. Most important is its role in bioproductivity, as many soils are P-deficient, and surface accumulations or sub-surface depletions of P are excellent geochemical measures of the depth of open-system biotic influence. Phosphorus is also fixed by calcareous horizons and is thus a secondary indicator of extensive pedogenic accumulations.

3.2.4 Hypothesis and Goals

The principle objective of this study was the compilation and interpretation of comparable, climate-induced, mass-balance trends for selected elements with a modern Vertisol climosequence. It was hoped that the trends identified in modern Vertisols, obtained under relatively well-constrained environmental conditions, would provide useful baselines for assessing mass-balance trends previously determined for analog Appalachian basin paleo-Vertisols, and would be able to provide finer-resolution climatic interpretations for those paleogeographic settings in which the paleosols occurred (Driese et al., 2000). Mass balance trends were compiled from both microhigh and microlow profiles across the climosequence. Correlation analyses of microlow depth trends are used to evaluate whether the elements acted similarly in the profiles, and whether the responses were directly related to mean annual precipitation or precipitation deficit. Amplitude of difference between microhigh and microlow trends provide information as to the intensity of internal mechanical deformation processes on hydrochemical activity. Finally, mass flux

assessments of total elemental translocations are used to evaluate whether the profiles are in relative steady-state with climate.

3.3 Materials and Methods

3.3.1 Geographic Setting and Sampling

The setting for this investigation has been described in Chapter 1 (Fig.1-1; Tables A1-1 through 3). Samples for this investigation were recovered from large soil pits (2m wide, 3-5m long) excavated at each site, transecting microhighs and microlows in each pit. Bulk soil samples were collected at 10 cm intervals from microtopographic pairs (pedon) to the base of each pit for geochemical analysis, and from each pedogenic horizon for bulk density.

3.3.2 Analytical Methods

To maintain uniform analytical procedure for analog soil-paleosol comparisons, soil samples were treated as whole rock samples and most analytical procedures performed on soils are also applicable to lithified paleosol samples. Soil samples were oven-dried at 60°C, ground in a shatterbox, and pelleted for bulk geochemical analysis using X-ray fluorescence (EG&G ORTEC TEFA III, Singer and Janitsky, 1986; all data, instrumental detection limits and precision are compiled in Table A3-1). Bulk density was determined by the paraffin-coated, air-dried, clod method (Blake and Hartge, 1986; data in Table A3-2). Particle size analysis was carried out at the National Soil Survey Laboratory in Lincoln, Nebraska, using the pipet method (Gee and Bauder, 1986; Table A2-5).

Elemental weight percentages were corrected for carbonate content dilution prior to mass-balance calculations (for method, see Chapter 2). Carbonate correction factors (CCF) are given in Table A2-3. The depths to which CaO wt % was at or below mean background CaO wt %, along with descriptive data from NRCS (Table A2-1) were used to determine the DCH of each profile. Ten cm depth interval data have been converted to mean values for specific pedogenic horizons to allow for more direct comparison between NRCS data/ descriptions and whole rock geochemistry. Thus, depth interval data within each horizon act as sub-samples and tend to smooth data uncertainties for any single point. All XRF data for 10-cm intervals are presented in Table A3-1, with carbonate-corrected data presented in Table A3-2.

3.4 Results and Discussion

3.4.1 Parent Material and Strain

Mass-balance relationships require a known composition for relatively unweathered parent material in weathering profiles. In the case of the Vertisol climosequence, formed on a complex of fluvio-deltaic deposits, there is no primary parent material composition that covers all locations. Rather, the parent material for each pedon set (microhigh and microlow) is assumed to be the composition of the deepest sample collected. This assumption may be problematic in that the deep samples collected were sometimes found to be lithologically "dissimilar" to overlying sediments, indicated as lithologic discontinuities in NRCS descriptions (Table A1-1). Deep samples removed from two of the pedons (LEG 245A and LAW 239) were found to be strongly influenced by

groundwater, such that the deepest sample showed significant morphological and geochemical differences (Table 3-1). For these profiles, parent material compositions were defined at slightly shallower depths. All elemental compositions of the pedogenically altered material collected to depths (~2.5 m) and parent sediment were determined to be significantly different ($P \leq 0.001$), indicating that mass-balance trends are due primarily to pedogenesis rather than sedimentological differences. Compositional differences in parent material between locations are within statistically acceptable ranges and do not vary significantly across the climosequence.

Strain is calculated as the ratio of volumetric elemental content (calculated as wt% times bulk density) of parent material to weathered interval (Eq.1). Residual enrichment (RE), or the ratio of bulk densities (ρ_p/ρ_w), shows trends of mineral dissolution and leaching (RE > 1) or secondary accumulations {RE <1; Figure 3-1 [note: In all figures, series localities listed in order of decreasing mean annual precipitation regime (MAP) from top left (League series) to bottom right (Victoria Series)]}, which are reflected in strain calculations. Bulk density changes in the climosequence profiles are relatively conservative, varying no more than 20% of the overall mean ρ_p (1.8657 g cm^{-3}; Fig. 3-1) The upper horizons in most of the profiles have experienced some dilation ($\rho_w < \rho_p$) due to bioturbation and mineral dissolution, particularly in the microlows (Fig. 3-1). These RE patterns are similar to, though less pronounced as, those noted by Chadwick et al. (1990), where RE values in surface horizons of a climosequence in Hawaii were as great as 150% of mean ρ_p. Microhigh RE values have overall broader scatter and are skewed toward

Table 3-1. Mean whole soil compositions for pedon deep (parent material) samples.

Profile	Sampling Depth	Element										Bulk Density
		Al_2O_3	CaO	Fe_2O_3	K_2O	MgO	MnO	P_2O_5	Rb	SiO_2	Sr	
	cm	wt%										g cm^{-3}
LEG 245A	280	17.52*[a]	1.46*	6.53*	2.00	1.86	0.262*	0.07	0.013*	68.79	0.013*	1.931*
LAC 201	300	12.18	12.49	5.36	2.46	4.01	0.073	0.14	0.010	59.86	0.016	1.870
LAC 157	280	12.28	11.71	6.62*	2.54	3.77	0.091	0.14	0.011	57.43	0.019	1.852
LAC 481	430	11.51	11.54	5.62	2.52	3.45	0.060	0.13	0.010	58.88	0.018	1.880
LAW 239	325	10.30	0.47*	3.09*	0.91*	1.10*	0.064	<0.01*	0.009	83.19*	0.010*	1.805
LAW 469	230	10.73	13.10	4.60	1.51	2.06	0.050	0.10	0.008	72.08	0.015	1.861
LAW 391	240	10.01	14.41	4.28	1.80	2.48	0.034	0.10	0.009	65.61	0.014	1.909
VIC 409	270	8.29*	12.66	3.92	1.31	2.21	0.061	0.10	0.007*	57.76	0.017	1.750*
99% CI Low[b]		9.13	4.74	3.86	1.33	1.69	0.021	0.06	0.008	57.25	0.014	1.910
99% CI High		14.08	14.97	6.14	2.54	4.55	0.153	0.14	0.012	73.65	0.019	1.805
Proxy PM[c]												
LEG 245A	250	11.55	11.83	5.21	1.39	1.69	0.119	0.09	0.009	72.64	0.012	1.926
LAW 239	295	10.79	10.61	4.35	2.09	2.56	0.054	0.10	0.009	68.59	0.020	1.824

[a] * indicates a wt % value that falls outside the statistically acceptable range as determined by mean whole soil compositional values for all profile deep samples

[b] Ranges of acceptable compositions for parent materials in the climosequence are based on mean whole soil compositions for all profiles ± 99% confidence interval

[c] Proxy parent material composition derived from next deepest sample in pedon

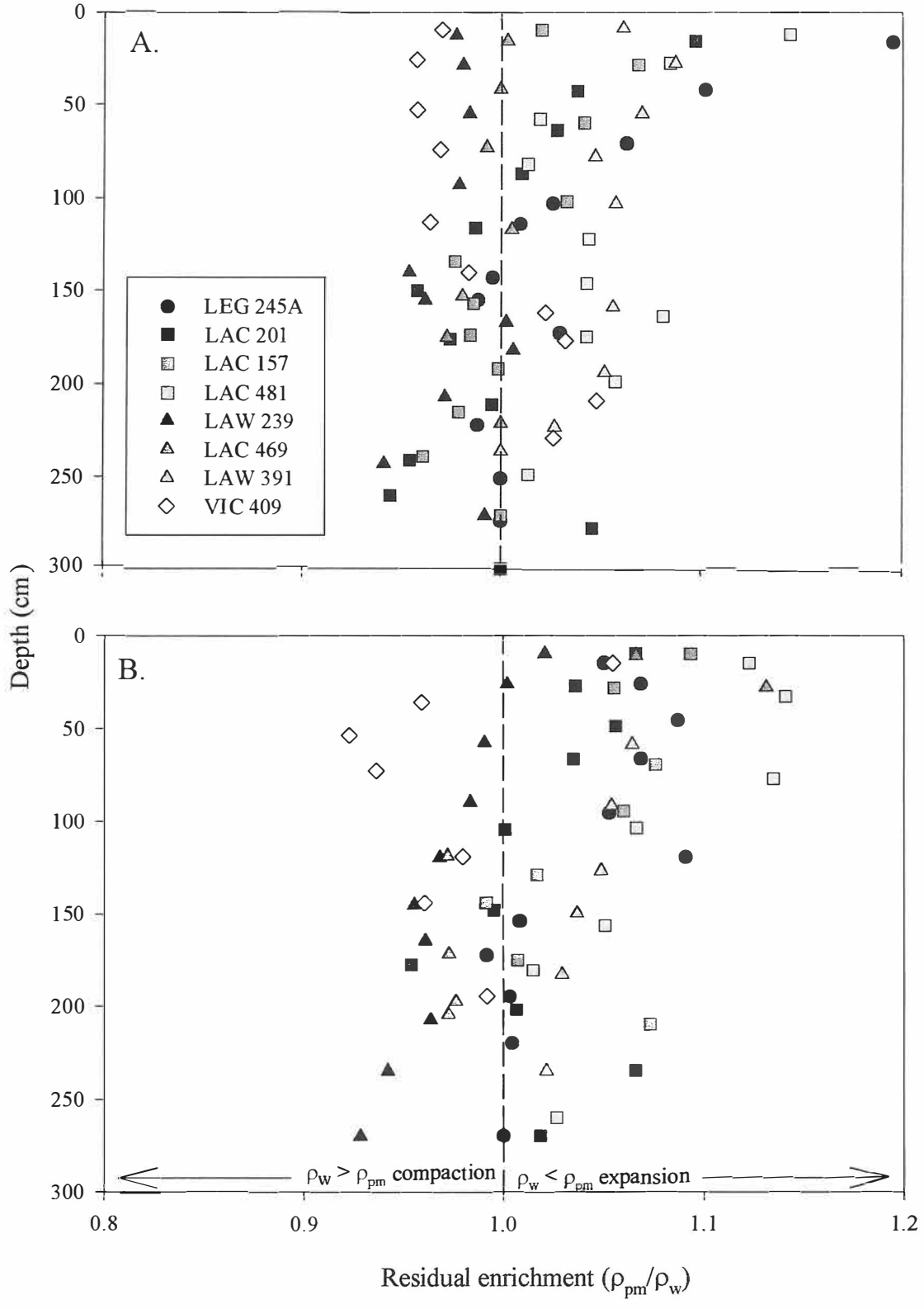

Figure 3-1. Residual enrichment for all profiles: A) microlows, B) microhighs.

dilation compared to the microlows. Lower ρ_w values at depth in both microhighs and microlows, with subsequent RE values greater than 1.0, may be attributed to higher clay contents at depth, with lower overall component ρ (mean < 2.0 g cm^{-3}) compared to quartz or carbonate-enriched parent material (ρ = 2.65 and 2.71 g cm^{-3}, respectively).

Strain for each profile was initially determined using titanium (Ti) as the conservative element in Equation (1). Figure 3-2 shows Ti-strain (ϵ_{Ti}) as a function of depth in all profiles. Strain in the microlows (Fig. 3-2A) follows a marked sigmoidal trend with depth, with greatest volumetric loss (compaction) between 50-150 cm, corresponding to the maximum slickenside expression in the profiles, as described in the field (Table A1-1). Most of the microlow profiles show slightly less compaction within the surface (A) horizons than in the underlying horizons, indicative of bioturbation dilational processes, such as burrowing and rooting in the A horizons that are obliteratedat depth by the effects of seasonal shrink-swell cycles. Microhigh ϵ_{Ti} trends show overall lower volumetric loss, greater scatter, and a less direct relationship with surface features and slickenside expression. Volumetric gains in both microlows and microhighs correspond to carbonate and gypsum accumulations at depth, which are somewhat shallower and more pronounced in the microhighs.

Strain estimates determined using Ti as the immobile indicator are more conservative than zirconium (Zr)-based values (Fig. 3-3). Zirconium strain (ϵ_{Zr}) exaggerates volumetric losses and gains due to compositional discrepancies in the upper portion of the profile

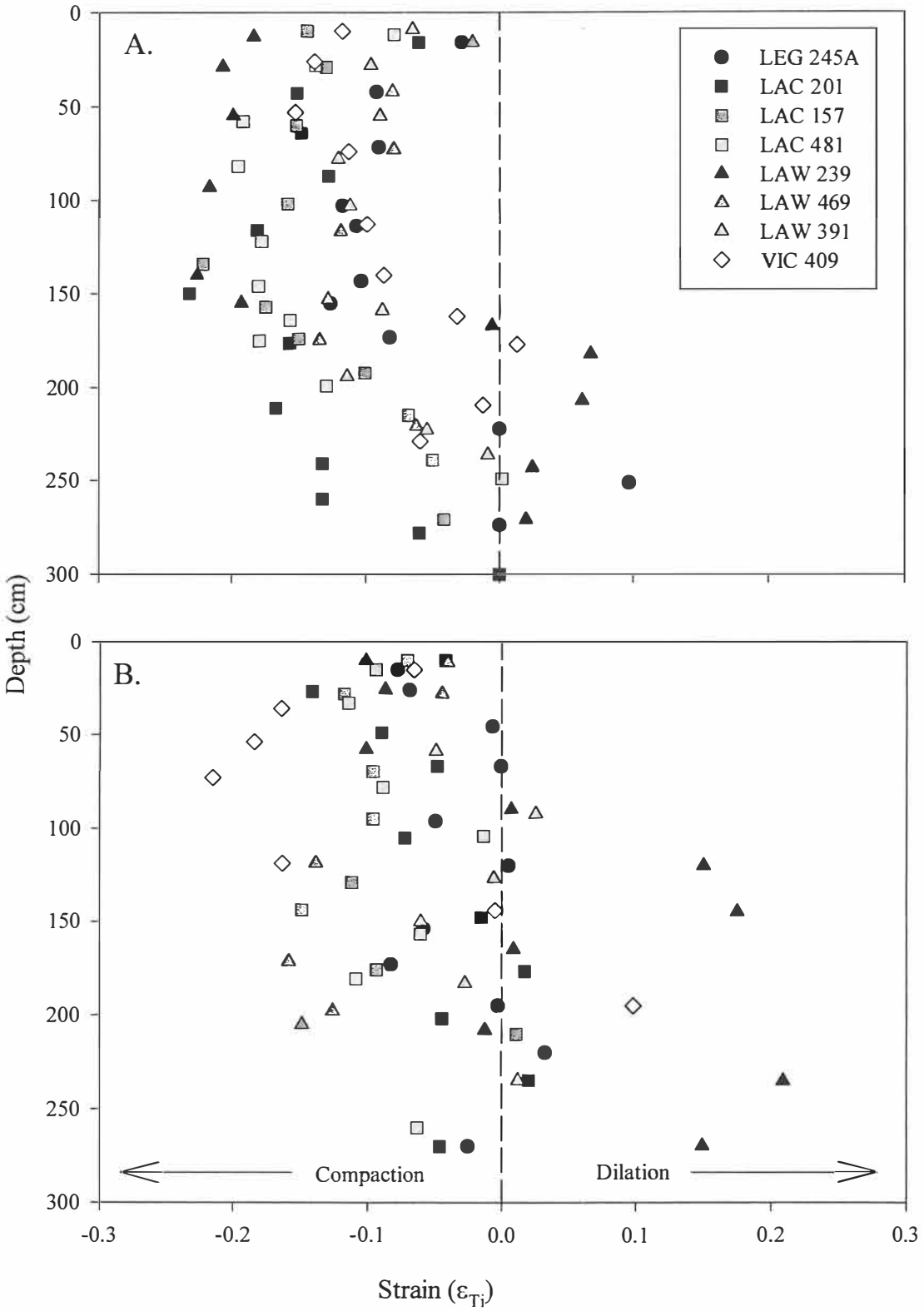

Figure 3-2. Titanium-based strain for all profiles: A) microlows, B) microhighs.

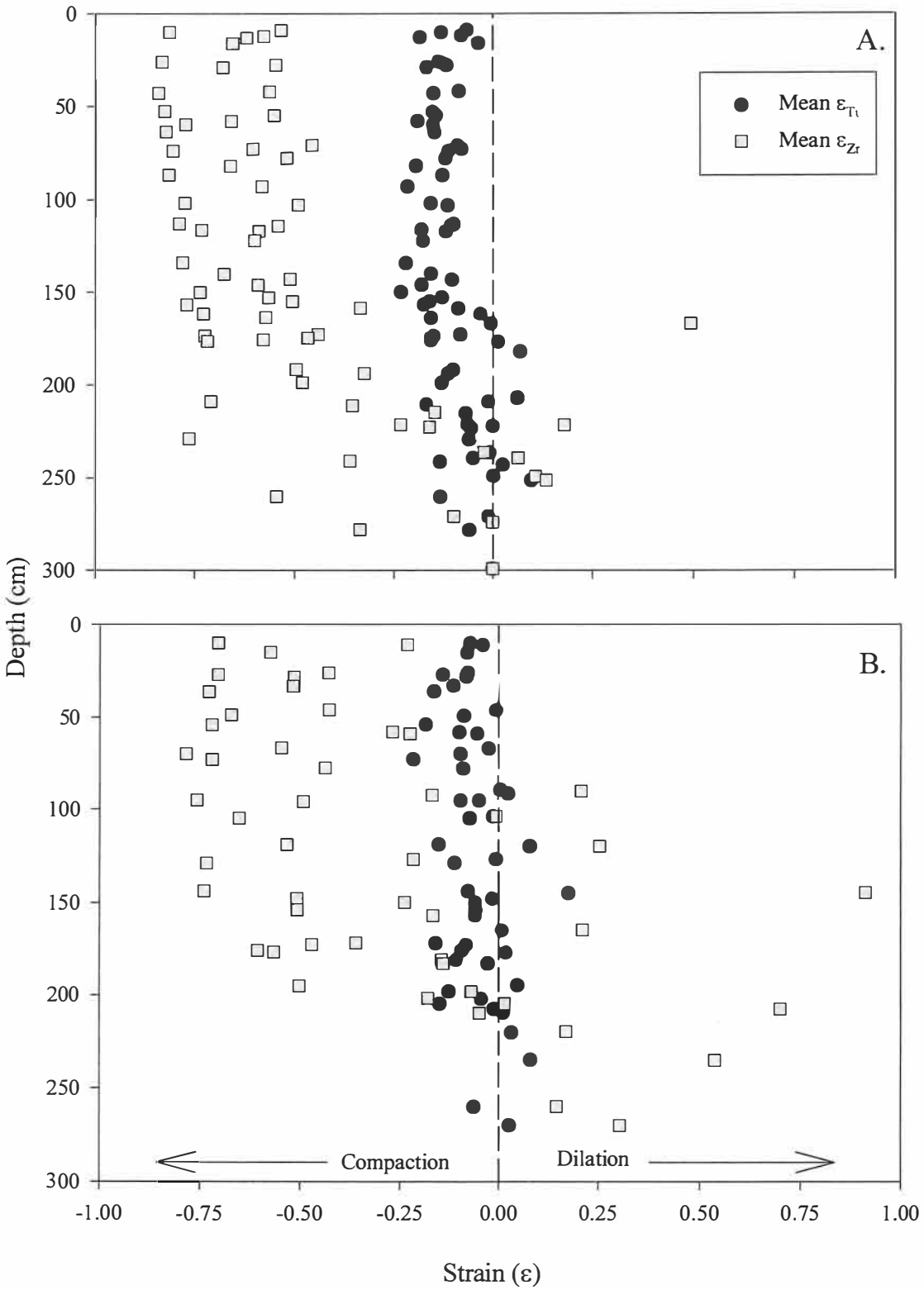

Figure 3-3. Mean Ti- and Zr-strain values: A) microlows, B) microhighs.

versus the parent material, which is possibly attributed to addition of exotic zircon into the upper, active portion of the profiles (see Chapter 2). Similarly, Brimhall et al. (1991a, 1994) demonstrated that most Zr in upper portions of weathering laterites was mostly associated with zircons accumulating, along with other translocated minerals, in clay-rich illuvial horizons. Thus, volumetric changes as determined by ϵ_{Zr} shown in Fig. 3-3 are exaggerated in the upper ~2.5 m of all the profiles, suggesting compaction as low as 84% and dilation up to 92% of original parent material volume. The exaggerated ϵ_{Zr} values are unrealistic for Vertisol pedogenesis in fine-textured distal alluvial parent material, in which volume losses and gains are minimized by pre-existing textural conditions, i.e., well-sorted silt to clay and high bulk densities. Without using correction factors for translocated zircon (e.g., Brimhall et al., 1991a), this comparison suggests that ϵ_{Ti} is more useful to describe overall geochemical changes in profiles that are attributable to pedogenic intensity, rather than exaggerated estimates of strain.

3.4.2 Mass-Balance Trends

The ten elements chosen for this study (Al, Ca, Fe, K, Mg, Mn, P, Rb, Si, and Sr) comprise roughly 97 wt % (± 1) of the total composition in all profiles. Profiles are dominated by Si ($\bar{x}$ = 69.93 ± 0.78 wt.%) followed by Al ($\bar{x}$ = 11.43 ± 0.28 wt.%). Both Al and Si are components of the dominant minerals (phyllosilicates, quartz, and feldspars), and are therefore expected to behave conservatively in the profiles. Aluminum translocations (Fig. 3-4) show some systematic differences, both between and within series pedons, which are indirectly attributable to climatic conditions. Microlows from the

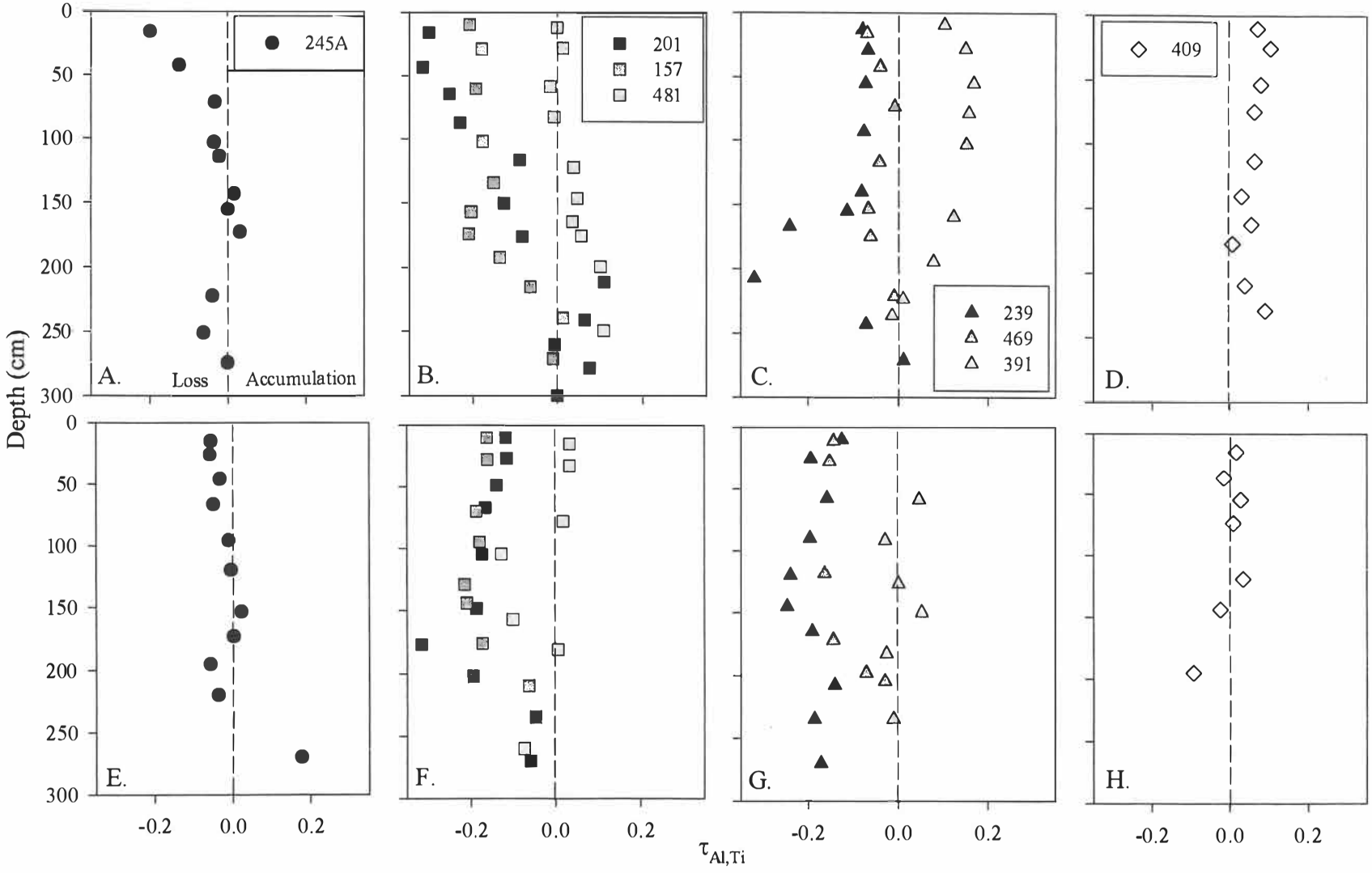

Figure 3-4. Translocations of Al in profiles: A-D) Microlows, E-H) Microhighs. A & E, League series; B & F Lake Charles series; C & G Laewest series: and D & H Victoria series.

wettest profiles (LEG 245A & LAC 201) show maximum losses in the upper portions, lessening with depth, and conservation in horizons with maximum slickenside and higher clay wt % (Tables A1-1, A2-5) . Both LAC 157 and 481 microlows show modest losses to around 170 cm. Aluminum behaves very conservatively in the driest profiles (LAW 391 and VIC 409, Fig. 3:C & D), with overall gains possibly as the result of wind-borne addition of relatively unweathered feldspar grains, particularly in the microlow. Trends in climosequence microhigh Al translocations do not correspond to those in adjacent microlow trends, and there is no discharge/recharge trend (i.e. overall microlow Al loss is offset by microlow Al gain) across the profile pairs. Microhigh trends in LAC series (MAP 1321-1124 mm) have similar patterns to those in LAW 239 and 469 microlows (MAP 1066 and 1000 mm, respectively).

Silicon behaves more conservatively than Al in most profiles (Fig. 3-5). The exceptions are profiles at the extreme MAP regimes (LEG 245A and VIC 409; Fig. 3-5 A & E, D & H), where Si behavior is dictated by high leaching and aeolian influx, respectively. The behavior of Si is largely dictated by the abundance of sand in all the profiles, except LEG 245A, where acid hydrolysis easily dissolves and removes excess Si, maintaining a relative steady-state. Upper portions of LAC 201 profiles (Fig. 3-5, B & F) show Si gains attributable to overwash sand deposition from the nearby waterway, as horizons down to ~170 cm have >100% higher sand content than deeper horizons (Fig. 3-6; Table A2-5). Conservative trends in the other LAC and the LAW microlow profiles are ascribed to relatively constant sand + silt contents. Slight differences, particularly attenuated losses or

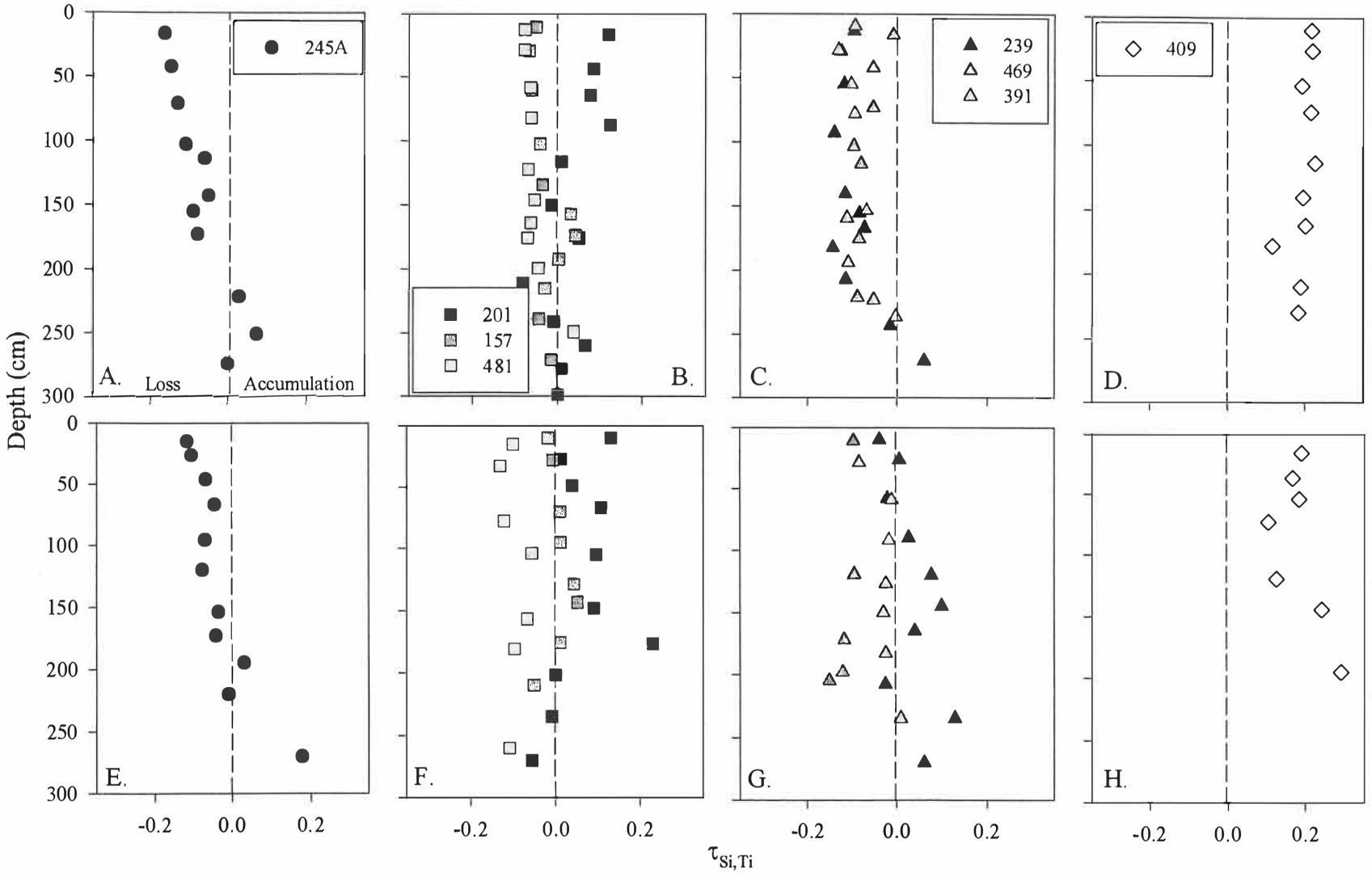

Figure 3-5. Translocations of Si in profiles: A-D) Microlows, E-H) Microhighs. A & E, League series; B & F Lake Charles series; C & G Laewest series: and D & H Victoria series.

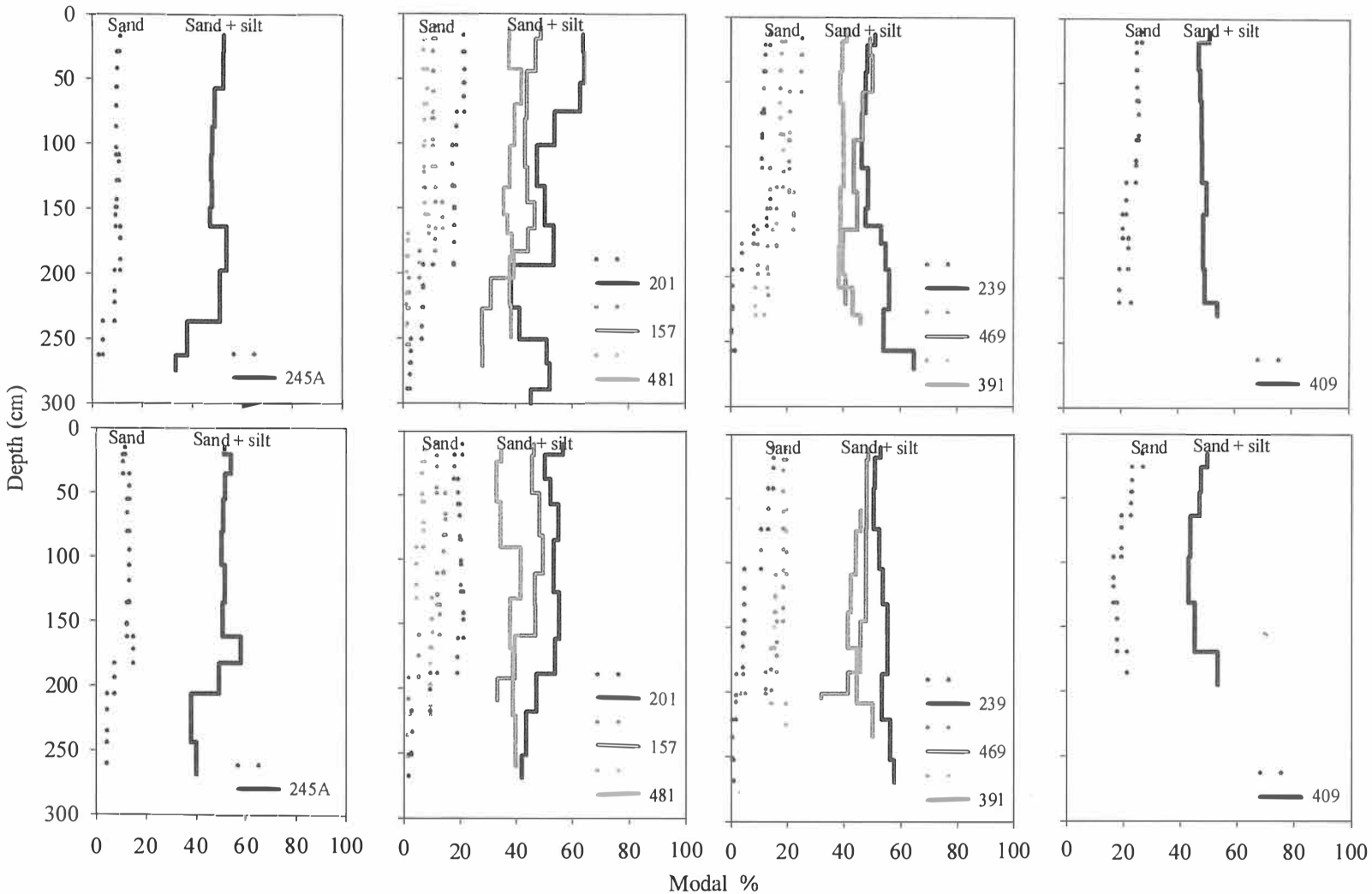

Figure 3-6. Particle size modal percentages: A-D) Microlows, E-H) Microhighs; A & E, League series, B & F, Lake Charles series; C & G, Laewest series; and D & H, Victoria series.

accumulations, can be roughly matched to silt content increases in these profiles (Fig. 3-6). The driest MAP profile, VIC 409, shows significant Si accumulations in both microhighs and microlows, ascribed to the aeolian influx of sand borne on winds sweeping across the large sand sheet just to the south of this pedon location.

Trends of Ca, Mg, and Sr translocations (Figs. 3-7,-8,-9) are nearly identical to each other within profiles, with Ca the most mobile of the three. Correlations of the three elements demonstrate similar behavior (Ca x Mg, R = 0.896, P = 0.014; Ca x Sr, R = 0.878, P = <0.001; Mg x Sr, R = 0.906, P = 0.023). Calcium has experienced the greatest relative losses in the microlow profiles, with the depth of effective leaching (i.e., $\tau_{Ca,Ti} < -0.850$, or >85% loss) roughly shallowing with lower MAP. This relationship of effective leaching depth with MAP is also evident in microlow Mg and Sr trends, although maximum losses are significantly lower ($\tau_{w,Ti}$ = -0.450 for Mg and -0.400 for Sr), because these elements both act more conservatively than Ca. Magnesium is often associated with isomorphic substitution within the clay structure, and the geochemical kinetics of Sr are slowed by the larger atomic radius and slightly lower electronegativity (0.95 vs 1.00 for Ca and 1.31 for Mg). Microhigh profiles from LAC, LAW and VIC pedons have not been leached as deeply or extensively as their adjacent microlows, and some profiles have significant accumulations (LAW 239). In the microlows, translocation trends for both Mg and Sr show more linear relationships overall with depth (less is removed as depth increases). Magnesium translocation shows some correlative response to MAP, as upper portions of the microlow profiles (to 150 cm depth) have decreasing loss of Mg as MAP decreases

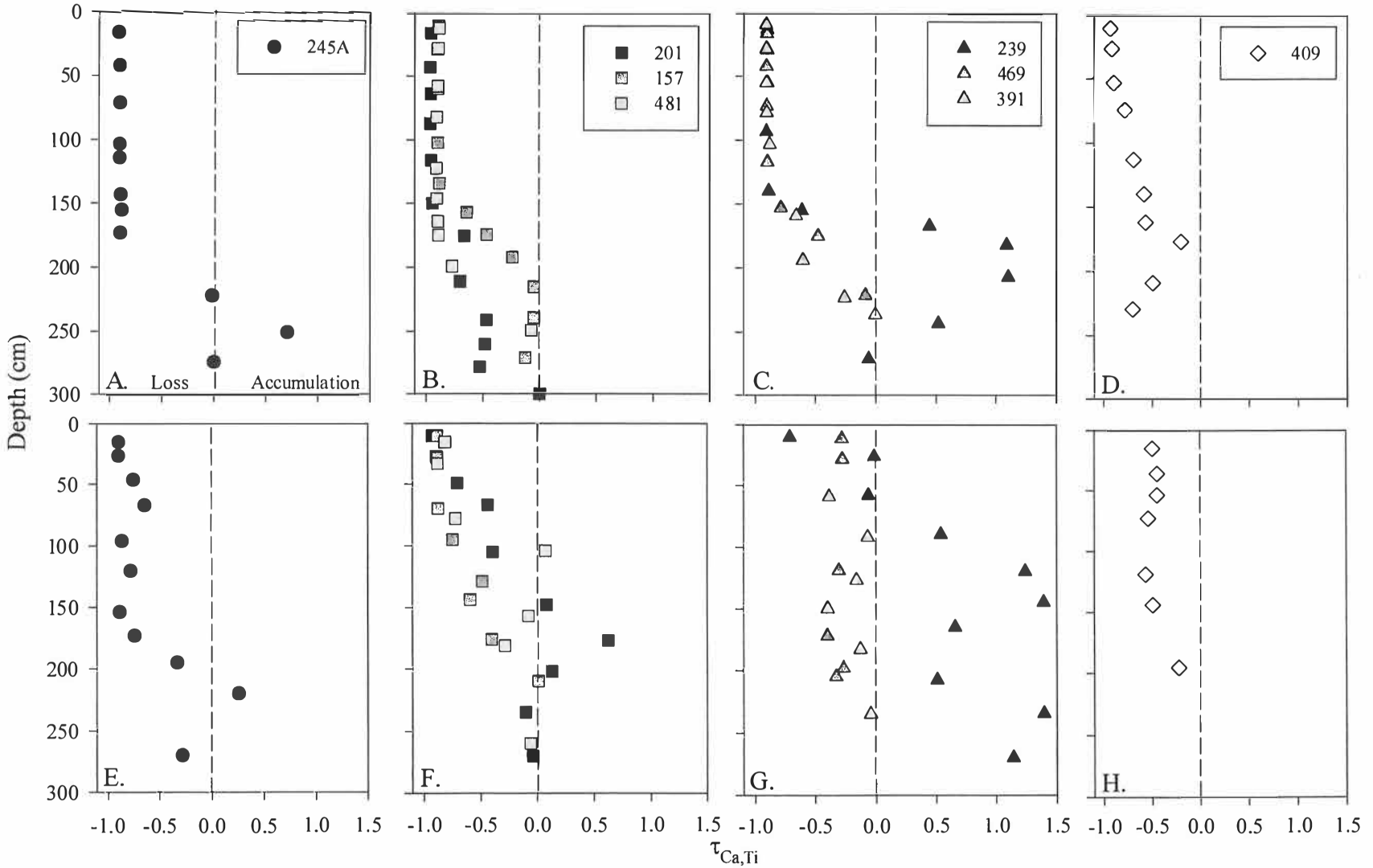

Figure 3-7. Translocations of Ca in profiles: A-D) Microlows, E-H) Microhighs. A & E, League series; B & F, Lake Charles series; C & G, Laewest series: and D & H, Victoria series.

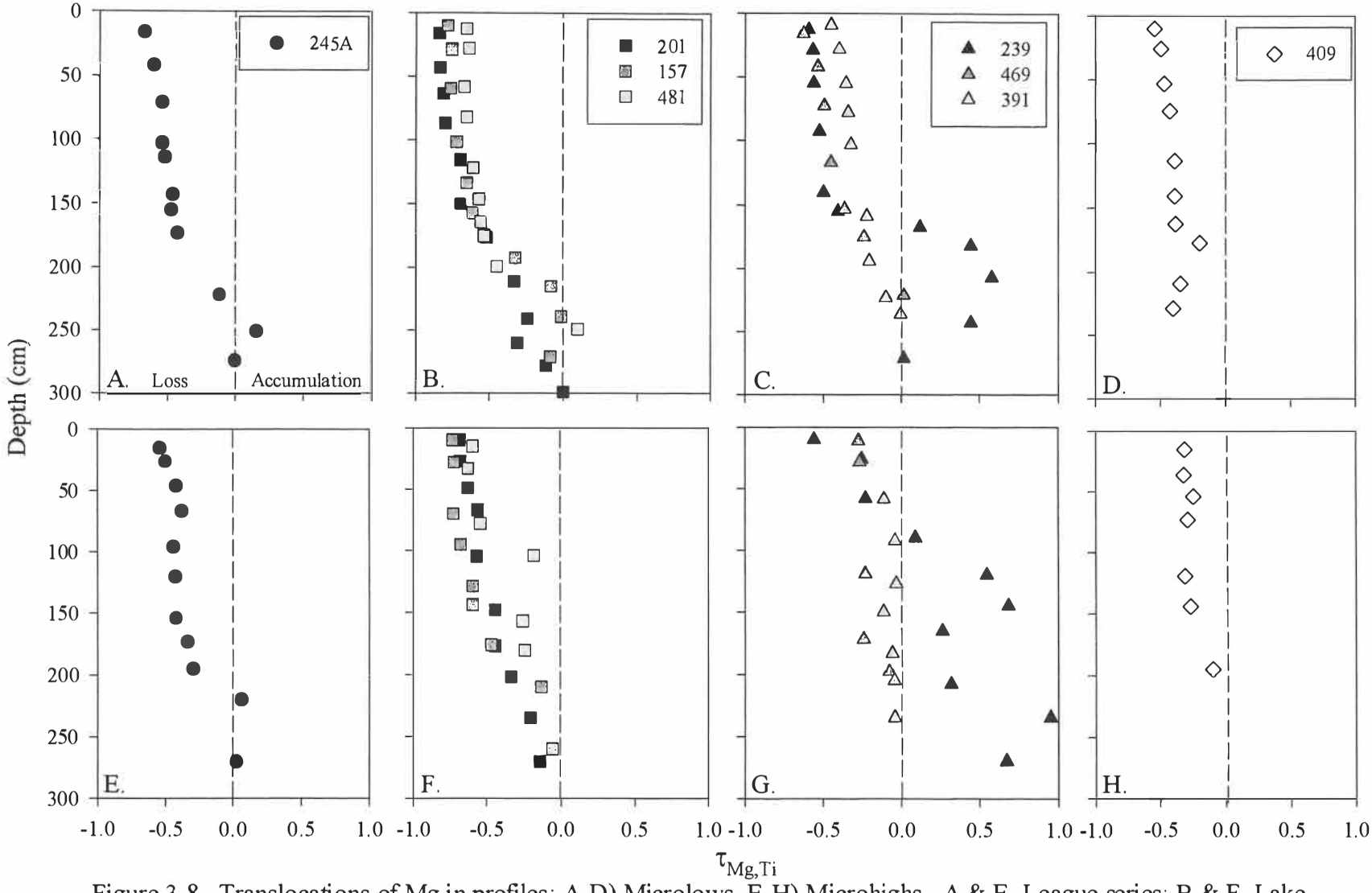

Figure 3-8. Translocations of Mg in profiles: A-D) Microlows, E-H) Microhighs. A & E, League series; B & F, Lake Charles series; C & G, Laewest series: and D & H, Victoria series.

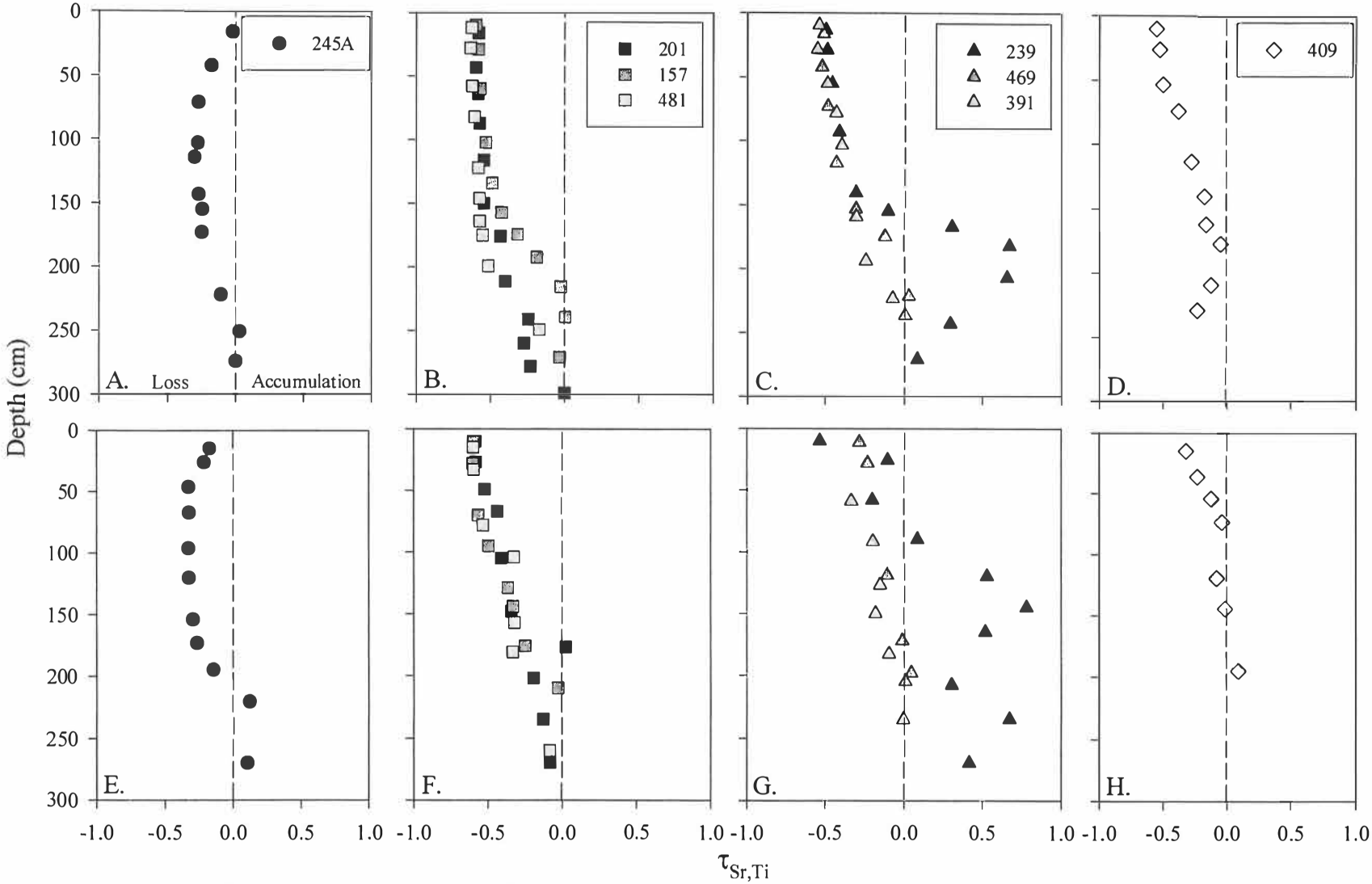

Figure 3-9. Translocations of Sr in profiles: A-D) Microlows, E-H) Microhighs. A & E, League series; B & F, Lake Charles series; C & G, Laewest series; and D & H, Victoria series.

(Fig. 3-8). Strontium is the most conservative of the three alkaline earth elements (Fig. 3-9) due to slower geochemical kinetics. No clear correlations with MAP are evident in Sr trends. Strontium trends noted in the LEG 245A profiles indicate slight losses at the surface and increasing losses at depth, and are attributed to Sr biocycling in these soils. Plants take up Sr along with Ca (up to 12% substitution; Kabata-Pendias, 2001), where it accumulates in the surface in decomposing vegetation. Crayfish bioturbation may also contribute, as sediments with higher Sr contents are brought up from depth in the soil and deposited on the surface. The slow kinetics of Sr relative to Ca and Mg result in higher accumulations at the surface, as biocycling exceeds effective leaching rates.

Profiles from LAW 239 are problematic, in that accumulations of the alkaline earth elements below 150 cm in the microlow and below 90 cm in the microhigh are very high compared to the other profiles. Calcium accumulations reach nearly 150%, and Mg and Sr nearly 100% and 75%, respectively, in this profile. This pedon also has exaggerated strain trends (Fig. 3-2) that suggest differences in alluvial parent materials at depth. Descriptions of LAW 239 microhigh and microlow pedons indicate there are distinct breaks in the morphology of carbonate masses, from hard glaebular concretions to fine-grained powdery masses. These trends in LAW 239 may reflect relict pedogenic features and, thus, this pedon may be truncated and polygenetic and may not reflect recent climatic conditions. Relatively high accumulations of alkaline earth elements at 230-250 cm depth in LEG 245A are due to crayfish-moderated carbonate precipitation, where cation-charged soil solution contacts atmospheric pCO_2 through crayfish burrows.

Potassium behaves very similarly to the leaching/exchange-sensitive elements, Ca, Mg, and Sr (Fig. 3-10), particularly Mg (R = 0.756, $P = 0.016$), if profile LAW 239 is excluded due to its unusual trends for all alkaline earth elements. Potassium mass-balance trends are nearly identical to Sr, where the statistical F-test shows an overlap probability of 0.626. Thus, behavior of K in the climosequence profiles is primarily influenced by the leaching regime. However, Rb behaves differently than K (Fig. 3-11), corresponding more closely to Al translocation trends (R = 0.895, $P = 0.027$). As Al is most closely associated with clay composition and content, it is reasonable to infer that Rb resides within the clay interlayer sites, forming a relatively stable complex in these alkaline trend soils.

Iron translocation patterns in microlows are similar to the other leachable elements such as Mg and K, showing losses in the upper 200 cm and conservative behavior below that depth (Fig. 3-12). Loss patterns are similar between microlows and microhighs in all pedons. This similarity suggests that mechanisms controlling Fe translocation are relatively uniform (i.e., matrix-dominated) and are controlled by the redox status of the soil. Organic matter acidolysis of Fe-bearing primary mineral constituents (i.e., pyroxenes and amphiboles) releases Fe^{2+}, which leaches downward in the soil profile and is precipitated in secondary minerals within favorable redox conditions usually occurring at depth (Montgomery et al., 2000). Generally, Fe losses increase with increasing MAP. The driest MAP profile, VIC 409 (Fig. 3-12, D & H), displays very conservative Fe behavior, although losses center on about -0.28. The bulk Fe composition in these profiles

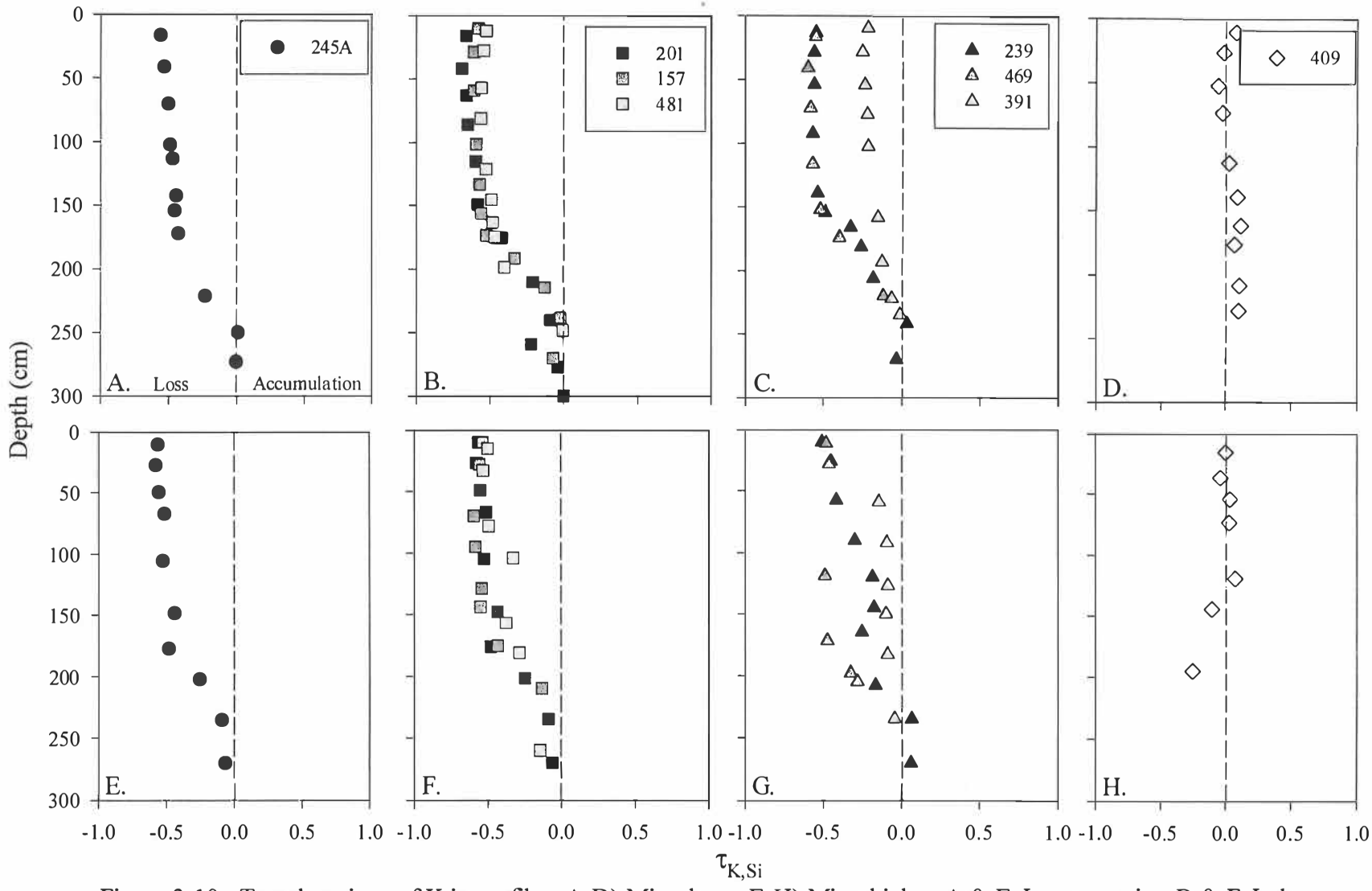

Figure 3-10. Translocations of K in profiles: A-D) Microlows, E-H) Microhighs. A & E, League series; B & F, Lake Charles series; C & G, Laewest series; and D & H, Victoria series.

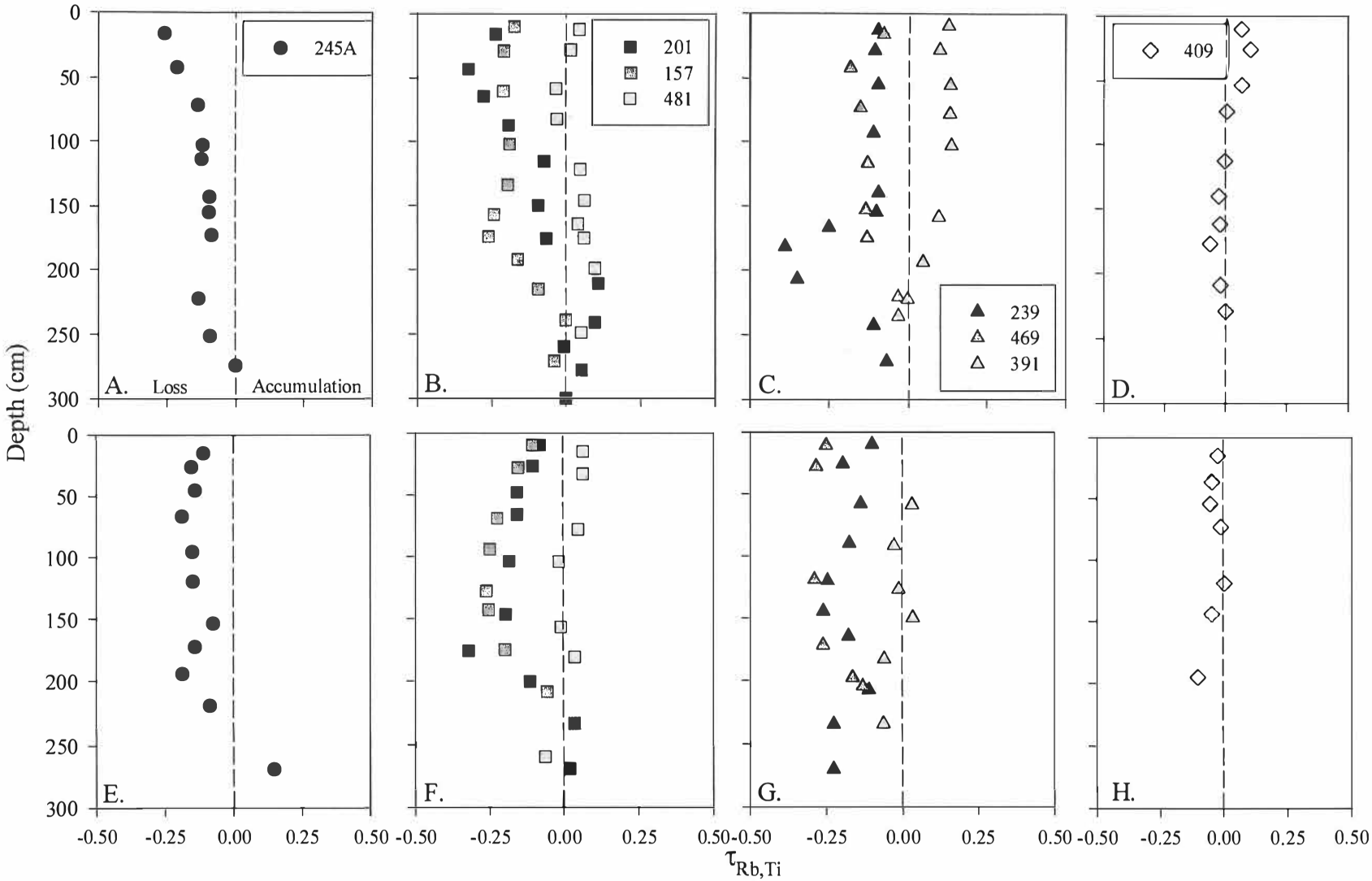

Figure 3-11. Translocations of Rb in profiles: A-D) Microlows, E-H) Microhighs. A & E, League series; B & F, Lake Charles series; C & G, Laewest series; and D & H, Victoria series.

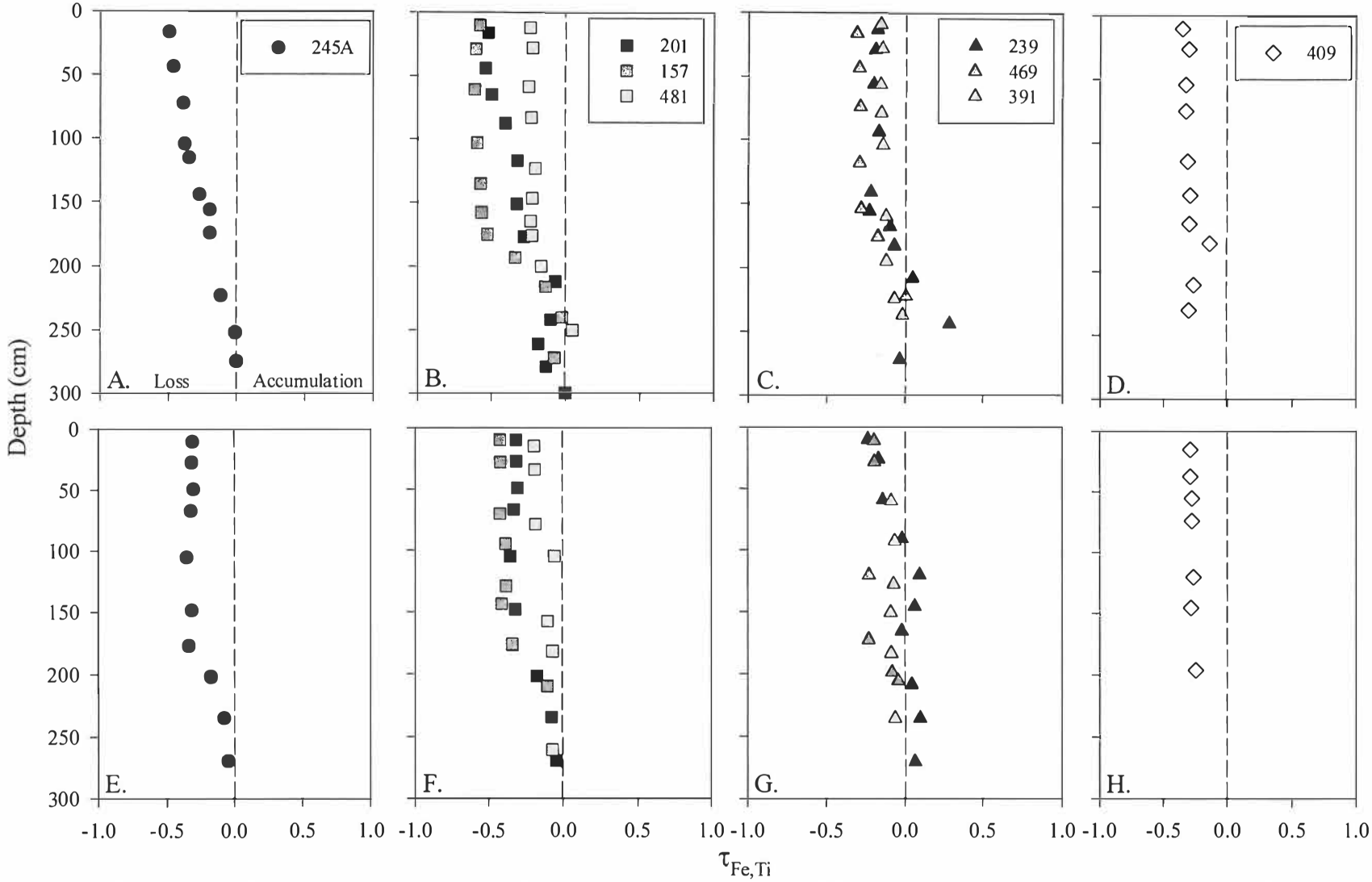

Figure 3-12. Translocations of Fe in profiles: A-D) Microlows, E-H) Microhighs. A & E, League series; B & F, Lake Charles series; C & G, Laewest series: and D & H, Victoria series.

is fairly consistent throughout, except in the deepest portion, where it increases slightly. Overall, the Fe content of VIC 409 profiles is the lowest of all the climosequence profiles (Table 3-1), and the moisture deficient conditions of the profiles restricts translocation.

Translocation patterns of Mn in the profiles are very complicated, with generalized patterns recognized for each of the different series (Fig. 3-13). Complicated loss/ accumulation trends are likely due to the complex behavior of ionic Mn, which can exist in several oxidation states in ambient soil solutions. Organic acids can cause dissolution of metastable Mn oxyhydroxides found as grain coatings in shallower horizons, reprecipitating Mn deeper in the profile (McKenzie, 1989; Montgomery et al., 2000). Climosequence Mn trends change from recording overall loss in the wettest MAP pedons to overall gains in the drier MAP profiles, with most the conservative behavior noted again in the driest pedon (VIC 409). The translocations patterns for the microhighs are more conservative than those for the microlows, as generally wetter conditions induce higher productivity, with subsequently more acidic conditions, and higher Mn mobility. Accumulations greater than 100% in LAW 239 and 391 microlows (Fig. 3-13, C) are somewhat problematic, suggesting Mn content was low or depleted in the deep (parent material) sample used for the mass-balance calculations, or the pedon was affected by outside additions of Mn. Manganese is a necessary nutrient, and can be removed to rooting depth and readily biocycled, but such recycling doesn't totally explain the accumulations, because the highly bioproductive LEG 245A and LAC 201 profiles do not show any accumulations over 100%. A more likely explanation involves Mn-removal by

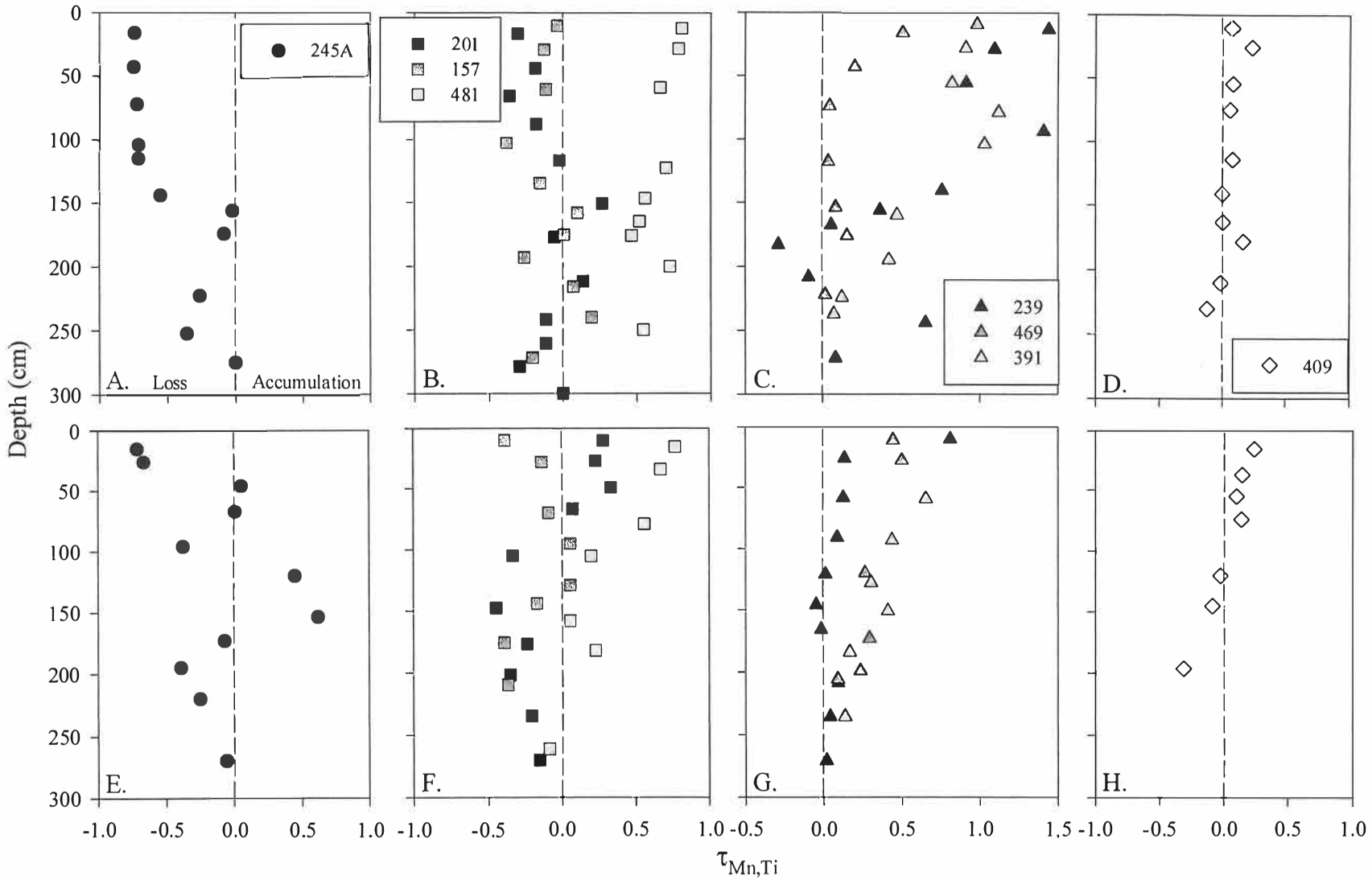

Figure 3-13. Translocations of Mn in profiles: A-D) Microlows, E-H) Microhighs. A & E, League series; B & F, Lake Charles series; C & G, Laewest series; and D & H, Victoria series.

periodic groundwater in the deeper portions of the pedons. Because pedon LAW 239 shows erratic translocations of other elements and it is possible that there is a truncated soil underlying the surface soil at a depth of around 2 m, there is some doubt as to its sedimentological continuity and polygenetic nature. Not all elements are affected by this discontinuity, suggesting that the break is a product of depositional processes (i.e., erosion, reposition of alluvium from the same source early in the history of the Beaumont, followed by subsequent pedogenesis of the more recent alluvium) rather than different parent material altogether.

Phosphorus loss is more pronounced in pedon microlows than microhighs (Fig. 3-14) and the depth to which P is depleted decreases with decreasing MAP. Most P-bearing minerals are relatively insoluble under well-oxidized, neutral to alkaline soil conditions, but are effectively dissolved by organic acid exudates in plant roots. Because P is a necessary macronutrient for most living organisms, P losses are directly related to biological productivity of the pedons and translocations in the microlows approach 100%. Phosphorus is more conservative in the microhighs, due to a combination of lower bioproductivity and generally higher pH (i.e, lower P mineral solubility). The climatic signature in P translocation can be seen in contrasting patterns between microlows and microhighs, with greatest contrast in the LAW profiles (MAP ca. 900-1100 mm).

Correlations amongst the element translocations (with the exception of pedon LAW 239) show overall similarities in the general geochemical behavior of these elements (Table 3-

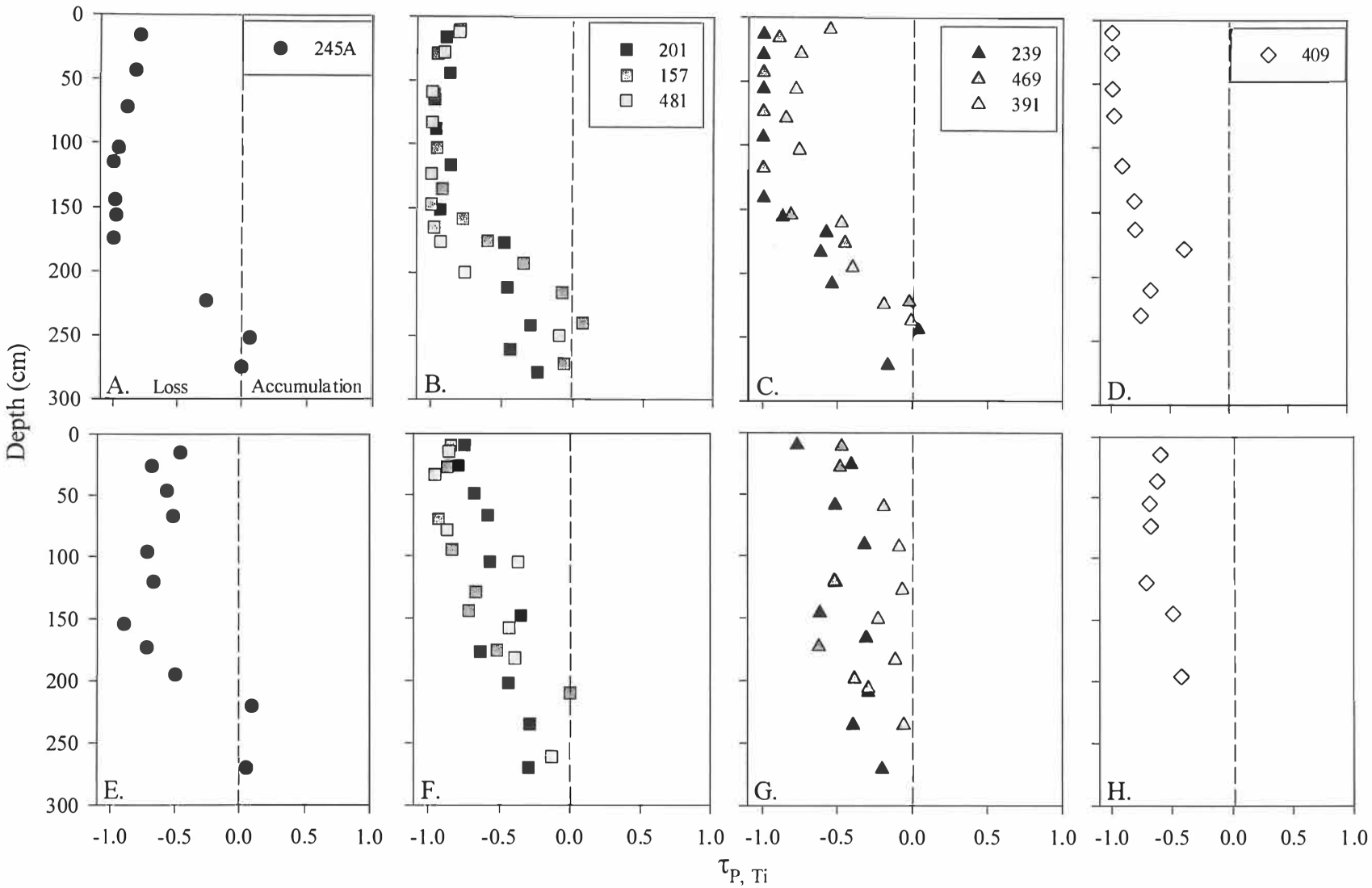

Figure 3-14. Translocations of P in profiles: A-D) Microlows, E-H) Microhighs. A & E, League series; B & F, Lake Charles series; C & G, Laewest series; and D & H, Victoria series.

2). Using these relationships, it is possible to categorize the elements based on broader geochemical behavior. In essence, there are four basic mass-balance trends with depth noted in the climosequence Vertisols:

1) A *framework trend* represented by Si, behaves conservatively in response to hydrogeochemical translocation and corresponds more closely to coarse to medium size-fraction (sand- and silt-sized) grain composition and distribution. Silicon is not correlated to any other elements in the matrix (Table 3-2).

2) A *clay-related trend* represented by Al and Rb. These elements behave less conservatively than Si under leaching conditions, are generally more conservative than most of the other elements, and are strongly related to the clay-fraction distribution in profiles.

3) A trend in *leachable/biocycled* elements represented by the alkaline earth elements (Mg, Ca, and Sr), K, Fe, and P, which show significant depletions in the microlows and generally differentiated depletions/accumulations in microhighs. Some of the elements show distinct MAP responses, but for the most part have reached a steady-state depletion to the depth of effective leaching. Correlations show the strongest relationships between the alkaline earth elements and P, although P data overlap significantly with Ca.

4) A *climate-redox sensitive trend* represented by Mn, which actually has the best overall correlation with MAP compared to other elements, despite the generally exaggerated depth trends. No other elements correlate to Mn trends.

Table 3-2. Correlation matrix for all elemental translocations in microlow and microhigh profiles (excluding pedon LAW 239).

Dependent element	Independent element								
	Ca	Fe	K	Mg	Mn	P	Rb	Si	Sr
Al	-0.0940	0.6046*[b]	0.6196*	0.4408	0.4652	0.1103	0.8787***	-0.0812	0.1190
(*P* value)[a]		(<0.0001)	(<0.0001)				(0.0217)		
Ca		0.5479*	0.5027*	0.7738***	-0.1608	0.8365***	-0.0277	0.1509	0.7392**
(*P* value)		(<0.0001)	(<0.0001)	(0.0144)		(0.3063)			(<0.0001)
Fe			0.5720*	0.8215***	0.3651	0.6764**	0.5739*	-0.2315	0.4994
(*P* value)			(0.0023)	(<0.0001)		(<0.0001)	(<0.0001)		
K				0.7563***	0.0522	0.5673*	0.5950*	0.3844	0.6218**
(*P* value)				(0.0160)		(<0.0001)	(<0.0001)		(0.6259)
Mg					0.0496	0.8502***	0.3557	-0.0209	0.8185***
(*P* value)						(<0.0001)			(0.0227)
Mn						-0.0988	0.4973	-0.1793	-0.3486
P							0.1489	-0.0630	0.7306**
(*P* value)									(<0.0001)
Rb								-0.0174	-0.0078
Si									0.0868

[a] ANOVA probability of data set overlap

[b] * Significant at $P \leq 95\%$, ** significant at $P \leq 97.5$, *** significant at $P \leq 99\%$

3.4.3 Mass Fluxes

The overall loss or accumulation of elements within individual profiles is termed net mass flux. Comparisons of these values may be more valuable than the translocation trends for individual elements when assessing the effects of long-term weathering under differing pedogenic factors.

In the climosequence profiles, elemental fluxes are generally higher in the microlows than microhighs (Table 3-3), except in the driest MAP profile (VIC 409). Only Mn showed a significant correlation to MAP (R = -0.725**), and most elements have only weak negative correlations. Essentially, drier profiles experienced lower losses. The Victoria pedon (VIC 409) was also the only one to show net accumulation of elements relative to parent composition. Pedon LAW 239 is again problematic and will be not be discussed further, as mass-balance behavior of elements in this profile may have been influenced by a pedologic discontinuity at depth and do not reflect long-term pedogenic effects. The overall mass flux percentages of the remaining profiles (Figure 3-15) show that the climosequence Vertisols have achieved a relative steady-state net mass flux of around -16% (±3%) when MAP exceeds 900 mm. Below this critical MAP, Vertisols do not experience the same pedogenic processes as their wetter counterparts. In the drier Vertisols, carbonates are more likely to accumulate and be retained within the profile. Another cumulant in theses profiles is aeolian sand and silt, which carry in Si in the form of quartz and feldspars (Table 3-3). Attenuated hydrogeochemical weathering rates limits leaching and secondary phyllosilicate formation, and thus enriches these elements in the

Table 3-3. Elemental mass fluxes for climosequence profiles samples.

Profile	Position[a]	Element										
		Al	Ca	Fe_2O_3	K_2O	MgO	MnO	P_2O_5	Rb	SiO_2	Sr	Summed
		g cm^{-2}										
LEG 245A	ML	-1.3792	-22.2756	-4.7924	-1.9694	-1.8557	-0.2215	-0.1288	-0.0057	-9.6777	-0.0100	-42.3159
	MH	0.4456	-25.1852	-2.4874	-1.4729	-1.5295	-0.0268	-0.0916	-0.0037	-8.1033	-0.0104	-38.4652
	Mean	*-0.4668*	*-23.7304*	*-3.6399*	*-1.7211*	*-1.6926*	*-0.1241*	*-0.1102*	*-0.0047*	*-8.8905*	*-0.0102*	**-40.3906**
LAC 201	ML	-3.1975	-36.7002	-5.7739	-4.6849	-7.0951	-0.0220	-0.2276	-0.0042	4.2842	-0.0373	-53.4585
	MH	-5.0305	-7.1590	-4.7000	-3.8827	-5.2623	-0.0464	-0.1580	-0.0064	8.5711	-0.0225	-17.6967
	Mean	*-4.1140*	*-21.9296*	*-5.2370*	*-4.2838*	*-6.1787*	*-0.0342*	*-0.1928*	*-0.0053*	*6.4277*	*-0.0299*	**-35.5776**
LAC 157	ML	-4.3779	-23.9739	-9.8326	-4.4736	-5.5721	-0.0394	-0.1800	-0.0093	-3.7148	-0.0325	-52.2062
	MH	-4.2270	-18.3945	-6.3014	-3.9281	-4.9232	-0.0441	-0.1467	-0.0087	0.6589	-0.0276	-37.3423
	Mean	*-4.3024*	*-21.1842*	*-8.0670*	*-4.2009*	*-5.2477*	*-0.0418*	*-0.1633*	*-0.0090*	*-1.5279*	*-0.0300*	**-44.7742**
LAC 481	ML	1.2819	-28.1444	-3.0562	-4.0748	-4.4968	0.1466	-0.2097	0.0016	-5.6227	-0.0438	-44.2182
	MH	-1.4406	-11.5752	-2.1558	-3.4270	-2.8795	0.0485	-0.1303	0.0000	-13.0661	-0.0292	-34.6551
	Mean	*-0.0793*	*-19.8598*	*-2.6060*	*-3.7509*	*-3.6882*	*0.0976*	*-0.1700*	*0.0008*	*-9.3444*	*-0.0365*	**-39.4366**
LAW 239	ML	-3.2071	-9.4752	-1.2560	-3.0480	-1.1884	0.1314	-0.1427	-0.0064	-13.3939	-0.0043	-31.5908
	MH	-5.1390	26.3636	0.0385	-1.6682	2.4316	0.0166	-0.0825	-0.0083	5.6317	0.0231	27.6071
	Mean	*-4.1731*	*8.4442*	*-0.6087*	*-2.3581*	*0.6216*	*0.0740*	*-0.1126*	*-0.0074*	*-3.8811*	*0.0094*	**-1.9919**
LAW 469	ML	-0.8928	-26.0315	-2.9113	-2.3452	-1.7881	0.0171	-0.1282	-0.0040	-9.4252	-0.0189	-43.5281
	MH	-3.0370	-11.4981	-2.4523	-2.1663	-1.0162	0.0435	-0.0866	-0.0083	-13.5554	-0.0045	-33.7813
	Mean	*-1.9649*	*-18.7648*	*-2.6818*	*-2.2557*	*-1.4022*	*0.0303*	*-0.1074*	*-0.0062*	*-11.4903*	*-0.0117*	**-38.6547**
LAW 391	ML	2.5947	-33.5872	-1.6623	-1.1049	-1.7271	0.0728	-0.1090	0.0032	-13.0173	-0.0205	-48.5576
	MH	0.1991	-13.1625	-1.3824	-0.8577	-0.5954	0.0572	-0.0321	-0.0009	-2.4640	-0.0139	-18.2526
	Mean	*1.3969*	*-23.3749*	*-1.5223*	*-0.9813*	*-1.1612*	*0.0650*	*-0.0706*	*0.0012*	*-7.7406*	*-0.0172*	**-33.4051**
VIC 409	ML	1.3479	-9.2902	-1.5431	0.5630	-1.6563	0.0426	-0.1261	-0.0012	27.2810	-0.0136	16.6040
	MH	-0.0480	-16.2776	-2.8188	-0.1173	-1.3465	0.0054	-0.1033	-0.0009	18.2188	-0.0051	-2.4933
	Mean	*0.6500*	*-12.7839*	*-2.1810*	*0.2228*	*-1.5014*	*0.0240*	*-0.1147*	*-0.0010*	*22.7499*	*-0.0094*	**7.0553**

[a] Microtopographic positions: ML = microlow, MH = microhigh.

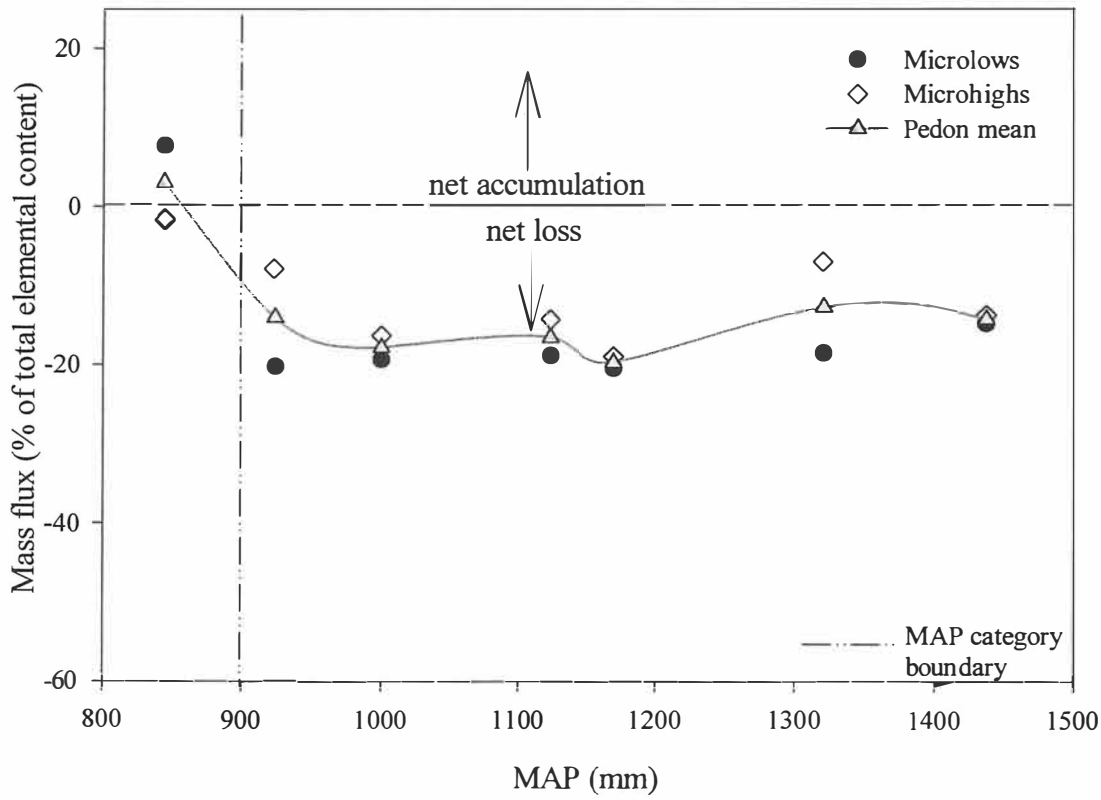

Figure 3-15. Mass flux as a function of MAP.

surface horizons. The overall mass flux assessments can differentiate only two broad precipitation regimes at > or < 900 mm MAP.

3.5 Conclusions

Geochemical mass balance trends in the Vertisol climosequence profile are comparable, with most of the ten elements examined showing reponses to MAP. The complex fluvio-deltaic sediments serving as parent material for the climosequence Vertisols were similar enough to allow for meaningful mass-balance comparisons on a whole-soil basis across the entire MAP range. Using Ti rather than Zr as the immobile element in this clay-enriched setting allowed for a conservative strain factor and maximized the likelihood that mass-balance trends are the products of actual geochemical changes, rather than responses to shifts in particle-size fraction. Only one pedon out of eight (LAW 239) showed significant evidence of erosional truncation and overprinting. It was not included in the final mass flux comparison.

Some mass-balance trends can be directly correlated to intensity of precipitation, whereas others are related indirectly through clay illuviation and biocycling. Mass-balance trends varied not only between locations, but also between microtopographic (microhigh and microlow) positions within each Vertisol pedon. Most Vertisol microlows show greater translocation and material losses than microhighs, although both have experienced net mass losses in all but the driest pedon. Basic trends in the climosequence profiles fall into four broad categories depending on the relative mobility and geochemical reactivity of the

individual elements: 1) framework, 2) clay fraction, 3) leachable/biocycle, and 4) climatic/redox-sensitive. Net mass flux percentages show that climosequence Vertisol pedons with MAP > 900 mm have achieved a relative steady-state with a net material loss of approximately -16% (±3%), with slightly less loss in microhighs. The driest Vertisol pedon had a net mass flux gain of around +3%, and the microlow gain was greater than the microhigh. In this pedon, high gains of silicon, particularly in the microlow, suggest that accumulation of aeolian silt and sand is outstripping weathering and these soils are not within the same geochemcial constraints as wetter Vertisol pedons.

Mass-balance relationships of individual elements allow for relatively fine-resolution comparisons to be made between U.S. Soil Taxonomy-designated series in the Vertisol climosequence. Most depth trends fall within relatively narrow MAP regimes, as the series are somewhat constrained to specific moisture regimes. Net mass flux trends gave only broad MAP resolution, essentially differentiating only two MAP regimes. The comprehensive trends noted in the modern Vertisols under known environmental conditions can now be compared with paleo-Vertisols to assess post-pedogenic changes and to reinforce their usefulness in paleoenvironmental reconstructions.

Chapter 4

Pedogenic Iron-Manganese Nodules in Vertisols: A New Proxy for Paleoprecipitation?

4.1 Abstract

The total Fe content of pedogenic iron-manganese (Fe-Mn) nodules taken from a Vertisol climosequence on the Texas Gulf Coastal Plain correlates with mean annual precipitation (MAP, $r^2 = 0.92$). No significant trend of Fe_{TOT} with depth was noted in profiles. Using the regression developed from modern Vertisol data, Fe_{TOT} contents of Paleozoic paleo-Vertisol Fe-Mn nodules yielded MAP regimes comparable to previously inferred paleoenvironmental interpretations. Paleoprecipitation estimates derived from Fe-Mn nodules for an uneroded, Late Mississippian paleo-Vertisol are very close to estimates determined from a depth-to-pedogenic-carbonate horizon (DCH) proxy determined from the modern Vertisol climosequence. Because the Fe-Mn nodule proxy is independent of depth, it provides consistent paleoprecipitation estimates even in eroded paleo-Vertisols and, in combination with the DCH, may be useful in determining original paleosol thickness.

4.2 Introduction

Pedogenic iron and manganese (Fe-Mn) minerals are abundant in many soils, commonly precipitating as macroscopically visible nodules (glaebules) or concretions (McKenzie, 1989; Schwertmann and Taylor, 1989). Nodules form authigenically from extant Fe and Mn pools in soils; the predominant mineralogy is controlled by soil environmental conditions, particularly the oxidation state, pH, and ionic strength of soil solution. All of

these factors vary with free-water availability; thus, formation of pedogenic Fe-Mn nodules in relatively uniform-textured soils on similar landscape positions is largely dictated by precipitation trends.

Pedogenic Fe-Mn nodules occur most frequently in fine-textured (silt- or clay-rich) soils with restricted permeability or imperfect drainage under moderate continental to warm subtropical temperature regimes. Vertisols, an order in Soil Taxonomy which are characterized by both high clay content and shrink-swell potential (Soil Survey Staff, 1998), may contain abundant pedogenic Fe-Mn nodules. Vertisols are well-preserved in the geologic record (Mora and Driese, 1999; Driese et al., 2000) and paleo-Vertisols containing Fe-Mn nodules have been identified over a range of geologic time, including the Mississippian (Caudill et al., 1996), Permian (Fastovsky et al., 1995), Cretaceous (McSweeney and Fastovsky, 1987; McCarthy et al., 1999), and Tertiary (Smith et al., 1994).

4.2.1. Formation and Preservation of Fe-Mn Nodules in Vertisols

The relationship of Fe and Mn in pedogenic nodules has been widely studied (Golden et al., 1993). The primary mode of formation is mineral dissolution and precipitation along a redox gradient (Schwertmann and Taylor, 1989) that can be either microbially or abiotically induced. Manganese oxides containing structural Mn^{4+} precipitate initially, and subsequent oxidation of Fe^{2+} by Mn^{4+} causes Fe^{3+} phases to precipitate (Golden et al., 1988). Vadose hydrology, dictated by seasonal wetting and drying cycles, is the primary control on these reactions. Hydrous Fe and Mn mineral phases (ferrihydrite, birnessite)

form in hydrochemically favorable soil micropores, proceeding to more stable crystalline lattices (goethite, lepidocrocite, hollandite) as water becomes limiting.

Pedogenic Fe-Mn nodules initially coalesce as hydrous-phase assemblages in micropores and accrete outward in concentric fashion. Nodules (Fig. 4-1A) grow displacively and incorporate resistant grains, such as quartz and zircon, into their matrix (Cescas et al., 1970). Nodules are well-formed within 3000 - 4000 yr. of pedogenic development in Vertisols (A. Robinson, 2001). Accretionary banding, as noted by White and Dixon (1996), occurs in response to seasonal deficits in soil moisture relative to phase saturation. Although individual bands may reveal a detailed history of small-scale redox variations, whole nodule compositions are integrated proxies for longer- term hydrologic conditions. The micromorphology of Fe-Mn nodules in ancient paleosols is remarkably similar to that of modern counterparts, including the accretionary growth patterns (Fig. 4-1B). Modern pedogenic Fe-Mn nodule mineralogy is dominated by goethite and lepidocrocite, whereas paleonodules are primarily hematite, reprecipitated during postpedogenic dehydroxylation (Schwertmann and Taylor, 1989).

Thin-section evidence suggests strong persistence of nodules in fine-textured matrices having low hydraulic conductivity and high base status. There are only shallow solutional halos into the matrix (Fig. 4-1B) and limited penetration into the surrounding clay. Reducing diagenetic fluids will rapidly mobilize Mn, as is witnessed by the significant Mn content in secondary diagenetic carbonate cements (Driese and Mora, 1993). However, Fe requires significantly lower eH for mobilization (Fig. 4.1 of

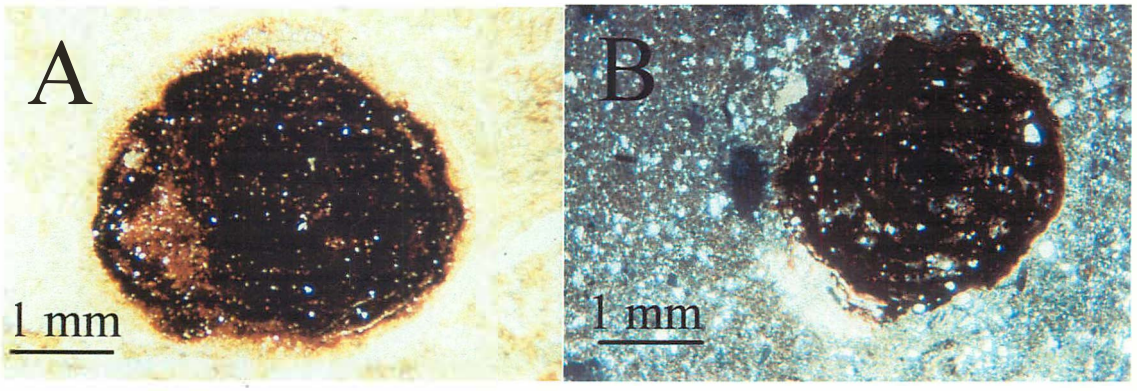

Figure 4-1. Thin-section views of pedogenic Fe-Mn nodules. A) modern Vertisol, Lake Charles series, 80 cm depth; B) Pennington Formation paleosol 2. Both views under cross-polarized light.

Vepraskis and Faulkner, 2001) and reduction of either element is inhibited because hydrogen ions are neutralized by base-saturated, smectitic clay matrices.

4.2.2. Depth to Carbonate as Precipitation Proxy

The composition of pedogenic Fe-Mn nodules provides one way of estimating the general hydrologic status of soil, but the power of such proxies in soils outside of the Vertisol order may be strengthened by using a second indicator. Depth-to-carbonate-enriched (calcic or Bk) horizons (DCH) has been utilized as a proxy for climatic conditions in several classic climosequence studies (Jenny and Leonard, 1934; Jenny, 1941b; Arkley, 1963). Secondary carbonate mineral accumulations occur just below effective meteoric infiltration. Estimations using DCH are not without problems, as comparisons between soils with widely differing textures and primary carbonate mineral contents cannot be easily made. Royer (1999) found a very weak relationship between a large data set of depths to top of carbonate horizon derived from the USDA - Natural Resource Conservation Service (NRCS) database and mean annual precipitation (MAP; $r^2 = 0.31$; $P < 0.001$). Royer (1999) suggests more robust correlations may be obtained if there is stricter control on edaphic conditions within modeled climoseries, such as vegetation type, hydraulic conductivies, and precipitation patterns. Data for both Fe-Mn nodule compositions and DCH in a series of Vertisol profiles having well-constrained pedologic conditions will provide a valid correlative data set to use with similar features found in paleo-Vertisols.

4.2.3. Hypotheses and goals

Much of the current interest in paleosols is driven by their potential value as climatic proxies of ancient environments; paleosol proxies must first be carefully defined in modern soil analogues. The bulk geochemistry of Fe-Mn nodules from a modern Vertisol climosequence (i.e., a transect of soils for which soil-forming factors are constant, except for climate) was examined in this portion of the study. Because of the strong precipitation control on both formation and mineralogy of Fe-Mn nodules, compositional variations across the climosequence should define, by proxy, differences in mean annual precipitation (MAP) for the selected sites. No previous study has investigated compositional differences within nodules on a regional climosequence scale, nor evaluated whether observed compositional trends persist into the rock record. Nor have past studies compared one precipitation estimator such as Fe-Mn nodule composition with other such indicators, i.e., DCH. With this in mind, purposes of the investigation are: 1) to derive a quantitative relationship between MAP and Fe-Mn nodule bulk chemistry using modern Vertisols, 2) evaluate its validity in the paleosol record by applying it to a suite of paleo-Vertisols for which the paleoclimate and/or paleoenvironment have been otherwise constrained, and 3) utilize DCH in combination with Fe-Mn nodule composition to estimate paleoprecipitation in one well-preserved paleo-Vertisol.

4.3 Materials and Methods

4.3.1 Geologic Setting and Sample Localities

The setting for this investigation has been described in Chapter 1 and sampling locations

for modern Vertisols are shown in Fig.1-1. Samples for this investigation were recovered from large soil pits (2m wide, 3-5m long) transecting microtopographic features peculiar to Vertisols (Lynn and Williams, 1992), herein referred to as microhighs and microlows. Bulk soil samples were collected at 10 cm intervals from microtopographic pairs to the base of each pit for geochemical analysis, and from each pedogenic horizon for bulk density. Paleo-Vertisol Fe-Mn nodules were taken from sample billets previously examined by the University of Tennessee research group, including materials from the Maccrady Formation (Middle Missisippian, West Virginia; Stefaniak et al., 1993), Pennington Formation (Upper Mississippian, Tennessee; Caudill et al., 1996), and Dunkard Formation (Lower Permian, Ohio; Fastovsky et al., 1995); paleosol locations are shown in Figure 4-2.

4.3.2 Geochemical Analysis

Modern Vertisol Fe-Mn nodules (0.125 – 2 mm) were visually separated from the coarse fraction of bulk samples shaken overnight in buffered Calgon solution. Nodules in paleosols were drilled out of billets using a ceramic dental drill bit. The <2mm nodule size may better reflect pedogenic hydrochemical conditions, as larger nodules may be relict. Collected nodules were then digested in a HF-HCL-HNO_3 solution in a microwave oven to achieve total dissolution (Nadkarni, 1984). The extracts were analyzed using a Thermo Jarrel Ash model ICAP 61 (Thermo Jarrel Ash Corp., Franklin, Massachusetts) with internal checks for extraction recovery (accuracy ±2.2%) and instrumental error (precision ±5%).

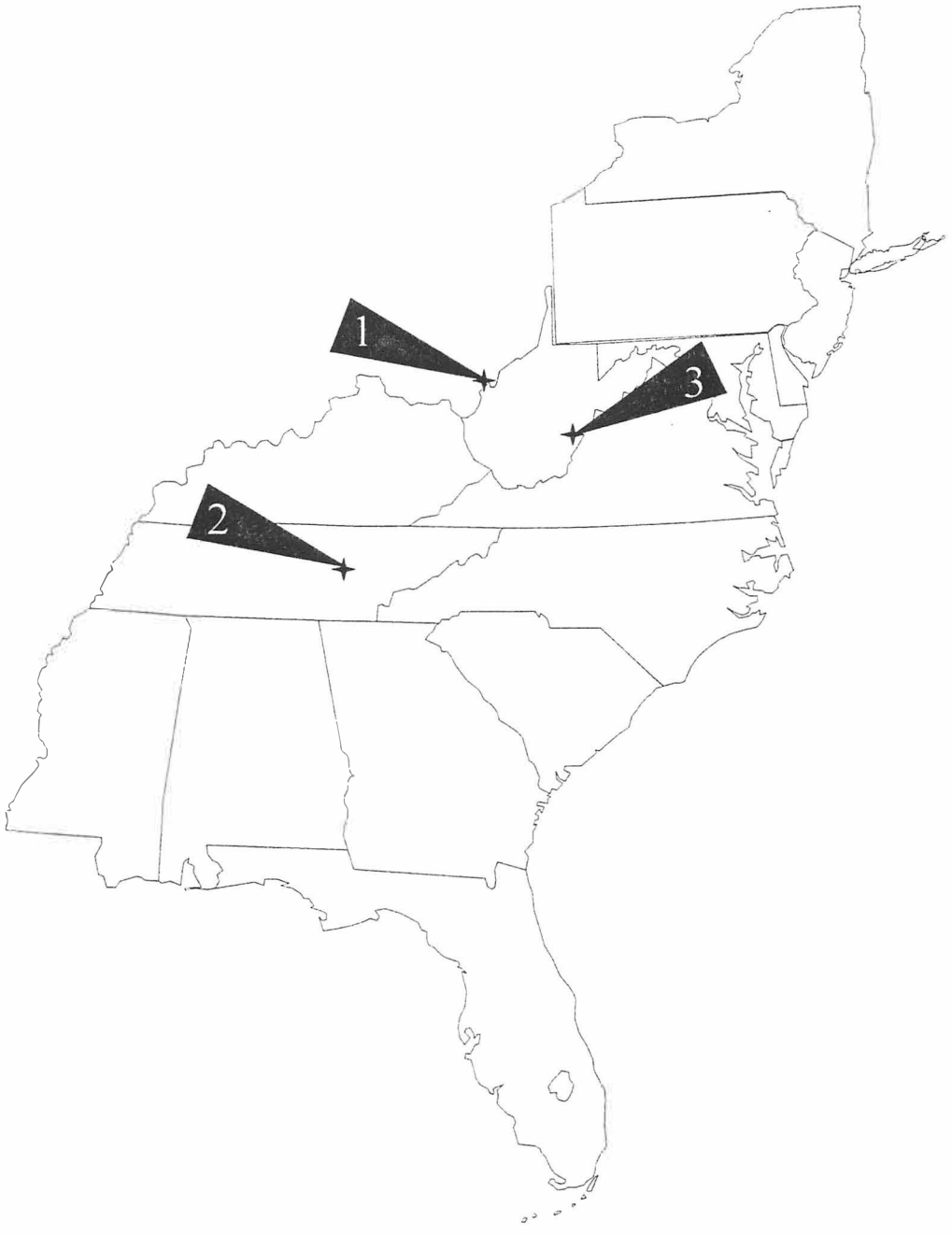

Figure 4-2. Paleosol sampling locations: 1- Dunkard Group, 2- Pennington Formation, 3 - Maccrady Formation.

Depth-to-carbonate horizon data used to determine the relationship with mean annual precipitation (MAP) were taken from field descriptions (Table A1-1) and the NRCS databases for these soils, which are available to the public at under the NRCS field pedon code listed with each profile in Table A1-1 at the National Soils Laboratory website found at www.iastate.statlab/soils.

4.4 Results and Discussion

4.4.1 Variation of Total Iron with Precipitation

The mean total Fe (Fe_{TOT}) content of nodules from eight modern Vertisol profile sets (i.e., microhigh-microlow pairs) increases linearly with increasing MAP (Fig. 4-3A). Nodules from the wettest profiles have Fe_{TOT} in the range 21.3 to 28.4 wt %, whereas the driest profiles have Fe_{TOT} of about 3 wt % (elemental compositions are given in Table A4-1 in the appendix). The MAP data are from the nearest recording station to each profile set location. The range of Fe_{TOT} within any given profile (up to 24 samples at 10 cm intervals) was limited, typically varying by only 1.8 wt % about the profile mean. Total Mn (Mn_{TOT}) shows an inverse relationship to MAP, although this trend is subdued compared to Fe_{TOT} trends. Statistical separation of Fe_{TOT} to Mn_{TOT} ratios using Duncan's Multiple Range yielded three MAP "climozones", which correlate to the modern Vertisol series moisture regimes: <900 mm (Victoria series; ustic), 900-1200 mm (Laewest and Lake Charles series; ustic to udic), and >1200 mm (League series; udic to aquic; data shown in Table A4-2). Regression analysis of mean Fe_{TOT} values for nodules versus MAP from each site yielded a regression equation of $Fe_{TOT} = -15.51 + 0.027$ MAP ($r^2 = 0.92$, $P<0.001$). Rearranging the equation as a predictive model to solve for MAP from

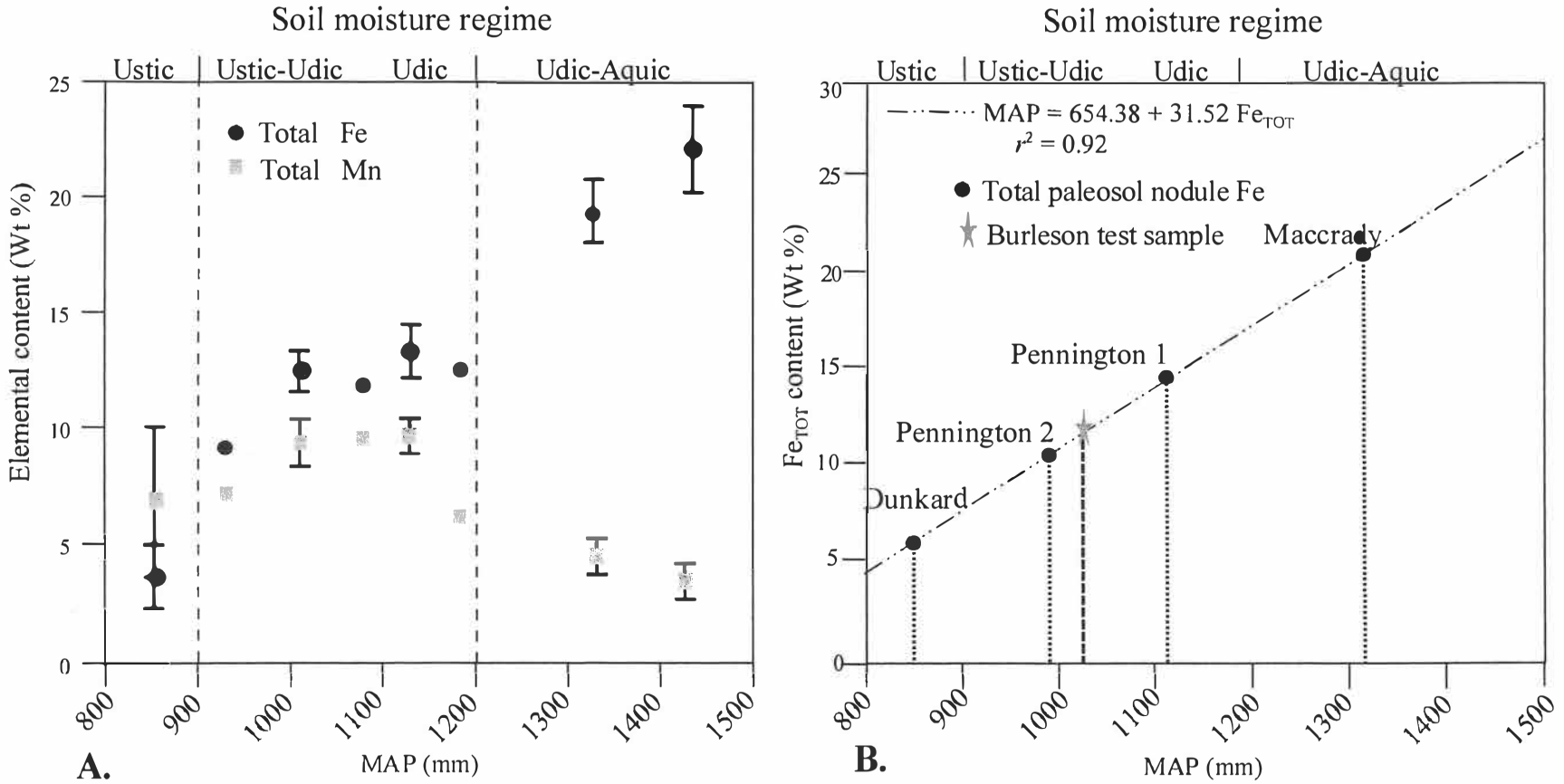

Figure 4-3. Data and regression from modern Vertisol Fe-Mn nodules. A) Mean total Fe and Mn (modern Vertisols) versus MAP; bars indicating 95% confidence intervals on data sets (points with no bars represent sets where $n \leq 4$); dashed lines define climozones; B) Regression relationship between modern Vertisol Fe_{TOT} and MAP, with Burleson test sample and projected paleoprecipitation estimates for Appalachian paleosols.

nodule Fe_{TOT} gives an equation of MAP = 654.38 + 31.52 Fe_{TOT} (Fig. 4-3B).

To test the regression relationship, the predictive equation was applied to previously published Fe-Mn nodule data reported for a Burleson series Vertisol pedon near College Station, Texas, formed on 16 ka Brazos River alluvium (White and Dixon, 1996). Mean nodule Fe_{TOT} in the Burleson soil was 11.61 ± 0.26 wt %, yielding an MAP estimate of 1020 ± 8 mm (Fig. 4-3B), within 3.5% of the actual measured 985 mm MAP for the nearest recording station.

4.4.2 Proxy for Paleoprecipitation

Previous workers identified examples of Paleozoic paleo-Vertisols for which the paleosol moisture regime can be inferred, on the basis of interpretive features in the paleosols as well as the enclosing stratigraphy (Table 4-1). All of these paleosols contain Fe-Mn nodules, which were analyzed for Fe_{TOT} content. These analyses and the linear relationship derived from modern Vertisols were used to determine paleoprecipitation estimates for the paleo-Vertisols (Fig. 4-3B). Post-pedogenic transformation of goethite to hematite, other constituents being equal, would produce slightly larger Fe_{TOT} in the paleosol nodules and, thus, slightly higher predicted MAP. No corrections were applied to the paleosol data presented here.

Nodule composition in a paleosol in the Maccrady Formation (mean Fe_{TOT} = 20.9 wt %), interpreted to have formed under conditions of relatively high soil moisture and relatively wet paleoclimate compared to the other paleosols examined, had a predicted MAP of

Table 4-1. Paleosol outcrop features and paleoclimate interpretation

Group or formation	Age (Ma)	Interpretive features	Estimated paleoclimatic regime and corresponding Vertisol series
Maccrady Fm.	350-353	High sinousity channel fills Abundant coal measures Strongly gleyed fabric	Udic-Aquic regime (soil moisture not seasonally limited); League series
Pennington Fm. (P1)	332-335	Paleokarst Limited coal measures	Udic regime with some seasonal limitations; Lake Charles series
Pennington Fm. (P2)	332-335	Evaporite pseudomorphs Sabkha-type restricted basins	Udic-Ustic regime (noticeable seasonal moisture deficit); Laewest series
Dunkard Grp.	280-292	Extensive redbeds Absence of plant traces	Ustic regime (seasonal to constant moisture deficit); Victoria series

1314 mm, roughly equivalent to the League series of eastern Texas. Nodules in Pennington Formation paleosols (two examples, mean Fe_{TOT} = 14.7 & 10.6 wt %, respectively), interpreted to have formed in humid to semi-arid paleoenvironments, had predicted MAP values of 1117 and 989 mm, equivalent to the Lake Charles and Laewest series, respectively. The Dunkard Formation paleosol nodules (mean Fe_{TOT} = 6.1 wt %) predicted MAP of 846 mm, equivalent to the Victoria series. On the basis of various paleosol and stratigraphic interpretive features, these paleosols formed under the driest conditions. Thus, in each case, the MAP predicted by Fe_{TOT} in pedogenic Fe-Mn nodules from paleo-Vertisols, a proxy quantified in analogous modern soils, corresponds well with independently derived interpretations of the paleoclimate and ancient soil moisture regime.

4.4.3 Comparison with Depth to Pedogenic Carbonate Horizons

Using field descriptions from the Vertisol microlow profiles and MAP data for the nearest recording stations, a linear relationship between MAP and DCH (Fig. 4-4) was

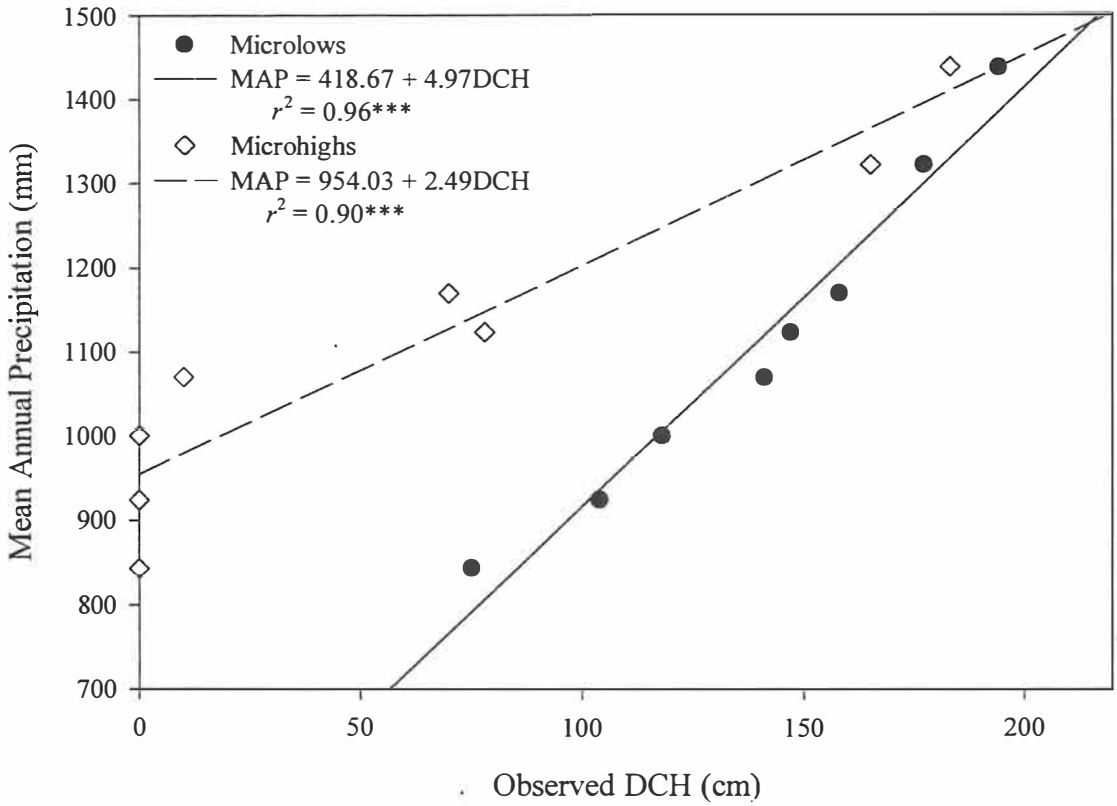

Figure 4-4. Mean annual precipitation as a function of DCH in modern Vertisol microtopographic positions. *** indicates significance at $P \geq 99\%$.

defined. This relationship is expected to be strong because of tightly constrained parent material and soil texture across the Vertisol climosequence. Measurements from both microhighs and microlow profiles show strong linear relationships From this data set, primary regression equations of DCH = -75.54 + 0.19 MAP (r^2 = 0.96, P<0.001) for microlows and DCH = -337.50 + 0.36 MAP (r^2 = 0.90, P<0.001) for microhighs, were obtained. Rearranged to predict MAP from DCH, the linear relationship is MAP = 418.67 + 4.97 microlow DCH and MAP = 954.03 + 2.49 microhigh DCH (Fig. 4-4). Microlows show their conservative nature, as MAP required for surface expression of pedogenic carbonate are less than half that shown in the microhigh relationship (419 mm vs 954mm). The intercept of the microlow linear regression is similar to Jenny and Leonard's (1934) relationship of 420.2 + 2.32DCH derived from 104 samples taken along a climatic gradient from eastern Colorado to central Missouri. Microhighs had functional slopes similar to the equations summarized in Royer (1999), which ranged from 1.19 to 3.73, and steeper slopes in the microlows are most likely an expression of the low hydraulic conductivities of smectitic clays, which tend to concentrate in these features.

Two problematic aspects of DCH proxies in paleosols are erosional truncation and/or compaction, which decreases apparent DCH and leads to underestimation of paleoprecipitation. Paleo-Vertisol microlows are less likely to be eroded, because of their low relief and higher overall clay content, thus, the microlow DCH curve is more useful for paleo-Vertisol paleoprecipitation estimates. Using the paired comparison of DCH and Fe-Mn nodule composition should clarify some of these confusing post-

pedogenic factors. Within the Paleozoic paleo-Vertisol database, only Pennington Formation paleosol 2 preserves a microlow profile that is considered complete (Caudill et al., 1996). A cross-check of both (paleo)precipitation proxies is thus possible. Caudill et al. (1996) noted pre-burial DCH of 100 cm and estimated paleoprecipitation to have been 648 ± 141 mm, on the basis of Retallack's (1994) relationship and accounting for an estimated 10% compaction. This estimate would be revised to 916 mm if the modern Vertisol regression relationship is used (Fig. 4-5). Paleoprecipitation based on the Fe_{TOT} of Fe-Mn nodules in this same paleosol was 989 mm, within 8% of the DCH estimate. This cross-check suggests that DCH may indeed "work," provided that a relationship is derived in analogous modern soils and there has been complete preservation of the soil (now paleosol) profile, and it further reinforces the value of Fe-Mn nodule chemistry as a paleohydrology indicator.

4.4.4 Determining Paleosol Erosion

Whole Fe-Mn nodule compositions do not exhibit lateral or depth trends, varying only slightly about the whole pedon mean. Thus, nodules collected from any part of a truncated paleosol yield Fe_{TOT} - MAP proxy data. In cases where paleosols contain pedogenic carbonates, Fe_{TOT} - MAP proxy can be used in combination with the preserved DCH to reconstruct original paleosol thickness. Such information is useful when determining pedogenic maturity – indicative of exposure time and climatic intensity – along with the energy of transgressive erosional post-pedogenic events.

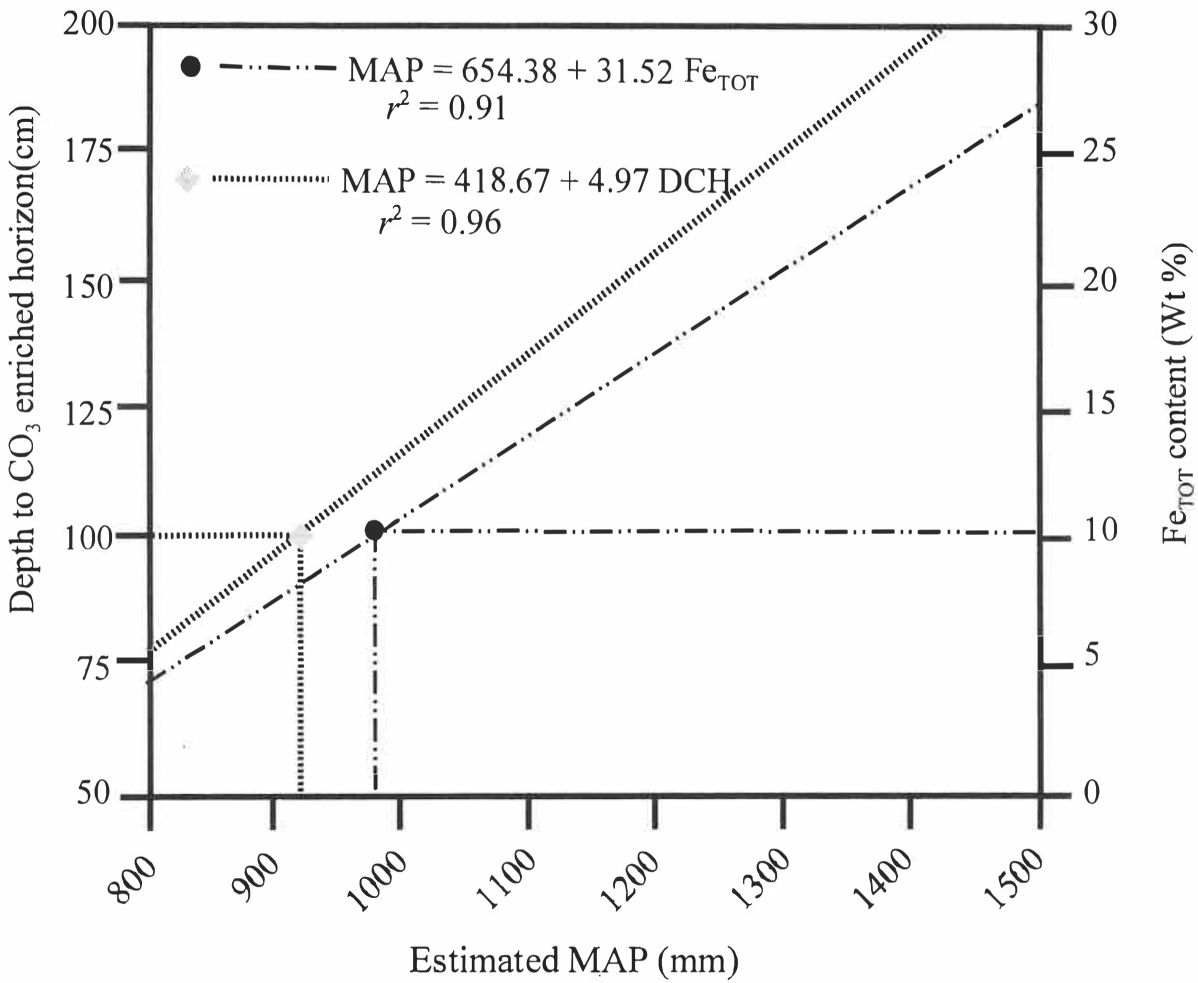

Figure 4-5. Paleoprecipitation estimates for Pennington Formation paleosol 2 based on nodule Fe_{TOT} and DCH from modern Vertisols.

4.5 Conclusions

Iron-manganese nodules, present in many fine-textured modern soils and preserved paleosols, provide an excellent and robust paleoclimate proxy. The Fe_{TOT} content of these nodules is easily analyzed and has a linear relationship with MAP that translates well between the modern and ancient setting, *provided that the soil type is analogous.* Paleo-Vertisol precipitation regimes estimated from this proxy agree well with paleoenvironmental interpretations based on a range of soil textural and mineralogical and stratigraphic evidence. Paleoprecipitation estimates based on Fe-Mn nodules can be used to reconstruct the original DCH and thus provide a mechanism for determining the extent of paleosol erosion.

Chapter 5

Overall Conclusions and Future Research

5.1 Modern Climosequence Vertisols - What Do They Tell Us?

The primary purpose of this research was to determine baseline Vertisol geochemical trends in a well-constrained pedogenic setting that may serve as a comparative baseline for understanding the pedogenic environment of Appalachian paleo-Vertisols. A secondary purpose was to test mass-balance applications to soils formed in complex fluvio-deltaic deposits analogous to many of the parent sediments of paleo-Vertisols. The final goal was to ascertain whether geochemical signatures formed in response to climatic forcing and easily deduced from modern Vertisol data, could be translated for applications to paleo-Vertisols, to give finer resolution to paleoclimate reconstructions.

The Texas climosequence Vertisols revealed a relatively straight-forward picture of their pedogenic behavior. Essentially, these soils have reached a relative steady state within their formational environment, and differences in geochemical trends between pedons are signatures of hydrogeochemical and physical actions under the long-term influences of climate. Despite discernible differences in sedimentary material from different fluvial sources, the overall power of mass-balance comparison is supported by the similarity in geochemical compositions of deep parent material samples, as well as the conservative behavior of the strain-indicator element, titanium (Ti), within the profiles. Deciding which element to use as a strain indicator is an important step and preliminary examination of thin-sections and individual heavy mineral grains assists in the choice. Textural

classification based on surface features of the minerals which concentrate the indicators helps with the decision, but in lithified paleo-Vertisols, thin-section examination must be carried out to ensure proper choice.

The mass-balance trends show that these soils behave conservatively, losing only an average of 15% of their total volumetric elemental content over the extent of their pedogenic exposure (35 ka). Translocation of most elements is ascribable to precipitation regime (MAP), and patterns of translocation with depth of individual elements can be grouped into broader categories of elements which behave in similar fashion. Some elements, such as phosphorus (P), are lost completely in the super-active solum, but are retained at depth. Can these fine-resolution geochemical trends can be discerned in paleo-Vertisols? Presently, trends in net mass flux can only discern two broad MAP regimes, above or below 900 mm. More useful tools may indeed be pedogenic minerals such as pedogenic carbonate and the small glaebular iron-manganese (Fe-Mn)nodules, which apparently capture evidence of pedogenic conditions, and hold it in translatable form through advancing pedogenesis and eventual burial diagenesis.

5.2 Future research

The work ahead involves looking in more detail at the climosequence components, fine-tuning the mass-balance methodology, and comparing the baseline data with paleo-Vertisols and other modern soil types.

5.2.1 Strain elements

The two most problematic issues presently plaguing the validity of mass-balance relationships are: 1) which elements behave truly conservatively in weathering profiles regardless of composition and textural considerations and 2) how can true protolith or parent material composition be resolved, particularly in complex fluvial and alluvial depositional systems? With increasingly sensitive analytical capability, more and more elements can be routinely assessed with greater accuracy. Recent studies (Hill et al., 2000, and Kurtz et al., 2000) have already suggested the use of rare earth or trace elements such as yttrium(Y), niobium (Nb), and tantalum (Ta), elements not normally quantified in soil analyses, as ideal indicators of weathering intensity and protolith volumetric loss. Where do these elements lie within the mineralogical framework of the weathering profile? Brimhall et al. (1991b) suggested that these elements may be found in zircon, but this is not yet substantiated. There is some indication that these elements may be associated with iron (Fe) oxides, and are thus susceptible to relocation in profiles within secondary Fe oxyhydroxide minerals. The stable thermodynamics of the transition (4d) elements suggests they will reside within the mineral phase until total disintegration, and it is an intuitive suggestion that these grains will become finer and finer with age. No studies have been carried out to discern the size fraction in which most potentially immobile elements reside, and whether or not the overall trend of element accumulation is a function of true volume loss or gain, or a relict of particle size distribution.

Protolith, or parent material, composition will always be problematic in alluvial settings.

Alluvial parent materials are nearly impossible to ascertain on an absolute basis, as the materials have undergone numerous phases of reworking prior to depositions. In conducting regional comparisons such as this, statistical constraints are a necessary pre-requisite, to minimize the differences which may be caused by localized events. A suggestion for any study in which parent material compositions may be questionable is to take several samples from throughout the extent of the deposit studied and derive a composite proxy.

Three suggestions for future research in this area can be made. First, further analysis of climosequence whole soil samples for trace elements such as Y, Nb, Ta, and the rare earth elements (REE) may determine if any of these elements are more effective at determining volumetric losses and translocation, and if their behavior is comparable to Ti-based trends. The second effort would involve similar analysis on size-fraction separates from the same soil samples, to determine which size fraction predominantly controls strain and whether the strain expressed is a true volume change or an artifact of particle-size distribution. Finally, the third effort would determine if the size fractions are truly representative of the soil itself, or indicate exotic introductions, similar to the study conducted by Brimhall et al. (1991b). This project would involves examining silt- and sand-sized fractions from shallow and deep domains to determine any fundamental differences in the geochemistry. This analysis might include chronometric measurements and electron microprobe analysis of individual grains, with the idea that if the weathering profile is indeed uniform throughout, then trace element geochemistry and general age will show low variance

within the profile.

5.2.2 Mass Balance Relationships

No attempt was made in this study to compare the translocation trends found in the climosequence with paleosol data. This is a necessary next step. With the assistance of the Fe-Mn nodule paleoprecipitation and the depth-to-carbonate-enriched horizons (DCH) relationships defined in Chapter 4, the mass-balance trends of paleosols containing these features may be compared with modern analog baselines presented in Chapter 3. The Fe-Mn / DCH depth reconstruction process resolves the problem of mass-balance depth functions being rendered useless due to post-pedogenic paleosol erosion and truncation. Thus, a whole series of comparisons can begin. First, which mass-balance trends are best preserved in the paleosols? One-to-one comparisons of elemental trends between paleosols and analog climosequence Vertisols can proceed once Fe-Mn nodule paleoprecipitation and DCH depth reconstruction are resolved. The most important finding here would be to determine post-pedogenic/diagenetic changes which occur in the paleosols.

Another implication for future research efforts lies in the utility of net mass-flux assessments in different soil types. The net mass-flux analysis in this study indicates that Vertisols are geochemically conservative soils, losing only around 16% or their total parent material compositions. Caudill et al. (1997) demonstrated that paleo-Vertisols are conservatively compacted in the rock record. Are Vertisols the *most* conservative soil

order? With more studies of surface processes relying on net mass flux assessments, it will soon be possible to compile comparisons of different soils orders with respect to elemental translocations. For example, silicon (Si) is conservative in the Vertisols measured in this study, losing no more that 10.6% within any one profile (Table 3-3), yet Si has been shown to be lost to a much greater extent in Costa Rican Andisols (up to 93% of parent composition; Nieuwenhuyse and van Breeman, 1997) and in California coastal Alfisols (around 50% of parent composition; Chadwick et al., 1990). Perhaps the conservative nature of Vertisols is a relict of their derivation from reworked alluvial material. It would be useful to study a set of Vertisols formed in residuum, such as those formed on basalt in India or central Africa. This might also help with the previously mentioned research efforts involving strain analysis - as the residual soils should not experience extensive overwash additions.

Vertisols are currently being submerged by gradually rising sea levels along the Texas Gulf Coast (Wes Miller, personal communication, 2000), permitting an expansion of modern analog studies to evaluate the effects of early post-pedogenic effects of sea-water incursion. Many occurrences of paleo-Vertisols in the Appalachian Foreland Basin successions are overlain by transgressive marine surfaces. The mass-balance trends noted in this study may serve as baselines to determine the effects of post-pedogenic marine influences on the Vertisols as they began the transformation from soils to palesols.

Three efforts for further study using mass-balance relationships are presented here. First,

comparison of mass-balance trends in reconstructed paleo-Vertisols with their modern analogs to determine post-pedogenic alterations. Secondly, net mass-flux comparisons between the alluvially-derived climosequence Vertisols with residually-derived Vertisols, and the overall comparison of Vertisol geochemical conservation with mass-flux trends found in other soil types. Finally, determining mass-balance relationships within Vertisols being invaded by sea water along the Texas Gulf Coast will give greater insight into early post-pedogenic effects, and may help to prove the conservative nature of these soils.

5.2.3 Iron-Manganese Nodule Geochemistry

The finding that Fe-Mn nodule Fe composition can serve as a proxy for precipitation regime lays the groundwork for much more research. In this study, only the whole nodule trends from whole profiles were utilized, but these larger nodules have concentric growth habits incorporating other minerals and pores within them. For pedologists, Fe-Mn nodules have always been evidence of fluctuating Eh-pH conditions and have been otherwise ignored for interpretive power. The preliminary work in this study suggests there are much broader applications for these features, which are often found in paleo-Vertisols.

Further research efforts involving the Fe-Mn nodules from modern soils include: 1) microscopic examination of internal structure and mineralogical composition; 2) Determination of elemental compositions within bands of larger nodules to determine if relict paleohydrologic regimes are present; 3) Expanding the comparison to include Fe-Mn

nodules from other soil types, such as Ultisols, Andisols, and Alfisols, which have textural differences from the clay-rich setting of this investigation. Paleo-nodules could also be examined for mineralogic composition and slight geochemical variations within large nodule transects. Another aspect of this research effort is documenting the complex relationship these features have with pedogenic carbonates. As MAP decreases, the Fe-Mn nodules in the climosequence are enriched with Mn and alkaline earth elements, suggesting that siderite ($FeCO_3$) and rhodochrosite ($MnCO_3$) are more likely to be formed than the Fe/Mn-oxyhydroxides found in the wetter MAP soils.

The integration of all the aspects of this study will strengthen the relationship between modern pedology and paleopedology. Using modern analog settings to define what is found within the rock record is a basic tenet of the uniformitarianist theory of geology. We cannot know what is in the distant past, but we can know what happens within recent times - and use that knowledge to expand our comprehension of an ever-evolving Earth.

References

Ahmad, N., 1983, Vertisols: p. 91-123 *In* Wilding, L.P., Smeck, N.E., and Hall, G.F., (eds.) Pedogenesis and soil taxonomy. II: The soil orders, Amsterdam, Elsevier Scientific Publishing.

Arkley, R.J., 1963, Calculation of carbonate and water movement in soil from climatic data: Soil Science, v. 96, p. 239-248.

Aslan, A., and Autin, W.J., 1998, Holocene flood-plain soil formation in the southern lower Mississippi Valley: implications for interpreting alluvial paleosols: Geological Society of America Bulletin, v. 110, p. 433-449.

Bernal, J.O., Dasgupta, D.R., MacKay, A.L., 1959, The oxides and hydroxides of iron and their structural interrelationships: Clay Minerals Bulletin, v. 4, p. 15-30.

Bernard, H.A., and LeBlanc, R.J., 1965, Resumé of the Quaternary geology of the northwestern Gulf of Mexico province: *In* Wright, H.E., and Frey, D.G., (eds.) The Quaternary of the United States: Princeton, New Jersey, Princeton University Press, p. 137-185.

Birdseye, H.A., and Aronow, S., 1991, New evidence for a young late Wisconsin age for the Prairie Formation, Texas, USA: Geological Society of America, Abstracts with Programs, v. 23, p. A223.

Birkeland, P.W., 1999, Soils and Geomorphology (Third Edition): Oxford University Press, New York, 430 p.

Blake, G.R., and Hartge, K.H.,1986, Bulk density: *In* Klute, A., (ed.) Methods of Soil Analysis, Pt. 1. Physical and Mineralogical Methods, Agronomy Monographs 9 - 2nd edition, Madison, WI, American Society of Agronomy, p. 363-375.

Blum, M.D., and Price, D.M., 1994, Glacio-eustatic and climatic controls on Quaternary alluvial plain deposition: Texas Coastal Plain: Gulf Coast Association of Geological Societies Transactions, v. 44, p. 85-92.

Bomar, G.W., 1995, Texas Weather: Austin, TX, University of Austin Press, 275 p.

Brewer, R., 1964, Fabric and Mineral Analysis of Soils: New York, Wiley and Sons, 470 p.

Brimhall, G.H., Alpers, C.N., and Cummingham, A.B., 1985, Analysis of supergene ore-forming processes and ground-water solute transport using mass balance principles: Economic Geology, v. 80, p.1227-1256.

Brimhall, G.H., and Dietrich, W.E., 1987, Constitutive mass balance relations between chemical composition, volume, density, porosity, and strain in metasomatic hydrochemical systems: results on weathering and pedogenesis: Geochimica et Cosmochimica Acta, v. 51, p. 567-587.

Brimhall, G.H., Chadwick, O.A., Lewis, C.J., Compston, W., Williams, I.S., Danti, K.J., Dietrich, W.E., Power, M.E., Hendricks, D., and Bratt, J., 1991a, Deformational mass transport and invasive processes in soil evolution: Science, v. 255, p. 695-702.

Brimhall, G.H., Lewis, C.J., Ford, C., Bratt, J., Taylor, G., and Warin, O., 1991b, Quantitative geochemical approach to pedogenesis: importance of parent material reduction, volumetric expansion, and eolian influx in laterization: Geoderma, v. 51, p. 51-91.

Brimhall, G.H., Compston, W., Williams, I.S., Reinfrank, , R.F., and Lewis, C.J., 1993

Darwinian zircons as provenance tracers of dust-sized exotic components in laterites: mass-balance and SHRIMP ion microprobe results: *In* Ringrose-Voase, A.J., and Humphreys, G.S., (eds.) Soil micromorphology - studies in management and genesis, Developments in Soil Science, v. 22. Amsterdam, Elsevier Science Publishers, p. 65-81.

Bullock, P., Federoff, N., Jongerius, A., Stoops, G., Tursina, T., and Babel, U., 1985, Handbook of Soil Thin Section Description: Wolverhampton, United Kingdom, Waine Research Publications, 152 p.

Caudill, M.R., Driese, S.G., and Mora, C.I., 1996, Preservation of a paleo-Vertisol and an estimate of late Mississippian paleoprecipitation: Journal of Sedimentary Research, v. 66, p. 58-70.

Caudill, M.R., Driese, S.G., and Mora, C.I., 1997, Physical compaction of vertic palaeosols: implications for burial diagenesis and palaeo-precipitation estimates: Sedimentology, v. 44, p. 673-685.

Cescas, M.P., Tyner, E.H., and Harner, R.S., III., 1970, Ferromanganiferous soil concretions: A scanning electron microscope study of their micropore structures: Soil Science Society of America Proceedings, v. 34, p. 641-644.

Cerling, T.E., Quade, J., Wang, Y., and Bowman, J.R., 1989, Carbon isotopes in soils and palaeosols as ecology and palaeoecology indicators: Nature, v. 341, p. 138-139.

Chadwick, O.A., Brimhall, G.H., Hendricks, D.M., 1990, From a black to a gray box - a mass balance interpretation of pedogenesis: Geomorphology, v. 3, p. 369-390.

Chadwick, O.A., and Chorover, J., 2001, The chemistry of pedogenic thresholds:

Geoderma 100:321-353.

Chadwick, O.A., and Davis, J.O., 1990, Soil-forming intervals caused by eolian sediment pulses in the Lahontan Basin, northwestern Nevada: Geology, v.18, p. 243-246.

Chadwick, O.A., and Nettleton, W.D., 1993, Quantitative relationships between net volume change and fabric properties during soil evolution: *In* Ringrose-Voase, A.J., and G.S. Humphreys (eds.) Soil Micromorphology - Studies in Management and Genesis, Developments in Soil Science v. 22, Amsterdam, Elsevier Science Publishers, p. 353-359.

Chadwick, O.A., Olson, C.G., Hendricks, D.M., Kelley, E.F., and Gavenda, G.T., 1994, quantifying climatic effects on mineral weathering and neoformation in Hawaii: Proceedings of the 15th International Soil Science Congress, v. 8A, p. 94-105.

Chesworth, W., 1991, Weathering systems: *In* Martini, I.P., and Chesworth, W. (eds.) Weathering, Soils and Paleosols, Developments in Earth Science Processes 2, Amsterdam, Elsevier Science Publishers, p. 19-40.

Colin, F., Alarçon, C., and Viellard, P., 1993, Zircon: an immobile index in soils?: Chemical Geology v. 107, p. 273-276.

Correns, C.W., 1978, Titanium: *In* Wedepohl, K.H. (ed.) Handbook of Geochemistry, Berlin, Springer-Verlag, Vol.II-2, Sec. 22B-22O.

Coulombe, C.E., Dixon, J.B., and Wilding, L.P., 1996a, Mineralogy and chemistry of Vertisols: *In* Ahmad, N., and Mermut, A., (eds.) Vertisols and Technologies for their Management: Developments in Soil Science v. 24, Amsterdam, Elsevier Science Publishers, p. 115-200.

Coulombe, C.E., Wilding, L.P., and Dixon, J.B., 1996b, Overview of Vertisols: characteristics and impacts on society: Advances in Agronomy, v. 57, p. 289-375.

Cremeens, D.L., Brown , R.B., Huddleston, J.H., 1994, Whole Regolith Pedology: Soil Science Society of America Special Publication 34, Madison, WI, Soil Science Society of America, 167 p.

Darmody, R.G.,1985, Weathering assessment of quartz grains: a semi-quantitative approach: Soil Science Society of America Journal, v. 49, p. 1322-1324.

Dixon, J.B., 1982, Mineralogy of Vertisols: *In* Vertisols and Rice Soils of the Tropics: Symposia Papers II, 12th International Congress of Soil Science, New Delhi, India, p.48-59

Doering, J.A., 1956, Review of Quaternary surface formations of the Gulf Coast region: American Association of Petroleum Geologists Bulletin, v. 40, p. 1816-1862.

Driese, S.G., and Foreman, J.L., 1992, Paleopedology and paleoclimatic implications of late Ordovician vertic paleosols, Juniata formation, southern Appalachians: Journal of Sedimentary Petrology, v. 62, p. 71-83.

Driese, S.G., and Mora, C.I., 1993, Physico-chemical environment of pedogenic carbonate formation in Devonian vertic palaeosols, central Appalachia, USA: Sedimentology, v. 40, p. 199-216.

Driese, D.G., Mora, C.I., Stiles, C.A., Joeckel, R.M., and Nordt, L.C., 2000, Mass-balance reconstruction of a modern Vertisol: Implications for interpreting the geochemistry and burial alteration of paleo-Vertisols: Geoderma, v. 95, p. 179-204.

Dudal,R., and Eswaran, H., 1988, Distribution, properties and classification of Vertisols: *In* Wilding, L.P., and Puentes, R., (eds.) Vertisols: Their Distribution, Properties, Classification, and Management, Technical Monograph 18, Texas A&M Univ. Printing Center, College Station, TX, p. 1-22.

Eswaran, H., and Bin, W.C., 1978, A study of deep weathering profiles granite in peninsular Malaysia: I., Physicochemical and micromorphological properties: Soil Science Soceity of America Journal, v. 42, p. 144-149.

Fastovsky, D.E., Veeger, A.I., Strater, K.P., Mora, C.I., and Driese, S.G., 1995, Preliminary analysis of stable isotopes in vertic featured paleosols from the Dunkard Group (Permian), Ohio: Geological Society of America Abstracts with Programs, v. 27, no. 2, p. 53.

Franz, G., and Carlson, R.M., 1987, Effects of rubidium, cesium, and thallium on interlayer potassium released from Transvaal vermiculite: Soil Science Society of America Journal, v. 51, p. 305-311.

Gee, G.W., and Bauder, J.W., 1986, Particle-size analysis: *In* Klute, A., (ed.) Methods of Soil Analysis, Pt. 1. Physical and Mineralogical Methods, Agronomy Monographs 9 - 2nd ed., Madison, WI, American Society of Agronomy, p. 383-411.

Golden, D.C., Dixon, J.B., and Kanchiro, Y., 1993, The manganese oxide mineral lithiophorite in an Oxisol from Hawaii: Australian Journal of Soil Research, v. 31, p. 56-66.

Golden, D.C., Chen, C.C., Dixon, J.B., and Tokashiki, Y., 1988, Pseudomorphic replacement of manganese oxides by iron oxide minerals: Geoderma, v. 42, p.199-

211.

Gustavson, T.C., 1991, Buried Vertisols in lacustrine facies of the Pliocene Fort Hancock formation, Hueco Bolson, west Texas and Chihuahua, Mexico: Geological Society of America Bulletin, v.103, p. 448-460.

Hallsworth, E.G., Robertson, G.W., and Gibbons, F.R., 1955, Studies in pedogenesis in New South Wales. VII. The Gilgai soils: Journal of Soil Science, v.6, p. 1-31.

Harden, J.W., 1988, Genetic interpretations of elemental and chemical differences in a soil chronosequence, California: Geoderma, v. 43, p. 179-193.

Harrassowitz, H., 1926, Laterit: Fortschungeschrift vor Geologie und Paleontologie, v.4, p. 253-566.

Hartmann, D.L., 1994, Global physical climatology: International Geophysics Series, v. 56, San Diego, CA, Academic Press, 411 p.

Heimsath, A.M., Dietrich, W.E., Nishiizumi, K., and Finkel, R.C., 1997, The soil production function and landscape equilibrium: Nature, v. 388, p. 358-361.

Hill, I.G., Worden, R.H., and Meighan, I.G., 2000, Yttrium: the immobility-mobility transition during basaltic weathering: Geology, v. 28, p. 923-926.

Huang, P.M., 1989, Feldspars, olivines, pyroxenes, amphiboles: *In* Dixon, J.B., and Weed, S.B., (eds.) Minerals in Soil Environments (2nd Edition): Madison, WI, Soil Science Society of America Book Series, no. 1, p. 975-1050.

Jackson, M.L., and Sherman, G.D., 1953, Chemical weathering of minerals in soils: Advances in Agronomy, v. 5, p. 219-318.

Jenny, H., 1941a, Factors of Soil Formation: New York, McGraw-Hill, 281 p.

Jenny, H., 1941b, Calcium in the soil: III. Pedologic relations: Soil Science Society of America Proceedings, v.6, p. 27-37.

Jenny, H., and Leonard, C.D., 1934, Functional relationships between soil properties and rainfall: Soil Science, v. 38, p. 363-381.

Kabata-Pendias, A., 2001, Trace Elements in Soils and Plants: Boca Raton, FL, CRC Press, 413 p.

Kurtz, A.C., Derry, L.A., Chadwick, O.A., and Alfano, M.J., 2000, Refractory element mobility in volcanic soils: Geology, v. 28, p. 683-686.

Langley-Turnbaugh, S.J., and Bockheim, J.G., 1998, Mass balance of soil evolution on late Quaternary marine terraces in coastal Oregon: Geoderma, v. 84, p. 265-288.

Kutílek, M., 1973, The influence of clay minerals and exchangeable cations on soil moisture potential: *In* Hadas, A., Swartzendruber, D., Rijtema, P.E., Fuchs, M., and Yaron, B., (eds.) Physical Aspects of Soil Water and Salts in Ecosystems: Ecological Studies v.4, Berlin, Springer-Verlag, p. 153-160.

Lindsay, W.L., 1979, Chemical Equilibria in Soils: New York, John Wiley, 449 p.

Lindsay, W.L., Vlek, P.L.G., Chien, S.H., 1989. Phosphate minerals: *In* Dixon, J.B., and Weed, S.B., (eds.) Minerals in Soil Environments (2nd Edition): Madison, WI, Soil Science Society of America Book Series, no. 1, p. 1089-1130.

Lynn, W.C., and Williams, D., 1992, The making of a Vertisol: Soil Survey Horizons, v. 33, p. 45-50.

Mack, G.H., James, W.C., and Monger, H.C., 1993, Classification of paleosols: Geological Society of America Bulletin, v.105, p. 129-136.

Mack, G.H., and James, W.C., 1994, Paleoclimate and the global distribution of paleosols: Journal of Geology, v.102, p. 360-366.

Marbut, C.F., 1935, Soils of the United States: Atlas of American Agriculture, Pt. 3: Washington, DC, U.S. Gov. Print. Off., 127 p.

Marshall, B., 1967, The present status of zircon: Sedimentology, v. 9, p. 119-136.

Marshall, C.E., and Haseman, J.F.,1942, The quantitative evaluation of soil formation and development by heavy mineral studies: a Grundy silt loam profile: Soil Science Society of America Proceedings, v. 7, p. 448-453.

Mason, J.A., and Jacobs, P.M., 1998, Chemical and particle-size evidence for addition of fine dust to soils of the midwestern United States: Geology, v. 26, p. 1135-1138.

McCarthy, P.J., Martini, I.P., Leckie, D.A., 1999, Pedogenic and diagenetic influences on void coating formation in Lower Cretaceous paleosols of the Mill Creek Formation, Alberta, Canada: Geoderma, v. 87, p. 209-237.

McFadden, L.D., Amundson, R.G., and Chadwick, O.A., 1991, Numerical modeling, chemical, and isotopic studies of carbonate accumulations in soils or arid regions: *In* Nettleton, W.D., (ed.) Occurrence, Characteristics, and Genesis of Carbonate, Gypsum, and Silica Accumulations in Soils, Soil Science Society of America Special Publication 26, Madison, WI, Soil Science Society of America, p. 17-35.

McKenzie, R.M, 1989, Manganese oxides and hydroxides, *In* Dixon, J.B., and Weed, S.B., (eds.) Minerals in Soil Environments (2nd Edition): Madison, WI, Soil Science Society of America Book Series, no. 1, p. 439-465.

McSweeney, K., and Fastovsky, D.E., 1987, Micromorphological and SEM analysis of

Cretaceous-Paleogene petrosols from eastern Montana and western North Dakota: Geoderma, v. 40, p. 49-63.

Mermut, A.R., Padmanabham, E., Eswaran, H., and Dasog, G.S., 1996, Pedogenesis: *In* Ahmad, N., and Mermut, A., (eds.) Vertisols and Technologies for their Management: Developments in Soil Science v. 24, Amsterdam, Elsevier Scientific Publishing, p. 43-61.

Merritts, D.J., Chadwick, O.A., and Hendricks, D.M., 1991, Rates and processes of soil evolution on uplifted marine terraces, northern California: Geoderma, v. 51, p. 241-275.

Miller, D., 2000, Occurrence and stable isotope composition of soil carbonate and organic matter within a climatic transect of modern Vertisols along the coastal prairie of Texas: Masters Thesis, The University of Tennessee - Knoxville.

Millot, G., 1982, Weathering sequences, 'climatic' planations, leveled surfaces and paleosurfaces: *In* van Olphen, H., and Veniale, F., (eds.) International Clay Conference 1981, Developments in Sedimentology, v. 35, New York, Elsevier-North Holland Inc., p. 585-593.

Milnes, A.R., and Fitzpatrick, R.W., 1985, Titanium and zirconium minerals: *In* Dixon, J.B., and Weed, S.B., (eds.) Minerals in Soil Environments (2nd Edition): Madison, WI, Soil Science Society of America Book Series, no. 1, p.1131-1205.

Montgomery, D.R., Zabowski, D., Ugolini, F.C., Hallberg, R.O., and Spaltenstein, H., 2000, Soils, watershed processes, and marine sediments: *In* Jacobson, M.C., Charlson, R.J., Rhode, H., and Orians, G.H., (eds.) Earth System Science: San

Diego, CA, Academic Press, International Geophysics Series Volume 72, p. 159-194.

Mora, C.I., and Driese, S.G., 1999, Palaeoenvironment, palaeoclimate, and stable carbon isotopes of Palaeozoic red-bed palaeosols, Appalachian Basin, USA and Canada: *In* Thiry, A., and Simon-Coinçon, R., (eds.) Palaeoweathering, Palaeosurfaces and Related Continental Deposits, Special Publications of the International Association of Sedimentologists 27, p. 61-84.

Mora, C.I., Driese, S.G., and Colarusso, L., 1996, Middle to Late Paleozoic atmospheric CO_2 levels from soil carbonate and organic matter: Science, v. 271, p. 1105-1107.

Nadkarni, R.A., 1984, Applications of microwave oven sample dissolution in analysis: Analytical Chemistry, v. 56, p. 2233-2237.

Nesbitt, H.W., and Young, G.M., 1984, Prediction of some weathering trends of plutonic and volcanic rocks on thermodynamic considerations: Geochimica et Cosmochimica Acta, v. 48, p. 1523-1534.

Newman, A.L., 1986, Vertisols in Texas: Temple, TX, Soil Conservation Service, 58 p.

Nikoforov, C.C., 1949, Weathering and soil evolution: Soil Science, v. 67, p. 219-223.

Nieuwenhuyse, A., and van Breeman, N., 1997, Quantitative aspects of weathering and neoformation in selected Costa Rican volcanic soils: Soil Science Society of America Journal, v. 61, p. 1450-1458.

Nordt, L.C., Boutton, T.W., Hallmark, C.T., and Waters, M.R., 1994, Late Quaternary vegetation and climate change in central Texas based on the isotopic composition of organic carbon: Quaternary Research, v. 41, p.109-120.

Retallack, G.J., 1990, Soils of the past: an introduction to paleopedology: Boston, MA, Unwin Hyman Publishers, 520 p.

Retallack, G.J., 1994, The environmental factor approach to the interpretation of paleosols: *In* Amundson, R., Harden, J., and Singer, M.,(eds.) Factors of Soil Formation: Fiftieth Anniversary Retrospective, Soil Science Society of America Special Publication 33, Madison, WI, Soil Science Society of America, p. 31-64.

Richter, D.D., and Markewitz, D., 1995, How deep is soil? BioScience, v. 45, p. 600-609.

Robinson, A., 2001, A chronosequence study of modern Vertisols and application to interpreting the time significance of Paleozoic paleo-Vertisols: Masters Thesis, The University of Tennessee - Knoxville.

Rosenberg, N.J., Blad, B.L., and Verma, S.B., 1983, Microclimate: the Biological Environment: New York, John Wiley & Sons, 283 p.

Royer, D.L., 1999, Depth to pedogenic carbonate horizon as a paleoprecipitation indicator?: Geology, v. 27, p. 1123-1126.

Ruhe, R.V., 1984, Loess-derived soils of the Mississippi Valley region: I. Soil-sedimentation system: Soil Science Society of America Journal, v. 48, p. 859-863.

Ruhe, R.V., and Olson, C.G., 1980, Soil welding: Soil Science, v. 130, p.132-139

Sadleir, S.B., and Gilkes, R.J., 1976, Bauxite in relation to parent material: Journal of the Geological Society of Australia, v. 23, p. 333-344.

Schwertmann, U. and Taylor, R.M. 1989. Iron oxides: *In* Dixon, J.B., and Weed, S.B., (eds.) Minerals in Soil Environments (2nd Edition): Madison, WI, Soil Science Society of America Book Series, no. 1, p. 379-438.

Schwartzman, D.W., and Volk, T., 1989, Biotic enhancement of weathering and the habitability of the earth: Nature, v. 340, p. 457-460.

Shackleton, N.J., 1988, Oxygen isotopes, ice volume, and sea level: Quaternary Science Reviews, v.6, p. 183-190.

Singer, M.J., and Janitsky, P.,1986, Field and laboratory procedures used in a soil chronosequence study: U.S. Geological Survey Bulletin 1648, 49 p.

Smeck, N.E., and Wilding, L.P., 1980, Quantitative evaluation of pedon formation in calcareous glacial deposits in Ohio: Geoderma, v. 24, p. 1-16.

Smith, C.A.S., Fox, C.A., and Kodama, H., 1994, Paleosols associated with Miocene basalts, Porcupine River, northeastern Alaska: Implications for regional paleoclimates: Quaternary International, v. 22/23, p. 79-90.

Soil Survey Staff, 1998, Keys to Soil Taxonomy, (8th edition): Washington, D.C., U.S. Government Printing Office, 324 p.

Soil Survey Staff, 1995, Soil Survey Laboratory Information Manual: Soil survey investigations report no. 45, Version 1.0.: Washington, DC., U.S. Government Printing Office, 305 p.

Sommer, M., Halm, D., Weller, U., Zarie, M., and Stahr, K., 2000, Lateral podzolization in a granite landscape: Soil Science Society of America Journal, v. 64, p.1434-1442.

Speer, J.A., 1982, Zircon: *In* Ribbe, P.H., (ed.) Orthosilicates: Mineralogical Society of America, Washington, DC, Reviews in Mineralogy, v.5, p. 67-112.

Spiers, G.A., Pawluk, S., and Dudas, M.J., 1984, Authigenic mineral formation in

solodization: Canadian Journal of Soil Science, v. 64, p. 515-532.

Stallard, R.F., 1995, Relating chemical and physical erosion: *In* White, E.F., and Brantley, S.L., (eds.) Chemical Weathering Rates of Silicate Minerals: Mineralogical Society of America, Washington, DC, Reviews in Mineralogy, v. 31, p. 543-564.

Stefaniak, A., Mora, C.I., and Driese, S.G., 1993, Pedogenic and groundwater carbonates in vertic paleosols in the Mississippian Maccrady Formation: Geological Society of America Abstracts with Programs, v. 25, no. 7, p. A399.

Stephen, I., 1953, A petrographic study of tropical black earth and grey earth from the Gold Coast: Journal of Soil Science, v. 4, p. 211-219.

Tejan-Kella, M.S., Fitzpatrick, R.W., and Chittleborough, D.J., 1990, Scanning electron microscope study of zircons and rutiles from a podzol chronosequence at Cooloola, Queensland, Australia: Catena, v. 18, p. 11-30.

Templin, E.H., Mowery, I.C., and Kunze, G.W., 1956, Houston black clay, the type grumosol: I Field morphology and geography: Soil Science Society of America Proceedings, v. 20, p. 88-90.

Thornthwaite, C.W., and Mather, J.R., 1955, The water balance: Climatology, v. 8, p. 1-104.

Torrent, J., and Schwertmann, U., 1987, Influence of hematite on the color of red beds: Journal of Sedimentary Petrology, v. 57, p. 121-125.

Torrent, J., Schwertmann, U., Fechter, H., Alferez, F., 1983, Quantitative relationships between soil colour and hematite content: Soil Science, v. 136, p. 354-358.

Van Andel, Tj. H., and Poole, D.M., 1960, Sources of recent sediments in the northern

Gulf of Mexico: Journal of Sedimentary Petrology, v. 30, p. 910-922.

Vepraskis, M.J., and Faulkner, S.P., 2001, Redox chemistry of wetland soils: *In* Richardson, J.L., and Vepraskis, M.J., (eds.) Wetland Soils: Genesis, Hydrology, Landscapes, and Classification, Boca Raton, FL, Lewis Publishers, p. 85-106.

Vitousek, P.M., Chadwick. O.E., Crews, T.E., Fownes, J.H., Hendricks, D.M., and Herbert, D., 1997, Soil and ecosystem across the Hawaiian Islands: GSA Today, v. 7, no. 9, p. 1-8.

Wang, H.D., White, G.N., Turner, F.T., and Dixon, J.B., 1993, Ferrihydrite, lepidocrocite, and goethite in coatings from East Texas Vertic Soils: Soil Science Society of America Journal, v. 57, p.1381-1386.

Weber, N.A., 1966, Fungus growing ants: Science, v. 153, p. 587-604.

White, A.F., and Brantley, S.L., 1995, Chemical weathering rates of silicate minerals: An overview: *In* White, A.F., and Brantley, S.L., (eds.) Chemical Weathering Rates of Silicate Minerals: Mineralogical Society of America, Washington, DC, Reviews in Mineralogy, v. 31, p. 1-22.

White, G.N., and Dixon, J.B., 1996, Iron and manganese distribution in nodules from a young Texas Vertisol: Soil Science Society of America Journal, v. 60, p. 1254-1262.

Wilding, L.P., and Couloumbe, C.E, 1996, Expansive soils: distribution, morphology, and genesis: *In* Baveye, P., and McBride, M.B., (eds.) Proceedings of the NATO-ARW on Clay Swelling and Expansive Soils, Amsterdam, Kluwer Academic Press, p. 78-92

Wilding, L.P., and Tessier, D., 1988, Genesis of Vertisols: shrink-swell phenomena: *In* Wilding, L.P., and Puentes, R., (eds.) Vertisols: Their Distribution, Properties, Classification, and Management, Technical Monograph 18, College Station, TX, Texas A&M Univ. Printing Center, p. 23-57.

Wilding, L.P., Williams, D., Miller, W., Cook, T., and Eswaran, H., 1990, Interval spatial variability of Vertisols: A case study in Texas: *In* Kimble J.M., (ed.) Proceedings of the Sixth International Soil Correlation Meeting (VI ISCOM): Characterization, Classification, and Utilization of Cold Aridisols and Vertisols: Washington, DC, USDA-NRCS Soil Survey Division, p. 232-247.

Yaalon, D.H., 1987, Saharan dust and desert loess: effect on surrounding soils: Journal of African Earth Science, v. 6, p. 569-571.

Yaalon, D.H., 1971, Soil-forming processes in space and time: *In* Yaalon, D.H., (ed.) Paleopedology - Origin, Nature and Dating of Palesols, Jerusalem, Israel Univ. Press, p. 29-39.

Yaalon, D.H., and Kalmar, D., 1978, Dynamics of cracking and swelling clay soils: Displacement of skeleton grains, optimum depth of slickensides, and rate of intra-pedonic turbation: Earth Surface Processes, v. 3, p. 31-42.

Yule, D.F., and Ritchie, J.T., 1980, Soil shrinkage relationships of Texas Vertisols: I. Small cores: Soil Science Society of America Journal, v.44, p. 1285-1291.

Appendices

Appendix 1: Data for Chapter 1

Table A1-1: Pedon Field Descriptions

Description Date: 5/16/2000

Soil Series: League
Site Identification #: **99 LEG 245A L** (00TX245001[a] - microlow)

Location Information
Soil Survey Area Name: Jefferson County, Texas
Latitude: 30 degrees 02 minutes 22.1 seconds North
Longitude: 94 degrees 11 minutes 36.0 seconds West
Described by: Jon Wiedenfeld

Classification: fine, smectitic,hyperthermic Oxyaquic Hapluderts

Microrelief: micro-low

Ap--0 to 16 cm; very dark gray (2.5Y 3/1), clay; weak fine subangular blocky structure; firm, very hard; common very fine and fine roots; common fine vesicular pores; 3 percent fine prominent (2.5Y 4/8) masses of oxidized iron with clear boundaries lining pores; 6 percent fine prominent yellowish red (5YR 5/8) masses of oxidized iron with diffuse boundaries lining pores; clear smooth boundary.

Bss1--16 to 43 cm; black (2.5Y 2.5/1), clay; moderate fine and medium subangular blocky structure; firm, very hard; common very fine and fine roots; common fine tubular pores; 10 percent distinct black (2.5Y 2.5/1) pressure faces; 30 percent distinct black (2.5Y 2.5/1) slickensides tilted at 20 to 40 degrees from the horizontal; 1 percent fine spherical moderately cemented very dark brown (10YR 2/2) iron-manganese nodules; 1 percent fine faint olive brown (2.5Y 4/3) iron-manganese masses with diffuse boundaries on faces of peds; 1 percent crayfish krotovinas 2 centimeters wide filled with pale yellow (2.5Y 7/4) clay and lined with very dark gray (2.5y 3/1) clay; clear smooth boundary.

Bss2--43 to 72 cm; very dark gray (10YR 3/1), clay; weak medium wedge structure parts to moderate medium angular blocky; firm, very hard; common very fine and fine roots; common fine tubular pores; 55 percent distinct very dark gray (10YR 3/1) slickensides tilted at 30 to 50 degrees; 1 percent fine faint olive brown (2.5Y 4/3) iron-manganese masses with diffuse boundaries on faces of peds; 1 percent fine spherical moderately cemented very dark brown (10YR 2/2) iron-manganese nodules; 2 percent crayfish krotovinas 2 centimeters wide filled with pale yellow (2.5Y 7/4) clay and lined with very dark gray(2.5Y 3/1) clay;gradual wavy boundary.

Bss3--72 to 104 cm; dark gray (10YR 4/1), clay; weak fine wedge structure parts to moderate medium angular blocky; firm, very hard; few very fine and fine roots; common very fine and fine tubular pores; 60 percent prominent dark gray (10YR 4/1) slickensides tilted at 40 to 60 degrees to the horizontal; 1 percent fine prominent strong brown (7.5YR 5/6) iron-manganese masses with diffuse boundaries on faces of peds; 1 percent fine spherical moderately cemented very dark brown (10YR 2/2) iron-manganese nodules; 2 percent crayfish krotovinas 2 centimeters wide filled with pale yellow (2.5Y 7/4) clay and lined with very dark gray(2.5Y 3/1) clay; gradual wavy boundary.

Bss4--104 to 115 cm; gray (10YR 5/1), clay; weak fine wedge structure parts to moderate medium angular blocky; firm, very hard; few very fine roots; few very fine tubular pores; 60 percent prominent gray (10YR 5/1) slickensides are tilted at 40 to 60 degrees to the horizontal; 1 percent fine and medium prominent strong brown (7.5YR 5/6) masses of oxidized iron with diffuse boundaries on faces of peds; 1 percent fine

[a] NRCS (Natural Resources Conservation Service) pedon designation code.

spherical moderately cemented very dark brown (10YR 2/2) iron-manganese nodules; 1 percent fine prominent brownish yellow (10YR 6/6) masses of oxidized iron with diffuse boundaries in matrix surrounding redox concentrations; 1 percent crayfish krotovinas 2 centimeters wide filled with pale yellow (2.5Y 7/4)clay and lined with dark gray (10YR 4/1) clay; gradual smooth boundary.

Bss5--115 to 144 cm; gray (10YR 5/1), clay; moderate medium wedge parts to moderate medium angular blocky structure; firm, very hard; few very fine roots; 45 percent distinct gray (10YR 5/1) slickensides tilted at 40 to 50 degrees to the horizontal; 1 percent fine prominent very dark brown (10YR 2/2) manganese masses; 5 percent fine distinct light yellowish brown (10YR 6/4) masses of oxidized iron with clear boundaries on faces of peds; 10 percent fine and medium prominent brownish yellow (10YR 6/6) masses of oxidized iron with clear boundaries on faces of peds; 1 percent crayfish krotovinas filled with dark gray(10YR 4/1) clay; gradual wavy boundary.

Bss6--144 to 156 cm; gray (10YR 5/1), clay; weak medium wedge structure parts to moderate medium angular blocky; firm, very hard; few very fine roots; 70 percent distinct gray (10YR 5/1) slickensides tilted at 20 to 50 degrees to the horizontal; 1 percent fine prominent dark yellowish brown (10YR 4/6) iron-manganese masses with sharp boundaries in matrix; 2 percent fine and medium prominent yellow (10YR 7/8) masses of oxidized iron with diffuse boundaries in matrix; 18 percent fine and medium prominent yellow(2.5Y 7/6) masses of oxidized iron with diffuse boundaries on faces of peds; 1 percent fine moderately cemented carbonate nodules; 1 percent crayfish krotovinas filled with gray (10YR 5/1)clay; gradual smooth boundary.

Bkss1--156 to 174 cm; gray (10YR 6/1), clay; weak medium wedge structure parts to moderate medium angular blocky; firm, very hard; few very fine roots; 70 percent distinct gray (10YR 6/1) slickensides tilted at 20 to 50 degrees to the horizontal; 3 percent fine and medium prominent yellow (2.5Y 7/6) masses of oxidized iron with diffuse boundaries in matrix; 3 percent fine and medium prominent brownish yellow (10YR 6/6) masses of oxidized iron with diffuse boundaries in matrix; 1 percent fine moderately cemented carbonate nodules; 1 percent crayfish krotovinas filled with gray (10yr 5/1) clay; strong effervescence; clear smooth boundary.

Bkss2--174 to 223 cm; gray (2.5Y 6/1), clay; moderate coarse wedge structure parts to moderate medium and coarse angular blocky; firm, very hard; few very fine roots; 45 percent distinct gray (2.5Y 6/1) slickensides tilted at 40 to 60 degrees to the horizontal; 1 percent fine black (7.5YR 2.5/1) manganese masses with sharp boundaries in matrix; 1 percent fine prominent reddish yellow (7.5YR 6/6) masses of oxidized iron with sharp boundaries around carbonate nodules; 5 percent fine and medium prominent yellowish brown (10YR 5/8) masses of oxidized iron with diffuse boundaries in matrix and 10 percent fine and medium prominent yellow (10YR 7/8) masses of oxidized iron with diffuse boundaries in matrix surrounding redox concentrations; 1 percent fine moderately cemented carbonate nodules; 1 percent crayfish krotovinas filled with gray (10YR 5/1) clay; strong effervescence; gradual wavy boundary.

B'kss1--223 to 252 cm; light gray (2.5Y 7/1), clay; moderate medium and coarse wedge structure parts to moderate medium angular blocky; firm, very hard; few very fine roots; 20 percent distinct yellowish brown (10YR 5/6) slickensides and 70 percent distinct light gray (2.5Y 7/1) slickensides tilted at 20 to 45 degrees to the horizontal; 1 percent medium prominent strong brown (7.5YR 5/6) masses of oxidized iron with sharp boundaries in matrix; 3 percent fine prominent dendritic black (10YR 2/1) manganese masses with sharp boundaries on faces of peds; 5 percent fine and medium carbonate nodules; 1 percent crayfish krotovinas filled with gray (10YR 5/1) clay and few fine calcium carbonate nodules; gradual smooth boundary.

B'kss2--252 to 275 cm; strong brown (7.5YR 5/6), clay; moderate medium and coarse wedge parts to moderate medium angular blocky structure; very firm, very hard; few very fine roots; 70 percent distinct

light gray (2.5Y 7/1) slickensides tilted at 20 to 30 degrees to the horizontal; 1 percent medium prominent strong brown (7.5YR 5/6) masses of oxidized iron with sharp boundaries in matrix; 3 percent fine prominent dendritic black(10YR 2/1) manganese masses with sharp boundaries on faces of peds; 1 percent crayfish krotovinas filled with gray (10YR 5/1) clay and few fine calcium carbonate nodules.

Description Date: 5/16/2000

Soil Series: League
Site Identification #: **99 LEG 245A H** (00TX245001A - microhigh)

Location Information
Soil Survey Area Name: Jefferson County, Texas
Latitude: 30 degrees 02 minutes 22.1 seconds North
Longitude: 94 degrees 11 minutes 36.0 seconds West
Described by: Jon Wiedenfeld

Classification: fine, smectitic, hyperthermic Oxyaquic Hapluderts

Microrelief: micro-high

Ap--0 to 15 cm; very dark gray (2.5Y 3/1), clay; weak medium subangular blocky structure; very firm, very hard; common very fine and fine roots; few fine tubular pores; 1 percent very coarse prominent yellowish brown (10YR 5/6) masses of oxidized iron with clear boundaries around carbonate nodules; 3 percent fine and medium prominent spherical moderately cemented very dark brown (7.5YR 2/2) iron-manganese nodules; 4 percent fine prominent brown (7.5YR 4/4) masses of oxidized iron with clear boundaries lining pores; 1 percent medium and coarse weakly cemented carbonate nodules; 5 percent crayfish krotovinas filled with very dark gray (2.5Y 3/1) clay; abrupt smooth boundary.

A--15 to 26 cm; black (2.5Y 2.5/1), clay; weak medium subangular blocky structure; very firm, very hard; common very fine and fine roots; few fine tubular pores; 1 percent fine prominent brown (7.5YR 4/4) masses of oxidized iron with clear boundaries lining pores; 1 percent very coarse prominent yellowish brown (10YR 5/6) masses of oxidized iron with clear boundaries around carbonate nodules; 3 percent fine and medium prominent spherical moderately cemented very dark brown (7.5YR 2/2) iron-manganese nodules; 20 percent medium distinct light olive brown (2.5Y 5/3) masses of oxidized iron with clear boundaries throughout; 1 percent medium and coarse weakly cemented carbonate nodules; 5 percent crayfish krotovinas filled with very dark gray (2.5Y 3/1) clay; clear wavy boundary.

Bkg--26 to 46 cm; grayish brown (2.5Y 5/2), clay; moderate fine and medium angular blocky structure; very firm, very hard; common very fine and fine roots; few fine tubular pores; 10 percent prominent grayish brown (2.5Y 5/2) pressure faces; 2 percent very coarse prominent brownish yellow (10YR 6/8) masses of oxidized iron with clear boundaries around carbonate nodules; 2 percent fine and medium prominent spherical moderately cemented very dark brown (7.5YR 2/2) iron-manganese nodules; 4 percent fine prominent brown (7.5YR 4/4) masses of oxidized iron with clear boundaries throughout; 5 percent medium distinct light olive brown (2.5Y 5/6) masses of oxidized iron with clear boundaries throughout; 2 percent medium and coarse weakly cemented carbonate nodules with a thin soft shell and a hard interior; 5 percent crayfish krotovinas filled with very dark gray (2.5y 3/1) clay; gradual wavy boundary.

Bkssg1--46 to 67 cm; grayish brown (2.5Y 5/2), clay; moderate fine and medium wedge structure parts to moderate fine and medium angular blocky; very firm, very hard; few very fine and fine roots; few fine tubular pores; 20 percent distinct grayish brown (2.5Y 5/2) slickensides tilted at 10 to 25 degrees from the horizontal; 75 percent prominent grayish brown (2.5Y 5/2) pressure faces; 2 percent fine and medium prominent spherical moderately cemented very dark brown (7.5YR 2/2) iron-manganese nodules; 2 percent very coarse prominent brownish yellow (10YR 6/8) masses of oxidized iron with clear boundaries around carbonate nodules; 20 percent medium distinct light olive brown (2.5Y 5/6) masses of oxidized iron with clear boundaries throughout; 1 percent medium and coarse moderately cemented carbonate

nodules with a thin soft shell and a hard interior; 5 percent crayfish krotovinas filled with very dark gray (2.5Y 3/1) clay; gradual wavy boundary.

Bkssg2--67 to 96 cm; gray (2.5Y 5/1), clay; moderate fine and medium wedge structure parts to moderate fine and medium angular blocky; very firm, very hard; few very fine and fine roots; few fine tubular pores; 35 percent prominent gray (2.5Y 5/1) slickensides tilted at 30 to 35 degrees from the horizontal; 65 percent prominent gray (2.5Y 5/1) pressure faces; 2 percent medium distinct light olive brown (2.5Y 5/6) masses of oxidized iron with sharp boundaries throughout; 2 percent fine and medium prominent spherical moderately cemented very dark brown (7.5YR 2/2) iron-manganese nodules; 20 percent medium prominent brownish yellow (10YR 6/8) masses of oxidized iron with clear boundaries around carbonate nodules with a thin soft shell and a hard interior; 1 percent medium and coarse weakly cemented carbonate nodules; 5 percent crayfish krotovinas filled with dark gray (2.5y 4/1) clay; gradual wavy boundary.

Bkssg3--96 to 120 cm; gray (2.5Y 5/1), clay; moderate medium and coarse wedge structure parts to moderate fine and medium angular blocky; very firm, very hard; few very fine and fine roots; few very fine tubular pores; 20 percent prominent gray (2.5Y 5/1) slickensides tilted at 30 to 40 degrees from the horizontal; 80 percent prominent gray (2.5Y 5/1) pressure faces; 1 percent very coarse prominent brownish yellow (10YR 6/8) masses of oxidized iron with clear boundaries around carbonate nodules; 2 percent fine and medium prominent spherical very weakly cemented brown (7.5YR 4/4) iron-manganese nodules; 5 percent medium prominent light olive brown (2.5Y 5/6) masses of oxidized iron with clear boundaries throughout; 20 percent medium distinct light olive brown (2.5Y 5/4) masses of oxidized iron with clear boundaries throughout; 1 percent medium and coarse weakly cemented carbonate nodules with a thin soft shell and a hard interior; 5 percent crayfish krotovinas filled with dark gray (2.5Y 4/1) clay; gradual wavy boundary.

Bkssg4--120 to 154 cm; dark gray (2.5Y 4/1), clay; moderate medium and coarse wedge structure parts to moderate fine and medium angular blocky; very firm, very hard; few very fine roots; few very fine tubular pores; 35 percent prominent dark gray (2.5Y 4/1) slickensides tilted at 20 to 40 degrees from the horizontal; 65 percent prominent dark gray (2.5Y 4/1) pressure faces; 1 percent very coarse prominent brownish yellow (10YR 6/8) masses of oxidized iron with clear boundaries around carbonate nodules; 2 percent fine prominent light olive brown (2.5Y 5/6) masses of oxidized iron with clear boundaries throughout; 12 percent fine and medium prominent spherical very weakly cemented black (10YR 2/1) iron-manganese nodules;12 percent medium prominent brown (7.5YR 4/4) iron-manganese masses with clear boundaries in matrix surrounding redox concentrations; 20 percent medium distinct light olive brown (2.5Y 5/4) masses of oxidized iron with clear boundaries throughout; 1 percent medium and coarse weakly cemented carbonate nodules; 10 percent crayfish krotovinas filled with very dark gray (N 3/) clay; gradual wavy boundary.

Bkssg5--154 to 173 cm; gray (2.5Y 5/1), clay; moderate coarse wedge parts structure to moderate medium and coarse angular blocky; very firm, very hard; few very fine roots; few very fine tubular pores; 25 percent prominent gray (2.5Y 5/1) slickensides tilted at 25 to 45 degrees from the horizontal; 75 percent prominent gray (2.5Y 5/1) pressure faces; 1 percent fine prominent spherical very weakly cemented dark yellowish brown (10YR 4/6) iron-manganese nodules; 5 percent medium prominent yellowish brown (10YR 5/6) masses of oxidized iron with clear boundaries around rock fragments; 20 percent medium prominent light olive brown (2.5Y 5/6) masses of oxidized iron with clear boundaries throughout; 5 percent medium strongly cemented carbonate nodules; 1 percent medium carbonate masses with hard centers; 5 percent crayfish krotovinas filled with very dark gray (N/3) clay; very slight effervescence; gradual wavy boundary.

Bkssg6--173 to 195 cm; gray (2.5Y 5/1), clay; moderate coarse wedge structure parts to moderate medium and coarse angular blocky; very firm, very hard; few very fine roots; few very fine tubular pores; 25 percent prominent dark gray (2.5Y 4/1) slickensides tilted at 10 to 40 degrees from the horizontal; 75 percent prominent dark gray (2.5Y 4/1) pressure faces; 1 percent very coarse prominent strong brown (7.5YR 4/6) masses of oxidized iron with clear boundaries around carbonate nodules; 3 percent coarse distinct very dark grayish brown (2.5Y 3/2) iron-manganese masses with clear boundaries in matrix surrounding redox concentrations; 1 percent black (2.5Y 2/1) iron-manganese masses with sharp boundaries throughout; 20 percent medium prominent light olive brown (2.5Y 5/6) masses of oxidized iron with clear boundaries throughout; 3 percent medium and coarse carbonate nodules; 5 percent crayfish krotovinas filled with very dark gray (N/3); slight effervescence clear wavy boundary.

Bkssg7--195 to 220 cm; light gray (5Y 7/1), clay; moderate medium and coarse wedge structure parts to moderate coarse angular blocky; very firm, very hard; few very fine roots; few very fine tubular pores; 10 percent prominent light gray (5Y 7/1) slickensides tilted at 30 to 60 degrees from the horizontal and are well developed; 75 percent prominent light gray (5Y 7/1) pressure faces; 1 percent coarse prominent brown (7.5YR 4/4) masses of oxidized iron with clear boundaries around carbonate nodules; 5 percent fine and medium strongly cemented carbonate nodules; 7 percent crayfish krotovinas filled with dark gray (2.5Y 4/1) clay; strong effervescence; clear smooth boundary.

Bkssg8--220 to 270 cm; light gray (5Y 7/1), clay; weak very coarse wedge structure parts to strong very coarse angular blocky structure; very firm, very hard; few very fine roots; few very fine tubular pores; 20 percent prominent light gray (5Y 7/1) slickensides tilted at 20 to 60 degrees from the horizontal;; 80 percent prominent light gray (5Y 7/1) pressure faces; 15 percent fine and medium prominent spherical very weakly cemented black (10YR 2/1)iron-manganese nodules; 20 percent medium prominent strong brown (7.5YR 5/6) masses of oxidized iron with clear boundaries throughout; 1 percent fine and medium strongly cemented carbonate nodules; 7 percent crayfish krotovinas filled with gray (2.5Y 6/1) clay; very slight effervescence; clear smooth boundary.

Bss--355 to 390 cm; strong brown (7.5YR 4/6), clay; moderate fine and medium angular blocky structure that is concoidally fractured and rock-like; very firm, very hard; few very fine roots; 1 percent prominent light gray (5Y 7/2) slickensides tilted at 25 to 45 degrees from the horizontal; 10 percent prominent light gray (5Y 7/2) pressure faces; 4 percent fine and medium prominent spherical very weakly cemented black (10YR 2/1) iron-manganese nodules; 10 percent medium prominent dark gray (10YR 4/1) iron depletions with clear boundaries throughout; 10 percent medium prominent reddish brown (5YR 5/4) masses of oxidized iron with clear boundaries throughout; 40 percent medium prominent light gray (5Y 7/2) iron depletions with clear boundaries throughout; 3 percent crayfish krotovinas filled with gray (2.5y 6/1) and cupped with very dark gray (10yr 3/1) clay; slight effervescence.

Lake Charles Series Pedon Descriptions

Description date: 6/24/1999

Soil Series: Lake Charles
Site Identification #: **99 LAC 201 L** (99TX201001 - microlow)

Location Information
Soil Survey Area Name: Harris County, Texas (Armand Bayou)
Latitude: 29 degrees 35 minutes 40 seconds North
Longitude: 95 degrees 04 minutes 14 seconds West
Described by: Lee Nordt and Jon Wiedenfeld

Classification: Fine, smectitic, hyperthermic Aquic Hapludert

A--0 to 16 cm; very dark gray (10YR 3/1) clay; weak fine and medium subangular blocky structure; firm, very sticky and very plastic; many very fine and fine roots; common very fine and fine interstitial pores; few fine pores filled with coarse material; few active unfilled krotovinas 1 to 5 cm wide; 3 percent fine distinct brown (7.5YR 4/4) iron concentrations with sharp boundaries along root pores linings; few fine iron-manganese nodules; clear smooth boundary.

Bw--16 to 44 cm; black (2.5Y 2/1) clay; weak medium prismatic structure parting to moderate medium and coarse angular blocky; firm, very sticky and very plastic; common very fine and fine roots; common fine tubular pores; very few faint intersecting slickensides; very few distinct pressure faces; 1 percent fine prominent strong brown (7.5YR 5/6) iron concentrations with clear boundaries along root pore linings; 1 percent fine faint gray (2.5Y 5/1) iron depletions with clear boundaries on surfaces of peds; few fine and medium iron-manganese nodules; gradual smooth boundary.

Bss1--44 to 65 cm; dark gray (2.5Y 4/1) clay; moderate medium prismatic structure parting to moderate medium angular blocky; firm, very sticky and very plastic; common very fine and fine roots; common fine tubular pores; common distinct intersecting slickensides that tilt 30 to 45 degrees from the horizontal; 3 percent fine prominent yellowish red (5YR 5/6) iron concentrations with sharp boundaries along root pore linings; few medium iron-manganese nodules; gradual wavy boundary.

Bss2--65 to 88 cm; dark gray (2.5Y 4/1) clay; weak coarse prismatic structure parting to moderate medium angular blocky; firm, very sticky and very plastic; common very fine and fine roots; common very fine and fine tubular pores; common distinct intersecting slickensides that tilt 35 to 55 degree from the horizontal; 10 percent fine faint light yellowish brown (2.5Y 6/3) iron concentrations with diffuse boundaries on surfaces of slickensides and peds; 3 percent fine faint gray (2.5Y 5/1) iron depletions with clear boundaries on surfaces of slickensides and peds; few medium iron-manganese nodules; gradual wavy boundary.

Bss3--88 to 117 cm; gray (2.5Y 5/1) clay; moderate medium angular blocky structure; very firm, very sticky and very plastic; common fine roots; very fine and fine tubular pores; few crawfish krotovina 1 to 5 cm wide filled with grayish brown (2.5Y 5/2) and very dark gray (2.5Y 3/1) material; few active unfilled krotovinas; common distinct intersecting slickensides that tilt 40 to 55 degrees from the horizontal; 15 percent fine faint light yellowish brown (2.5Y 6/3) and 3 percent fine and medium distinct light yellowish brown (2.5Y 6/4) iron concentrations with diffuse boundaries on surfaces and interiors of peds; few fine and medium iron-manganese nodules; clear wavy boundary.

Bss4--117 to 151 cm; light brownish gray (2.5Y 6/2) clay; moderate medium angular blocky structure;

very firm, very sticky and very plastic; common fine roots; very fine and fine tubular pores; few crawfish krotovinas 1 to 5 cm wide filled with grayish brown (2.5Y 5/2) and very dark gray (2.5Y 3/1) material; common distinct intersecting slickensides that tilt 30 to 40 degrees from the horizontal; 15 percent fine and medium faint light yellowish brown (2.5Y 6/4) iron concentrations with diffuse boundaries on surfaces of slickensides and on interiors of peds; 1 percent fine distinct greenish gray (5BG 6/1) iron depletions with diffuse boundaries on surfaces of slickensides and on interiors of peds; few fine and medium iron-manganese nodules; clear wavy boundary.

Bkss1--151 to 177 cm; light yellowish brown (2.5Y 6/3) clay; weak medium and coarse subangular blocky structure; very firm, very sticky and very plastic; common fine roots; very fine and fine tubular pores; few crawfish krotovinas 1 to 5 cm wide filled with yellowish red (5YR 5/6) and very dark gray (2.5YR 3/1) material; common distinct intersecting slickensides that tilt 30 degrees from the horizontal; 5 cm wide arcing yellowish red (5YR 5/6) clay intrusion from Bkss2 horizon; 3 percent fine faint gray (2.5Y 5/1) iron depletions with clear boundaries on surfaces of slickensides; less than 1 percent fine prominent strong brown (7.5YR 5/6)iron concentrations with diffuse boundaries along surfaces of slickensides and as a halo around manganese nodules; 1 percent fine faint greenish gray (5BG 6/1) iron depletions with sharp boundaries along root pore linings; common fine rounded strong brown (7.5YR 5/6) iron-manganese concretions; few fine nodules of calcium carbonate; slightly effervescent; gradual smooth boundary.

Bkss2--177 to 212 cm; reddish brown (5YR 5/4) clay; weak coarse subangular blocky structure; very firm, very sticky and very plastic; very few very fine and fine roots; very fine and fine tubular pores; few crawfish krotovinas filled with dark gray (10YR 4/1) and reddish brown (5YR 5/4) material; common faint intersecting slickensides that tilt 20 degrees from the horizontal; 7 percent fine prominent gray (2.5Y 6/1) iron depletions with clear boundaries on surfaces of slickensides; 1 percent fine prominent greenish gray (5BG 6/1) iron depletions along root pore linings; 1 percent fine prominent light yellowish brown (10YR 6/4) iron concentrations with diffuse boundaries between peds; common fine nodules of calcium carbonate; strongly effervescent; gradual wavy boundary.

B'ss1--212 to 242 cm; red (2.5YR 5/6) clay; weak medium and coarse prismatic structure; very firm, very sticky and very plastic; very few very fine and fine roots; very few very fine and fine tubular pores; few crawfish krotovinas 0.5 to 1.5 cm wide filled with dark gray (2.5Y 4/1) and red (2.5YR 4/8) material; common faint intersecting slickensides that tilt 20 degrees from the horizontal; 5 percent fine and medium prominent yellow (2.5Y 7/6) iron concentrations with diffuse boundaries on surfaces of peds; 3 percent fine prominent greenish gray (5BG 6/1)iron depletions with clear boundaries on root pore linings; few fine and medium nodules of calcium carbonate; strongly effervescent; clear smooth boundary.

B'ss2--242 to 261 cm; red (2.5YR 5/6) clay; moderate fine and medium platy structure parting to moderate fine angular blocky; very firm, very sticky and very plastic; very fine and fine roots; very fine and fine tubular pores; few crawfish krotovinas 1 to 2 cm wide filled with gray (2.5Y 6/1), red (2.5YR 5/6) clay and few fine very pale brown (10YR 8/2) nodules of calcium carbonate; common faint intersecting slickensides that tilt 15 to 20 degrees from the horizontal; common fine and medium prominent light greenish gray (10Y 7/1) iron depletions with clear boundaries on root pore linings; common fine nodules of iron-manganese at top of horizon; strongly effervescent.

B'ss3--261 to 279 cm; red (2.5YR 4/6) clay; moderate fine and medium platy structure parting to moderate fine angular blocky; very firm, very sticky and very plastic; very few very fine and fine roots; very few very fine and fine tubular pores; 10 percent of horizon are red (2.5YR 4/8) fractured conchoidal blocks; common faint intersecting slickensides that tilt 15 to 20 degrees from the horizontal; 10 percent fine and medium prominent light greenish gray (10Y 7/1) iron depletions with clear boundaries along root pore linings; strongly effervescent.

B'ss4--279 to 300 cm; red (2.5YR 5/6) clay; moderate fine and medium platy structure parting to moderate fine angular blocky; very firm, very sticky and very plastic; very fine and fine roots; very fine and fine tubular pores; 15 percent of horizon are red (2.5YR 4/8) fractured conchoidal blocks; 10 percent lenses 1 to 2 cm thick of light yellowish brown (10YR 6/4) silt loam; few faint intersecting slickensides; common fine and medium prominent light greenish gray (10Y 7/1) iron depletions with clear boundaries along root pore linings; strongly effervescent.

Description date: 6/24/1999

Soil Series: Lake Charles
Site Identification #: **99 LAC 201 H** (99TX201001A - microhigh)

Location Information
Soil Survey Area Name: Harris County, Texas (Armand Bayou)
Latitude: 29 degrees 35 minutes 40 seconds North
Longitude: 95 degrees 04 minutes 14 seconds West
Described by: Wes Miller and Larry Wilding

Classification: Fine, smectitic, hyperthermic Aquic Hapludert

Ak--0 to 10 cm; dark gray (2.5Y 4/1) clay; weak coarse angular blocky structure parting to moderate medium granular; firm, very sticky and very plastic; many fine roots; common fine interstitial pores; very few faint intersecting slickensides; 2 percent fine prominent strong brown (7.5YR 4/6) iron concentrations along root pore linings; few fine uncoated nodules of calcium carbonate; matrix is non-calcareous; clear smooth boundary.

Bkssg1--10 to 27 cm; grayish brown (2.5Y 5/2) clay; moderate medium angular blocky structure; firm, very sticky and very plastic; common fine roots; few fine interstitial pores; common faint intersecting slickensides; few rounded 2 to 4 mm black (10YR 2/1) nodules of iron-manganese; 2 percent fine prominent yellowish red (5YR 5/8) iron concentrations with clear boundaries on surfaces of peds and on root pore linings; few 2 to 10 mm weakly indurated nodules of calcium carbonate coated with olive yellow (2.5Y 6/6) iron; few masses of calcareous red (2.5YR 5/8) clay 5mm to 1cm in size mixed with calcium carbonate nodules; matrix is non-calcareous; clear wavy boundary.

Bkssg2--27 to 49 cm; grayish brown (2.5Y 5/2) clay; moderate fine and medium angular blocky structure; firm, very sticky and very plastic; common fine roots; few fine tubular pores; common distinct weakly grooved intersecting slickensides that are tilted 20 to 40 degrees from the horizontal; 1 percent fine prominent strong brown (7.5YR 5/6) iron concentrations with clear boundaries on root pore linings; few rounded 2 to 4 mm black (10YR 2/1) nodules of iron-manganese; common weakly indurated nodules of calcium carbonate coated with olive yellow (2.5Y 6/6) iron; few masses of calcareous red (2.5YR 5/8) clay 5mm to 1cm in size mixed with calcium carbonate nodules; matrix is non-calcareous; clear wavy boundary.

Bkssg3--49 to 67 cm; grayish brown (2.5Y 5/2) clay; moderate fine and medium angular blocky structure; firm, very sticky and very plastic; common fine roots; few fine tubular pores; many weakly grooved distinct intersecting slickensides that are tilted at 30 to 40 degrees from the horizontal; 5 percent fine distinct dark grayish brown (2.5Y 4/2) iron depletions on surfaces of slickensides; few rounded 2 to 10 mm black (10YR 2/1) nodules of iron-manganese; common weakly indurated nodules of calcium carbonate coated with olive yellow (2.5Y 6/6) iron; common masses of calcareous red (2.5YR 5/8) clay 5mm to 2cm in size mixed with calcium carbonate nodules; slightly effervescent; abrupt wavy boundary.

Bkssg4--67 to 105 cm; grayish brown (2.5Y 5/2) clay; moderate medium and coarse angular blocky structure; firm, very sticky and very plastic; common fine roots; few fine tubular pores; many weakly grooved distinct intersecting slickensides that are tilted at 15 to 30 degrees from the horizontal; 15 percent medium faint olive brown (2.5Y 4/4)iron concentrations with diffuse boundaries on surfaces of slickensides; 10 percent medium faint dark gray (2.5Y 4/1) iron depletions with diffuse boundaries on surfaces of slickensides; common uncoated rounded nodules of calcium carbonate 2 to 5mm in size; few

rounded nodules of black (10YR 2/1) of iron-manganese 4 to 8 mm in size; strongly effervescent; clear wavy boundary.

Bkssg5--105 to 148 cm; gray (2.5Y 5/1) clay; moderate medium and coarse angular blocky structure; firm, very sticky and very plastic; common fine roots between peds; few very fine tubular pores; many prominent coarsely grooved intersecting slickensides; 35 percent fine and medium distinct light yellowish brown (2.5Y 6/4) iron concentrations with diffuse boundaries on surfaces of slickensides; 10 percent fine prominent dark gray (2.5Y 4/1) iron depletions with clear boundaries on surfaces of slickensides; common rounded black (10YR 2/1) nodules of iron-manganese 2 to 8mm in size; common rounded uncoated nodules of calcium carbonate 2 to 15mm in size; slightly effervescent; clear wavy boundary.

Bkssg6--148 to 177 cm; gray (5Y 6/1) clay; moderate medium and coarse angular blocky structure; firm, very sticky and very plastic; common fine roots; few fine tubular pores; common distinct finely grooved intersecting slickensides that are tilted at 30 to 35 degrees to the horizontal; 40 percent coarse prominent light yellowish brown (2.5Y 6/3) iron concentrations with diffuse boundaries on surfaces of slickensides; common rounded black (10YR 2/1) iron-manganese concretions; few rounded uncoated strongly indurated nodules of calcium carbonate 2 to 3 mm in size; slightly effervescent; clear wavy boundary.

B'kss1--177 to 202 cm; yellowish red (5YR 5/6) clay; weak coarse angular blocky structure; firm, very sticky and very plastic; common fine roots between peds; common distinct finely grooved intersecting slickensides that are tilted 35 to 50 degrees to the horizontal; 5 percent fine distinct pale brown (10YR 6/3) iron concentrations with diffuse boundaries; 2 percent fine prominent gray (5Y 5/1) iron depletions with clear boundaries throughout; few fine dendritic black (10YR 2/1) iron-manganese concentrations in gray (5Y 5/1) iron depletions; common rounded nodules of black (10YR 2/1) iron-manganese 1 to 2 mm in size; few rounded uncoated strongly indurated nodules of calcium carbonate 2 to 3 mm in size; strongly effervescent; clear wavy boundary.

B'ss1--202 to 235 cm; yellowish red (5YR 4/6) clay; weak coarse angular blocky structure; firm, very sticky and very plastic; common very fine and fine roots; few distinct finely grooved intersecting slickensides that are tilted at 20 to 40 degrees to the horizontal; 5 percent medium prominent light yellowish brown (2.5Y 6/3) iron concentrations with clear boundaries on surfaces of peds; common rounded nodules of black (10YR 2/1) iron-manganese 1 to 2mm in size; few medium masses of iron manganese on surfaces of slickensides; few masses of calcium carbonate 3 to 5mm in size; strongly effervescent; clear wavy boundary.

B'ss2--235 to 270 cm; red (2.5YR 4/6) clay; strong coarse angular blocky structure parting to moderate medium angular blocky; very firm, very sticky and very plastic; common very fine and fine roots; common prominent coarsely grooved intersecting slickensides that are tilted 35 to 45 degrees to the horizontal; 5 percent fine and medium prominent light greenish gray (10Y 7/1) iron depletions with clear boundaries on surfaces of slickensides; 1 percent fine prominent light yellowish brown (2.5Y 6/3) iron depletions on surfaces of slickensides; common rounded black nodules of (10YR 2/1) iron-manganese 1 to 2mm in size; common fine masses of black (10YR 2/1) iron-manganese on surfaces of slickensides; strongly effervescent.

Description date: 6/22/1999

Soil Series: Lake Charles
Site Identification #: **99 LAC 157 L** (99TX157001- microlow)

Location Information
Soil Survey Area Name: Fort Bend County, Texas.
Latitude: 29 degrees 24 minutes 12 seconds North
Longitude: 95 degrees 43 minutes 42 seconds West
Described by: Edward Griffin and Jon Wiedenfeld

Classification: Fine, smectitic, hyperthermic Typic Hapludert

A1--0 to 10 cm; black (2.5Y 2/1) clay; moderate fine and medium subangular blocky structure parting to moderate medium granular; very hard, very firm, moderate, very sticky and very plastic; common very fine and fine roots; common fine interstitial pores; few faint pressure surfaces; abrupt smooth boundary.

A2--10 to 29 cm; black (2.5Y 2/1) clay; moderate fine and medium subangular blocky structure; very hard, very firm, very sticky and very plastic; common fine and medium roots; common fine tubular pores; common distinct pressure surfaces; clear smooth boundary.

Bss1--29 to 61 cm; black (2.5Y 2/1) clay; weak medium wedge-shaped structure parting to moderate medium subangular blocky; very hard, very firm, very sticky and very plastic; common fine roots; common fine tubular pores; common distinct intersecting slickensides that are tilted at 50 to 65 degrees to the horizontal; clear wavy boundary.

Bss2--61 to 103 cm; very dark gray (2.5Y 3/1) clay; strong medium and coarse wedge-shaped structure parting to moderate medium angular blocky; very hard, very firm, very sticky and very plastic; common fine roots; common fine tubular pores; very few crayfish krotovina filled with yellowish red (5YR 5/6) and very dark gray (2.5Y 3/1) clay; many prominent intersecting slickensides that are tilted 30 to 40 degrees to the horizontal; very slightly effervescent; gradual wavy boundary.

Bss3--103 to 135 cm; very dark gray (2.5Y 3/1) clay; strong medium and coarse wedge-shaped structure parting to moderate medium angular blocky; very hard, very firm, very sticky and very plastic; common fine roots; very few crayfish krotovina filled with yellowish red (5YR 5/6) and very dark gray (2.5Y 3/1) clay; many prominent intersecting slickensides that are tilted at 45 to 60 degrees to the horizontal; few fine black (10YR 2/1) nodules of iron-manganese; very slightly effervescent; gradual wavy boundary.

Bkss1--135 to 158 cm; dark gray (2.5Y 4/1) clay; moderate medium and coarse wedge-shaped structure parting to moderate medium and coarse angular blocky; very hard, very firm, very sticky and very plastic; common very fine and fine roots; very few crayfish krotovina filled with yellowish red (5YR 5/6) and very dark gray (2.5Y 3/1) clay; common prominent intersecting slickensides that are tilted 35 to 45 degrees to the horizontal; 1 percent fine uncoated nodules of calcium carbonate; 2 percent nodules of calcium carbonate coated with strong brown (7.5YR 5/6) iron; very slightly effervescent; gradual wavy boundary.

Bkss2--158 to 175 cm; 60 percent gray (2.5Y 5/1), 20 percent light olive brown (2.5Y 5/3), 20 percent light yellowish brown (2.5Y 6/3) clay; weak coarse wedge-shaped structure parting to moderate medium and coarse angular blocky; very hard, very firm, very sticky and very plastic; common very fine and fine roots; common prominent intersecting slickensides that are tilted at 30 to 45 degrees to the horizontal; 3 percent fine and medium nodules of calcium carbonate coated with brown (10YR 4/3) iron; 2 percent uncoated nodules of calcium carbonate; strongly effervescent; gradual smooth boundary.

Bkss3--175 to 193 cm; yellowish red (5YR 5/6) clay; moderate coarse prismatic structure parting to moderate medium and coarse subangular blocky; extremely hard, extremely firm, very sticky and very plastic; common very fine and fine roots; 5 percent crayfish krotovinas filled with yellowish red (5YR 5/6) and very dark gray (10YR 3/1) clay and few fine nodules of calcium carbonate; common distinct intersecting slickensides that are tilted at 35 to 40 degrees to the horizontal on horizontal faces of peds; 1 percent fine prominent light greenish gray (5GY 7/1) iron depletions with clear boundaries on surfaces of slickensides; strongly effervescent; clear wavy boundary.

B'ss1--193 to 216 cm; yellowish red (5YR 5/6) clay; weak coarse wedge-shaped structure parting to weak medium and coarse subangular blocky; extremely hard, extremely firm, very sticky and very plastic; common distinct dark gray (10YR 4/1) intersecting slickensides that are tilted 30 to 35 degrees to the horizontal; 7 percent fine and medium prominent light greenish gray (5GY 7/1) iron depletions with sharp boundaries on surfaces of slickensides; few fine rounded concretions of calcium carbonate coated with yellow (10YR 7/8) iron; strongly effervescent; gradual smooth boundary.

B'ss2--216 to 240 cm; yellowish red (5YR 4/6) clay; moderate coarse wedge-shaped structure parting to moderate medium and coarse subangular blocky; extremely hard, extremely firm, very sticky and very plastic; very few very fine roots between peds; common prominent intersecting slickensides that are tilted 25 to 35 degrees to the horizontal; 10 percent fine prominent light greenish gray (10GY 7/1,8/1) iron depletions with sharp boundaries on the surfaces of slickensides; strongly effervescent; gradual smooth boundary.

B'ss3--240 to 272 cm; yellowish red (5YR 5/6) clay; weak coarse angular blocky structure parting to weak medium angular blocky; extremely hard, extremely firm, very sticky and very plastic; very few very fine roots between peds; few faint intersecting slickensides that are tilted 15 to 25 percent to the horizontal; 4 percent fine prominent light olive gray (5Y 6/2) iron depletions with sharp boundaries on root traces in interiors of peds and on surfaces of slickensides; few fine and medium black (10YR 2/1) masses of iron manganese on root traces; strongly effervescent; gradual smooth boundary.

B'ss4--272 to 300 cm; yellowish red (5YR 5/6) clay extremely hard, extremely firm, very sticky and very plastic; very few very fine roots between peds; few prominent intersecting slickensides that are tilted 15 to 25 percent to the horizontal; 6 percent fine and medium light gray (5Y 7/2) iron depletions with sharp boundaries on root traces in interiors of peds and on surfaces of slickensides; strongly effervescent.

Description Date: 6/22/1999

Soil Series: Lake Charles
Site Identification #: **99 LAC 157 H** (99TX157001A - microhigh)

Location Information
Soil Survey Area Name: Fort Bend County, Texas.
Latitude: 29 degrees 24 minutes 12 seconds North
Longitude: 95 degrees 43 minutes 42 seconds West
Described by: Wes Miller and Larry Wilding

Classification: Fine, smectitic, hyperthermic Typic Hapludert

Ak1--0 to 10 cm; very dark gray (10YR 3/1) clay; weak fine granular structure; firm; many fine roots; common fine and few medium interstitial pores; common medium rounded white (2.5Y 8/1) nodules of calcium carbonate and few calcium carbonate nodules are coated with yellowish brown (10YR 5/6) iron; clear smooth boundary.

Ak2--10 to 28 cm; very dark gray (10YR 3/1) clay; weak medium subangular blocky structure parting to moderate fine and medium granular; firm; common fine roots; few fine interstitial and few fine tubular pores; common fine and medium rounded white (2.5Y 8/1) nodules of calcium carbonate and few calcium carbonate nodules are coated with yellowish brown (10YR 5/6) iron; slightly effervescent; clear wavy boundary.

Bkss1--28 to 70 cm; dark gray (10YR 4/1) clay; moderate fine and medium angular blocky structure; firm; common fine roots; few fine tubular pores; common distinct intersecting slickensides that are tilted 55 to 60 degrees to the horizontal; common fine and medium rounded white (10YR 8/1) nodules of calcium carbonate and few calcium carbonate nodules are coated with yellowish brown (10YR 5/6) iron; slightly effervescent; clear smooth boundary.

Bkss2--70 to 95 cm; dark grayish brown (2.5Y 4/2) clay; moderate fine and medium angular blocky structure; firm; common fine roots; few fine tubular pores; common intersecting slickensides that are tilted 40 to 50 degrees to the horizontal; few distinct pressure surfaces; common fine and medium white (10YR 8/1) nodules of calcium carbonate; 5 percent fine and medium yellowish brown (10YR 5/6) masses of iron with sharp boundaries; slightly effervescent; gradual wavy boundary.

Bkss3--95 to 129 cm; dark grayish brown (2.5Y 4/2) clay; moderate fine and medium angular blocky structure; firm; common fine roots; few fine tubular pores; common intersecting slickensides that are tilted 40 to 50 degrees to the horizontal; few distinct pressure surfaces; common fine and medium white (10YR 8/1) nodules of calcium carbonate; 5 percent fine and medium yellowish brown (10YR 5/6) masses of iron with sharp boundaries; slightly effervescent; gradual wavy boundary.

Bkss4--129 to 144 cm; 60 percent olive brown (2.5Y 4/3), 20 percent dark gray (10YR 4/1), 20 percent yellowish brown (10YR 5/6) clay; strong medium and coarse angular blocky structure; very firm; common fine roots; common intersecting slickensides that are tilted 35 to 45 degrees to the horizontal; dark gray (10YR 4/1) matrix material are filled cracks 5mm to 2.5 cm wide mixed within the olive brown (2.5Y 4/3) matrix material; yellowish brown (10YR 5/6) matrix material is an oval mass about 10 cm wide and 8 cm thick and is bounded by the olive brown (2.5Y 4/3) material; common fine to coarse rounded light brownish gray (10YR 6/2) and white (10YR 8/1) nodules of calcium carbonate; slightly effervescent; clear wavy boundary.

Bkss5--144 to 176 cm; dark yellowish brown (10YR 4/4), dark gray (10YR 4/1), strong brown (7.5YR 5/8) clay; strong medium and coarse angular blocky structure; very firm; common fine roots; common intersecting slickensides that are tilted 30 to 40 degrees to the horizontal; dark gray (10YR 4/1) matrix material are filled cracks 5mm to 2 cm wide throughout the horizon; strong brown (7.5YR 5/8) matrix material dominates the lower 5 cm of the horizon; common fine to coarse rounded light brownish gray (10YR 6/2) and white (10YR 8/1) nodules and masses of calcium carbonate that are concentrated near the contact with the Bss1 horizon; strongly effervescent; clear wavy boundary.

Bss1--176 to 210 cm; strong brown (7.5YR 4/6) clay; moderate medium and coarse angular blocky structure; very firm; common fine roots; common distinct intersecting slickensides that are tilted 30 to 40 degrees to the horizontal; 6 percent fine and medium prominent greenish gray (5G 6/1) iron depletions with clear boundaries on surfaces of slickensides and on root pore linings; few fine rounded white (10YR 8/1) nodules of calcium carbonate; strongly effervescent; gradual wavy boundary.

Bss2--210 to 240 cm; yellowish red (5YR 4/6) clay; moderate medium and coarse angular blocky structure; extremely firm; common fine roots; many prominent intersecting slickensides that are tilted 20 to 30 degrees to the horizontal; 8 percent fine prominent light greenish gray (5GY 7/1) iron depletions with clear boundaries on surfaces of slickensides; few fine dendritic black (10YR 2/1) masses of iron-manganese on surfaces of slickensides within the light greenish gray (5GY 7/1) iron depletions; strongly effervescent gradual wavy boundary.

Description Date: 6/23/1999

Soil Series: Lake Charles
Site Identification #: **99 LAC 481 L** (99TX481001 - microlow)

Location Information
Soil Survey Area Name: Wharton County, Texas.
Latitude: 29 degrees 25 minutes 21 seconds North
Longitude: 96 degrees 04 minutes 22 seconds West
Described by: Edward Griffin and Jon Wiedenfeld

Classification: Fine, smectitic, hyperthermic Typic Hapludert

A1--0 to 12 cm; black (2.5Y 2/1) clay; moderate fine and medium subangular blocky structure; hard, firm, very sticky and very plastic; common fine roots; common fine tubular pores; less than 1 percent vey fine and fine rounded nodules of iron-manganese; less than 1 percent fine rounded nodules of calcium carbonate coated with brownish yellow (10YR 6/8) iron; clear smooth boundary.

A2--12 to 28 cm; black (2.5Y 2/1) clay; moderate fine and medium subangular blocky structure; hard, firm, very sticky and very plastic; common fine roots; common fine tubular pores; very few distinct pressure surfaces; clear smooth boundary.

Bss1--28 to 59 cm; black (2.5Y 2/1) clay; moderate medium and coarse subangular blocky structure; very hard, firm; common fine roots; many fine tubular pores; common distinct intersecting slickensides that are tilted 60 to 70 degrees to the horizontal; few fine rounded nodules of calcium carbonate coated with brownish yellow (10YR 6/8) iron; clear smooth boundary.

Bss2--59 to 83 cm; black (2.5Y 2/1) clay; moderate medium and coarse subangular blocky structure; very hard, very firm; common fine roots; common fine and medium tubular pores; common distinct intersecting slickensides that are tilted 60 to 70 degrees to the horizontal; less than 1 percent fine rounded nodules of calcium carbonate coated with brownish yellow (10YR 6/8) iron; less than 1 percent very fine and fine rounded nodules of iron-manganese; gradual wavy boundary.

Bss3--83 to 123 cm; very dark gray (2.5Y 3/1) clay; moderate medium wedge-shaped structure parting to moderate fine and medium angular blocky; very hard, very firm; common fine roots along surfaces of slickensides; common fine and medium tubular pores; many prominent intersecting slickensides that are tilted 50 to 60 degrees to the horizontal; gradual wavy boundary.

Bss4--123 to 147 cm; dark gray (2.5Y 4/1) clay; moderate medium wedge-shaped structure parting to moderate fine and medium angular blocky; very hard, very firm; common fine roots along surfaces of slickensides; many prominent intersecting slickensides that are tilted 40 to 50 degrees to the horizontal; few crawfish krotovinas 3 to 4 cm in diameter filled with a mixture of grayish brown (2.5Y 5/2), dark gray (2.5Y 4/1), and yellowish red (5YR 5/6) clay; less than 1 percent fine faint light olive brown (2.5Y 5/3) iron concentrations with diffuse boundaries along surfaces of slickensides; very slightly effervescent; clear smooth boundary.

Bkss1--147 to 165 cm; dark gray (2.5Y 4/1) clay; moderate medium and coarse wedge-shaped structure parting to moderate fine and medium angular blocky; very hard, very firm; common fine roots on surfaces of slickensides; many prominent intersecting slickensides that are tilted 30 to 40 degrees to the horizontal; few crawfish krotovinas 3 to 4 cm wide and filled with a mixture of grayish brown (2.5Y 5/2), dark gray

(2.5Y 4/1), and yellowish red (5YR 5/6) clay; few fine rounded uncoated nodules of calcium carbonate; very slightly effervescent; clear smooth boundary.

Bkss2--165 to 176 cm; grayish brown (2.5Y 5/2) clay; weak medium and coarse wedge-shaped structure parting to moderate medium and coarse angular blocky; very hard, very firm, very sticky and very plastic; common very fine and fine roots along surfaces of slickensides; common distinct intersecting slickensides that are tilted 30 to 40 degrees to the horizontal; few crawfish krotovinas 3 to 4 cm in diameter and filled with a mixture of grayish brown (2.5Y 5/2), dark gray (2.5Y 4/1), and yellowish red (5YR 5/6) clay; 5 percent fine and medium rounded nodules of calcium carbonate and 1 percent of the nodules are coated with brownish yellow (10YR 6/8) iron; strongly effervescent; abrupt smooth boundary.

Bkss3--176 to 200 cm; reddish brown (5YR 5/4); weak medium and coarse subangular blocky structure; extremely hard, extremely firm, slightly sticky and slightly plastic; very few very fine and fine roots; few crawfish krotovinas 3 to 4 cm in diameter and filled with a mixture of grayish brown (2.5Y 5/2), dark gray (2.5Y 4/1), yellowish red (5YR 5/6) clay, and few fine rounded masses and nodules of calcium carbonate; common distinct intersecting slickensides that are tilted 15 to 25 degrees to the horizontal; 7 percent fine and medium grayish green (5G 5/2) iron depletions with sharp boundaries on surfaces of slickensides; 1 percent fine and medium rounded nodules of calcium carbonate in matrix; strongly effervescent; gradual wavy boundary.

Bkss4--200 to 250 cm; yellowish red (5YR 5/6) clay; moderate medium and coarse wedge-shaped structure parting to moderate medium and coarse subangular blocky; extremely hard, extremely firm, slightly sticky and slightly plastic; very few very fine roots; common prominent intersecting slickensides that are tilted 10 to 20 degrees to the horizontal; 5 percent fine and medium grayish green (5G 5/2) and 2 percent fine gray (2.5Y 5/1) iron depletions with sharp boundaries on surfaces of slickensides; 1 percent fine and medium rounded nodules of calcium carbonate; strongly effervescent.

Description Date: 6/23/1999

Soil Series: Lake Charles
Site Identification #: **99 LAC 481 H** (99TX481001A - microhigh)

Location Information
Soil Survey Area Name: Wharton County, Texas
Latitude: 29 degrees 25 minutes 21 seconds North
Longitude: 96 degrees 04 minutes 22 seconds West
Described by: Wes Miller and Larry Wilding

Classification: Fine, smectitic, hyperthermic Typic Hapludert

Ak1--0 to 15 cm; very dark gray (10YR 3/1) clay; weak medium subangular blocky structure parting to moderate fine and medium granular; friable; many fine roots; common fine and few medium interstitial pores; few fine masses of grayish brown (2.5Y 5/2) clay throughout; 3 percent subrounded nodules of calcium carbonates 2 to 4 mm in size; matrix is non-calcareous; clear smooth boundary.

Ak2--15 to 33 cm; very dark gray (2.5Y 3/1) clay; moderate fine and medium angular blocky structure; friable; common fine roots; few fine tubular and interstitial pores; common distinct pressure surfaces; few distinct intersecting slickensides; 20 percent light yellowish brown (2.5Y 6/3) masses and nodules of calcium carbonates along surfaces of slickensides; slightly effervescent; clear smooth boundary.

Bkss1--33 to 78 cm; dark gray (2.5Y 4/1) clay; strong fine and medium angular blocky structure; friable; common fine roots; few fine tubular pores; common distinct intersecting slickensides that are tilted 40 to 50 degrees to the horizontal; 30 percent fine and medium rounded nodules of calcium carbonate and 1 percent nodules of calcium carbonate coated with brownish yellow (10YR 6/8) iron; strongly effervescent; abrupt wavy boundary.

Bkss2--78 to 104 cm; weak red (7.5R 4/4) clay; moderate fine and medium angular blocky structure; firm; common fine roots; few very fine tubular pores; many distinct intersecting slickensides that are tilted 30 to 45 degrees to the horizontal; 5 percent of matrix are cracks filled with very dark gray (2.5Y 3/1) clay 1 cm to 3 cm wide; 5 percent subrounded nodules of calcium carbonate 2 to 4 mm in size; 10 percent masses of olive brown (2.5Y 4/3) clay 1 to 3 cm in size mixed within the weak red (7.5YR 4/4) matrix material; 5 percent of the horizon is a reddish yellow (7.5YR 6/6) strongly effervescent clay intrusion 4 to 8 cm wide that arcs from the upper part of the Bkss3 horizon and extends to the lower part of the Bkss1 horizon; strongly effervescent; abrupt wavy boundary.

Bkss3--104 to 157 cm; dark grayish brown (2.5Y 4/2) clay; strong medium and coarse angular blocky structure; firm; common fine roots; very few very fine tubular pores; common distinct intersecting slickensides that are tilted 30 to 50 degrees to the horizontal; 5 percent fine and medium subrounded nodules of calcium carbonate; 5 percent of the horizon is a strong brown (7.5YR 5/6) strongly effervescent clay intrusion 4 to 8 cm wide that arcs from the upper part of the Bkss4 horizon and extends to the lower part of the Bkss2 horizon; strongly effervescent; abrupt wavy boundary.

Bkss4--157 to 181 cm; light olive brown (2.5Y 5/4) clay; strong medium and coarse angular blocky structure; firm; common fine roots; very few very fine pores; common distinct coarsely grooved intersecting slickensides tilted 30 to 60 degrees to the horizontal; 10 percent fine and medium nodules of calcium carbonate concentrated near contact with Bss1 horizon; 10 percent of the horizon is a strong brown (7.5YR 4/6) strongly effervescent clay intrusion 4 to 10 cm wide that arcs from the Bss1 horizon and extends to the lower part of the Bkss3 horizon; 4 percent fine rounded black (10YR 2/1)

iron-manganese nodules and masses; strongly effervescent; clear wavy boundary.

Bss1--181 to 260 cm; yellowish red (5YR 5/6) clay; strong medium to very coarse angular blocky structure; firm; common fine roots; common distinct intersecting slickensides that are tilted 20 to 60 degrees to the horizontal; 2 percent fine and medium prominent light brownish gray (2.5Y 6/2) iron depletions on surfaces of slickensides; 10 percent fine rounded black (10YR 2/1) iron-manganese nodules and masses; 2 percent fine nodules of calcium carbonate; 10 percent of the horizon is reddish yellow (7.5YR 7/6) clay mixed with the yellowish red (5YR 5/6) matrix material; strongly effervescent; abrupt wavy boundary.

Bss2--260 to 300 cm; yellowish red (5YR 5/6) clay; strong very coarse angular blocky structure; very firm; very few very fine roots; common prominent intersecting slickensides that are tilted 20 to 40 degrees to the horizontal; 8 percent fine and medium light brownish gray (2.5Y 6/2) iron depletions on surfaces of slickensides; 1 percent fine masses of black (10YR 2/1) dendritic masses of iron-manganese on surfaces of slickensides; less than 1 percent fine nodules of calcium carbonate; strongly effervescent.

Laewest Series Pedon Descriptions

Description Date: 11/18/1999

Soil Series: Laewest
Site Identification #: **99 LAW 239 L** (99TX239001 - microlow)

Location Information
Soil Survey Area Name: Jackson County, Texas
Latitude: 28 degrees 52 minutes 47.6 seconds North
Longitude: 96 degrees 24 minutes 11.4 seconds West
Site Note: The site fits the Lake Charles series.
Described by: Jon Wiedenfeld

Classification: Fine, smectitic, hyperthermic Typic Hapluderts

A1--0 to 13 cm; black (N 2.5/) clay; moderate fine and medium subangular blocky structure; firm, very hard; common very fine and fine roots; common fine interstitial pores; 5 percent faint pressure surfaces; less than 1 percent fine distinct spherical black (7.5YR 2.5/1) iron-manganese masses on surfaces of peds with sharp boundaries; clear smooth boundary.

A2--13 to 29 cm; black (N 2.5/) clay; strong fine and medium subangular blocky structure; firm, very hard; common very fine and fine roots; common very fine tubular pores; 10 percent faint slickensides; 15 percent distinct pressure surfaces; less than 1 percent fine distinct spherical black (7.5YR 2.5/1) iron-manganese masses on surfaces of peds with sharp boundaries; clear wavy boundary.

Bss1--29 to 56 cm; very dark gray (N 3/) clay; strong medium subangular blocky structure; firm, very hard; common very fine and fine roots; common very fine tubular pores; 30 percent distinct slickensides tilted at 50 to 60 degrees from the horizontal; less than 1 percent fine distinct spherical black (7.5YR 2.5/1) iron-manganese masses on surfaces of peds with sharp boundaries; gradual wavy boundary.

Bss2--56 to 94 cm; dark gray (N 4/) clay; moderate medium wedge structure parts to strong medium and coarse angular blocky; firm, very hard; common very fine roots; few very fine tubular pores; 55 percent prominent slickensides tilted at 50 to 60 degrees from the horizontal; less than 1 percent fine distinct spherical black (7.5YR 2.5/1) iron-manganese masses on surfaces of peds with sharp boundaries; 1 percent fine spherical carbonate nodules; few carbonate nodules coated with brownish yellow (10YR 6/8) iron concentrations; gradual wavy boundary.

Bss3--94 to 141 cm; dark gray (2.5Y 4/1) clay; moderate medium wedge structure parts to strong medium and coarse angular blocky; firm, very hard; common very fine roots; few very fine tubular pores; 75 percent prominent slickensides tilted at 40 to 60 degrees from the horizontal; less than 1 percent fine spherical black (7.5YR 2.5/1) iron-manganese nodules; less than 1 percent fine distinct spherical black (7.5YR 2.5/1) iron-manganese masses on surfaces of peds with sharp boundaries; less than 1 percent fine spherical carbonate nodules; clear wavy boundary.

Bkss1--141 to 156 cm; dark gray (10YR 4/1) clay; moderate coarse wedge structure parts to moderate medium and coarse angular blocky; firm, very hard; common very fine roots; 45 percent prominent slickensides tilted at 10 to 20 degrees from the horizontal; less than 1 percent fine spherical black (7.5YR 2.5/1) iron-manganese nodules; less than 1 percent fine distinct spherical black (7.5YR 2.5/1) iron-manganese masses on surfaces of peds with sharp boundaries; 8 percent medium and coarse spherical carbonate nodules; 1 percent medium and coarse irregular carbonate masses; slightly effervescent; clear

wavy boundary.

Bkss2--156 to 168 cm; 80 percent reddish yellow (7.5YR 6/6) and 20 percent strong brown (7.5YR 5/6) clay; moderate medium and coarse angular blocky structure; firm, very hard; few very fine roots; 30 percent distinct slickensides are tilted at 10 to 20 degrees from the horizontal; less than 1 percent fine spherical black (7.5YR 2.5/1) iron-manganese nodules; 20 percent medium and coarse irregular carbonate masses; 2 percent medium and coarse spherical carbonate nodules; carbonate masses and nodules or on top of a 4 centimeter wide reddish yellow (5YR 6/6) layer of clay is at the contact between the Bkss2 and Bkss3 horizons; few cracks 5millimeters to 1.5 centimeters wide filled with dark gray (10YR 4/1) clay; strongly effervescent; clear smooth boundary.

Bkss3--168 to 183 cm; 70 percent strong brown (7.5YR 5/6) and 30 percent reddish yellow (7.5YR 6/6) clay; weak medium and coarse subangular blocky structure; firm, very hard; few very fine roots; 20 percent slickensides tilted at 10 to 20 degrees from the horzontal with gray (7.5YR 5/1) iron depletions on 20 percent of the slickenside surfaces; 3 percent fine and medium prominent light gray (7.5YR 7/1) iron depletions on surfaces of peds with diffuse boundaries not associated with the slickensides; 10 percent fine and medium irregular carbonate masses; 3 percent fine and medium spherical carbonate nodules; a gray (7.5YR 5/1) clay layer 3 centimeters wide is at the contact between the Bkss3 and Bkss4 horzons with less than 1 percent fine rounded iron-manganese nodules; strongly effervescent; clear smooth boundary.

B'ss1--183 to 208 cm; 65 percent yellowish red (5YR 5/6), and 25 percent light gray (2.5Y 7/2) clay; weak coarse prismatic structure parts to moderate medium subangular blocky; firm, very hard; few very fine roots between peds; 30 percent distinct slickensides tilted at 20 to 40 degrees from the horizontal; less than 1 percent fine and medium prominent light gray (7.5YR 7/1) iron depletions vertical on surfaces of peds with diffuse boundaries; 1 percent fine prominent yellow (2.5Y 7/8) masses of oxidized iron in matrix surrounding redox depletions with diffuse boundaries; 10 percent fine and medium irregular carbonate masses in center of light gray (2.5Y 7/2) matrix; 6 percent of the total area consists of brittle masses of strong brown (7.5YR 5/6) fine sandy loam 5 millimeters to 2 centimeters in size with few fine iron-manganese masses in center; strongly effervescent; clear smooth boundary.

B'ss2--208 to 244 cm; 70 percent reddish yellow (5YR 6/6), and 30 percent light gray (2.5Y 7/2) clay; weak coarse prismatic structure parts to moderate medium subangular blocky ; firm, very hard; few very fine roots between peds; 25 percent distinct slickensides tilted at 20 to 50 degrees from the horizontal; 1 percent fine prominent black (7.5YR 2.5/1) iron-manganese masses with sharp boundaries; 2 percent fine and medium prominent yellow (2.5Y 7/8) masses of oxidized iron in matrix surrounding redox depletions with diffuse boundaries; 2 percent fine prominent dendritic black (7.5YR 2.5/1) manganese coatings on surfaces of slickensides with sharp boundaries; 1 percent medium irregular carbonate nodules; 6 percent of the total area consists of brittle masses of strong brown (7.5YR 5/6) fine sandy loam 5 millimeters to 5 centimeters in size with few fine iron-manganese masses in center ; few crawfish krotovinas 2 to 5 centimeters in width filled with gray (10YR 6/1) clay extending from the bottom to midway through the horizon; strongly effervescent; gradual wavy boundary.

BC--244 to 272 cm; 55 percent light gray (2.5Y 7/2) and 45 percent reddish yellow (5YR 6/6) clay; weak coarse prismatic structure parts to moderate medium subangular blocky ; firm, very hard; 10 percent distinct slickensides tilted at 20 to 30 degrees from the horizontal; 1 percent fine prominent dendritic black (7.5YR 2.5/1) manganese coatings surfaces of slickensides with sharp boundaries and 2 percent fine and medium prominent brownish yellow (10YR 6/8) masses of oxidized iron in matrix surrounding redox concentrations with clear boundaries; 2 percent fine and medium prominent yellow (2.5Y 7/8) masses of oxidized iron in matrix surrounding redox depletions with diffuse boundaries; 1 percent fine irregular carbonate masses; 3 percent of the total area consists of pink (5YR 7/4) brittle masses of silt loam texture and are in the light gray (2.5Y 7/2) matrix material; few crawfish krotovinas filled with gray (10YR 6/1)

clay extending from the bottom to midway through the horizon; strongly effervescent clear wavy boundary.
2BC--272 to 320 cm; reddish yellow (7.5YR 6/6), fine sandy loam; weak coarse subangular blocky structure; friable, hard; few thin strata of yellowish red (5YR 5/6) sandy clay loam; strongly effervescent; clear smooth boundary.

3BC1--320 to 360 cm; 60 percent red (2.5YR 5/6) and 40 percent light gray (2.5Y 7/1) clay; weak coarse subangular blocky structure; firm, very hard; 1 percent fine prominent olive yellow (2.5Y 6/8) masses of oxidized iron in matrix surrounding redox depletions with sharp boundaries; 1 percent fine irregular carbonate masses; 1 percent fine spherical carbonate nodules; strongly effervescent; clear smooth boundary.

3BC2--360 to 405 cm; light gray (5Y 7/2) clay; weak coarse subangular blocky structure; firm, very hard; 2 percent fine prominent olive yellow (2.5Y 6/8) masses of oxidized iron on surfaces of peds with diffuse boundaries; strongly effervescent; gradual smooth boundary.

3BC3--405 to 425 cm; light gray (5Y 7/2) clay; 5 percent medium and coarse faint pale olive (5Y 6/3) mottles; weak coarse subangular blocky structure; firm, very hard; 1 percent fine prominent reddish yellow (7.5YR 6/8) masses of oxidized iron in matrix surrounding redox concentrations with clear boundaries; 1 percent fine prominent yellowish red (5YR 5/8) masses of oxidized iron on surfaces of peds with sharp boundaries; strongly effervescent.

Description Date: 11/18/1999

Soil Series: Laewest
Site Identification #: **99 LAW 239 H** (99TX239001A - microhigh)

Location Information
Soil Survey Area Name: Jackson County, Texas
Latitude: 28 degrees 52 minutes 47.6 seconds North
Longitude: 96 degrees 24 minutes 11.4 seconds West
Site Note: The site fits the Lake Charles series.
Described by: Larry Wilding and Lee Nordt

Classification: Fine, smectitic, hyperthermic Chromic Hapluderts

A--0 to 10 cm; 70 percent very dark gray (10YR 3/1) and 30 percent dark gray (10YR 4/1) clay; weak fine and medium subangular blocky structure; firm, very hard; common very fine and fine roots on surfaces of slickensides and common medium roots between peds; common fine interstitial pores; 2 percent fine faint very dark brown (10YR 2/2) iron-manganese nodules with sharp boundaries; 2 percent fine and medium carbonate nodules; gradual smooth boundary.

Ak--10 to 26 cm; 70 percent dark gray (2.5Y 4/1), 20 percent gray (2.5Y 5/1), and 10 percent light brownish gray (2.5Y 6/2) clay; weak medium and coarse angular blocky structure; firm, very hard; common very fine roots on surfaces of slickensides; common very fine and fine interstitial and tubular pores; 10 percent faint slickensides; 2 percent fine faint very dark brown (10YR 2/2) iron-manganese nodules with sharp boundaries; 5 percent medium carbonate nodules; 8 percent medium and coarse carbonate masses with few having nodules in the center; very slightly effervescent; gradual wavy boundary.

Bkss1--26 to 58 cm; 85 percent dark gray (2.5Y 4/1) and 15 percent light yellowish brown (2.5Y 6/3) clay; moderate coarse wedge structure parts to moderate medium angular blocky; firm, very hard; common medium roots and common very fine roots on surfaces of slickensides; few very fine tubular pores; 40 percent distinct slickensides tilted at 30 to 40 degrees from the horizontal; 1 percent fine faint very dark brown (10YR 2/2) iron-manganese nodules with sharp boundaries; 10 percent medium and coarse carbonate masses and nodules in centers of carbonate masses in light olive brown matrix; very slightly effervescent; clear wavy boundary.

Bkss2--58 to 90 cm; 55 percent dark grayish brown (2.5Y 4/2), 30 percent gray (2.5Y 5/1), and 15 percent olive yellow (2.5Y 6/6) clay; moderate fine and medium wedge structure parts to moderate fine angular blocky; very firm, very hard; common very fine and fine roots on surfaces of slickenside; few very fine tubular pores; 50 percent distinct slickensides tilted at 40 to 50 degrees from the horizontal with few slickensides tilted at 60 to 70 degrees from the horizontal at interface between the microhigh and microlow; 1 percent fine faint very dark brown (10YR 2/2) iron-manganese nodules with sharp boundaries; 5 percent medium and coarse carbonate masses; 10 percent medium and coarse carbonate nodules with few in the centers of carbonate masses;; few crawfish krotovinas; slightly effervescent; gradual wavy boundary.

Bkss3--90 to 120 cm; 70 percent light yellowish brown (2.5Y 6/4) and 25 percent yellow (10YR 7/6) clay; moderate coarse wedge structure parts to moderate fine and medium angular blocky; very firm, very hard; common very fine roots on surfaces of slickensides; few very fine tubular pores; 55 percent prominent slickensides tilted at 40 to 50 degrees from the horizontal with few slickensides tilted at 60 to 70 degrees from the horizontal at interface between the microhigh and microlow; 1 percent fine and

medium faint very dark brown (10YR 2/2) iron-manganese nodules with sharp boundaries; 1 percent fine and medium carbonate masses; 2 percent medium and coarse carbonate nodules; common cracks 1 to 2 centimeters wide filled with black (2.5Y 2/1) clay; strongly effervescent; gradual wavy boundary.

Bkss4--120 to 145 cm; 80 percent light yellowish brown (2.5Y 6/3) and 15 percent yellow (10YR 7/8) clay; moderate coarse wedge structure parts to moderate fine and medium angular blocky; very firm, very hard; common very fine roots on surfaces of slickensides; few very fine tubular pores; 50 percent distinct slickensides tilted at 45 to 75 degrees from the horizontal with few slickensides tilted at 60 to 70 degrees from the horizontal at interface between the microhigh and microlow; 3 percent fine and medium distinct very dark brown (10YR 2/2) iron-manganese nodules with sharp boundaries; 1 percent fine and medium carbonate masses; less than 1 percent medium and coarse carbonate nodules; common cracks 1 to 2 centimeters wide filled with black (2.5Y 2/1) clay; strongly effervescent; gradual wavy boundary.

Bkss5--145 to 165 cm; 50 percent light brownish gray (2.5Y 6/2) and 50 percent strong brown (7.5YR5/6), clay; moderate coarse wedge structure parts to moderate medium and coarse angular blocky; very firm, very hard; common very fine and fine roots on surfaces of slickensides; few very fine tubular pores; 45 percent distinct slickensides tilted at 25 to 30 degrees from the horizontal with few slickensides tilted at 55 degrees from the horizontal at interface between the microhigh and microlow; 1 percent fine iron-manganese masses lining root pores; 1 percent fine distinct very dark brown (10YR 2/2) iron-manganese nodules with sharp boundaries; 1 percent fine and medium carbonate masses; 3 percent medium and coarse carbonate nodules; few cracks 1 to 2 centimeters wide filled with black (2.5Y 2/1) clay; strongly effervescent; gradual wavy boundary.

Bkss6--165 to 208 cm; 55 percent yellow (10YR 7/8) and 45 percent strong brown (7.5YR 4/6) clay; moderate coarse wedge structure parts to moderate medium and coarse angular blocky; very firm, very hard; common very fine roots between peds; 35 percent distinct slickensides tilted at 25 to 30 degrees from the horizontal; 1 percent fine distinct very dark brown (10YR 2/2) iron-manganese nodules with sharp boundaries; 2 percent fine and medium distinct black (7.5YR 2/1) manganese masses on surfaces of peds with sharp boundaries; 10 percent coarse prominent light gray (2.5Y 7/1) iron depletions in matrix with sharp boundaries; 1 percent fine and medium carbonate masses; 1 percent medium and coarse carbonate nodules; strongly effervescent; gradual wavy boundary.

Bss--208 to 235 cm; 45 percent light gray (2.5Y 7/1) and 55 percent strong brown (7.5YR 5/8), silty clay; moderate coarse wedge structure parts to weak fine and medium angular blocky; very firm, very hard; common very fine roots between peds; 25 percent distinct slickensides and 50 percent prominent pressure faces; 1 percent fine distinct very dark brown (10YR 2/2) iron-manganese nodules with sharp boundaries and 2 percent fine and medium distinct black (7.5YR 2/1) manganese masses with sharp boundaries; 35 percent coarse prominent light gray (2.5Y 7/1) iron depletions with sharp boundaries; 1 percent fine and medium carbonate nodules; strongly effervescent; clear smooth boundary.

BC1--235 to 270 cm; 50 percent light gray (2.5Y 7/1), 35 percent strong brown (7.5YR 5/8), and 15 percent light yellowish brown (10YR 6/4) silty clay; weak coarse angular blocky structure; very firm, very hard; common very fine roots; 20 percent faint pressure faces; 1 percent fine and medium distinct very dark brown (10YR 2/2) iron-manganese nodules with sharp boundaries; strongly effervescent; gradual smooth boundary.

BC2--270 to 300 cm; 45 percent light gray (2.5Y 7/1), 40 percent strong brown (7.5YR 5/8), and 15 percent light yellowish brown (10YR 6/4) silty clay; weak coarse angular blocky structure; very firm, very hard; violent effervescent.

Description Date: 11/17/1999

Soil Series: Laewest
Site Identification #: **99 LAW 469 L** (99TX469001 - microlow)

Location Information
Soil Survey Area Name: Victoria County, Texas
Latitude: 28 degrees 43 minutes 12.0 seconds North
Longitude: 96 degrees 45 minutes 23.3 seconds West
Described by Jon Wiedenfeld and Cynthia Stiles

Classification: Fine, smectitic, hyperthermic Typic Hapludert

A--0 to 16 cm; black (10YR 2/1) clay, black (10YR 2/1), dry; moderate fine and medium subangular blocky structure; firm, hard; common very fine and fine roots and common coarse roots; common fine vesicular pores; 10 percent faint pressure faces; few insect casts; clear smooth boundary.

Bss1--16 to 43 cm; black (10YR 2/1), clay, black (10YR 2/1), dry; moderate medium subangular blocky structure; firm, very hard; common very fine and fine roots; few fine tubular pores; 20 percent distinct slickensides tilted at 20 to 40 degrees from the horizontal; 30 percent distinct pressure faces; less than 1 percent fine spherical black (7.5YR 2/1)iron-manganese nodules; less than 1 percent fine iron manganese masses; common cracks 0.5 to 2.5 centimeters wide; gradual smooth boundary.

Bss2--43 to 74 cm; black (10YR 2/1), clay, black (10YR 2/1), dry; moderate medium subangular blocky structure; firm, very hard; common very fine and fine roots; common very fine tubular pores; 60 percent prominent slickensides tilted at 50 degrees from the horizontal; less than 1 percent fine black (7.5YR 2/1) iron-manganese nodules; less than 1 percent fine iron manganese masses; gradual smooth boundary.

Bss3--74 to 118 cm; black (10YR 2/1), clay, very dark gray (10YR 3/1), dry; moderate medium angular blocky and moderate fine and medium wedge structure; firm, very hard; common very fine and fine roots; 70 percent prominent slickensides tilted at 50 degrees from the horizontal.; 1 percent fine snail shell fragments; less than 1 percent fine iron-manganese nodules; gradual wavy boundary.

Bkss1--118 to 154 cm; very dark gray (10YR 3/1), clay, very dark gray (10YR 3/1), dry; moderate medium and coarse wedge parts to strong medium and coarse angular blocky structure; firm, very hard; common very fine roots; 60 percent prominent slickensides are tilted at 40 to 50 degrees from the horizontal; 5 percent fine spherical carbonate nodules with few having a hollow center; 1 percent medium plant phytoliths; less than 1 percent fine iron-manganese masses; slightly effervescent; clear wavy boundary.

Bkss2--154 to 176 cm; 70 percent dark gray (10YR 4/1) and 30 percent yellowish brown (10YR 5/8) clay; moderate medium and coarse angular blocky structure; firm, very hard; common very fine roots on surfaces of slickensides; 45 percent distinct slickensides tilted at 40 degrees from the horizontal with dark gray (10YR 4/1) organic coats on slickenside surfaces; less than 1 percent fine prominent strong brown (7.5YR 5/8) masses of oxidized iron with sharp boundaries in matrix; 1 percent fine carbonate nodules; 2 percent medium and coarse carbonate masses with few having fine nodules in the center; common cracks 5 centimeters wide filed with black (10YR 2/1) clay; strongly effervescent; gradual wavy boundary.

B'ss1--176 to 222 cm;„ 80 percent brownish yellow (10YR 6/6) and light yellowish brown (10YR 6/4) clay; moderate medium and coarse angular blocky structure; firm, hard; common very fine roots on

surfaces of slickensides; 40 percent distinct slickensides tilted at 20 to 30 degrees from the horizontal with dark gray (10YR 4/1) organic coats on slickenside surfaces; 1 percent fine and medium distinct dark grayish brown (2.5Y 4/2) iron depletions with clear boundaries lining root pores and on slickenside surfaces; 1 percent fine distinct strong brown (7.5YR 5/8) masses of oxidized iron with sharp boundaries in matrix; 1 percent fine distinct very dark brown (7.5YR 2/2) iron-manganese masses along ped faces with sharp boundaries; 1 percent very fine iron-manganese masses on slickenside surfaces; less than 1 percent fine carbonate nodules; less than 1 percent fine and medium carbonate masses ; less than 1 percent medium gypsum nests; less than 1 percent medium gypsum crystals; strongly effervescent; gradual wavy boundary.

B'ss2--222 to 245 cm; 80 percent brownish yellow (10YR 6/6) and 20 percent light gray (2.5Y 7/1), clay; moderate medium and coarse angular blocky structure; firm, hard; common very fine roots; common very fine tubular pores; 30 percent distinct slickensides tilted at 20 to 30 degrees from the horizontal; 1 percent fine prominent dendritic very dark brown (7.5YR 2/2) iron-manganese masses on slickenside surfaces with sharp boundaries; 1 percent fine prominent reddish yellow (5YR 6/8) masses of oxidized iron in matrix with sharp boundaries; 2 percent fine distinct reddish yellow (7.5YR 6/8) masses of oxidized iron in matrix with clear boundaries; light gray (2.5Y 7/1) matrix is mostly along slickenside surfaces and as a depletion on root pores; less than 1 percent fine cylindrical carbonate nodules; very few very fine clean rounded quartz grains throughout; strongly effervescent; gradual wavy boundary.

B'ss3--245 to 265 cm; 70 percent yellow (10YR 7/6) and 25 percent light gray (2.5Y 7/1) clay; moderate coarse angular blocky structure; firm, hard; 25 percent distinct slickensides tilted at 20 to 30 degrees from the horizontal; 1 percent fine prominent yellowish red (5YR 4/6) masses of oxidized iron lining pores with sharp boundaries; 1 percent fine distinct strong brown (7.5YR 5/6) masses of oxidized iron lining pores with clear boundaries; 2 percent fine prominent dendritic black (7.5YR 2.5/1) iron-manganese masses on slickenside surfaces with sharp boundaries; less than 1 percent fine cylindrical carbonate masses; lightr gray (2.5Y 7/1 matrix is mostly along slickenside surfaces; strongly effervescent.

Description Date: 11/17/1999

Soil Series: Laewest
Site Identification: **99 LAW 469 H** (99TX469001A - microhigh)

Location Information
Soil Survey Area Name: Victoria County, Texas
Latitude: 28 degrees 43 minutes 12.0 seconds North
Longitude: 96 degrees 45 minutes 23.3 seconds West
Described by: Larry Wilding, Lee Nordt,and Corey Crawford

Classification: Fine, smectitic, hyperthermic Chromic Hapludert

Ak--0 to 11 cm; dark gray (10YR 4/1), clay, dark gray (10YR 4/1), dry; moderate medium subangular blocky and moderate fine and medium angular blocky structure; very firm, very hard; common very fine, fine, and medium roots; common fine interstitial pores; 5 percent fine and medium white (10YR 8/1) and very pale brown (10YR 8/3) pedogenic carbonate nodules; strongly effervescent; gradual wavy boundary.

Bk--11 to 28 cm; dark grayish brown (2.5Y 4/2), clay, grayish brown (2.5Y 5/2), dry; moderate medium angular blocky structure; very firm, very hard; common very fine and fine roots roots; common fine tubular pores; common cracks 1 centimeter to 3 centimeters in width filled with dark gray (10YR 4/1) clay; 1 percent fine spherical very dark brown (10YR 2/2) nodules of iron-manganese; 8 percent fine and medium carbonate nodules; about 4 percent of the horizon is brown (10YR 5/3) clay; strongly effervescent; gradual wavy boundary.

Bkss1--28 to 119 cm; dark grayish brown (2.5Y 4/2) clay, grayish brown (2.5Y 5/2), dry; moderate medium wedge and moderate coarse wedge structure parts to moderate coarse platy structure; very firm, very hard; very few very fine roots between peds; common fine tubular pores; 45 percent distinct gray (2.5Y 5/1) slickensides tilted at 50 to 65 degrees from the horizontal; common cracks 1 centimeter to 3 centimeters in width filled with dark gray (10YR 4/1) clay; 1 percent fine very dark brown (10YR 2/2) nodules of iron-manganese; 15 percent fine and medium carbonate nodules; violently effervescent; gradual wavy boundary.

Bkss2--119 to 172 cm; light olive brown (2.5Y 5/3) clay, light yellowish brown (2.5Y 6/3), dry; moderate medium wedge and coarse structure; very firm, very hard; very few very fine roots between peds; very few very fine tubular pores; 55 percent prominent grayish brown (2.5Y 5/2) and dark gray (10YR 4/1) slickensides tilted at 40 to 65 degrees from the horizontal; 1 percent fine very dark brown (10YR 2/2) nodules of iron-manganese; 2 percent fine, medium and coarse carbonate nodules; violently effervescent; clear wavy boundary.

Bkss3--172 to 198 cm; yellowish brown (10YR 5/4) clay; moderate medium and coarse wedge structure; very firm, very hard; very few very fine roots; very few very fine tubular pores; 40 percent distinct grayish brown (2.5Y 5/2) slickensides tilted at 55 degrees from the horizontal; 1 percent fine very dark brown (10YR 2/2) nodules of iron-manganese; 3 percent worm casts; 2 percent medium and coarse carbonate nodules; common cracks 0.5 to 1.5 centimeters wide filled with dark gray (10YR 4/1) clay; violently effervescent; clear wavy boundary.

Bss--198 to 205 cm; 80 percent brownish yellow (10YR 6/6) and 20 percent light gray (2.5Y 7/1), clay; moderate medium and coarse angular blocky structure; firm, hard; common very fine roots; common very fine tubular pores; 30 percent distinct slickensides tilted at 20 to 30 degrees from the horizontal; 1 percent fine prominent dendritic very dark brown (7.5YR 2/2) iron-manganese masses on slickenside

surfaces with sharp boundaries; 1 percent fine prominent reddish yellow (5YR 6/8) masses of oxidized iron in matrix with sharp boundaries; 2 percent fine distinct reddish yellow (7.5YR 6/8) masses of oxidized iron in matrix with clear boundaries; light gray (2.5Y 7/1) matrix is mostly along slickenside surfaces and as a depletion on root pores; less than 1 percent fine cylindrical carbonate nodules; very few very fine clean rounded quartz grains throughout; strongly effervescent; gradual wavy boundary.

B'ss3--205 to 265 cm; 70 percent yellow (10YR 7/6) and 25 percent light gray (2.5Y 7/1) clay; moderate coarse angular blocky structure; firm, hard; 25 percent distinct slickensides tilted at 20 to 30 degrees from the horizontal; 1 percent fine prominent yellowish red (5YR 4/6) masses of oxidized iron lining pores with sharp boundaries; 1 percent fine distinct strong brown (7.5YR 5/6) masses of oxidized iron lining pores with clear boundaries; 2 percent fine prominent dendritic black (7.5YR 2.5/1) iron-manganese masses on slickenside surfaces with sharp boundaries; less than 1 percent fine cylindrical carbonate masses; light gray (2.5Y 7/1 matrix is mostly along slickenside surfaces; strongly effervescent.

Description Date: 11/19/1999

Soil Series: Laewest
Site Identification #: **99 LAW 391 L** (99TX391001 - microlow)

Location Information
Soil Survey Area Name: Refugio County, Texas
Latitude: 28 degrees 28 minutes 27.4 seconds North
Longitude: 97 degrees 07 minutes 0.0 seconds West
Site Note: The site fits the Laewest series.
Described by: Jon Wiedenfeld

Classification: Fine, smectitic, hyperthermic Typic Hapludert

A1--0 to 9 cm; black (2.5Y 2.5/1) clay; moderate fine subangular blocky structure; firm, very hard; common fine and medium roots; common fine interstitial pores; clear smooth boundary.

A2--9 to 28 cm; black (2.5Y 2.5/1) clay; moderate fine and medium subangular blocky structure; firm, very hard; common very fine and fine roots; few very fine tubular pores; 10 percent faint pressure surfaces; gradual smooth boundary.

Bss1--28 to 56 cm; black (2.5Y 2.5/1) clay; moderate medium angular blocky structure; firm, very hard; common very fine and fine roots between peds; few very fine tubular pores; 30 percent distinct slickensides tilted at 25 to 30 degrees from the horizontal; less than 1 percent fine iron-manganese masses gradual wavy boundary.

Bss2--56 to 79 cm; black (2.5Y 2.5/1) clay; moderate medium wedge structure parts to strong medium and coarse angular blocky; firm, very hard; common very fine and fine roots in cracks and common medium roots between peds; few very fine tubular pores; 50 percent prominent slickensides tilted at 35 to 45 degrees from the horizontal; less than 1 percent fine iron-manganese masses; less than 1 percent medium carbonate nodules; clear wavy boundary.

Bkss1--79 to 104 cm; very dark gray (10YR 3/1) clay; moderate medium wedge structure parts to strong medium and coarse angular blocky; firm, very hard; common fine roots between peds; few very fine tubular pores; 70 percent prominent slickensides tilted at 40 to 50 degrees from the horizontal; less than 1 percent fine iron-manganese masses; 1 percent fine and medium carbonate masses ; 5 percent medium carbonate nodules; gradual wavy boundary.

Bkss2--104 to 160 cm; dark gray (10YR 4/1) clay; strong medium and coarse wedge structure parts to moderate medium and coarse angular blocky; firm, very hard; common very fine and fine roots between peds; few very fine tubular pores; 70 percent prominent slickensides tilted at 40 to 60 degrees from the horizontal; less than 1 percent fine iron-manganese masses; 14 percent fine and medium carbonate nodules; very slightly effervescent; clear wavy boundary.

Bkss3--160 to 195 cm; 35 percent pale yellow (2.5Y 7/3) and 65 percent dark gray (10YR 4/1) clay; moderate medium and coarse wedge structure parts to strong medium and coarse angular blocky; firm, very hard; common very fine roots between peds; few very fine tubular pores; 50 percent prominent slickensides tilted at 40 to 60 degrees from the horizontal with dark gray (10YR 4/1) organic stains on upper surfaces of slickensides; less than 1 percent fine iron-manganese masses; 1 percent fine carbonate masses; 8 percent fine carbonate nodules; slightly effervescent; clear wavy boundary.

Bkss4--195 to 224 cm; 50 percent light gray (2.5Y 7/2) and 50 percent gray (10YR 5/1), clay; weak coarse wedge structure parts to moderate coarse angular blocky; firm, very hard; few very fine roots between peds; few very fine tubular pores; 50 percent prominent slickensides tilted at 40 to 60 degrees from the horizontal with dark gray (10YR 4/1) organic stains on upper surfaces of slickensides; 4 percent fine and medium prominent brownish yellow (10YR 6/8) masses of oxidized iron in light gray (2.5Y 7/2) matrix with sharp boundaries; 2 percent fine carbonate nodules; 5 percent medium and coarse carbonate masses; strongly effervescent; clear smooth boundary.

B'ss--224 to 239 cm; light gray (2.5Y 7/2), clay; weak coarse wedge structure parts to moderate medium and coarse angular blocky; firm, very hard; 30 percent distinct slickensides tilted at 30 to 40 degrees from the horizontal with gray (10YR 5/1) organic stains on upper surfaces of peds; less than 1 percent fine distinct very dark brown (10YR 2/2) iron-manganese nodules; less than 1 percent fine distinct black (10YR 2/1) iron-manganese masses; 2 percent fine distinct yellow (2.5Y 7/6) masses of oxidized iron and 3 percent fine and medium prominent brownish yellow (10YR 6/8) masses of oxidized iron with clear boundaries on surfaces of peds; less than 1 percent fine and medium carbonate nodules; strongly effervescent;

Description Date: 11/19/1999

Soil Series: Laewest
Site Identification #: **99 LAW 391 H** (99TX391001A - microhigh)

Location Information
Soil Survey Area Name: Refugio County, Texas
Latitude: 28 degrees 28 minutes 27.4 seconds North
Longitude: 97 degrees 07 minutes 0.0 seconds West
Site Note: The site fits the Laewest series.
Described by: Larry Wilding and Lee Nordt

Classification: Fine, smectitic, hyperthermic Chromic Hapluderts

A--0 to 12 cm; black (2.5Y 2.5/1) clay; moderate fine and medium subangular blocky structure; firm, hard; common fine and medium roots; common very fine and fine interstitial pores; very slightly effervescent; gradual wavy boundary.

Ak--12 to 33 cm; dark gray (2.5Y 4/1) clay; moderate medium and coarse angular blocky structure; firm, very hard; common fine roots; common very fine and fine interstitial pores; less than 1 percent fine spherical iron-manganese masses; 10 percent fine and medium irregular light gray (10YR 7/2) carbonate nodules; slightly effervescent; gradual wavy boundary.

Bkss1--33 to 59 cm; gray (2.5Y 5/1) clay; moderate medium and coarse angular blocky structure; firm, very hard; common fine roots; common very fine tubular pores; 4 percent faint slickensides tilted at 40 to 60 degrees from the horizontal; 4 percent faint pressure faces; 1 percent fine spherical iron-manganese nodules; 15 percent fine and medium irregular carbonate nodules; few cracks 1 to 2 centimeters wide filled with black (2.5Y 2.5/1) clay; slightly effervescent; gradual wavy boundary.

Bkss2--59 to 92 cm; gray (10YR 5/1) clay; moderate medium wedge structure parts to moderate medium angular blocky ; firm, very hard; common fine roots; common very fine tubular pores; 3 percent faint light gray (10YR 7/2) carbonate coats on surfaces along pores; 20 percent distinct slickensides tilted at 40 to 60 degrees from the horizontal; 1 percent fine spherical iron-manganese nodules; 15 percent fine and medium irregular carbonate nodules; few cracks 1 to 2 centimeters in size filled with black (2.5Y 2.5/1) clay; slightly effervescent; gradual wavy boundary.

Bkss3--92 to 127 cm; gray (10YR 5/1) clay; moderate medium and coarse wedge structure parts to moderate medium and coarse angular blocky; firm, very hard; common very fine and fine roots; common very fine tubular pores; 60 percent prominent slickensides tilted at 40 to 60 degrees from the horizontal; 1 percent fine spherical iron-manganese nodules; 5 percent fine and medium irregular carbonate nodules; few cracks 1 to 3 centimeters in size filled with black (2.5y 2.5/1) clay; slightly effervescent; gradual wavy boundary.

Bkss4--127 to 150 cm; 40 percent gray (2.5Y 6/1), 30 percent yellow (2.5Y 7/6) and 30 percent light brownish gray (2.5Y 6/2) clay; moderate medium wedge structure parts to moderate medium and coarse angular blocky; firm, very hard; common very fine and fine roots; common very fine tubular pores; 55 percent slickensides tilted at 40 to 60 degrees from the horizontal; 1 percent fine spherical iron-manganese nodules; 10 percent medium and coarse irregular carbonate nodules; slightly effervescent; gradual wavy boundary.

Bkss5--150 to 183 cm; 50 percent gray (2.5Y 5/1) and 50 percent light yellowish brown (2.5Y 6/4), clay; moderate medium and coarse angular blocky structure; firm, very hard; common very fine and fine roots; 40 percent slickensides tilted at 40 to 60 degrees from the horizontal; 1 percent fine distinct brownish yellow (10YR 6/8) masses of oxidized iron on surfaces of peds with sharp boundaries; 3 percent medium carbonate nodules ; 5 percent very coarse carbonate masses with hard centers; slightly effervescent; gradual wavy boundary.

Bkss6--183 to 235 cm; pale yellow (2.5Y 7/3), clay; moderate coarse angular blocky structure; firm, very hard; common very fine and fine roots; 40 percent distinct slickensides tilted 40 to 60 degrees from the horizontal; 2 percent fine prominent brownish yellow (10YR 6/8) masses of oxidized iron adjacent to masses of calcium carbonate with sharp boundaries; 5 percent very coarse carbonate masses with hard centers; strongly effervescent

Victoria Series Pedon Description

Date Sampled: 10/ 6/1999

Soil Series: Victoria
Sample Identification #: **99 VIC 409 L** (99TX409003 - microlow)

Location Information
Soil Survey Area Name: San Patricio County, Texas (Welder Wildlife Refuge)
Latitude: 28degrees 06 minutes 44.5 seconds North
Longitude: 97 degrees 20 minutes 55.4 seconds West
Described by: Dennis Brezina, Alan Stahnke, Wes Miller, Ramiro Molina, Jon Wiedenfeld, Warren Lynn, Conrad Neitsch.

Classification: fine, smectitic, hyperthermic Udic Haplusterts

A--0 to 10 cm; black (10YR 2/1); moderate fine and medium subangular blocky structure; hard, firm; many fine roots and common medium; many fine vesicular pores and common fine dendritic tubular pores; clear smooth boundary.

Bw--10 to 26 cm; black (10YR 2/1); moderate medium subangular blocky structure; hard, firm; common fine and medium roots; common fine and medium tubular pores; few faint pressure faces; clear smooth boundary.

Bss1--26 to 54 cm; black (10YR 2/1); weak fine and medium prismatic structure parting to moderate medium angular blocky; hard, firm; common fine roots; common fine tubular pores; common faint intersecting slickensides; few distinct pressure faces; very slightly effervescent; gradual wavy boundary.

Bss2--54 to 75 cm; 80 percent black (10YR 2/1), 20 percent black (10YR 2/1); moderate medium prismatic structure parting to moderate medium angular blocky; hard, firm; common fine roots; common fine tubular pores; few snail shell fragments; common distinct intersecting slickensides, few prominent intersecting slickensides; few fine nodules of calcium carbonate; slightly effervescent; gradual wavy boundary.

Bkss1--75 to 114 cm; 70 percent very dark gray (10YR 3/1), 30 percent black (10YR 2/1); weak medium and coarse prismatic structure parting to moderate medium angular blocky; hard, firm; common fine roots; common fine tubular pores; few snail shell fragments; black (10YR 2/1) clay matrix consists of vertical backfilled cracks; common prominent intersecting slickensides; common fine nodules of calcium carbonate, common fine masses of calcium carbonate; strongly effervescent; gradual wavy boundary.

Bkss2--114 to 141 cm; 60 percent light yellowish brown (2.5Y 6/3), 40 percent dark gray (10YR 4/1); weak coarse prismatic structure parting to moderate medium subangular blocky; very hard, firm; common fine roots; common fine tubular pores; 5 percent fine distinct brown (10YR 4/3) iron-manganese concentrations with sharp boundaries on surfaces of peds in light yellowish brown (2.5Y 6/3) matrix; dark gray (10YR 4/1) clay consists of backfilled cracks; common prominent intersecting slickensides; common fine and medium masses of calcium carbonate, few fine nodules of calcium carbonate; strongly effervescent; gradual wavy boundary.

Bkss3--141 to 163 cm; 80 percent light brownish gray (2.5Y 6/2), 20 percent dark gray (2.5Y 4/1); moderate medium subangular blocky structure; very hard, firm; common fine roots; common fine tubular pores; 5 percent fine distinct brown (10YR 4/3) iron-manganese concentrations with sharp boundaries on

surfaces of peds in light brownish gray (2.5Y 6/2) matrix; dark gray (2.5Y 4/1) clay consists of backfilled cracks; common distinct intersecting slickensides; common medium and coarse masses of calcium carbonate, few fine nodules of calcium carbonate, few fine gypsum crystals; strongly effervescent; gradual wavy boundary.

Bkss4--163 to 178 cm; light brownish gray (2.5Y 6/2); moderate medium subangular blocky structure; hard, firm; common fine roots; common fine tubular pores; 5 percent vertical cracks filled with dark gray (10YR 4/1) clay; common distinct intersecting slickensides; common medium and coarse masses of calcium carbonate, common fine gypsum crystals; strongly effervescent; gradual wavy boundary.

Bkssy1--178 to 210 cm; see Bkssy1 of Victoria (high) description; strongly effervescent.

Bkssy2--210 to 230 cm; see Bkssy2 horizon from Victoria (high) description.

Sample Date: 10/6/99

Soil Series: Victoria
Site Identification #: **99 VIC 409 H** (99TX409003A - microhigh)

Soil Survey Area Name: San Patricio County, Texas (Welder Wildlife Refuge)
Latitude: 28degrees 06 minutes 44.5 seconds North
Longitude: 97 degrees 20 minutes 55.4 seconds West
Described by: Dennis Brezina, Alan Stahnke, Wes Miller, Ramiro Molina, Jon Wiedenfeld, Warren Lynn, Conrad Neitsch.

Classification: fine, smectitic, hyperthermic Calcic Haplusterts (may make Udic Calciusterts)

A--0 to 15 cm; very dark gray (10YR 3/1) clay; moderate fine and medium subangular blocky structure; hard, firm; many fine roots and common medium; common medium vesicular pores and many fine dendritic tubular pores; few snail shell fragments; few insects casts; slightly effervescent; clear smooth boundary.

Bw--15 to 36 cm; dark gray (10YR 4/1) clay; moderate fine and medium subangular blocky structure; hard, firm; common fine and medium roots; common fine dendritic tubular pores; few snail shell fragments; few faint intersecting slickensides, few faint pressure faces; few insects casts; slightly effervescent; gradual smooth boundary.

Bss1--36 to 54 cm; dark gray (2.5Y 4/1) clay; moderate fine and medium subangular blocky structure; very hard, very firm; common fine roots; common fine tubular pores; few snail shell fragments; common prominent intersecting slickensides; few insects casts, few nodules of calcium carbonate; slightly effervescent; clear smooth boundary.

Bss2--54 to 73 cm; dark gray (10YR 4/1) clay; moderate medium subangular blocky structure; very hard, very firm; common fine roots; common fine tubular pores; few snail shell fragments; less than 1 percent fine faint brown (10YR 4/3) iron-manganese masses with sharp boundaries on surfaces of slickensides; many prominent intersecting slickensides; few nodules of calcium carbonate; strongly effervescent; gradual wavy boundary.

Bkss1—73 to 119 cm; dark gray (10YR 4/1) clay; moderate medium prismatic structure parting to moderate medium angular blocky; extremely hard, extremely firm; common fine roots; common fine tubular pores; many prominent intersecting slickensides; few nodules of calcium carbonate; strongly effervescent; gradual smooth boundary.

Bkss2--119 to 144 cm; 80 percent dark gray (10YR 4/1), 20 percent light yellowish brown (2.5Y 6/3) clay; moderate medium prismatic structure parting to moderate medium angular blocky; extremely hard, very firm; common fine roots; common fine tubular pores; common prominent intersecting slickensides; common medium and coarse masses of calcium carbonate; strongly effervescent; gradual wavy boundary.

Bkss3--144 to 195 cm; light brownish gray (2.5Y 6/2) clay; moderate medium and coarse prismatic structure parting to moderate medium angular blocky; extremely hard, firm; common fine roots; common fine tubular pores; 5 percent fine distinct brown (10YR 4/3) iron-manganese masses on surfaces of slickensides; common prominent intersecting slickensides; common medium and coarse masses of calcium carbonate, common fine gypsum crystals; strongly effervescent; gradual wavy boundary.

Bkssy1--195 to 214 cm; light gray (2.5Y 7/2) clay; weak medium and coarse prismatic structure parting to moderate medium and coarse angular blocky; very hard, very firm; common fine roots; common fine tubular pores; 1 percent fine prominent reddish yellow (7.5YR 6/8) iron concentrations with sharp boundaries in pore linings along slickensides; few distinct intersecting slickensides; few fine and medium masses of calcium carbonate; common fine and medium gypsum crystals; strongly effervescent; gradual wavy boundary.

Bkssy2--214 to 231 cm; 70 percent light yellowish brown (2.5Y 6/3), 30 percent brownish yellow (10YR 6/6) clay; weak coarse prismatic structure parting to weak medium and coarse subangular blocky; hard, firm; common fine roots; common fine tubular pores; few distinct intersecting slickensides; few fine and medium nodules of calcium carbonate; common fine and medium gypsum crystals; common fine very dark brown (7.5YR 2/2) masses of manganese on surfaces of slickensides; strongly effervescent; gradual wavy boundary.

Bkssy2--231 to 275 cm; 70 percent light yellowish brown (2.5Y 6/3), 30 percent brownish yellow (10YR 6/6) clay; weak coarse subangular blocky structure; hard, firm; common fine roots; common fine tubular pores; few distinct intersecting slickensides; common fine and medium gypsum crystals; common fine very dark brown (7.5YR 2/2) masses of manganese; strongly effervescent; gradual smooth boundary.

Bssy1--275 to 300 cm; 20 percent brownish yellow (10YR 6/8) clay, 80 percent light gray (2.5Y 7/2) dry; weak medium platy structure; hard, firm; few faint intersecting slickensides; common fine and medium gypsum crystals, common fine and medium masses of gypsum, common fine very dark brown (7.5YR 2/2) masses of manganese; strongly effervescent; gradual smooth boundary.

Bssy2--300 to 330 cm; 60 percent brownish yellow (10YR 6/8), 40 percent light gray (2.5Y 7/2) clay; weak medium platy structure; hard, firm; few faint intersecting slickensides; few fine gypsum crystals; common fine and medium masses of gypsum; strongly effervescent.

Table A1-2. Mean monthly ambient temperatures for pedon locations. (Source: National Climate Data Center, Asheville, NC)

Month	Pedon Designation											
	LEG 245A			LAC 201			LAC 157			LAC 481		
	High	Low	Mean	High	Low	Mean	High	Low	Mean	High	Low	Mean
	°C											
JAN	18.5	7.1	12.8	16.7	6.1	11.4	16.6	5.3	11.0	16.9	7.2	12.0
FEB	18.5	7.4	13.0	18.7	7.8	13.3	18.5	6.9	12.7	18.5	8.7	13.6
MAR	20.4	9.5	15.0	21.9	11.0	16.4	22.3	10.6	16.5	22.1	12.5	17.3
APR	23.6	13.0	18.3	25.6	15.6	20.6	26.3	15.2	20.7	25.4	17.1	21.2
MAY	26.9	16.6	21.7	28.8	19.7	24.2	29.8	19.1	24.4	28.2	20.8	24.5
JUN	29.8	19.8	24.8	31.9	22.9	27.4	32.8	22.1	27.4	30.6	23.8	27.2
JUL	31.7	21.9	26.8	33.2	24.0	28.6	34.2	23.2	28.7	32.0	25.3	28.6
AUG	32.4	22.3	27.3	33.4	23.5	28.5	34.3	22.9	28.6	31.8	24.8	28.3
SEP	31.2	20.3	25.8	31.3	20.8	26.1	32.0	20.6	26.3	29.9	22.2	26.1
OCT	28.4	16.8	22.6	27.5	15.7	21.6	28.2	15.4	21.8	27.0	17.7	22.3
NOV	24.4	12.6	18.5	22.2	10.7	16.5	22.4	10.2	16.3	22.3	13.0	17.6
DEC	20.7	9.0	14.8	18.5	7.6	13.1	18.5	6.7	12.6	18.5	9.1	13.8
Annual	25.5	14.7	20.1	25.8	15.4	20.6	26.3	14.8	20.6	25.2	16.8	21.0

Month	Pedon Designation											
	LAW 239			LAW 469			LAW 391			VIC 409		
	High	Low	Mean	High	Low	Mean	High	Low	Mean	High	Low	Mean
	°C											
JAN	16.9	7.2	12.0	17.2	6.1	11.7	18.5	7.0	12.7	18.5	7.0	12.7
FEB	18.5	8.7	13.6	19.4	7.7	13.6	20.6	8.3	14.5	20.6	8.3	14.5
MAR	22.1	12.5	17.3	23.3	11.8	17.6	24.4	12.5	18.4	24.4	12.5	18.4
APR	25.4	17.1	21.2	27.0	16.3	21.6	27.5	16.7	22.1	27.5	16.7	22.1
MAY	28.2	20.8	24.5	29.7	19.9	24.8	30.1	20.0	25.1	30.1	20.0	25.1
JUN	30.6	23.8	27.2	32.6	22.9	27.7	32.8	23.0	27.9	32.8	23.0	27.9
JUL	32.0	25.3	28.6	34.2	23.9	29.1	34.3	23.8	29.1	34.3	23.8	29.1
AUG	31.8	24.8	28.3	34.4	23.7	29.0	34.7	23.5	29.1	34.7	23.5	29.1
SEP	29.9	22.2	26.1	32.0	21.4	26.7	32.6	21.3	27.0	32.6	21.3	27.0
OCT	27.0	17.7	22.3	28.4	16.3	22.3	29.1	16.6	22.9	29.1	16.6	22.9
NOV	22.3	13.0	17.6	23.1	11.4	17.3	24.2	11.9	18.1	24.2	11.9	18.1
DEC	18.5	9.1	13.8	19.0	7.7	13.3	20.2	8.2	14.2	20.2	8.2	14.2
Annual	25.2	16.8	21.0	26.7	15.8	21.2	27.4	16.1	21.8	27.4	16.1	21.8

Table A1-3. Mean monthly precipitation (MMP), potential evapotranspiration (ET_p), and estimated moisture deficits for pedon locations. (Source: National Climate Data Center, Asheville, NC)

Month	Pedon Designation											
	LEG 245A			LAC 201			LAC 157			LAC 481		
	MMP	ET_p	deficit	MMP	ET_p	deficit	MMP	ET_p	deficit	MMP	ET_p	deficit
	mm											
JAN	124	20	-104[a]	104	21	-83	93	22	-71	74	18	-60
FEB	100	28	-72	111	31	-80	84	29	-55	71	26	-45
MAR	84	66	-18	75	67	-8	70	68	-2	53	66	3
APR	99	131	32	88	131	43	87	128	41	76	137	61
MAY	132	237	105	116	240	125	117	226	109	108	248	135
JUN	138	339	201	139	344	205	120	328	209	131	351	247
JUL	139	386	247	103	399	296	85	381	296	85	411	323
AUG	131	362	231	105	375	271	102	371	288	93	388	303
SEP	141	259	117	128	260	132	119	258	138	151	270	153
OCT	107	136	29	116	140	25	103	142	39	118	146	44
NOV	110	53	-57	120	57	-64	103	57	-46	84	56	-30
DEC	132	26	-106	117	30	-87	88	27	-61	81	26	-58
Annual	1437	2042	604	1321	2095	774	1170	2036	866	1124	2143	1019

[a] Shown as 0 - (MMP-ET_p) and negative value indicates moisture surplus.

Month	Pedon Designation											
	LAW 239			LAW 469			LAW 391			VIC 409		
	MMP	ET_p	deficit	MMP	ET_p	deficit	MMP	ET_p	deficit	MMP	ET_p	deficit
	mm											
JAN	78	22	-43	60	29	-41	55	19	-25	45	19	-26
FEB	71	30	-34	53	39	-24	58	29	-19	50	29	-21
MAR	64	75	16	48	92	29	42	77	50	43	77	34
APR	76	147	74	76	165	78	61	154	104	60	154	94
MAY	113	253	152	134	267	128	118	262	149	99	262	163
JUN	104	351	252	124	379	251	108	375	271	79	375	296
JUL	88	421	343	83	423	361	67	444	356	71	444	374
AUG	85	387	312	78	411	344	75	421	336	76	421	345
SEP	116	271	165	134	297	158	148	292	149	132	292	160
OCT	102	158	66	89	168	70	96	159	72	91	159	68
NOV	85	69	-2	61	76	3	51	64	24	45	64	19
DEC	83	32	-45	60	37	-32	46	28	-10	52	28	-24
Annual	1066	2215	1149	1000	2381	1381	924	2326	1402	844	2326	1482

Appendix 2: Data and Statistical Tables for Chapter 2

Table A2-1. X-ray fluorescence (XRF) raw data for Ti and Zr.

	Ti in Microlows							
Depth	Pedon designation							
	LEG 245A	LAC 201	LAC 157	LAC 481	LAW 239	LAW 469	LAW 391	VIC 409
cm	wt %							
10	0.57	0.47	0.51	0.52	0.49	0.38	0.39	0.35
20	0.70	0.47	0.52	0.54	0.51	0.40	0.42	0.36
30	0.59	0.50	0.53	0.52	0.50	0.42	0.40	0.36
40	0.58	0.50	0.52	0.53	0.50	0.42	0.40	0.37
50	0.57		0.52	0.53	0.50	0.41	0.40	0.36
60	0.58	0.49	0.53	0.55	0.52	0.41	0.40	0.36
70	0.57	0.47	0.52	0.53	0.51	0.40	0.40	0.35
80	0.58	0.46	0.51	0.53	0.51	0.42	0.41	0.34
90	0.57	0.48	0.53	0.53	0.51	0.42	0.40	0.36
100		0.47	0.53	0.53	0.51	0.44	0.41	0.33
110	0.56	0.49	0.54	0.54	0.50	0.47	0.39	0.34
120	0.55	0.52	0.54	0.55	0.50	0.44	0.39	0.35
130	0.54	0.50	0.54	0.54	0.52	0.43	0.37	0.34
140	0.55	0.52	0.51	0.54	0.50	0.40	0.34	0.35
150	0.56	0.49	0.50	0.53	0.48	0.43	0.41	0.34
160	0.55	0.44	0.46	0.55	0.46	0.41	0.40	0.34
170	0.55	0.49	0.47	0.54	0.31	0.41	0.40	0.33
180	0.55	0.44	0.44	0.53	0.31	0.38	0.40	0.32
190	0.50		0.44	0.51	0.29	0.38	0.37	0.33
200	0.41	0.47	0.37	0.49	0.31	0.38	0.38	0.35
210	0.43		0.40	0.39	0.29	0.35	0.37	0.35
220	0.46		0.43	0.37	0.35	0.33	0.32	0.35
230	0.29	0.43	0.39	0.37	0.31	0.34	0.32	0.35
240	0.43		0.37	0.39	0.30		0.31	0.35
250	0.45	0.42		0.38				0.36
260	0.52		0.42		0.42			0.31
270	0.56	0.43			0.32			0.32
280	0.57				0.37			
290								
300		0.37						

Ti in Microhighs

Depth	Pedon designation							
	LEG 245A	LAC 201	LAC 157	LAC 481	LAW 239	LAW 469	LAW 391	VIC 409
cm	wt %							
10	0.55	0.45	0.50	0.51	0.47	0.38		0.35
20	0.59	0.48	0.52	0.54	0.38	0.38		0.33
30	0.54	0.49	0.50	0.54		0.39		0.35
40	0.53	0.46	0.51	0.55	0.48	0.37		0.35
50	0.52	0.45	0.51	0.54	0.34	0.39	0.35	0.33
60	0.52	0.44	0.50	0.54	0.41	0.37	0.37	0.35
70	0.50	0.40	0.51	0.52	0.35	0.39	0.30	0.33
80	0.55	0.45	0.50		0.38	0.38	0.33	0.35
90	0.56	0.46	0.50	0.45	0.28	0.39	0.33	0.36
100	0.54	0.38	0.46	0.37	0.29	0.37	0.33	0.36
110	0.50		0.45	0.41	0.25	0.42	0.32	0.36
120	0.55		0.47	0.44	0.29	0.39	0.35	0.36
130	0.51	0.38	0.45	0.40	0.27	0.39	0.32	0.36
140	0.53		0.47	0.45	0.25	0.38	0.36	0.35
150	0.53		0.50	0.34	0.27	0.43	0.35	0.36
160	0.55	0.34	0.48	0.48	0.34	0.40	0.33	0.35
170	0.54		0.42	0.46	0.36	0.42	0.34	
180	0.44		0.38	0.47	0.42	0.37	0.33	0.32
190	0.49		0.38	0.41	0.29	0.39	0.31	0.30
200	0.49	0.39	0.37	0.40	0.40	0.38	0.32	0.25
210	0.42		0.39	0.44	0.26	0.40	0.33	0.30
220	0.42			0.41	0.26		0.30	0.32
230	0.44	0.39		0.39	0.23		0.32	
240	0.49				0.31		0.30	
250	0.49				0.25			
260	0.48				0.26			
270	0.47				0.28			
280	0.40							
290								
300				0.38				

Zr in Microlows								
Depth	Pedon designation							
	LEG 245A	LAC 201	LAC 157	LAC 481	LAW 239	LAW 469	LAW 391	VIC 409
cm	wt %							
10	0.095	0.101	0.060	0.045	0.083	0.104	0.056	0.123
20	0.086	0.110	0.055	0.045	0.074	0.103	0.051	0.113
30	0.090	0.124	0.057	0.045	0.078	0.098	0.056	0.114
40	0.082	0.100	0.055	0.049	0.076	0.030	0.052	0.109
50	0.078		0.058	0.049	0.078	0.095	0.055	0.108
60	0.070	0.093	0.060	0.053	0.074	0.086	0.054	0.112
70	0.074	0.104	0.059	0.051	0.075	0.091	0.054	0.095
80	0.074	0.088	0.062	0.052	0.072	0.090	0.054	0.095
90	0.084	0.088	0.057	0.041	0.073	0.088	0.053	0.098
100		0.068	0.053	0.054	0.075	0.089	0.052	0.090
110	0.088	0.059	0.054	0.040	0.076	0.084	0.045	0.091
120	0.082	0.054	0.054	0.042	0.078	0.088	0.042	0.080
130	0.081	0.055	0.056	0.042	0.077	0.087	0.039	0.075
140	0.078	0.063	0.058	0.042	0.073	0.070	0.028	0.081
150	0.073	0.068	0.051	0.045	0.066	0.085	0.042	0.079
160	0.071	0.048	0.048	0.042	0.060	0.072	0.039	0.072
170	0.070	0.072	0.048	0.042	0.013	0.058	0.039	0.076
180	0.076	0.019	0.032	0.040	0.009	0.034	0.038	0.071
190	0.067		0.025	0.035	0.008	0.024	0.034	0.069
200	0.033	0.025	0.012	0.030	0.009	0.025	0.036	0.079
210	0.043		0.014	0.015	0.009	0.023	0.036	0.069
220	0.052		0.011	0.014	0.030	0.040	0.022	0.086
230	0.023	0.024	0.011	0.013	0.009	0.032	0.024	0.088
240	0.031		0.009	0.014	0.010		0.023	0.082
250	0.035	0.033		0.014				0.090
260	0.058		0.016		0.034			0.038
270	0.036	0.025			0.044			0.020
280	0.030				0.028			
290								
300		0.016						

Zr in Microhighs

Depth	Pedon designation							
	LEG 245A	LAC 201	LAC 157	LAC 481	LAW 239	LAW 469	LAW 391	VIC 409
cm	wt %							
10	0.079	0.070	0.056	0.038	0.082	0.045		0.075
20	0.080	0.061	0.057	0.039	0.042	0.047		0.063
30	0.081	0.056	0.057	0.040		0.049		0.069
40	0.068	0.054	0.059	0.040	0.063	0.044		0.062
50	0.074	0.051	0.063	0.039	0.024	0.044	0.032	0.061
60	0.072	0.052	0.064	0.038	0.038	0.049	0.036	0.061
70	0.072	0.041	0.064	0.036	0.026	0.053	0.027	0.060
80	0.082	0.055	0.062		0.034	0.049	0.030	0.063
90	0.078	0.061	0.052	0.023	0.013	0.052	0.029	0.064
100	0.085	0.039	0.042	0.013	0.014	0.045	0.028	0.061
110	0.067		0.042	0.016	0.010	0.055	0.029	0.062
120	0.065		0.047	0.022	0.016	0.049	0.033	0.064
130	0.078	0.031	0.047	0.017	0.014	0.051	0.027	0.065
140	0.081		0.049	0.023	0.011	0.040	0.036	0.063
150	0.082		0.054	0.013	0.014	0.065	0.035	0.066
160	0.072	0.033	0.047	0.022	0.024	0.048	0.027	0.071
170	0.077		0.029	0.021	0.026	0.050	0.031	
180	0.056		0.014	0.022	0.031	0.031	0.026	0.077
190	0.075		0.016	0.015	0.012	0.042	0.025	0.051
200	0.069	0.019	0.011	0.013	0.025	0.029	0.026	0.035
210	0.046		0.010	0.014	0.007	0.032	0.024	0.054
220	0.030	0.018		0.013	0.010		0.024	0.059
230	0.025			0.013	0.007		0.031	
240	0.036			0.015	0.019		0.039	
250	0.037				0.012			
260	0.030				0.010			
270	0.020				0.019			
280								
290								
300				0.018				

Table A2-2. Carbonate correction factors (as determined using procedure in Chapter 2).

Depth	Microlows							
	Profile							
	LEG 245A	LAC 201	LAC 157	LAC 481	LAW 239	LAW 469	LAW 391	VIC 409
cm								
10	1.00	1.00	1.00	1.00	1.00	1.00	1.00	1.00
20	1.00	1.00	1.00	1.00	1.00	1.00	1.00	1.00
30	1.00	1.00	1.00	1.00	1.00	1.00	1.00	1.00
40	1.00	1.00	1.00	1.00	1.00	1.00	1.00	1.00
50	1.00		1.00	1.00	1.00	1.00	1.00	1.00
60	1.00	1.00	1.00	1.00	1.00	1.00	1.00	1.00
70	1.00	1.00	1.00	1.00	1.00	1.00	1.00	1.03
80	1.00	1.00	1.00	1.00	1.00	1.00	1.00	1.01
90	1.00	1.00	1.00	1.00	1.00	1.00	1.00	1.01
100	1.00	1.00	1.00	1.00	1.00	1.00	1.00	1.05
110	1.00	1.00	1.00	1.00	1.00	1.00	1.01	1.03
120	1.00	1.00	1.00	1.00	1.00	1.00	1.01	1.04
130	1.00	1.00	1.00	1.00	1.00	1.00	1.04	1.05
140	1.00	1.00	1.01	1.00	1.01	1.04	1.07	1.04
150	1.00	1.00	1.03	1.00	1.04	1.01	1.01	1.05
160	1.00	1.04	1.07	1.00	1.05	1.04	1.02	1.05
170	1.00	1.00	1.05	1.00	1.25	1.05	1.03	1.04
180	1.00	1.04	1.11	1.00	1.28	1.11	1.03	1.09
190	1.03		1.08	1.01	1.26	1.12	1.05	1.05
200	1.14	1.02	1.15	1.03	1.28	1.12	1.05	1.04
210	1.10		1.12	1.11	1.25	1.13	1.04	1.05
220	1.08		1.10	1.12	1.13	1.11	1.10	1.03
230	1.24	1.04	1.11	1.13	1.20	1.12	1.09	1.03
240	1.12		1.14	1.10	1.19		1.09	1.03
250	1.10	1.04		1.11			1.09	1.01
260	1.02		1.10		1.06			1.08
270	1.00	1.03			1.12			1.07
280	1.00		1.13					
300		1.07			1.11			
340					1.00			
380					1.00			

Depth	Microhighs							
	Profile							
	LEG 245A	LAC 201	LAC 157	LAC 481	LAW 239	LAW 469	LAW 391	VIC 409
cm								
10	1.00	1.00	1.00	1.00	1.00	1.11		1.06
20	1.00	1.00	1.00	1.00	1.12	1.11		1.08
30	1.00	1.00	1.00	1.00		1.10		1.07
40	1.02	1.02	1.00	1.00	1.02	1.13		1.08
50	1.02	1.02	1.00	1.00	1.17	1.12	1.07	1.07
60	1.03	1.03	1.00	1.00	1.10	1.11	1.05	1.08
70	1.04	1.06	1.00	1.02	1.15	1.10	1.10	1.07
80	1.00	1.02	1.00		1.12	1.11	1.08	1.07
90	1.00	1.02	1.02	1.09	1.23	1.09	1.08	1.07
100	1.00	1.07	1.06	1.17	1.22	1.14	1.08	1.07
110	1.04		1.07	1.15	1.26	1.08	1.09	1.06
120	1.00		1.05	1.10	1.22	1.10	1.07	1.06
130	1.01		1.07	1.15	1.24	1.10	1.09	1.06
140	1.00	1.08	1.05	1.11	1.26	1.16	1.05	1.06
150	1.00		1.02	1.20	1.24	1.04	1.05	1.06
160	1.00		1.04	1.07	1.16	1.08	1.09	1.05
170	1.00	1.12	1.08	1.08	1.15	1.06	1.07	
180	1.09		1.16	1.07	1.09	1.13	1.09	1.00
190	1.04		1.13	1.11	1.21	1.09	1.10	1.00
200	1.04	1.09	1.13	1.14	1.10	1.12	1.09	1.00
210	1.12		1.11	1.13	1.26	1.10	1.10	1.00
220	1.14			1.13	1.23		1.10	1.00
230	1.11	1.07		1.11	1.25		1.08	
240	1.03				1.17		1.06	
250	1.03				1.22			
260	1.06	1.08			1.22			
270	1.08				1.19			
370							1.10	
430				1.12				

Table A2-3. Carbonate-corrected XRF element wt % (as determined using procedure in Chapter 2).

Ti in Microlows								
Depth	Pedon designation							
	LEG 245A	LAC 201	LAC 157	LAC 481	LAW 239	LAW 469	LAW 391	VIC 409
cm	wt%							
10	0.57	0.47	0.51	0.52	0.49	0.38	0.39	0.35
20	0.70	0.47	0.52	0.54	0.51	0.40	0.42	0.36
30	0.59	0.50	0.53	0.53	0.50	0.41	0.40	0.36
40	0.58	0.50	0.52	0.53	0.50	0.42	0.40	0.37
50	0.57		0.52	0.53	0.50	0.41	0.40	0.36
60	0.58	0.49	0.53	0.55	0.52	0.41	0.40	0.36
70	0.57	0.47	0.52	0.53	0.51	0.40	0.40	0.35
80	0.58	0.46	0.51	0.53	0.51	0.42	0.41	0.34
90	0.57	0.48	0.53	0.53	0.51	0.42	0.40	0.36
100		0.47	0.53	0.53	0.51	0.44	0.41	0.33
110	0.56	0.49	0.54	0.54	0.50	0.44	0.39	0.34
120	0.55	0.52	0.54	0.55	0.50	0.44	0.40	0.35
130	0.54	0.50	0.54	0.54	0.52	0.43	0.39	0.34
140	0.55	0.52	0.52	0.54	0.50	0.42	0.37	0.35
150	0.56	0.49	0.52	0.53	0.49	0.43	0.41	0.34
160	0.55	0.45	0.49	0.55	0.48	0.42	0.41	0.34
170	0.55	0.49	0.50	0.54	0.39	0.43	0.42	0.33
180	0.55	0.46	0.49	0.54	0.39	0.42	0.41	0.32
190	0.52		0.48	0.51	0.37	0.43	0.39	0.33
200	0.47	0.48	0.43	0.51	0.39	0.43	0.39	0.35
210	0.48		0.45	0.44	0.36	0.39	0.39	0.35
220	0.50		0.48	0.42	0.39	0.37	0.35	0.35
230	0.36	0.44	0.43	0.42	0.38	0.38	0.35	0.35
240	0.49		0.42	0.43	0.36		0.34	0.35
250	0.49	0.44		0.42				0.36
260	0.53		0.46		0.45			0.31
270	0.56	0.45			0.36			0.32
280	0.57				0.41			
290								
300		0.40						

Ti in Microhighs								
Depth	Pedon designation							
	LEG 245A	LAC 201	LAC 157	LAC 481	LAW 239	LAW 469	LAW 391	VIC 409
cm	wt%							
10	0.55	0.45	0.50	0.51	0.47	0.42		0.37
20	0.59	0.48	0.52	0.54	0.44	0.42		0.35
30	0.54	0.49	0.50	0.54		0.43		0.37
40	0.54	0.47	0.51	0.55	0.50	0.42		0.38
50	0.53	0.46	0.51	0.54	0.40	0.43	0.37	0.35
60	0.53	0.45	0.50	0.54	0.46	0.41	0.39	0.37
70	0.52	0.42	0.51	0.52	0.42	0.43	0.33	0.36
80	0.55	0.46	0.50		0.44	0.42	0.35	0.38
90	0.56	0.46	0.51	0.50	0.35	0.43	0.36	0.39
100	0.54	0.41	0.49	0.43	0.35	0.42	0.36	0.39
110	0.51		0.49	0.47	0.32	0.45	0.35	0.38
120	0.55		0.50	0.49	0.36	0.43	0.37	0.38
130	0.52	0.41	0.48	0.46	0.34	0.43	0.35	0.38
140	0.53		0.49	0.50	0.32	0.44	0.38	0.37
150	0.53		0.51	0.41	0.34	0.45	0.37	0.38
160	0.55	0.38	0.50	0.51	0.40	0.43	0.36	0.37
170	0.54		0.45	0.50	0.42	0.45	0.37	
180	0.48		0.44	0.50	0.46	0.42	0.36	0.32
190	0.51		0.43	0.46	0.36	0.43	0.34	0.30
200	0.51	0.42	0.42	0.46	0.45	0.42	0.34	0.25
210	0.47		0.43	0.50	0.33	0.44	0.36	0.30
220	0.48	0.42		0.46	0.32		0.33	0.32
230	0.49			0.44	0.29		0.34	
240	0.51				0.37		0.32	
250	0.50				0.31			
260	0.50				0.32			
270	0.51				0.34			
280	0.43							
290								
300				0.42				

Zr in Microlows

Depth	Pedon designation							
	LEG 245A	LAC 201	LAC 157	LAC 481	LAW 239	LAW 469	LAW 391	VIC 409
cm	wt%							
10	0.095	0.101	0.060	0.045	0.083	0.104	0.056	0.123
20	0.086	0.110	0.055	0.045	0.074	0.103	0.051	0.113
30	0.090	0.124	0.057	0.045	0.078	0.098	0.056	0.114
40	0.082	0.100	0.055	0.049	0.076	0.093	0.052	0.109
50	0.078		0.058	0.049	0.078	0.096	0.055	0.108
60	0.070	0.093	0.060	0.053	0.074	0.086	0.054	0.112
70	0.074	0.104	0.059	0.051	0.075	0.090	0.054	0.095
80	0.074	0.088	0.062	0.052	0.072	0.090	0.054	0.095
90	0.084	0.088	0.057	0.041	0.073	0.088	0.053	0.098
100		0.068	0.053	0.054	0.075	0.089	0.052	0.090
110	0.088	0.059	0.054	0.040	0.076	0.085	0.046	0.091
120	0.082	0.054	0.054	0.042	0.078	0.088	0.043	0.080
130	0.081	0.055	0.056	0.042	0.077	0.088	0.040	0.075
140	0.078	0.063	0.059	0.042	0.073	0.072	0.030	0.081
150	0.073	0.068	0.053	0.045	0.068	0.086	0.042	0.079
160	0.071	0.050	0.051	0.042	0.063	0.075	0.040	0.072
170	0.070	0.072	0.050	0.042	0.016	0.061	0.040	0.076
180	0.076	0.020	0.036	0.040	0.011	0.038	0.040	0.071
190	0.069		0.027	0.036	0.010	0.027	0.036	0.069
200	0.038	0.026	0.014	0.031	0.012	0.028	0.038	0.079
210	0.047		0.016	0.016	0.011	0.025	0.038	0.069
220	0.056		0.013	0.015	0.033	0.045	0.024	0.086
230	0.028	0.025	0.012	0.014	0.011	0.036	0.026	0.088
240	0.035		0.010	0.015	0.012		0.025	0.082
250	0.039	0.035		0.016				0.090
260	0.058		0.018		0.036			0.038
270	0.036	0.026			0.049			0.020
280	0.030				0.031			
290								
300		0.017						

Zr in Microhighs								
Depth	Pedon designation							
	LEG 245A	LAC 201	LAC 157	LAC 481	LAW 239	LAW 469	LAW 391	VIC 409
cm	wt%							
10	0.079	0.070	0.056	0.038	0.082	0.049		0.080
20	0.080	0.061	0.057	0.039	0.047	0.052		0.068
30	0.081	0.056	0.057	0.040		0.054		0.074
40	0.069	0.055	0.059	0.040	0.066	0.050		0.067
50	0.076	0.052	0.063	0.039	0.029	0.049	0.034	0.065
60	0.074	0.054	0.064	0.038	0.043	0.055	0.038	0.066
70	0.075	0.044	0.064	0.036	0.031	0.058	0.030	0.064
80	0.082	0.056	0.062		0.038	0.054	0.032	0.068
90	0.078	0.062	0.054	0.025	0.016	0.057	0.031	0.068
100	0.085	0.042	0.045	0.016	0.017	0.051	0.030	0.065
110	0.069		0.045	0.018	0.013	0.060	0.031	0.066
120	0.065		0.050	0.024	0.020	0.054	0.035	0.068
130	0.078	0.034	0.050	0.020	0.017	0.056	0.029	0.069
140	0.081		0.052	0.026	0.014	0.047	0.038	0.066
150	0.082		0.055	0.015	0.017	0.068	0.037	0.070
160	0.072	0.037	0.049	0.023	0.029	0.052	0.029	0.074
170	0.078		0.031	0.023	0.030	0.053	0.033	
180	0.061		0.016	0.023	0.034	0.035	0.029	0.077
190	0.078	0.020	0.018	0.017	0.015	0.046	0.027	0.051
200	0.072		0.012	0.015	0.028	0.032	0.028	0.035
210	0.051	0.019	0.011	0.016	0.009	0.035	0.026	0.054
220	0.034			0.015	0.012		0.027	0.059
230	0.028			0.015	0.009		0.033	
240	0.037				0.022		0.041	
250	0.038	0.016			0.015			
260	0.032				0.012			
270	0.021				0.023			
280								
290								
300				0.017				

Table A2-4. Dry clod bulk density (BD) values

LEG 245 A					
Microhigh			Microlow		
Horizon	Depth	BD	Horizon	Depth	BD
	cm	Mg m^{-3}		cm	Mg m^{-3}
Ap	0-15	1.839	Ap	0-16	1.598
A	15-26	1.806	Bss1	16-43	1.765
Bkg	26-46	1.763	Bss2	43-72	1.827
Bsskg1	46-67	1.799	Bss3	72-104	1.895
Bsskg2	67-96	1.840	Bss4	104-115	1.885
Bsskg3	96-120	1.759	Bss5	115-144	1.934
Bsskg4	120-154	1.907	Bss6	144-156	1.962
Bsskg5	154-173	1.952	Bss7	156-174	1.845
Bkssg4	260	1.917	Bkss	174-223	1.966
Bss	320	1.951	B′ss1	223-252	1.926
			B′ss2	252-275	1.931
LAC 201					
Ak	10	1.754	A	10	1.686
Bkss1	20	1.836	Bw	20	1.737
Bkss2	30	1.762		30	1.758
	40	1.795		40	1.858
Bkssg1	50	1.746	Bss1	50	1.757
	60	1.790		60	1.822
Bkssg2	70	1.841	Bss2	70	1.763
	80	1.898		80	1.834
	90	1.844	Bss3	90	1.909
	100	1.866		100	1.930
Bkssg3	105-148	1.879		110	1.832
B′kss1	148-177	1.961	Bss4	120	1.929
B′ss1	202-235	1.754		130	1.686
B′ss2	235-270	1.836		140	1.737
			Bkss1	150	1.758

LAC 201					
Microhigh			Microlow		
Horizon	Depth	BD	Horizon	Depth	BD
	cm	Mg m^{-3}		cm	Mg m^{-3}
				160	1.858
				170	1.757
			Bkss2	180	1.929
LAC 157					
Ak1	10	1.693	A2	10	1.815
Ak2	20	1.736		20	1.762
	30	1.777	Bss1	30	1.700
Bkss1	40	1.666		40	1.761
	50	1.705		50	1.706
	60	1.754	Bss2	60	1.878
Bkss2	70	1.745		70	1.733
	80	1.771		80	1.787
Bkss3	90	1.686		90	1.841
	100	1.816	Bss3	100	1.785
	110	1.837		110	1.862
	120	1.822		120	1.880
Bkss4	130	1.805	Bkss1	130	1.913
	140	1.868		140	1.911
Bkss5	150	1.883		150	1.888
	160	1.783	Bkss2	160	1.844
	170	1.858		170	1.900
Bss1	180	1.854	Bkss3	180	1.857
	190	1.844		190	1.855
	200	1.848		200	1.845
Bss2	210	1.775	B′ss1	210	1.916
			B′ss2	220	1.915
				230	2.008
			B′ss3	240-272	1.852

LAC 481					
Microhigh			Microlow		
Horizon	Depth	BD	Horizon	Depth	BD
	cm	Mg m^{-3}		cm	Mg m^{-3}
Ak1	10	1.679	A1	10	1.634
Ak2	20	1.663	A2	20	1.691
	30	1.639	Bss1	30	1.776
Bkss1	40	1.652		40	1.787
	50	1.673		50	1.873
	60	1.619	Bss2	60	1.893
	70	1.617		70	1.888
Bkss2	80	1.643		80	1.822
	90	1.720	Bss3	90	1.844
Bkss3	100	1.717		100	1.713
	110	1.823		110	1.824
	120	1.742		120	1.822
	130	1.781	Bss4	130	1.848
	140	1.712		140	1.761
Bkss4	150	1.818	Bkss1	150	1.817
	160	1.884		160	1.720
	170	1.773	Bkss2	170	1.728
Bss1	180	1.860	Bkss3	180	1.865
	190	1.863		190	1.865
	200	1.899	Bkss4	200	1.856
	210	1.803		210	1.789
	220	1.853		220	1.896
	230	1.776		230	1.807
				240	1.917
2C	440	1.880		250	1.865

LAW 239					
Microhigh			Microlow		
Horizon	Depth	BD	Horizon	Depth	BD
	cm	Mg m^{-3}		cm	Mg m^{-3}
A	0-10	1.768	A1	0-13	1.847
Ak	10-26	1.797	A2	13-29	1.835
Bsskl	26-58	1.824	Bss1	29-56	1.834
Bkss2	58-90	1.836	Bss2	56-94	1.842
Bssk3	90-120	NA	Bss3	94-141	1.896
Bssk4	120-145	1.892	Bkssl	141-156	1.898
Bssk5	145-165	1.881	Bkss2	156-168	1.844
Bssk6	165-208	1.869	Bkss3	168-183	1.778
Bss	208-235	1.915	B′ssl	183-208	1.857
BC1	235-270	1.947	B′ss2	208-244	1.929
			BCx	244-272	1.805
			2C	272-320	1.704
LAW 469					
Ak	0-11	1.745	A	0-21	1.855
Bk	11-28	1.742	Bssl	21-42	1.857
Bkssl	28-119	1.918	Bss2	42-63	1.897
Bkss2	119-172	NA	Bss3	63-82	1.847
Bkss3	172-198	1.906	Bkssl	82-113	1.848
Bss	198-205	1.858	Bkss2	113-141	1.865
Bss2	205-265	1.916	Bkss3	141-155	1.949
			B′ssl	155-166	1.922
			B′ss2	166-197	1.861
LAW 391					
A	0-12	1.690	A1	0-9	1.799
Ak	12-33	1.730	A2	9-28	1.719
Bkssl	33-59	1.777	Bssl	28-56	1.783
Bkss2	59-92	1.810	Bss2	56-79	1.827

LAW 391					
Microhigh			Microlow		
Horizon	Depth	BD	Horizon	Depth	BD
	cm	Mg m^{-3}		cm	Mg m^{-3}
Bkss3	92-127	1.815	Bkss1	79-104	1.804
Bkss4	127-150	1.842	Bkss2	104-160	1.808
Bkss5	150-183	1.853	Bkss3	160-195	1.813
Bkss6	183-235	1.867	Bkss4	195-224	1.840
			B′ss	224-239	1.909
VIC 409					
A	0-15	1.622	A	0-10	1.804
Bw	15-36	1.842	Bw	10-26	1.828
Bss1	36-54	1.905	Bss1	26-54	1.832
Bss2	54-73	1.893	Bss2	54-75	1.805
Bkss1	73-119	1.869	Bkss1	75-114	1.821
Bkss2	119-144	1.789	Bkss2	114-141	1.781
Bkss3	144-195	1.711	Bkss3	141-163	1.710
Bkssyl	195-214	1.777	Bkss4	163-178	1.725
			Bkssy1	178-210	1.670
			Bkssy2	210-230	1.705
			Bkssy3	230-275	1.750
			Bssv1	275-300	1.833

Table A2-5. Volumetric elemental content.

Ti in Microlows								
Depth	Pedon designation							
	LEG 245A	LAC 201	LAC 157	LAC 481	LAW 239	LAW 469	LAW 391	VIC 409
cm	mg cm^{-3}							
10	9.052	7.936	9.223	8.536	8.971	7.075	6.946	6.359
20	11.179	8.151	9.139	9.102	9.434	7.440	7.517	6.513
30	10.442	8.779	8.996	9.325	9.264	7.677	6.840	6.515
40	10.160	9.240	9.243	9.450	9.163	7.750	7.086	6.755
50	10.419		8.885	9.872	9.193	7.787	7.192	6.625
60	10.594	8.913	9.928	10.371	9.479	7.812	7.229	6.430
70	10.465	8.468	9.035	9.996	9.446	7.429	7.377	6.358
80	10.992	8.395	9.196	9.717	9.469	7.770	7.471	6.145
90	10.733	9.078	9.705	9.826	9.448	7.852	7.302	6.512
100		9.039	9.381	9.023	9.465	8.075	7.404	5.995
110	10.626	8.894	10.147	9.778	9.548	8.130	7.090	6.247
120	10.588	9.987	10.112	10.023	9.457	8.228	7.184	6.242
130	10.474	9.649	10.287	10.046	9.788	8.060	6.976	5.999
140	10.547	10.268	9.917	9.479	9.564	7.791	6.656	6.265
150	10.850	9.580	9.831	9.659	9.359	8.407	7.444	5.875
160	10.843	8.869	9.066	9.385	8.907	8.257	7.406	5.732
170	10.199	9.416	9.466	9.349	6.876	8.328	7.526	5.771
180	10.150	8.403	9.048	9.979	6.949	7.823	7.502	5.348
190	10.197		8.943	8.538	6.885	7.997	7.048	5.580
200	9.144	9.048	7.885	9.449	7.272	7.998	7.201	5.769
210	9.411		8.611	7.782	6.688	7.346	7.118	5.767
220	9.856		9.122	7.939	7.543	6.899	6.582	5.899
230	6.977	8.681	8.594	7.549	7.260	7.062	6.616	6.031
240	9.361		7.771	8.211	6.908		6.493	6.186
250	9.470	8.680		7.813				6.349
260	10.227		8.486		8.127			5.342
270	10.815	8.011			6.452			5.610
280	11.097				7.401			
290								
300								

Ti in Microhighs

Depth	Pedon designation							
	LEG 245A	LAC 201	LAC 157	LAC 481	LAW 239	LAW 469	LAW 391	VIC 409
cm	$mg\ cm^{-3}$							
10	10.046	7.859	8.492	8.646	8.238	7.361		5.952
20	10.760	8.899	8.965	9.015	7.889	7.350		6.109
30	9.841	8.593	8.918	8.915		7.489		6.851
40	9.545	8.353	8.487	9.061	9.192	7.362		7.052
50	9.314	8.085	8.689	8.985	7.329	8.312		6.733
60	9.549	8.034	8.814	8.764	8.313	7.840	6.622	7.114
70	9.322	7.715	8.913	8.482	7.627	8.180	7.078	6.760
80	10.032	8.710	8.880		8.049	8.115	5.965	7.103
90	10.218	8.540	8.539	8.571	6.412	8.253	6.408	7.245
100	9.966	7.579	8.834	7.386	6.597	8.039	6.541	7.268
110	9.041		8.918	8.513	6.028	8.723	6.493	7.155
120	9.714		9.097	8.522	6.721	8.266	6.341	7.020
130	9.864	7.645	8.657	8.118	6.499	8.217	6.781	6.853
140	10.053		9.224	8.612	6.062	8.402	6.509	6.586
150	10.053		9.590	7.401	6.445	8.552	7.064	6.599
160	10.702	7.398	8.863	9.640	7.607	8.292	6.883	6.292
170	10.538		8.440	8.893	7.944	8.578	6.638	
180	9.290		8.142	9.366	8.621	7.999	6.792	5.444
190	9.769		7.927	8.514	6.712	8.138	6.678	5.269
200	9.862	7.880	7.682	8.640	8.389	7.887	6.403	4.452
210	9.043		7.668	9.033	6.257	8.343	6.430	5.359
220	9.194	7.379		8.599	6.160		6.754	5.707
230	9.419				5.637		6.220	
240	9.769				7.181		6.418	
250	9.740				6.076		6.110	
260	9.668	7.892			6.278			
270	9.707				6.672			
280								
290								
300				7.740				

Zr in Microlows								
Depth	Pedon designation							
	LEG 245A	LAC 201	LAC 157	LAC 481	LAW 239	LAW 469	LAW 391	VIC 409
cm	mg cm^{-3}							
10	1.519	1.706	1.081	0.741	1.535	1.927	1.009	2.215
20	1.369	1.904	0.978	0.765	1.369	1.904	0.910	2.072
30	1.590	2.186	0.977	0.806	1.427	1.826	0.954	2.084
40	1.455	1.865	0.962	0.882	1.397	1.722	0.927	2.006
50	1.428		0.984	0.927	1.435	1.820	0.975	1.977
60	1.278	1.692	1.132	0.999	1.359	1.640	0.977	2.016
70	1.349	1.862	1.022	0.968	1.384	1.658	0.984	1.708
80	1.393	1.617	1.110	0.946	1.323	1.667	0.979	1.711
90	1.592	1.673	1.058	0.764	1.344	1.621	0.958	1.783
100		1.306	0.953	0.924	1.410	1.642	0.936	1.633
110	1.659	1.083	0.999	0.726	1.449	1.575	0.830	1.660
120	1.593	1.040	1.015	0.768	1.483	1.646	0.769	1.418
130	1.560	1.072	1.080	0.768	1.467	1.639	0.725	1.340
140	1.515	1.245	1.120	0.746	1.390	1.349	0.545	1.439
150	1.410	1.332	1.004	0.817	1.298	1.676	0.761	1.357
160	1.388	0.983	0.941	0.723	1.156	1.463	0.730	1.231
170	1.286	1.390	0.949	0.718	0.284	1.177	0.732	1.308
180	1.404	0.372	0.664	0.748	0.203	0.706	0.719	1.189
190	1.364		0.496	0.597	0.195	0.494	0.652	1.150
200	0.746	0.482	0.261	0.571	0.215	0.517	0.689	1.327
210	0.926		0.303	0.291	0.209	0.473	0.696	1.148
220	1.110		0.242	0.292	0.646	0.834	0.455	1.460
230	0.540	0.486	0.237	0.260	0.204	0.667	0.495	1.493
240	0.680		0.194	0.291	0.240		0.471	1.431
250	0.746	0.686		0.290				1.567
260	1.128		0.327		0.650			0.673
270	0.703	0.468			0.893			0.350
280	0.577				0.567			
290								
300		0.312						

Zr in Microhighs								
Depth	Pedon designation							
	LEG 245A	LAC 201	LAC 157	LAC 481	LAW 239	LAW 469	LAW 391	VIC 409
cm	mg cm^{-3}							
10	1.461	1.233	0.941	0.644	1.452	0.863		1.290
20	1.463	1.117	0.988	0.652	0.853	0.914		1.179
30	1.462	0.987	1.008	0.651		0.934		1.371
40	1.224	0.983	0.991	0.657	1.197	0.874		1.250
50	1.337	0.904	1.072	0.659	0.532	0.942	0.612	1.247
60	1.327	0.963	1.124	0.617	0.786	1.046	0.683	1.260
70	1.342	0.802	1.111	0.580	0.572	1.106	0.539	1.207
80	1.511	1.059	1.090		0.706	1.042	0.584	1.284
90	1.431	1.146	0.902	0.427	0.295	1.096	0.569	1.275
100	1.562	0.788	0.821	0.267	0.324	0.973	0.553	1.219
110	1.213		0.819	0.327	0.237	1.151	0.571	1.233
120	1.143		0.904	0.422	0.365	1.030	0.638	1.262
130	1.493	0.634	0.910	0.356	0.323	1.072	0.534	1.235
140	1.541		0.973	0.443	0.264	0.895	0.706	1.188
150	1.562		1.034	0.280	0.325	1.295	0.686	1.223
160	1.409	0.717	0.878	0.442	0.544	0.996	0.544	1.268
170	1.513		0.576	0.405	0.569	1.017	0.620	
180	1.173		0.301	0.436	0.640	0.676	0.531	1.312
190	1.510		0.332	0.320	0.275	0.869	0.513	0.887
200	1.401	0.380	0.222	0.276	0.527	0.602	0.527	0.628
210	0.991		0.197	0.292	0.161	0.671	0.494	0.958
220	0.654	0.332		0.273	0.237		0.495	1.046
230	0.539				0.171		0.618	
240	0.718				0.430		0.779	
250	0.727				0.286			
260	0.607	0.302			0.233			
270	0.410				0.439			
280								
290								
300				0.259				

Table A2-6. Particle size distribution data.

LEG 245 A									
Microhigh					Microlow				
Horizon	Depth	Sand	Silt	Clay	Horizon	Depth	Sand	Silt	Clay
	cm	wt%				cm	wt%		
Ap	0-15	11.7	39.4	48.9	Ap	0-16	11.0	41.6	47.4
A	15-26	10.8	43.0	46.2	Bss1	16-43	10.1	42.2	47.7
Bkg	26-46	13.4	38.1	48.5	Bss2	43-72	9.7	39.2	51.1
Bsskg1	46-67	12.5	38.2	49.3	Bss3	72-104	9.7	38.4	51.9
Bsskg2	67-96	13.3	36.8	49.9	Bss4	104-115	10.9	36.7	52.4
Bsskg3	96-120	13.2	38.2	48.6	Bss5	115-144	10.0	37.9	52.1
Bsskg4	120-154	12.4	38.1	49.5	Bss6	144-156	9.5	37.7	52.8
Bsskg5	154-173	14.9	42.9	45.5	Bss7	156-174	11.4	42.3	46.3
Bkssg4	260	7.4	41.7	50.9	Bkss	174-223	9.2	41.8	49.0
Bss	320	4.3	35.8	59.9	B′ss1	223-252	4.5	33.6	61.9
					B′ss2	252-275	2.8	30.8	66.4
LAC 201									
Ak	0-10	20.7	35.8	43.5	A	0-16	21.3	42.6	36.2
Bkss1	10-27	17.7	32.4	49.9	Bw	16-44	21.6	42.6	35.8
Bkss2	27-49	19.1	33.0	47.9	Bss1	44-65	21.4	41.3	37.3
Bkssg1	49-67	19.7	35.2	45.1	Bss2	65-88	18.8	34.9	46.3
Bkssg2	67-105	20.2	33.0	46.8	Bss3	88-117	17.4	30.1	52.5
Bkssg3	105-148	21.1	34.1	44.8	Bss4	117-151	18.1	32.2	49.7
B′kss1	148-165	18.9	34.8	46.3	Bkss1	151-177	18.0	35.5	46.5
B′kss2	165-202	9.2	37.9	52.9	Bkss2	177-212	7.2	31.2	61.6
B′ss1	202-235	2.7	40.9	56.4	B′ss1	212-242	6.7	34.7	58.6
B′ss2	235-270	1.7	40.3	58.0	B′ss2	242-261	2.9	48.2	48.9
					B′ss3	261-279	2.6	49.6	47.8
					B′ss4	279-300	1.7	43.8	54.5
LAC 157									
Ak1	0-10	11.4	34.8	53.8	A1	0-10	11.4	37.4	51.2
Ak2	10-28	11.6	33.9	54.5	A2	10-29	10.5	36.4	53.1
Bkss1	28-70	14.7	33.4	51.9	Bss1	29-61	10.7	33.1	56.2
Bkss2	70-95	14.0	35.4	50.6	Bss2	61-103	10.3	33.0	56.7

LAC 157									
Microhigh					Microlow				
Horizon	Depth	Sand	Silt	Clay	Horizon	Depth	Sand	Silt	Clay
	cm	----------wt%----------				cm	----------wt%----------		
Bkss3	95-129	11.8	34.8	53.4	Bss3	103-135	11.5	32.6	55.9
Bkss4	129-144	12.7	34.3	53.0	Bkss1	135-158	13.9	32.8	53.3
Bkss5	144-176	5.2	34.1	60.7	Bkss2	158-175	11.4	33.0	55.6
Bss1	176-210	1.6	31.7	66.7	Bkss3	175-193	5.9	33.5	60.6
Bss2	210-240	1.3	26.8	71.9	B′ss1	193-216	2.2	29.0	68.8
					B′ss2	216-240	1.5	26.6	71.9
					B′ss3	240-272	2.3	26.0	71.7
					B′ss4	272-300	3.0	27.7	69.3
LAC 481									
Ak1	0-15	7.3	27.2	65.5	A1	0-12	7.7	29.9	62.4
Ak2	15-33	6.3	26.6	67.1	A2	12-28	7.1	30.4	62.5
Bkss1	33-78	6.9	27.5	65.6	Bss1	28-59	8.4	33.5	58.1
Bkss2	78-104	4.4	37.1	58.5	Bss2	59-83	7.4	32.1	60.5
Bkss3	104-157	9.8	27.9	62.3	Bss3	83-123	7.3	30.5	62.2
Bkss4	157-181	9.4	29.4	61.2	Bss4	123-147	7.7	28.0	64.3
Bss1	181-260	1.2	38.6	60.2	Bkss1	147-165	9.0	28.0	63.0
Bss2	260-300	1.0	43.2	55.8	Bkss2	165-176	1.8	36.9	61.3
2C	380-405	1.1	42.7	56.2	Bkss3	176-200	1.3	36.5	62.2
					Bkss4	200-250	1.0	37.4	61.6
LAW 239									
A	0-10	14.6	37.9	47.5	A1	0-13	14.1	36.9	49.0
Ak	10-26	14.9	35.7	49.4	A2	13-29	12.4	35.9	51.7
Bssk1	26-58	13.1	37.1	49.8	Bss1	29-56	11.9	35.8	52.3
Bssk2	58-90	10.6	41.5	47.9	Bss2	56-94	11.1	35.4	53.5
Bssk3	90-120	4.7	48.7	46.6	Bss3	94-141	14.1	34.6	51.3
Bssk4	120-145	4.7	50.3	45.0	Bkss1	141-156	12.9	34.9	52.2
Bssk5	145-165	4.2	50.9	44.9	Bkss2	156-168	8.3	45.0	46.7
Bssk6	165-208	1.7	51.4	46.9	Bkss3	168-183	4.1	50.8	45.1
Bss	208-235	0.4	55.7	43.9	B′ss1	183-208	0.8	55.4	43.8
BC1	235-270	0.9	56.6	42.5	B′ss2	208-244	0.5	53.7	45.8

LAW 239									
Microhigh					Microlow				
Horizon	Depth	Sand	Silt	Clay	Horizon	Depth	Sand	Silt	Clay
	cm	wt%				cm	wt%		
					BCx	244-272	1.7	63.2	35.1
					2C	272-320	62.9	29.2	7.9
LAW 469									
Ak	0-11	19.4	29.0	51.6	A	0-16	25.3	24.0	50.7
Bk	11-28	18.4	29.4	52.2	Bss1	16-43	25.0	25.2	49.8
Bkss1	28-119	18.4	29.2	52.4	Bss2	43-74	21.1	25.7	53.2
Bkss2	119-172	16.2	29.5	54.3	Bss3	74-118	20.8	22.9	56.3
Bkss3	172-198	12.3	29.1	58.6	Bkss1	118-154	22.4	22.5	55.1
Bss1	198-205	3.3	28.8	67.9	Bkss2	154-176	9.7	30.3	60.0
Bss2	205-245	4.0	28.7	67.3	B′ss1	176-222	13.5	27.4	59.1
					B′ss2	222-245	22.3	28.9	48.8
					B′ss3	245-265	17.0	29.4	53.6
LAW 391									
A	0-12	19.1	25.6	55.3	A1	0-9	19.4	21.7	58.9
Ak	12-33	19.7	25.4	54.9	A2	9-28	18.1	21.4	60.5
Bkss1	33-59	19.4	26.3	54.3	Bss1	28-56	17.6	21.2	61.2
Bkss2	59-92	19.6	24.5	55.9	Bss2	56-79	17.7	22.2	60.1
Bkss3	92-127	15.7	26.7	57.6	Bkss1	79-104	18.8	21.3	59.9
Bkss4	127-150	15.4	25.9	58.7	Bkss2	104-160	16.5	22.5	61.0
Bkss5	150-183	14.2	30.3	55.5	Bkss3	160-195	13.3	25.1	61.6
Bkss6	183-235	19.5	30.4	50.1	Bkss4	195-224	8.9	34.5	56.6
					B′ss	224-237	12.2	34.0	53.8
VIC 409									
A	0-15	26.7	22.7	50.6	A	0-10	27.2	23.6	49.2
Bw	15-36	22.9	24.2	52.9	Bw	10-26	25.4	21.8	52.8
Bss1	36-54	22.5	24.1	53.4	Bss1	26-54	25.5	22.2	52.3
Bss2	54-73	20.6	24.7	54.7	Bss2	54-75	26.1	22.1	51.8
Bkss1	73-119	19.2	24.2	56.6	Bkss1	75-114	25.2	23.2	51.6
Bkss2	119-144	16.4	26.5	57.1	Bkss2	114-141	21.9	28.2	49.9
Bkss3	144-195	17.7	27.4	54.9	Bkss3	141-163	20.6	28.3	51.1

VIC 409

Microhigh					Microlow				
Horizon	Depth	Sand	Silt	Clay	Horizon	Depth	Sand	Silt	Clay
	cm	----------wt%----------				cm	----------wt%----------		
Bkssy1	195-214	21.2	31.9	46.9	Bkss4	163-178	22.6	26.3	51.1
Bkssy2	214-231	19.5	34.9	45.6	Bkssy1	178-210	19.4	30.1	50.5
Bkssy3	231-275	18.4	37.2	44.4	Bkssy2	210-230	23.6	30.3	46.1
Bssy1	275-300	21.9	30.9	47.2					
Bssy2	300-330	6.3	39.9	53.8					

Table A2-7. Mean separations between upper and lower unit Ti and Zr contents.

Element	Profile	Statistical Criterion				
		Mean separation[a]	Least significant difference (lsd) values[b]			Significance[c]
			95%	97.5%	99%	
		mg cm^{-3}				
Ti	LEG 245A	0.8773	2.4541	2.9499	3.5443	ns
	LAC 201	0.6493	2.4449	2.9420	3.5398	ns
	LAC 157	0.9906	2.2872	2.7493	3.3034	ns
	LAC 481	1.6865	2.1027	2.5251	3.0296	ns
	LAW 239	2.2485	1.6160	1.9446	2.3398	97.5%
	LAW 469	0.3537	2.1230	2.5532	3.0700	ns
	LAW 391	0.6515	1.7387	2.0867	2.5368	ns
	VIC 409	0.6548	1.3585	1.6286	1.9500	ns
Zr	LEG 245A	0.6577	0.2193	0.2637	0.3168	99%
	LAC 201	1.0295	0.2527	0.3041	0.3659	99%
	LAC 157	0.7039	0.1051	0.1263	0.1518	99%
	LAC 481	0.5106	0.1021	0.1226	0.1471	99%
	LAW 239	0.9977	0.1364	0.1641	0.1974	99%
	LAW 469	1.0291	0.2078	0.2500	0.3005	99%
	LAW 391	0.3575	0.1610	0.1932	0.2349	99%
	VIC 409	1.0775	0.3098	0.3714	0.4447	99%

[a] Mean separation calculated as the absolute difference between the elemental (Ti or Zr) content of upper and lower units

[b] Least significant differences calculated as $t_{\alpha\ \text{one-tailed}} \times (\text{MSE} \times (1/n_1 + 1/n_2))^{1/2}$, where $t_{\alpha\ \text{one-tailed}}$ is Student's t normal distribution value at probability α, MSE is pooled variance, and n_i is the number of data points

[c] Significance is that level of probability at which mean separation is greater than lsd

Table A2-8. Mean separations in Ti or Zr contents between laterally adjacent profiles.

Profile combination	Statistical Criterion				
	Mean separation	Least significant difference (lsd) values			Significance
		95%	97.5%	99%	
	mg cm^{-3}				
Ti - Upper Units					
LEG 245A x LAC 201	1.4314	1.6860	2.0253	2.4326	ns
LEG 245A x LAC 157	0.9947	1.3140	1.5788	1.8956	ns
LEG 245A x LAC 481	0.9275	1.2739	1.5299	1.8355	ns
LEG 245A x LAW 239	1.1005	1.7573	2.1115	2.5352	ns
LEG 245A x LAW 469	2.5982	1.4135	1.6983	2.0391	99%
LEG 245A x LAW 391	3.2577	1.4482	1.7380	2.0837	99%
LAC 201 x LAC 157	0.4367	1.2000	1.4426	1.7327	ns
LAC 201x LAC 481	0.5039	1.4591	1.7515	2.1018	ns
LAC 201 x LAW 239	0.3308	0.2466	0.2968	0.3571	ns
LAC 201 x LAW 469	1.1668	0.9211	1.1082	1.3322	97.5%
LAC 157 x LAC 481	0.0672	1.1511	1.3818	1.6581	ns
LAC 157 x LAW 239	0.1058	1.2664	1.5224	1.8285	ns
LAC 157 x LAW 469	1.6035	0.7980	0.9593	1.1522	99%
LAC 481 x LAW 239	1.6707	1.5477	1.8577	2.2293	95%
LAC 481 x LAW 469	2.3302	1.1573	1.3892	1.6671	99%
LAW 239 x LAW 469	1.4977	0.9648	1.1608	1.3954	99%
LAW 469 x LAW 391	0.6595	1.2487	1.4986	1.7967	ns
LAW 391 x VIC 409	1.0844	1.6112	1.9191	2.2976	ns
Ti - Lower Units					
LEG 245A x LAC 201	1.2034	3.8546	4.6560	5.6303	ns
LEG 245A x LAC 157	1.1079	2.7143	3.2888	3.9948	ns
LEG 245A x LAC 481	1.7367	3.0286	3.6774	4.4805	ns
LEG 245A x LAW 239	2.4717	2.6895	3.2487	3.9285	ns
LEG 245A x LAW 469	2.5982	2.5791	3.1315	3.8154	ns

Ti - Lower Units					
Profile combination	Statistical Criterion				
	Mean separation	Least significant difference (lsd) values			Significance
		95%	97.5%	99%	
	mg cm^{-3}				
LEG 245A x LAW 391	3.0319	2.8740	3.4897	4.2518	95%
LEG 245A x VIC 409	4.1196	2.5999	3.1569	3.8463	99%
LAC 201 x LAC 157	0.0954	3.7309	4.5006	5.4339	ns
LAC 201 x LAC 481	0.5334	3.0537	3.7548	4.6581	ns
LAC 201 x LAW 239	1.2683	2.8590	3.4534	4.1761	ns
LAC 201 x LAW 469	0.8712	3.8658	4.6696	5.6467	ns
LAC 201 x LAW 391	1.8285	5.5739	6.7329	8.1418	ns
LAC 201 x VIC 409	2.9162	4.7131	5.6931	6.8844	ns
LAC 157 x LAC 481	0.6288	3.8019	4.5924	5.5534	ns
LAC 157 x LAW 239	1.3638	2.3585	2.8489	3.4450	ns
LAC 157 x LAW 469	0.9666	3.1397	3.8043	4.6209	ns
LAC 157 x LAW 391	1.9239	5.1080	6.1891	7.5177	ns
LAC 157 x VIC 409	3.0116	3.8425	4.6558	5.6552	ns
LAC 481 x LAW 239	0.7350	2.8009	3.3832	4.0912	ns
LAC 481 x LAW 469	0.3378	3.0468	3.7463	4.6476	ns
LAC 481 x LAW 391	1.2951	5.7044	7.1840	9.2274	ns
LAC 481 x VIC 409	2.3828	3.7824	4.7635	6.1184	ns
LAW 239 x LAW 469	0.3972	2.4513	2.9610	3.5806	ns
LAW 239 x LAW 391	0.5602	4.1519	5.0152	6.0647	ns
LAW 239 x VIC 409	1.6479	2.7951	3.3763	4.0828	ns
LAW 469 x LAW 391	0.9573	5.6522	6.9114	8.5037	ns
LAW 469 x VIC 409	2.0450	2.9938	3.6811	4.5667	ns
LAW 391 x VIC 409	1.0877	3.0059	4.5335	4.9392	ns

Zr - Upper Units					
Profile combination	Statistical Criterion				
	Mean separation	Least significant difference (lsd) values			Significance
		95%	97.5%	99%	
	---------- mg cm^{-3} ----------				
LEG 245A x LAC 201	0.0444	0.3050	0.3663	0.4400	ns
LEG 245A x LAC 157	0.4548	0.2238	0.2687	0.3224	99%
LAC 201 x LAC 157	0.4992	0.2517	0.3026	0.3635	99%
LAC 157 x LAC 481	0.2030	0.1340	0.1608	0.1930	99%
LAC 481 x LAW 239	0.5941	0.2346	0.2816	0.3379	99%
LAW 239 x LAW 469	0.2551	0.1689	0.2032	0.2443	99%
LAW 469 x LAW 391	0.8131	0.2692	0.3231	0.3874	99%
LAW 391 x VIC 409	0.7577	0.1626	0.1950	0.2335	99%
Zr - Lower Units					
LEG 245A x LAC 201	0.3273	0.3050	0.3663	0.4400	95%
LEG 245A x LAC 157	0.5010	0.2238	0.2687	0.3224	99%
LAC 201 x LAC 157	0.1736	0.1861	0.2245	0.2710	ns
LAC 201 x LAC 481	0.1833	0.1178	0.1449	0.1797	99%
LAC 157 x LAC 481	0.0096	0.1318	0.1592	0.1926	ns
LAC 157 x LAW 239	0.0973	0.1610	0.1944	0.2351	ns
LAC 157 x LAW 469	0.3210	0.2176	0.2636	0.3202	99%
LAC 4812 x LAW 239	0.1069	0.1824	0.2204	0.2665	ns
LAC 481 x LAW 469	0.3306	0.1302	0.1601	0.1986	99%
LAW 239 x LAW 469	0.2237	0.2388	0.2885	0.3489	ns
LAW 239 x LAW 391	0.0822	0.2566	0.3100	0.3749	ns
LAW 239 x VIC 409	0.1199	0.3018	0.3646	0.4409	ns

Table A2-9. SEM survey results.

Unit	Profile	SEM Survey Feature							
		Hydrogeochemical Features				Physical Features			
		Solution	Scale	Pits	Mean	Conch.	Round.	Cracks	Mean
		%--------							
Rutile									
Upper	245A	100.0	100.0	72.7	90.9	54.5	100.0	9.1	54.5
	201	92.3	100.0	69.2	87.2	46.2	84.6	15.4	48.7
	481	93.3	100.0	100.0	97.8	40.0	100.0	26.7	55.6
	469	76.9	92.3	76.9	82.1	38.5	92.3	7.7	46.2
	391	91.7	100.0	91.7	94.4	58.3	75.0	16.7	50.0
	409	100.0	100.0	87.5	95.8	50.0	100.0	37.5	62.5
Lower	245A	85.7	100.0	85.7	90.5	42.9	100.0	28.6	57.1
	201	64.7	100.0	88.2	84.3	35.3	100.0	23.5	52.9
	481	100.0	100.0	80.0	93.3	30.0	80.0	40.0	50.0
	469	81.8	100.0	72.7	84.8	27.3	81.8	36.4	48.5
	391	100.0	90.0	100.0	96.7	80.0	60.0	10.0	50.0
	409	37.5	62.5	75.0	58.3	87.5	25.0	50.0	54.2
Zircon									
Upper	245A	7.1	14.3	85.7	35.7	92.9	42.9	50.0	61.9
	201	16.7	41.7	8.3	22.2	75.0	91.7	41.7	69.4
	481	0.0	40.0	0.0	13.3	100.0	90.0	50.0	80.0
	469	0.0	41.7	8.3	16.7	58.3	91.7	25.0	58.3
	391	0.0	45.5	0.0	15.2	100.0	72.7	36.4	69.7
	409	7.1	71.4	14.3	31.0	92.9	92.9	64.3	83.3
Lower	245A	0.0	14.3	0.0	4.8	85.7	71.4	14.3	57.1
	201	0.0	25.0	12.5	12.5	75.0	62.5	62.5	66.7
	481	6.7	53.3	6.7	22.2	80.0	80.0	46.7	68.9
	469	7.1	64.3	0.0	23.8	64.3	92.9	21.4	59.5

Zircon									
Unit	Profile	SEM Survey Feature							
		Hydrogeochemical Features				Physical Features			
		Solution	Scale	Pits	Mean	Conch.	Round.	Cracks	Mean
		%							
	391	0.0	40.0	0.0	13.3	90.0	90.0	40.0	73.3
	409	0.0	45.5	45.5	30.3	90.9	63.6	45.5	66.7

Table A2-10. Mean separations between zircon and rutile SEM features in upper and lower units.

Mineral	Profile	Statistical Criterion			
		Hydrogeochemical[a]		Physical	
		mean separation	significance[b]	mean separation	significance
		%		%	
Rutile	LEG 245A	0.4	ns	2.6	ns
	LAC 201	2.9	ns	4.2	ns
	LAC 481	4.4	ns	4.6	95%
	LAW 469	2.8	ns	2.3	ns
	LAW 391	2.2	ns	0.0	ns
	VIC 409	37.5	99%	8.3	99%
Zircon	LEG 245A	30.9	99%	4.8	ns
	LAC 201	9.7	99%	2.8	ns
	LAC 481	8.9	97.5%	11.1	99%
	LAW 469	7.1	95%	1.2	ns
	LAW 391	1.8	ns	3.6	ns
	VIC 409	0.6	ns	16.7	99%

[a] Categories described in Table 2-3

[b] Least significant differences calculated as $t_{\alpha\ \text{two-tailed}} \times (\text{MSE} \times (1/n))^{1/2}$, where $t_{\alpha\ \text{two-tailed}}$ is Student's t normal distribution value at probability α, MSE is pooled variance, and n is the number of data points. Significance levels for rutile: 95% ms ≥4.6, 97.5% ms ≥6.2, and 99% ms ≥6.8; for zircon: 95% ms ≥6.4, 97.5% ms ≥8.5, and 99% ms ≥9.2.

Table A2-11. Mean separations between zircon and rutile SEM features in upper units of adjacent pedons.

Profile combination	Statistical Criterion			
	Hydrogeochemical[a]		Physical	
	mean separation	significance[b]	mean separation	significance
Rutile				
	%		%	
LEG 245A vs LAC 201	3.7	ns	5.8	95%
LEG 245A vs LAC 481	6.9	97.5%		
LAC 201 vs LAC 481	10.6	99%	6.8	97.5%
LAC 481 vs LAW 469	15.7	99%	9.4	99%
LAW 469 vs LAW 391			3.8	ns
LAW 469 vs VIC 409	12.4	99%	16.3	99%
LAW 391 vs VIC 409	13.8	99%	12.5	99%
Zircon				
LEG 245A vs LAC 201	13.5	99%	7.5	97.5%
LAC 201 vs LAC 481	8.9	97.5%	10.6	99%
LAC 481 vs LAW 469	3.3	ns	21.7	99%
LAC 481 vs LAW 391	1.8	ns		
LAC 481 vs VIC 409	17.6	99%		
LAW 469 vs LAW 391	11.82	99%	11.4	99%
LAW 391 vs VIC 409	38.33	99%	13.6	99%

[a] Categories described in Table 2-3

[b] Significance levels for rutile: 95% ms ≥5.2, 97.5% ms ≥6.2, and 99% ms ≥7.5; for zircon: 95% ms ≥5.6, 97.5% ms ≥6.8, and 99% ms ≥8.1.

Table A2-12. Mean strain values for all profiles.

Depth interval	Microlows			Microhighs		
	ϵ_{Ti}	ϵ_{Zr}	ϵ_{Zr}:ϵ_{Ti}	ϵ_{Ti}	ϵ_{Zr}	ϵ_{Zr}:ϵ_{Ti}
cm						
10	-0.0499	-0.6823	13.67	-0.0413	-0.5976	14.47
20	-0.1111	-0.6644	5.98	-0.0776	-0.5595	7.21
30	-0.1027	-0.6804	6.63	-0.0743	-0.6005	8.08
40	-0.1166	-0.6704	5.75	-0.0942	-0.5790	6.15
50	-0.1115	-0.6571	5.89	-0.0525	-0.4634	8.83
60	-0.1365	-0.6706	4.91	-0.0750	-0.5249	7.00
70	-0.1107	-0.6698	6.05	-0.0342	-0.4596	13.44
80	-0.1182	-0.6672	5.64	-0.0772	-0.5121	6.63
90	-0.1353	-0.6624	4.90	-0.0506	-0.3372	6.66
100	-0.1395	-0.6645	4.76	-0.0155	-0.2740	17.68
110	-0.1327	-0.6382	4.81	-0.0156	-0.1709	10.96
120	-0.1477	-0.6317	4.28	-0.0495	-0.3252	6.57
130	-0.1381	-0.6263	4.54	-0.0244	-0.2759	11.31
140	-0.1287	-0.5913	4.59	-0.0377	-0.2917	7.74
150	-0.1386	-0.6286	4.54	-0.0323	-0.2916	9.03
160	-0.1087	-0.5887	5.42	-0.0775	-0.3936	5.08
170	-0.0838	-0.3966	4.73	-0.0553	-0.3698	6.69
180	-0.0576	-0.1617	2.81	-0.0344	-0.2843	8.26
190	-0.0307	-0.0417	1.36	0.0206	-0.1121	-5.44
200	-0.0423	-0.0338	0.80	0.0107	-0.1203	-11.24
210	0.0099	0.0816	8.24	0.0238	0.2335	9.81
220	-0.0095	-0.2313	24.35	0.0763	0.1459	1.91
230	0.0513	0.2036	3.97	0.1119	0.4630	4.14
240	0.0293	0.0306	1.04	0.0798	-0.0878	-1.10
250	-0.0152	-0.3056	20.11	0.1838	0.3908	2.13
260	-0.0060	-0.3443	57.38	0.0936	0.4739	5.06
270	0.0378	-0.2723	-7.20	0.1164	0.3375	2.90

Appendix 3: Data and Statistical Tables for Chapter 3.

Table A3-1. Whole soil XRF data, uncorrected element oxide data[a].

LEG 245A microhigh										
	Element									
Depth	Al_2O_3	CaO	Fe_2O_3	K_2O	MgO	MnO	P_2O_5	Rb	SiO_2	Sr
cm	Wt %									
10	12.31	1.40	3.62	0.77	0.85	0.041	0.06	0.009	72.77	0.010
20	12.65	1.39	3.62	0.77	0.95	0.035	0.04	0.008	73.73	0.013
30	12.37	1.52	4.06	0.76	0.98	0.055	0.03	0.009	75.41	0.008
40	12.03	3.56	4.65	0.78	1.08	0.153	0.05	0.008	71.89	0.008
50	11.71	3.50	4.76	0.73	1.03	0.155	0.04	0.007	72.62	0.008
60	11.30	4.25	4.69	0.75	1.06	0.172	0.04	0.007	71.27	0.008
70	11.36	4.82	4.07	0.73	1.14	0.042	0.06	0.008	72.91	0.008
80	12.86	1.55	4.28	0.74	1.11	0.070	0.03	0.008	74.50	0.009
90	12.92	1.32	4.69	0.76	1.07	0.108	0.03	0.009	74.92	0.009
100	12.35	1.31	4.57	0.71	0.78	0.081	<dl[b]	0.008	75.23	0.008
110	11.88	4.72	4.30	0.73	1.18	0.067	0.07	0.008	71.20	0.008
120	12.76	1.30	6.61	0.70	0.97	0.359	<dl	0.008	70.66	0.008
130	12.32	2.12	4.48	0.73	1.05	0.095	0.02	0.008	74.61	0.009
140	12.59	1.18	4.72	0.72	1.01	0.087	<dl	0.009	75.00	0.008
150	12.80	1.20	4.13	0.77	1.03	0.461	<dl	0.009	75.27	0.009
160	13.03	1.52	5.92	0.79	1.13	0.154	0.01	0.009	73.77	0.009
170	12.98	1.82	4.57	0.76	1.24	0.092	0.02	0.008	75.79	0.009
180	9.28	9.80	4.24	0.73	1.14	0.129	0.06	0.006	68.92	0.008
190	11.05	4.70	3.72	0.76	1.05	0.043	0.03	0.007	74.04	0.010
200	11.14	5.42	3.63	0.79	1.07	0.049	0.03	0.007	72.11	0.009
210	8.87	12.68	3.53	0.84	1.34	0.067	0.07	0.006	65.92	0.010
220	9.01	14.21	4.18	1.05	1.52	0.074	0.09	0.006	61.66	0.011
230	10.70	11.65	4.92	1.36	1.70	0.088	0.09	0.008	61.12	0.012
240	13.88	4.53	5.14	1.60	1.65	0.092	0.07	0.010	67.48	0.012
250	14.01	4.00	4.84	1.71	1.59	0.101	0.08	0.010	68.59	0.012
260	12.84	6.91	5.14	1.59	1.61	0.113	0.08	0.010	63.74	0.012
270	12.47	8.93	6.06	1.77	1.89	0.107	0.12	0.010	60.30	0.014
. LEG 245A microlow										
10	11.37	1.19	3.26	0.69	0.68	0.039	0.01	0.008	76.94	0.010
20	11.67	1.35	3.13	0.72	0.70	0.034	0.04	0.008	72.12	0.022
30	11.84	1.35	3.21	0.72	0.76	0.033	0.01	0.008	76.15	0.010
40	12.66	1.35	3.47	0.74	0.87	0.039	0.02	0.009	75.23	0.098
50	12.89	1.41	3.60	0.74	0.89	0.041	0.01	0.009	74.30	0.010
60	13.47	1.48	3.89	0.77	0.93	0.037	<dl	0.009	72.88	0.010
70	13.22	1.41	3.80	0.76	0.90	0.033	<dl	0.009	73.73	0.009
80	13.27	1.46	3.73	0.77	0.91	0.038	<dl	0.009	74.12	0.010
90	12.60	1.33	3.68	0.77	0.89	0.048	<dl	0.009	77.11	0.010
100	NA[c]									

[a] accounted to ± 2% of the amount present for major elements, ± 5% for minor elements, and ± 10% for trace elements
[b] value below instrument detection limit
[c] analysis data not available

	LEG 245A microlow									
	Element									
Depth	Al_2O_3	CaO	Fe_2O_3	K_2O	MgO	MnO	P_2O_5	Rb	SiO_2	Sr
cm	Wt%									
110	12.67	1.31	3.65	0.76	0.86	0.035	<dl	0.009	77.62	0.009
120	12.90	1.28	4.02	0.77	0.96	0.044	<dl	0.009	76.91	0.009
130	12.98	1.41	4.12	0.78	1.01	0.051	<dl	0.009	77.31	0.009
140	13.20	1.31	4.21	0.81	1.01	0.061	<dl	0.009	76.86	0.009
150	12.97	1.72	4.47	0.80	0.96	0.096	<dl	0.009	75.41	0.010
160	13.20	1.39	4.96	0.78	1.05	0.168	<dl	0.009	74.81	0.010
170	13.54	1.44	4.65	0.84	1.06	0.118	<dl	0.009	74.95	0.010
180	13.21	1.35	4.54	0.84	1.14	0.092	<dl	0.009	76.45	0.010
190	12.02	4.41	4.36	0.84	1.19	0.060	0.03	0.008	73.69	0.009
200	8.67	14.87	4.28	0.92	1.57	0.135	0.09	0.006	62.24	0.010
210	9.98	10.94	4.08	0.99	1.41	0.059	0.07	0.007	67.03	0.010
220	10.31	9.01	4.21	0.90	1.20	0.076	0.06	0.007	69.69	0.010
230	5.49	23.84	3.13	0.80	1.48	0.030	0.05	0.004	55.23	0.007
240	9.88	12.77	4.42	1.14	1.62	0.047	0.09	0.007	63.76	0.011
250	10.50	10.75	4.73	1.17	1.54	0.108	0.08	0.008	66.00	0.010
260	13.34	2.84	4.66	1.26	1.25	0.069	0.03	0.010	72.30	0.010
270	17.47	1.42	5.36	2.01	1.71	0.140	0.05	0.013	70.26	0.013
280	17.51	1.46	6.52	2.00	1.86	0.261	0.07	0.013	68.73	0.013
	LAC 201microhigh									
10	11.95	0.98	4.10	1.19	1.39	0.104	0.04	0.010	75.49	0.007
20	13.22	1.02	4.38	1.25	1.54	0.106	0.03	0.011	73.41	0.008
30	12.67	2.38	4.46	1.24	1.54	0.112	0.05	0.010	72.54	0.008
40	12.16	4.20	3.92	1.26	1.70	0.059	0.06	0.009	70.81	0.008
50	11.54	4.74	4.53	1.23	1.71	0.168	0.05	0.009	70.65	0.009
60	10.98	5.90	3.94	1.25	1.79	0.104	0.06	0.009	71.21	0.009
70	10.00	9.32	3.46	1.25	1.89	0.043	0.08	0.008	66.60	0.009
80	9.23	12.63	3.40	1.29	2.09	0.038	0.09	0.007	61.03	0.010
90	11.35	4.13	3.63	1.16	1.60	0.050	0.06	0.009	74.26	0.009
100	11.87	3.96	3.93	1.22	1.67	0.077	0.05	0.009	71.41	0.009
127	11.17	4.06	3.57	1.14	1.57	0.049	0.06	0.009	73.07	0.009
163	6.98	17.05	2.97	1.07	1.86	0.047	0.05	0.006	61.85	0.013
190	9.48	13.64	4.27	1.77	2.58	0.046	0.08	0.008	57.83	0.012
219	11.35	10.97	4.84	2.18	3.11	0.057	0.10	0.010	58.01	0.013
253	11.37	11.89	5.06	2.28	3.41	0.061	0.10	0.010	56.06	0.014
	LAC 201microlow									
10	9.97	0.55	2.94	0.98	0.68	0.055	0.01	0.009	77.39	0.008
20	9.80	0.44	3.00	0.94	0.84	0.066	0.03	0.008	80.14	0.007
30	9.13	0.41	2.63	0.86	0.60	0.066	0.01	0.008	81.80	0.007
40	10.97	0.54	3.29	0.94	0.95	0.085	0.03	0.008	77.97	0.008
60	11.24	0.55	3.22	1.02	0.98	0.049	<dl	0.009	77.01	0.008
70	10.16	0.51	3.24	0.95	0.75	0.060	<dl	0.009	80.04	0.008

LAC 201microlow										
	Element									
Depth	Al_2O_3	CaO	Fe_2O_3	K_2O	MgO	MnO	P_2O_5	Rb	SiO_2	Sr
cm	Wt%									
80	11.31	0.48	3.64	1.00	1.04	0.045	0.01	0.009	77.55	0.007
90	10.72	0.51	4.08	1.00	0.84	0.107	<dl	0.009	77.64	0.008
100	12.81	0.60	3.94	1.14	1.30	0.062	0.02	0.011	73.81	0.008
110	13.87	0.64	4.39	1.22	1.60	0.056	0.03	0.011	72.62	0.009
120	14.41	0.68	5.16	1.29	1.64	0.164	0.03	0.011	70.53	0.009
130	13.92	0.63	4.85	1.25	1.65	0.158	0.01	0.011	72.00	0.009
140	12.97	0.63	4.51	1.28	1.23	0.108	<dl	0.012	74.26	0.009
150	12.81	0.56	3.99	1.24	1.52	0.071	0.01	0.011	75.58	0.009
160	10.91	6.62	3.70	1.30	1.79	0.076	0.06	0.009	69.96	0.010
170	12.62	1.06	3.81	1.34	1.60	0.058	<dl	0.010	78.90	0.009
180	14.91	6.75	5.92	2.33	3.43	0.106	0.23	0.012	62.71	0.012
195	15.88	4.38	5.88	2.27	3.14	0.098	0.09	0.013	64.56	0.011
227	13.73	7.01	5.12	2.36	3.22	0.068	0.11	0.011	62.81	0.012
252	12.71	6.71	4.60	2.01	2.90	0.068	0.09	0.010	66.99	0.012
270	14.11	6.36	5.02	2.53	3.81	0.055	0.12	0.011	65.02	0.013
300	11.34	11.63	4.99	2.29	3.73	0.068	0.14	0.009	55.74	0.015
LAC 157 microhigh										
10	12.11	1.52	4.47	1.38	1.18	0.066	0.03	0.012	66.37	0.009
20	12.45	1.66	4.51	1.37	1.31	0.077	0.02	0.012	68.39	0.009
30	12.13	1.50	4.61	1.30	1.19	0.114	0.02	0.012	68.10	0.009
40	12.26	1.54	4.47	1.28	1.26	0.080	0.02	0.011	67.99	0.009
50	11.73	1.75	4.44	1.21	1.19	0.098	0.01	0.011	69.49	0.010
60	11.58	1.96	4.35	1.18	1.16	0.082	0.01	0.010	69.66	0.010
70	11.91	1.57	4.66	1.17	1.25	0.131	<dl	0.010	69.72	0.010
80	11.93	1.54	4.75	1.17	1.26	0.121	<dl	0.010	69.11	0.010
90	11.77	3.35	4.62	1.22	1.37	0.100	0.03	0.010	66.25	0.011
100	10.43	7.65	4.56	1.23	1.63	0.110	0.06	0.009	63.26	0.012
110	10.27	7.70	4.67	1.22	1.63	0.161	0.05	0.009	62.95	0.013
120	10.83	6.21	4.31	1.27	1.65	0.081	0.04	0.010	65.95	0.012
130	9.98	7.86	4.07	1.22	1.66	0.061	0.05	0.009	65.52	0.014
140	10.43	6.65	4.21	1.23	1.71	0.081	0.05	0.009	66.67	0.014
150	11.92	3.12	4.61	1.33	1.62	0.100	0.03	0.011	68.98	0.013
160	11.20	5.47	4.41	1.40	1.81	0.055	0.05	0.010	66.30	0.014
170	10.37	9.41	4.49	1.52	2.00	0.048	0.08	0.009	56.67	0.014
180	8.61	16.25	4.51	1.64	2.77	0.041	0.10	0.008	49.52	0.017
190	9.67	13.58	4.81	1.73	2.61	0.046	0.11	0.009	50.51	0.015
200	10.00	13.81	5.18	1.96	2.96	0.055	0.13	0.010	46.30	0.016
210	11.47	11.75	5.94	2.20	3.12	0.050	0.14	0.011	47.38	0.017
LAC 157 microlow										
10	11.57	1.40	4.42	1.26	0.97	0.103	0.03	0.008	64.98	0.010
20	12.31	1.46	4.77	1.21	1.12	0.127	<dl	0.008	65.19	0.022

	LAC 157 microlow									
	Element									
Depth	Al_2O_3	CaO	Fe_2O_3	K_2O	MgO	MnO	P_2O_5	Rb	SiO_2	Sr
cm	Wt%									
30	12.43	1.46	4.63	1.21	1.12	0.063	<dl	0.008	66.59	0.010
40	12.28	1.45	4.96	1.20	1.13	0.145	0.01	0.009	65.28	0.010
50	12.25	1.42	4.62	1.19	1.09	0.065	<dl	0.009	65.92	0.010
60	11.97	1.36	4.64	1.20	1.09	0.096	<dl	0.011	67.82	0.010
70	12.15	1.34	4.39	1.23	1.11	0.046	<dl	0.011	66.96	0.010
80	11.94	1.32	4.38	1.19	1.08	0.050	<dl	0.011	67.58	0.010
90	12.33	1.31	4.51	1.25	1.21	0.063	0.01	0.012	66.82	0.011
100	12.83	1.83	4.79	1.33	1.59	0.102	0.02	0.012	68.57	0.011
110	13.31	1.33	4.95	1.38	1.59	0.109	<dl	0.012	69.18	0.012
120	13.64	1.32	4.84	1.42	1.78	0.070	0.01	0.012	69.94	0.012
130	12.86	1.49	4.91	1.31	1.57	0.131	0.01	0.012	69.09	0.012
140	12.12	2.75	4.41	1.25	1.48	0.071	0.02	0.011	68.80	0.011
150	11.53	4.44	4.87	1.30	1.66	0.143	0.03	0.011	68.26	0.012
160	10.33	7.54	4.38	1.23	1.79	0.106	0.05	0.009	67.30	0.013
170	11.03	6.08	4.53	1.28	1.78	0.099	0.05	0.010	66.52	0.013
180	9.60	11.27	4.46	1.36	2.18	0.096	0.08	0.008	61.06	0.015
190	11.66	9.23	5.05	1.79	2.58	0.048	0.09	0.011	58.97	0.015
200	9.41	15.37	5.11	1.89	3.09	0.082	0.10	0.009	50.90	0.016
210	10.92	12.79	5.50	2.05	3.21	0.064	0.12	0.010	53.25	0.017
220	12.40	10.87	6.71	2.30	3.43	0.154	0.14	0.011	51.28	0.020
230	11.89	11.61	6.20	2.32	3.32	0.064	0.13	0.011	50.55	0.016
240	10.20	14.28	6.44	2.14	3.37	0.110	0.13	0.010	48.00	0.017
250						NA				
260	11.93	10.73	5.64	2.20	3.14	0.050	0.12	0.011	55.15	0.017
270						NA				
280	10.89	13.20	5.87	2.25	3.35	0.080	0.12	0.010	50.96	0.017
	LAC 481 microhigh									
10	14.61	2.82	5.52	1.58	1.74	0.134	0.03	0.013	65.60	0.009
20	15.04	2.17	5.81	1.52	1.64	0.124	0.02	0.014	65.67	0.009
30	15.40	1.58	5.90	1.51	1.64	0.130	<dl	0.014	65.86	0.010
40	15.49	1.56	5.86	1.53	1.70	0.130	<dl	0.014	66.26	0.010
50	15.59	1.50	5.67	1.53	1.74	0.125	<dl	0.014	66.05	0.010
60	15.58	1.40	5.70	1.52	1.75	0.135	<dl	0.014	64.61	0.010
70	14.60	3.36	5.53	1.53	1.84	0.111	<dl	0.013	64.75	0.010
80	11.59	10.40	5.37	1.60	2.28	0.088	0.07	0.012	56.28	0.012
90						NA				
100	8.38	17.88	4.68	1.55	2.72	0.054	0.07	0.009	49.94	0.011
110	9.65	15.39	5.15	1.64	2.82	0.070	0.09	0.010	53.33	0.012
120	10.98	11.49	5.14	1.49	2.23	0.090	0.08	0.011	54.82	0.012
130	9.16	15.71	4.75	1.46	2.52	0.054	0.08	0.009	52.86	0.013
140	10.95	11.90	5.26	1.57	2.45	0.075	0.07	0.011	58.60	0.013

Depth	Al_2O_3	CaO	Fe_2O_3	K_2O	MgO	MnO	P_2O_5	Rb	SiO_2	Sr
	Element									
cm	Wt%									
LAC 481 microhigh										
150	7.22	20.71	4.19	1.37	2.75	0.036	0.06	0.007	49.01	0.012
160	12.98	8.45	5.72	1.76	2.51	0.079	0.08	0.012	57.28	0.012
170	12.41	9.37	5.47	1.71	2.49	0.062	0.08	0.012	55.91	0.012
180	13.32	8.28	5.76	1.84	2.61	0.102	0.06	0.012	59.17	0.012
190	10.99	12.05	5.17	1.91	2.84	0.060	0.10	0.010	52.00	0.013
200	9.81	14.58	4.96	2.04	3.16	0.056	0.11	0.009	51.13	0.016
210	10.35	13.54	5.29	2.09	3.24	0.059	0.11	0.009	53.32	0.018
220	10.25	13.58	4.99	2.08	3.20	0.048	0.12	0.009	50.83	0.017
230	10.88	12.17	5.00	2.14	3.03	0.049	0.11	0.010	49.00	0.015
430	10.23	12.98	5.00	2.24	3.07	0.053	0.12	0.009	52.36	0.016
LAC 481 microlow										
10	14.25	1.53	5.27	1.48	1.44	0.133	0.03	0.013	67.43	0.008
20	14.58	1.56	5.43	1.47	1.59	0.140	0.03	0.013	67.95	0.008
30	14.72	1.49	5.55	1.41	1.52	0.127	<dl	0.013	68.68	0.008
40	14.29	1.41	5.29	1.41	1.37	0.104	<dl	0.013	69.46	0.009
50	14.51	1.39	5.42	1.39	1.48	0.114	<dl	0.012	69.24	0.009
60	13.91	1.41	5.33	1.36	1.43	0.160	<dl	0.012	70.42	0.009
70	14.45	1.28	5.25	1.38	1.46	0.109	<dl	0.012	69.55	0.009
80	13.96	1.31	5.50	1.36	1.46	0.208	<dl	0.012	69.99	0.009
90	15.76	1.31	5.98	1.47	1.69	0.145	<dl	0.014	67.91	0.009
100	13.10	1.19	5.40	1.38	1.44	0.164	<dl	0.012	71.10	0.009
110	16.22	1.31	5.85	1.56	1.85	0.108	<dl	0.014	69.09	0.010
120	15.71	1.25	5.65	1.57	1.78	0.101	<dl	0.014	70.06	0.010
130	15.62	1.20	5.76	1.61	1.88	0.135	<dl	0.014	70.18	0.010
140	15.42	1.19	5.61	1.63	1.87	0.122	<dl	0.014	70.79	0.010
150	15.00	1.62	5.39	1.63	1.89	0.096	<dl	0.014	71.70	0.010
160	15.32	1.53	5.55	1.67	1.93	0.114	<dl	0.014	70.87	0.010
170	15.40	1.42	5.62	1.67	2.02	0.134	<dl	0.014	69.99	0.010
180	15.54	1.74	5.49	1.71	2.04	0.093	0.01	0.014	69.44	0.011
190	15.46	2.47	5.59	1.74	2.13	0.113	0.03	0.014	67.73	0.010
200	14.78	4.56	5.70	1.87	2.51	0.144	0.06	0.013	65.81	0.011
210	11.66	11.75	5.32	2.18	3.36	0.073	0.11	0.010	56.05	0.013
220	11.24	12.34	4.90	2.25	3.37	0.067	0.11	0.009	55.05	0.014
230	10.80	13.09	5.41	2.20	3.35	0.097	0.10	0.009	53.74	0.014
240	12.40	10.67	5.69	2.38	3.46	0.099	0.11	0.010	55.50	0.014
250	11.38	12.01	5.20	2.26	3.41	0.078	0.11	0.010	54.84	0.014
LAW 239 microhigh										
10	10.73	3.48	3.78	1.17	1.28	0.110	0.03	0.009	74.93	0.008
20	7.96	14.60	3.43	1.11	1.91	0.056	0.06	0.007	66.09	0.014
30						NA				
40	11.37	5.04	4.03	1.24	1.61	0.082	0.03	0.010	74.02	0.011

LAW 239 microhigh										
	Element									
Depth	Al_2O_3	CaO	Fe_2O_3	K_2O	MgO	MnO	P_2O_5	Rb	SiO_2	Sr
cm	Wt%									
50	7.06	19.30	3.32	1.17	2.27	0.034	0.05	0.006	59.38	0.013
60	8.98	12.65	3.83	1.24	1.84	0.071	0.06	0.008	65.97	0.129
70	7.42	17.81	3.54	1.19	2.17	0.053	0.07	0.007	60.23	0.014
80	8.54	14.59	3.65	1.24	2.04	0.051	0.06	0.007	64.54	0.013
90	5.62	24.69	3.31	1.17	2.61	0.038	0.04	0.005	49.73	0.015
100	5.94	23.58	3.44	1.22	2.57	0.036	0.04	0.005	50.96	0.016
110	4.89	27.62	3.02	1.08	2.83	0.036	0.01	0.004	46.01	0.017
120	5.77	23.87	3.17	1.13	2.54	0.038	0.04	0.005	51.96	0.016
130	5.40	25.38	3.03	1.10	2.64	0.037	0.03	0.005	49.77	0.017
140	4.96	27.25	2.91	1.09	2.86	0.031	0.02	0.004	46.49	0.019
150	5.40	25.52	2.95	1.12	2.76	0.030	0.03	0.005	49.57	0.019
160	7.47	18.45	3.54	1.28	2.50	0.045	0.06	0.006	58.97	0.019
170	7.74	17.53	3.66	1.30	2.44	0.052	0.07	0.007	60.19	0.019
180	10.33	11.45	4.24	1.54	2.37	0.059	0.07	0.009	64.48	0.016
190	6.30	22.82	3.56	1.39	2.96	0.041	0.05	0.006	50.85	0.017
200	9.98	12.71	4.28	1.67	2.48	0.056	0.08	0.009	61.71	0.016
210	4.96	27.25	3.13	1.29	3.25	0.040	0.02	0.004	43.70	0.018
220	5.56	24.50	2.76	1.43	3.10	0.032	0.04	0.004	47.83	0.017
230	4.89	26.88	2.90	1.32	3.21	0.033	0.02	0.004	43.93	0.016
240	7.06	19.44	3.57	1.48	2.74	0.043	0.07	0.006	56.76	0.015
250	5.41	24.22	2.60	1.40	2.88	0.029	0.04	0.004	50.08	0.015
260	5.61	23.76	3.70	1.45	2.91	0.044	0.05	0.005	48.21	0.014
270	6.17	20.96	2.61	1.51	2.67	0.032	0.06	0.005	55.65	0.015
LAW 239 microlow										
10	11.70	1.21	4.19	1.13	1.19	0.154	<dl	0.010	74.43	0.009
20	12.53	1.31	4.48	1.14	1.39	0.167	<dl	0.010	73.80	0.010
30	12.40	1.29	4.26	1.13	1.34	0.117	<dl	0.010	74.42	0.010
40	12.31	1.29	4.24	1.14	1.34	0.126	<dl	0.010	74.45	0.010
50	12.24	1.29	4.20	1.14	1.37	0.112	<dl	0.010	74.66	0.011
60	12.32	1.30	4.44	1.13	1.40	0.151	<dl	0.010	73.94	0.011
70	12.37	1.26	4.37	1.13	1.46	0.139	<dl	0.010	74.04	0.011
80	12.57	1.24	4.52	1.12	1.54	0.167	<dl	0.010	73.38	0.011
90	12.51	1.24	4.74	1.15	1.57	0.199	<dl	0.010	73.81	0.012
100	12.44	1.18	4.26	1.15	1.53	0.122	<dl	0.010	73.85	0.012
110	12.42	1.15	4.11	1.18	1.51	0.102	<dl	0.011	74.76	0.013
120	12.04	1.60	4.23	1.16	1.55	0.131	<dl	0.010	75.29	0.013
130	12.34	1.08	4.18	1.19	1.60	0.114	<dl	0.010	74.90	0.014
140	11.91	2.20	4.16	1.22	1.63	0.117	<dl	0.010	74.39	0.015
150	11.07	4.58	3.81	1.20	1.71	0.079	0.01	0.010	72.42	0.016
160	10.85	5.70	3.93	1.28	1.76	0.091	0.02	0.009	71.57	0.016
170	5.65	24.33	3.14	1.17	2.65	0.034	0.04	0.005	48.14	0.018

	LAW 239 microlow									
	Element									
Depth	Al_2O_3	CaO	Fe_2O_3	K_2O	MgO	MnO	P_2O_5	Rb	SiO_2	Sr
cm	Wt%									
180	4.93	27.16	2.81	1.11	2.72	0.024	0.02	0.004	42.68	0.021
190	5.41	25.67	3.54	1.24	2.90	0.039	0.03	0.005	43.77	0.017
200	4.97	27.29	2.86	1.13	2.95	0.030	0.02	0.004	43.07	0.020
210	5.64	24.28	3.61	1.37	2.91	0.038	0.05	0.005	45.34	0.019
220	8.62	13.28	4.02	1.65	2.56	0.083	0.08	0.007	61.97	0.015
230	7.33	19.77	5.00	1.76	3.22	0.086	0.08	0.006	47.75	0.016
240	7.59	19.15	4.23	1.68	2.94	0.051	0.08	0.006	50.19	0.016
250						NA				
260	11.79	7.19	4.83	1.89	2.43	0.069	0.07	0.009	65.41	0.015
270	8.14	12.03	2.43	1.71	1.95	0.034	0.07	0.006	67.45	0.014
295	9.70	11.79	3.91	1.88	2.30	0.048	0.09	0.008	61.69	0.014
310	10.29	0.49	3.07	0.92	1.11	0.056	<dl	0.009	83.39	0.010
325	10.32	0.46	3.11	0.91	1.09	0.071	<dl	0.009	82.98	0.010
	LAW 469 microhigh									
10	9.26	11.54	3.71	0.79	1.50	0.073	0.05	0.006	65.13	0.011
20	8.92	11.88	3.61	0.78	1.49	0.075	0.05	0.006	66.39	0.011
30	9.35	10.94	3.78	0.78	1.51	0.081	0.05	0.006	66.60	0.011
40	8.54	13.41	3.49	0.78	1.58	0.052	0.05	0.006	65.04	0.012
50	9.02	12.62	3.64	0.80	1.69	0.071	0.05	0.006	65.52	0.013
60	8.83	11.53	3.55	0.76	1.47	0.060	0.05	0.006	65.93	0.012
70	9.54	10.43	3.73	0.79	1.62	0.079	0.05	0.007	67.79	0.012
80	9.04	11.46	3.54	0.77	1.56	0.039	0.05	0.006	66.82	0.013
90	9.63	10.05	3.70	0.79	1.62	0.074	0.04	0.006	68.04	0.014
100	8.28	13.99	3.39	0.76	1.68	0.055	0.05	0.005	64.79	0.015
110	9.79	9.44	3.74	0.80	1.62	0.076	0.05	0.007	68.59	0.015
120	9.57	10.60	3.68	0.83	1.61	0.059	0.05	0.006	66.70	0.014
130	9.20	10.89	3.59	0.80	1.63	0.065	0.04	0.006	67.78	0.015
140	7.34	16.53	3.11	0.75	1.74	0.056	0.06	0.005	62.25	0.019
150	10.96	5.72	3.96	0.82	1.52	0.089	0.02	0.008	71.73	0.014
160	10.42	9.18	4.02	0.91	1.75	0.068	0.04	0.007	67.91	0.015
170	11.16	7.60	4.11	0.93	1.66	0.073	0.03	0.008	68.89	0.015
180	9.29	13.79	4.12	1.00	1.90	0.066	0.07	0.007	61.92	0.017
190	10.41	10.05	4.21	0.99	1.79	0.063	0.05	0.007	66.39	0.014
200	10.26	12.27	4.43	1.09	2.05	0.058	0.07	0.007	61.76	0.016
210	11.00	10.57	4.63	1.14	2.03	0.056	0.07	0.008	64.05	0.015
	LAW 469 microlow									
10	9.97	1.28	3.14	0.71	0.76	0.073	0.02	0.008	72.99	0.007
20	10.76	1.25	3.42	0.68	0.95	0.090	<dl	0.008	74.13	0.007
30	11.26	1.34	3.55	0.66	1.06	0.067	<dl	0.007	74.43	0.007
40	11.32	1.34	3.54	0.65	1.07	0.063	<dl	0.008	74.47	0.008
50	11.21	1.33	3.49	0.65	1.07	0.044	<dl	0.008	73.89	0.008

	LAW 469 microlow									
	Element									
Depth	Al_2O_3	CaO	Fe_2O_3	K_2O	MgO	MnO	P_2O_5	Rb	SiO_2	Sr
cm	Wt%									
60	11.82	1.40	3.51	0.68	1.13	0.050	<dl	0.008	72.03	0.008
70	11.26	1.35	3.50	0.69	1.10	0.073	<dl	0.008	74.62	0.008
80	11.59	1.40	3.61	0.70	1.20	0.064	<dl	0.008	75.07	0.009
90	11.72	1.47	3.67	0.73	1.22	0.068	<dl	0.008	75.60	0.009
100	11.84	1.50	3.74	0.74	1.34	0.065	<dl	0.008	76.11	0.010
110	12.22	1.43	3.76	0.76	1.19	0.050	<dl	0.009	75.66	0.010
120	11.70	1.46	3.73	0.77	1.36	0.050	<dl	0.009	76.14	0.010
130	11.65	1.39	3.69	0.77	1.39	0.054	<dl	0.009	75.77	0.010
140	10.33	5.18	3.61	0.83	1.50	0.063	0.04	0.008	72.61	0.012
150	11.43	2.21	3.64	0.81	1.42	0.059	0.01	0.008	74.64	0.011
160	10.55	5.38	3.64	0.84	1.52	0.077	0.04	0.008	72.31	0.013
170	11.00	6.03	4.01	0.95	1.61	0.058	0.05	0.008	71.05	0.014
180	10.18	10.66	4.32	1.08	1.86	0.051	0.09	0.008	65.24	0.014
190	10.86	11.61	4.95	1.28	2.11	0.054	0.09	0.008	61.02	0.015
200	10.83	11.27	4.63	1.31	2.08	0.056	0.10	0.008	61.06	0.016
210	9.88	12.17	4.51	1.27	2.15	0.049	0.10	0.008	59.99	0.015
220	9.15	10.70	3.70	1.26	1.77	0.036	0.09	0.007	66.38	0.013
230	9.54	11.65	4.09	1.34	1.83	0.045	0.09	0.008	64.07	0.013
	LAW 391 microhigh									
10						NA				
20						NA				
30						NA				
40						NA				
50	10.62	11.08	4.01	1.60	2.39	0.052	0.09	0.009	64.13	0.010
60	11.56	8.60	4.25	1.65	2.24	0.067	0.09	0.010	65.99	0.010
70	8.28	15.43	3.52	1.49	2.22	0.035	0.08	0.007	61.30	0.010
80	9.41	12.89	3.85	1.55	2.31	0.049	0.09	0.008	63.31	0.011
90	9.60	12.56	3.93	1.57	2.22	0.052	0.09	0.008	62.68	0.011
100	9.75	12.72	3.88	1.58	2.31	0.049	0.10	0.008	61.16	0.011
110	9.50	13.27	3.86	1.60	2.36	0.040	0.10	0.008	62.56	0.012
120	10.50	10.55	3.97	1.64	2.28	0.041	0.09	0.009	64.11	0.012
130	9.25	14.02	3.80	1.57	2.43	0.043	0.09	0.008	62.12	0.012
140	11.42	8.87	4.10	1.71	2.33	0.046	0.08	0.010	67.01	0.012
150	11.10	9.07	4.10	1.70	2.20	0.055	0.08	0.009	66.72	0.012
160	9.22	13.53	3.68	1.57	2.24	0.030	0.09	0.008	61.38	0.013
170	10.25	11.04	3.93	1.64	2.16	0.046	0.08	0.008	63.71	0.012
180	9.24	14.07	3.83	1.60	2.42	0.042	0.09	0.008	61.42	0.013
190	9.01	14.47	3.74	1.59	2.34	0.032	0.10	0.007	59.89	0.012
200	9.24	14.03	3.79	1.60	2.32	0.034	0.09	0.007	60.96	0.013
210	8.81	15.02	3.73	1.57	2.37	0.029	0.10	0.007	60.35	0.015
220	8.84	14.50	3.72	1.56	2.18	0.040	0.09	0.007	59.13	0.013

Depth	Al_2O_3	CaO	Fe_2O_3	K_2O	MgO	MnO	P_2O_5	Rb	SiO_2	Sr
	Element									
cm	Wt%									
LAW 391 microhigh										
230	9.68	11.85	3.75	1.65	2.05	0.041	0.09	0.008	62.61	0.012
240	9.82	10.19	3.47	1.63	1.77	0.040	0.08	0.008	65.09	0.012
370	7.49	14.63	2.76	1.64	1.63	0.025	0.08	0.006	63.26	0.011
LAW 391 microlow										
10	12.53	1.55	4.07	1.61	1.54	0.076	0.05	0.011	67.55	0.007
20	14.26	1.70	4.57	1.62	1.87	0.087	0.03	0.011	68.17	0.008
30	13.55	1.62	4.26	1.63	1.72	0.066	0.03	0.011	69.31	0.008
40	13.77	1.65	4.22	1.61	1.80	0.064	0.03	0.011	68.10	0.008
50	13.59	1.65	4.26	1.61	1.90	0.079	0.04	0.012	69.89	0.009
60	14.12	1.69	4.29	1.65	2.03	0.078	0.00	0.012	70.71	0.009
70	13.64	1.76	4.27	1.66	1.88	0.077	0.02	0.012	69.92	0.009
80	13.87	1.77	4.41	1.69	1.97	0.097	0.02	0.012	71.82	0.010
90	13.79	1.58	4.38	1.66	1.88	0.096	0.02	0.012	70.37	0.010
100	13.69	2.36	4.35	1.70	2.06	0.072	0.03	0.012	71.39	0.010
110	13.47	3.41	4.26	1.71	2.07	0.062	0.05	0.011	68.44	0.011
120	13.29	3.83	4.17	1.71	2.02	0.048	0.05	0.011	65.16	0.011
130	11.79	6.60	4.03	1.65	2.03	0.045	0.07	0.010	64.80	0.011
140	10.28	11.22	3.91	1.62	2.24	0.057	0.09	0.009	61.06	0.011
150	14.38	2.97	4.59	1.83	2.22	0.065	0.05	0.012	67.83	0.011
160	13.50	4.87	4.48	1.82	2.35	0.061	0.06	0.011	67.85	0.011
170	13.05	5.60	4.41	1.83	2.21	0.057	0.07	0.011	67.57	0.012
180	12.77	6.19	4.36	1.80	2.26	0.062	0.06	0.011	67.32	0.013
190	11.66	8.42	4.20	1.78	2.29	0.051	0.08	0.010	66.41	0.012
200	11.59	8.23	4.23	1.80	2.23	0.044	0.08	0.010	65.91	0.013
210	12.08	7.38	4.28	1.84	2.21	0.046	0.08	0.010	68.19	0.011
220	11.98	7.26	4.22	1.81	2.12	0.048	0.07	0.010	65.22	0.011
230	8.60	15.52	3.85	1.60	2.31	0.029	0.09	0.007	59.79	0.015
240	9.04	14.22	3.84	1.63	2.31	0.036	0.10	0.008	60.66	0.013
250	9.18	13.99	3.88	1.63	2.22	0.031	0.10	0.008	58.84	0.013
VIC 409 microhigh										
10	8.96	7.03	3.01	1.38	1.59	0.079	0.05	0.007	72.88	0.012
20	8.84	8.54	2.91	1.39	1.64	0.082	0.03	0.007	72.86	0.013
30	8.68	8.35	2.99	1.30	1.53	0.071	0.05	0.007	71.47	0.014
40	8.65	9.21	3.04	1.36	1.68	0.073	0.04	0.007	71.42	0.016
50	9.10	8.17	2.94	1.45	1.78	0.065	0.03	0.007	72.21	0.016
60	8.92	8.59	3.04	1.42	1.73	0.083	0.04	0.007	71.46	0.016
70	9.35	7.70	2.96	1.51	1.81	0.074	0.03	0.007	72.69	0.016
80	9.09	7.82	3.10	1.46	1.67	0.064	0.04	0.007	71.23	0.018
90	9.08	7.93	3.16	1.47	1.73	0.081	0.04	0.007	71.24	0.019
100	9.15	7.85	3.18	1.49	1.73	0.079	0.04	0.007	70.96	0.020
110	9.85	6.72	3.25	1.56	1.82	0.074	0.03	0.008	71.16	0.018

	VIC 409 microhigh									
	Element									
Depth	Al_2O_3	CaO	Fe_2O_3	K_2O	MgO	MnO	P_2O_5	Rb	SiO_2	Sr
cm	Wt%									
120	9.66	6.61	3.26	1.53	1.77	0.089	0.04	0.008	72.31	0.018
130	9.49	6.65	3.21	1.53	1.60	0.063	0.03	0.007	71.09	0.018
140	9.53	6.92	3.22	1.59	1.78	0.069	0.04	0.008	72.39	0.018
150	9.34	6.71	3.15	1.53	1.59	0.060	0.04	0.007	72.58	0.017
160	9.64	5.82	3.17	1.59	1.57	0.080	0.04	0.008	74.04	0.017
170	NA									
180	7.88	5.80	2.76	1.08	1.43	0.052	0.08	0.006	73.35	0.016
190	7.27	8.66	2.81	0.96	1.71	0.044	0.09	0.006	68.72	0.018
200	5.15	9.95	2.36	0.43	2.32	0.030	<dl	0.004	61.24	0.018
210	7.17	8.21	2.74	0.95	1.63	0.038	0.08	0.006	69.53	0.017
220	8.40	9.01	3.05	1.43	1.37	0.049	0.06	0.006	71.73	0.016
	VIC 409 microlow									
10	9.75	0.96	2.78	1.55	1.11	0.072	<dl	0.008	77.26	0.008
20	10.20	1.17	3.06	1.44	1.26	0.090	<dl	0.008	78.65	0.009
30	10.13	1.17	3.01	1.42	1.22	0.074	<dl	0.008	77.69	0.009
40	10.29	1.27	3.04	1.41	1.32	0.072	<dl	0.008	77.53	0.010
50	10.15	1.77	2.98	1.39	1.39	0.078	<dl	0.008	77.89	0.010
60	9.62	1.80	2.92	1.35	1.28	0.076	<dl	0.008	78.78	0.011
70	9.51	3.79	2.88	1.40	1.42	0.070	<dl	0.007	75.48	0.013
80	9.90	2.88	2.78	1.44	1.46	0.067	<dl	0.007	76.84	0.011
90	10.05	2.62	2.96	1.44	1.45	0.070	<dl	0.008	75.09	0.012
100	8.73	5.67	2.74	1.36	1.44	0.071	0.02	0.007	76.09	0.014
110	9.42	4.07	2.93	1.47	1.41	0.073	0.02	0.007	76.51	0.014
120	9.38	5.09	3.00	1.53	1.47	0.073	0.02	0.007	74.37	0.015
130	8.95	6.30	2.93	1.52	1.49	0.062	0.03	0.007	73.84	0.016
140	9.34	4.99	3.02	1.55	1.41	0.067	0.01	0.007	75.02	0.015
150	9.19	5.85	2.96	1.55	1.49	0.062	0.02	0.007	75.28	0.015
160	9.31	5.74	2.87	1.55	1.41	0.070	0.02	0.007	71.21	0.015
170	9.09	6.06	2.89	1.52	1.47	0.055	0.03	0.007	74.49	0.016
180	8.02	13.76	3.91	1.34	2.11	0.088	0.10	0.006	58.35	0.018
190	8.98	6.83	2.93	1.52	1.53	0.065	0.03	0.007	73.26	0.016
200	9.60	5.20	3.04	1.59	1.44	0.064	0.02	0.007	75.20	0.015
210	9.07	6.77	3.02	1.53	1.51	0.058	0.04	0.007	73.46	0.017
220	9.86	4.01	2.96	1.56	1.41	0.058	0.03	0.007	73.13	0.014
230	9.87	4.25	3.04	1.58	1.51	0.059	0.03	0.007	75.97	0.015
240	9.92	4.44	3.07	1.58	1.42	0.061	0.04	0.007	73.82	0.015
250	9.93	3.23	3.15	1.55	1.45	0.066	0.06	0.008	77.31	0.014
260	9.18	10.06	3.66	1.55	1.73	0.064	0.12	0.007	64.91	0.020
270	8.29	12.66	3.92	1.31	2.21	0.061	0.10	0.007	57.76	0.017
dl	0.08	0.06	0.02	0.02	0.04	0.004	0.01	0.001	0.24	0.001
prec[c]	0.11	0.02	0.08	0.01	0.05	0.002	0.03	0.0003	0.15	0.0003

[c] instrumental precision

Table A3-2. Whole soil carbonate-corrected element oxide data.

	LEG 245A microhigh									
	Element									
Depth	Al_2O_3	CaO	Fe_2O_3	K_2O	MgO	MnO	P_2O_5	Rb	SiO_2	Sr
cm	Wt%									
10	12.31	1.40	3.62	0.77	0.85	0.041	0.06	0.009	72.77	0.010
20	12.65	1.39	3.62	0.77	0.95	0.035	0.04	0.008	73.73	0.013
30	12.37	1.52	4.06	0.76	0.98	0.055	0.03	0.009	75.41	0.008
40	12.31	3.64	4.75	0.80	1.10	0.156	0.05	0.009	73.55	0.009
50	11.97	3.58	4.86	0.74	1.06	0.159	0.04	0.008	74.25	0.008
60	11.64	4.38	4.84	0.77	1.09	0.177	0.04	0.008	73.44	0.008
70	11.78	5.00	4.22	0.76	1.19	0.044	0.06	0.008	75.58	0.008
80	12.86	1.55	4.28	0.74	1.11	0.070	0.03	0.008	74.50	0.009
90	12.92	1.32	4.69	0.76	1.07	0.108	0.03	0.009	74.92	0.009
100	12.35	1.31	4.57	0.71	0.78	0.081	<dl	0.008	75.23	0.008
110	12.30	4.89	4.46	0.76	1.22	0.069	0.07	0.008	73.72	0.009
120	12.76	1.30	6.61	0.70	0.97	0.359	<dl	0.008	70.66	0.008
130	12.42	2.14	4.51	0.73	1.06	0.095	0.02	0.008	75.17	0.009
140	12.59	1.18	4.72	0.72	1.01	0.087	<dl	0.009	75.00	0.008
150	12.80	1.20	4.13	0.77	1.03	0.461	<dl	0.009	75.27	0.009
160	13.04	1.52	5.93	0.79	1.13	0.155	0.01	0.009	73.86	0.009
170	13.03	1.83	4.59	0.77	1.25	0.092	0.02	0.008	76.13	0.009
180	10.12	10.68	4.62	0.79	1.24	0.140	0.07	0.007	75.12	0.009
190	11.44	4.87	3.85	0.79	1.09	0.045	0.03	0.008	76.65	0.010
200	11.62	5.65	3.79	0.83	1.11	0.052	0.03	0.008	75.21	0.010
210	9.95	14.21	3.96	0.95	1.50	0.075	0.08	0.007	73.89	0.011
220	10.25	16.17	4.75	1.20	1.73	0.084	0.10	0.007	70.13	0.012
230	11.88	12.93	5.47	1.51	1.89	0.097	0.10	0.009	67.84	0.014
240	14.35	4.68	5.31	1.66	1.70	0.095	0.07	0.011	69.74	0.012
250	14.39	4.11	4.98	1.76	1.64	0.104	0.08	0.011	70.50	0.012
260	13.60	7.32	5.44	1.68	1.70	0.119	0.08	0.011	67.51	0.013
270	13.48	9.65	6.55	1.92	2.04	0.116	0.13	0.011	65.17	0.015
	LEG 245A microlow									
10	11.37	1.19	3.26	0.69	0.68	0.039	0.01	0.008	76.94	0.010
20	11.67	1.35	3.13	0.72	0.70	0.034	0.04	0.008	72.12	0.022
30	11.84	1.35	3.21	0.72	0.76	0.033	0.01	0.008	76.15	0.010
40	12.66	1.35	3.47	0.74	0.87	0.039	0.02	0.009	75.23	0.010
50	12.89	1.41	3.60	0.74	0.89	0.041	0.01	0.009	74.30	0.010
60	13.47	1.48	3.89	0.77	0.93	0.037	<dl	0.009	72.88	0.010
70	13.22	1.41	3.80	0.76	0.90	0.033	<dl	0.009	73.73	0.009
80	13.27	1.46	3.73	0.77	0.91	0.038	<dl	0.009	74.12	0.010
90	12.60	1.33	3.68	0.77	0.89	0.048	<dl	0.009	77.11	0.010
100	NA[b]									

[a] value below instrument detection limit

[b] analysis data not available

LEG 245A microlow										
	Element									
Depth	Al_2O_3	CaO	Fe_2O_3	K_2O	MgO	MnO	P_2O_5	Rb	SiO_2	Sr
cm	Wt%									
110	12.67	1.31	3.65	0.76	0.86	0.035	<dl	0.009	77.62	0.009
120	12.90	1.28	4.02	0.77	0.96	0.044	<dl	0.009	76.91	0.009
130	12.98	1.41	4.12	0.78	1.01	0.051	<dl	0.009	77.31	0.009
140	13.20	1.31	4.21	0.81	1.01	0.061	<dl	0.009	76.86	0.009
150	12.97	1.72	4.47	0.80	0.96	0.096	<dl	0.009	75.41	0.010
160	13.20	1.39	4.96	0.78	1.05	0.168	<dl	0.009	74.81	0.010
170	13.54	1.44	4.65	0.84	1.06	0.118	<dl	0.009	74.95	0.010
180	13.21	1.35	4.54	0.84	1.14	0.092	<dl	0.009	76.45	0.010
190	12.41	4.56	4.50	0.87	1.23	0.062	0.03	0.008	76.08	0.010
200	9.92	17.03	4.90	1.05	1.80	0.154	0.11	0.007	71.26	0.011
210	11.01	12.06	4.50	1.09	1.55	0.065	0.08	0.008	73.91	0.011
220	11.16	9.75	4.55	0.98	1.30	0.082	0.07	0.008	75.39	0.010
230	6.81	29.59	3.88	0.99	1.84	0.037	0.07	0.005	68.55	0.009
240	11.09	14.33	4.96	1.28	1.82	0.052	0.10	0.008	71.55	0.012
250	11.55	11.83	5.21	1.29	1.69	0.119	0.09	0.009	72.64	0.012
260	13.55	2.88	4.74	1.28	1.27	0.070	0.03	0.010	73.42	0.010
270	17.48	1.42	5.36	2.01	1.71	0.140	0.05	0.013	70.28	0.013
280	17.53	1.46	6.53	2.00	1.86	0.262	0.07	0.013	68.79	0.013
LAC 201microhigh										
10	11.95	0.98	4.10	1.19	1.39	0.104	0.04	0.010	75.49	0.007
20	13.22	1.02	4.38	1.25	1.54	0.106	0.03	0.011	73.41	0.008
30	12.71	2.39	4.47	1.25	1.55	0.112	0.05	0.010	72.79	0.008
40	12.37	4.27	3.99	1.29	1.72	0.060	0.06	0.010	72.04	0.009
50	11.79	4.84	4.62	1.25	1.75	0.172	0.06	0.009	72.17	0.009
60	11.31	6.08	4.06	1.28	1.85	0.107	0.06	0.009	73.38	0.009
70	10.56	9.85	3.65	1.32	2.00	0.046	0.08	0.009	70.38	0.010
80	12.05	4.02	3.99	1.24	1.70	0.078	0.05	0.009	72.52	0.009
90	11.35	4.13	3.63	1.16	1.60	0.050	0.06	0.009	74.26	0.009
100	9.88	12.01	3.61	1.25	1.97	0.040	0.08	0.008	69.13	0.011
127	9.99	13.67	3.68	1.39	2.26	0.041	0.10	0.008	66.04	0.010
163	7.79	19.03	3.31	1.19	2.08	0.052	0.05	0.006	69.02	0.015
190	10.33	14.86	4.66	1.93	2.81	0.050	0.09	0.009	63.01	0.013
219	12.14	11.73	5.17	2.33	3.33	0.061	0.11	0.011	62.04	0.014
253	12.24	12.80	5.44	2.45	3.67	0.066	0.11	0.011	60.34	0.015
LAC 201microlow										
10	9.97	0.55	2.94	0.98	0.68	0.055	0.01	0.009	77.39	0.008
20	9.80	0.44	3.00	0.94	0.84	0.066	0.03	0.008	80.14	0.007
30	9.13	0.41	2.63	0.86	0.60	0.066	0.01	0.008	81.80	0.007
40	10.97	0.54	3.29	0.94	0.95	0.085	0.03	0.008	77.97	0.008
60	11.24	0.55	3.22	1.02	0.98	0.049	<dl	0.009	77.01	0.008
70	10.16	0.51	3.24	0.95	0.75	0.060	<dl	0.009	80.04	0.008

LAC 201microlow										
	Element									
Depth	Al_2O_3	CaO	Fe_2O_3	K_2O	MgO	MnO	P_2O_5	Rb	SiO_2	Sr
cm	Wt%									
80	11.31	0.48	3.64	1.00	1.04	0.045	0.01	0.009	77.55	0.007
90	10.72	0.51	4.08	1.00	0.84	0.107	<dl	0.009	77.64	0.008
100	12.81	0.60	3.94	1.14	1.30	0.062	0.02	0.011	73.81	0.008
110	13.87	0.64	4.39	1.22	1.60	0.056	0.03	0.011	72.62	0.009
120	14.41	0.68	5.16	1.29	1.64	0.164	0.03	0.011	70.53	0.009
130	13.92	0.63	4.85	1.25	1.65	0.158	0.01	0.011	72.00	0.009
140	12.97	0.63	4.51	1.28	1.23	0.108	<dl	0.011	74.26	0.009
150	12.81	0.56	3.99	1.24	1.52	0.071	0.01	0.011	75.58	0.008
160	11.30	6.86	3.83	1.35	1.85	0.078	0.06	0.009	72.48	0.010
170	12.62	1.06	3.81	1.34	1.60	0.058	<dl	0.010	78.90	0.009
180	15.46	7.00	6.14	2.42	3.56	0.110	0.23	0.013	65.03	0.012
195	16.18	4.46	5.99	2.32	3.20	0.100	0.10	0.013	65.78	0.011
227	14.26	7.28	5.32	2.45	3.35	0.071	0.11	0.012	65.26	0.013
252	13.18	6.96	4.77	2.08	3.00	0.070	0.09	0.011	69.44	0.012
270	14.59	6.57	5.19	2.62	3.94	0.057	0.12	0.011	67.23	0.013
300	12.18	12.49	5.36	2.46	4.01	0.073	0.15	0.010	59.86	0.016
LAC 157 microhigh										
10	12.11	1.52	4.47	1.38	1.18	0.066	0.03	0.012	66.37	0.009
20	12.45	1.66	4.51	1.37	1.31	0.077	0.02	0.012	68.39	0.009
30	12.13	1.50	4.61	1.30	1.19	0.114	0.02	0.011	68.10	0.009
40	12.26	1.54	4.47	1.28	1.26	0.080	0.02	0.011	67.99	0.009
50	11.73	1.75	4.44	1.21	1.19	0.098	0.01	0.011	69.49	0.010
60	11.58	1.96	4.35	1.18	1.16	0.082	0.01	0.010	69.66	0.010
70	11.91	1.57	4.66	1.17	1.25	0.131	<dl	0.010	69.72	0.010
80	11.93	1.54	4.75	1.17	1.26	0.121	<dl	0.010	69.11	0.010
90	12.02	3.28	4.71	1.24	1.40	0.102	0.03	0.010	67.66	0.011
100	11.14	7.17	4.87	1.31	1.74	0.117	0.06	0.009	67.52	0.013
110	10.97	7.21	4.99	1.30	1.74	0.172	0.05	0.010	67.22	0.014
120	11.39	5.90	4.54	1.34	1.74	0.085	0.04	0.010	69.37	0.013
130	10.68	7.35	4.35	1.30	1.78	0.066	0.05	0.010	70.08	0.015
140	11.02	6.29	4.45	1.30	1.80	0.085	0.05	0.010	70.44	0.015
150	12.14	3.07	4.69	1.35	1.65	0.102	0.03	0.011	70.27	0.014
160	11.69	5.24	4.61	1.46	1.89	0.057	0.05	0.011	69.21	0.014
170	11.26	8.66	4.87	1.65	2.17	0.052	0.09	0.010	61.55	0.015
180	9.98	14.01	5.23	1.91	3.22	0.047	0.12	0.009	57.42	0.019
190	10.94	12.00	5.44	1.96	2.96	0.051	0.12	0.010	57.13	0.017
200	11.34	12.18	5.87	2.22	3.35	0.063	0.15	0.011	52.49	0.018
210	12.75	10.57	6.60	2.45	3.46	0.056	0.15	0.012	52.65	0.018
LAC 157 microlow										
10	11.57	1.40	4.42	1.26	0.97	0.103	0.03	0.011	64.98	0.009
20	12.31	1.46	4.77	1.21	1.12	0.127	<dl	0.011	65.19	0.009

LAC 157 microlow										
	Element									
Depth	Al_2O_3	CaO	Fe_2O_3	K_2O	MgO	MnO	P_2O_5	Rb	SiO_2	Sr
cm	Wt%									
30	12.43	1.46	4.63	1.21	1.12	0.063	<dl	0.011	66.59	0.009
40	12.28	1.45	4.96	1.20	1.13	0.145	0.01	0.011	65.28	0.010
50	12.25	1.42	4.62	1.19	1.09	0.065	<dl	0.011	65.92	0.010
60	11.97	1.36	4.64	1.20	1.09	0.096	<dl	0.011	67.82	0.010
70	12.15	1.34	4.39	1.23	1.11	0.046	<dl	0.011	66.96	0.010
80	11.94	1.32	4.38	1.19	1.08	0.050	<dl	0.011	67.58	0.010
90	12.33	1.31	4.51	1.25	1.21	0.063	0.01	0.012	66.82	0.011
100	12.83	1.83	4.79	1.33	1.59	0.102	0.02	0.012	68.57	0.011
110	13.31	1.33	4.95	1.38	1.59	0.109	<dl	0.012	69.18	0.012
120	13.64	1.32	4.84	1.42	1.78	0.070	0.01	0.012	69.94	0.012
130	12.86	1.49	4.91	1.31	1.57	0.131	0.01	0.012	69.09	0.012
140	12.30	2.71	4.47	1.26	1.51	0.072	0.02	0.011	69.81	0.012
150	11.91	4.30	5.03	1.35	1.72	0.148	0.03	0.011	70.50	0.012
160	11.01	7.07	4.67	1.31	1.91	0.113	0.06	0.010	71.75	0.014
170	11.58	5.79	4.76	1.34	1.87	0.104	0.05	0.010	69.88	0.014
180	10.61	10.19	4.93	1.51	2.41	0.106	0.09	0.009	67.55	0.017
190	12.64	8.51	5.47	1.94	2.79	0.052	0.10	0.012	63.94	0.016
200	10.82	13.36	5.88	2.18	3.55	0.094	0.11	0.010	58.55	0.018
210	12.25	11.39	6.17	2.30	3.60	0.072	0.13	0.011	59.77	0.019
220	13.66	9.86	7.39	2.54	3.78	0.170	0.16	0.012	56.51	0.022
230	13.20	10.46	6.88	2.57	3.69	0.071	0.14	0.013	56.10	0.018
240	11.61	12.54	7.33	2.44	3.84	0.125	0.15	0.011	54.65	0.019
250						NA				
260	13.13	9.75	6.21	2.42	3.45	0.055	0.13	0.012	60.69	0.019
270						NA				
280	12.28	11.71	6.62	2.54	3.77	0.091	0.14	0.010	59.86	0.016
LAC 481 microhigh										
10	14.61	2.82	5.52	1.58	1.74	0.134	0.03	0.013	65.60	0.009
20	15.04	2.17	5.81	1.52	1.64	0.124	0.02	0.014	65.67	0.009
30	15.40	1.58	5.90	1.51	1.64	0.130	<dl	0.014	65.86	0.010
40	15.49	1.56	5.86	1.53	1.70	0.130	<dl	0.014	66.26	0.010
50	15.59	1.50	5.67	1.53	1.74	0.125	<dl	0.014	66.05	0.010
60	15.58	1.40	5.70	1.52	1.75	0.135	<dl	0.014	64.61	0.010
70	14.60	3.36	5.53	1.53	1.84	0.111	<dl	0.013	64.75	0.010
80	12.71	9.48	5.89	1.75	2.50	0.096	0.08	0.013	61.73	0.013
90						NA				
100	9.87	15.19	5.51	1.82	3.20	0.064	0.09	0.010	58.79	0.013
110	11.10	13.38	5.92	1.89	3.24	0.081	0.10	0.011	61.35	0.014
120	12.17	10.36	5.70	1.65	2.47	0.099	0.09	0.012	60.77	0.013
130	10.57	13.62	5.49	1.69	2.90	0.062	0.09	0.010	61.00	0.015
140	12.19	10.69	5.86	1.75	2.72	0.084	0.08	0.012	65.21	0.014

Depth	Al_2O_3	CaO	Fe_2O_3	K_2O	MgO	MnO	P_2O_5	Rb	SiO_2	Sr
	LAC 481 microhigh									
	Element									
cm	Wt%									
150	8.72	17.15	5.06	1.65	3.32	0.044	0.08	0.009	59.18	0.015
160	13.97	7.86	6.16	1.89	2.70	0.085	0.08	0.013	61.63	0.013
170	13.47	8.63	5.94	1.86	2.71	0.068	0.08	0.013	60.71	0.013
180	14.31	7.71	6.19	1.98	2.80	0.109	0.07	0.013	63.56	0.013
190	12.25	10.81	5.77	2.13	3.17	0.067	0.11	0.011	57.96	0.015
200	11.20	12.77	5.67	2.33	3.61	0.064	0.12	0.010	58.38	0.018
210	11.70	11.98	5.98	2.37	3.66	0.067	0.12	0.011	60.29	0.020
220	11.59	12.01	5.64	2.35	3.61	0.055	0.13	0.010	57.49	0.019
230	12.14	10.90	5.57	2.39	3.38	0.055	0.13	0.011	54.68	0.017
430	11.51	11.54	5.62	2.52	3.45	0.060	0.13	0.010	58.88	0.018
	LAC 481 microlow									
10	14.25	1.53	5.27	1.48	1.44	0.133	0.03	0.013	67.43	0.008
20	14.58	1.56	5.43	1.47	1.59	0.140	0.03	0.013	67.95	0.008
30	14.72	1.49	5.55	1.41	1.52	0.127	<dl	0.013	68.68	0.008
40	14.29	1.41	5.29	1.41	1.37	0.104	<dl	0.013	69.46	0.009
50	14.51	1.39	5.42	1.39	1.48	0.114	<dl	0.012	69.24	0.008
60	13.91	1.41	5.33	1.36	1.43	0.160	<dl	0.012	70.42	0.009
70	14.45	1.28	5.25	1.38	1.46	0.109	<dl	0.012	69.55	0.009
80	13.96	1.31	5.50	1.36	1.46	0.208	<dl	0.012	69.99	0.009
90	15.76	1.31	5.98	1.47	1.69	0.145	<dl	0.014	67.91	0.009
100	13.10	1.19	5.40	1.38	1.44	0.164	<dl	0.012	71.10	0.009
110	16.22	1.31	5.85	1.56	1.85	0.108	<dl	0.014	69.09	0.010
120	15.71	1.25	5.65	1.57	1.78	0.101	<dl	0.014	70.06	0.010
130	15.62	1.20	5.76	1.61	1.88	0.135	<dl	0.014	70.18	0.010
140	15.42	1.19	5.61	1.63	1.87	0.122	<dl	0.014	70.79	0.010
150	15.00	1.62	5.39	1.63	1.89	0.096	<dl	0.014	71.70	0.010
160	15.32	1.53	5.55	1.67	1.93	0.114	<dl	0.014	70.87	0.010
170	15.40	1.42	5.62	1.67	2.02	0.134	<dl	0.014	69.99	0.010
180	15.54	1.74	5.49	1.71	2.04	0.093	0.01	0.014	69.44	0.011
190	15.64	2.44	5.66	1.76	2.16	0.115	0.03	0.014	68.52	0.010
200	15.28	4.41	5.89	1.93	2.60	0.149	0.06	0.013	68.06	0.012
210	12.96	10.57	5.91	2.42	3.73	0.081	0.12	0.011	62.29	0.015
220	12.56	11.04	5.48	2.51	3.77	0.075	0.13	0.011	61.53	0.015
230	12.16	11.63	6.09	2.48	3.77	0.109	0.11	0.010	60.50	0.015
240	13.64	9.70	6.26	2.62	3.80	0.109	0.12	0.011	61.04	0.015
250	12.68	10.78	5.79	2.52	3.80	0.087	0.12	0.011	61.10	0.016
	LAW 239 microhigh									
10	10.73	3.48	3.78	1.17	1.28	0.110	0.03	0.009	74.93	0.008
20	9.09	12.78	3.91	1.26	2.18	0.063	0.07	0.008	75.47	0.016
30						NA				
40	11.81	4.85	4.18	1.29	1.67	0.085	0.03	0.010	76.93	0.011

LAW 239 microhigh										
	Element									
Depth	Al_2O_3	CaO	Fe_2O_3	K_2O	MgO	MnO	P_2O_5	Rb	SiO_2	Sr
cm	Wt%									
50	8.42	16.18	3.96	1.40	2.70	0.040	0.07	0.008	70.81	0.016
60	10.06	11.29	4.29	1.38	2.07	0.079	0.06	0.009	73.96	0.014
70	8.73	15.14	4.17	1.40	2.55	0.062	0.08	0.008	70.86	0.016
80	9.76	12.77	4.17	1.42	2.33	0.058	0.07	0.008	73.70	0.015
90	7.03	19.74	4.14	1.47	3.26	0.048	0.05	0.006	62.18	0.019
100	7.36	19.04	4.26	1.51	3.18	0.044	0.05	0.006	63.11	0.019
110	6.27	21.54	3.87	1.38	3.63	0.047	0.02	0.005	58.98	0.021
120	7.17	19.23	3.93	1.40	3.15	0.047	0.05	0.006	64.51	0.020
130	6.79	20.18	3.81	1.39	3.32	0.046	0.04	0.006	62.61	0.021
140	6.34	21.32	3.72	1.40	3.66	0.039	0.02	0.005	59.41	0.024
150	6.79	20.26	3.71	1.41	3.48	0.038	0.04	0.006	62.42	0.024
160	8.84	15.59	4.19	1.52	2.96	0.053	0.07	0.008	69.78	0.022
170	9.08	14.94	4.29	1.53	2.87	0.061	0.08	0.008	70.63	0.022
180	11.45	10.33	4.70	1.70	2.63	0.065	0.08	0.010	71.45	0.017
190	7.76	18.55	4.38	1.71	3.64	0.050	0.07	0.007	62.56	0.020
200	11.19	11.33	4.80	1.88	2.78	0.062	0.09	0.010	69.21	0.018
210	6.33	21.32	4.00	1.65	4.16	0.052	0.02	0.005	55.84	0.023
220	6.95	19.62	3.45	1.78	3.87	0.040	0.05	0.006	59.70	0.021
230	6.23	21.10	3.70	1.68	4.09	0.042	0.03	0.005	55.97	0.021
240	8.43	16.28	4.26	1.77	3.27	0.051	0.08	0.007	67.77	0.018
250	6.74	19.45	3.24	1.74	3.58	0.036	0.05	0.005	62.36	0.019
260	6.96	19.16	4.60	1.79	3.60	0.055	0.06	0.006	59.80	0.018
270	7.47	17.32	3.16	1.83	3.23	0.039	0.07	0.006	67.35	0.018
LAW 239 microlow										
10	11.70	1.21	4.19	1.13	1.19	0.154	<dl	0.010	74.43	0.009
20	12.53	1.31	4.48	1.14	1.39	0.167	<dl	0.010	73.80	0.010
30	12.40	1.29	4.26	1.13	1.34	0.117	<dl	0.010	74.42	0.010
40	12.31	1.29	4.24	1.14	1.34	0.126	<dl	0.010	74.45	0.010
50	12.24	1.29	4.20	1.14	1.37	0.112	<dl	0.010	74.66	0.011
60	12.32	1.30	4.44	1.13	1.40	0.151	<dl	0.010	73.94	0.011
70	12.37	1.26	4.37	1.13	1.46	0.139	<dl	0.010	74.04	0.011
80	12.57	1.24	4.52	1.12	1.54	0.167	<dl	0.010	73.38	0.011
90	12.51	1.24	4.74	1.15	1.57	0.199	<dl	0.010	73.81	0.012
100	12.44	1.18	4.26	1.15	1.53	0.122	<dl	0.010	73.85	0.012
110	12.42	1.15	4.11	1.18	1.51	0.102	<dl	0.011	74.76	0.013
120	12.04	1.60	4.23	1.16	1.55	0.131	<dl	0.010	75.29	0.013
130	12.34	1.08	4.18	1.19	1.60	0.114	<dl	0.010	74.90	0.014
140	12.02	2.18	4.20	1.23	1.64	0.118	<dl	0.010	75.04	0.015
150	11.45	4.42	3.94	1.24	1.77	0.082	0.01	0.010	74.91	0.017
160	11.35	5.45	4.11	1.34	1.85	0.095	0.02	0.010	74.89	0.017
170	7.04	19.52	3.91	1.46	3.30	0.042	0.05	0.006	60.00	0.022

	LAW 239 microlow									
	Element									
Depth	Al_2O_3	CaO	Fe_2O_3	K_2O	MgO	MnO	P_2O_5	Rb	SiO_2	Sr
cm	Wt%									
180	6.29	21.27	3.59	1.42	3.47	0.031	0.03	0.005	54.50	0.026
190	6.82	20.36	4.47	1.56	3.66	0.049	0.04	0.006	55.19	0.022
200	6.35	21.35	3.65	1.44	3.77	0.038	0.02	0.005	55.06	0.026
210	7.02	19.49	4.50	1.71	3.63	0.048	0.06	0.006	56.49	0.023
220	9.73	11.77	4.53	1.86	2.88	0.094	0.09	0.007	69.89	0.017
230	8.77	16.51	5.99	2.11	3.85	0.103	0.10	0.008	57.19	0.020
240	9.03	16.08	5.04	2.00	3.50	0.061	0.10	0.008	59.76	0.019
250						NA				
260	12.52	6.77	5.13	2.00	2.59	0.073	0.08	0.010	69.49	0.016
270	9.08	10.80	2.71	1.90	2.18	0.038	0.08	0.007	75.17	0.016
295	10.79	10.61	4.35	2.09	2.56	0.054	0.10	0.009	68.59	0.016
310	10.29	0.49	3.07	0.92	1.11	0.056	<dl	0.009	83.39	0.010
325	10.32	0.46	3.11	0.91	1.09	0.071	<dl	0.009	82.98	0.010
	LAW 469 microhigh									
10	10.26	10.42	4.11	0.87	1.66	0.080	0.06	0.007	72.15	0.012
20	9.92	10.69	4.01	0.87	1.65	0.083	0.06	0.007	73.77	0.012
30	10.30	9.93	4.16	0.86	1.66	0.089	0.05	0.007	73.35	0.013
40	9.65	11.88	3.94	0.88	1.79	0.058	0.05	0.007	73.44	0.014
50	10.11	11.26	4.08	0.90	1.89	0.079	0.06	0.007	73.41	0.015
60	9.77	10.42	3.92	0.84	1.62	0.066	0.05	0.007	72.94	0.013
70	10.45	9.53	4.08	0.86	1.77	0.086	0.06	0.007	74.24	0.014
80	10.00	10.36	3.91	0.85	1.72	0.043	0.06	0.007	73.92	0.014
90	10.51	9.22	4.03	0.87	1.77	0.081	0.04	0.007	74.21	0.015
100	9.40	12.32	3.85	0.87	1.91	0.062	0.06	0.006	73.56	0.017
110	10.60	8.71	4.05	0.87	1.76	0.082	0.05	0.007	74.27	0.016
120	10.50	9.66	4.04	0.91	1.77	0.064	0.05	0.007	73.22	0.015
130	10.12	9.90	3.95	0.89	1.80	0.071	0.05	0.007	74.57	0.016
140	8.53	14.21	3.62	0.87	2.02	0.065	0.07	0.006	72.38	0.022
150	11.39	5.50	4.11	0.85	1.58	0.093	0.02	0.008	74.58	0.015
160	11.27	8.49	4.35	0.99	1.89	0.073	0.04	0.008	73.44	0.016
170	11.86	7.15	4.37	0.99	1.77	0.077	0.04	0.008	73.22	0.016
180	10.53	12.17	4.67	1.14	2.16	0.075	0.07	0.007	70.17	0.020
190	11.37	9.21	4.59	1.08	1.96	0.069	0.05	0.008	72.49	0.015
200	11.46	10.99	4.95	1.21	2.29	0.065	0.08	0.008	68.99	0.017
210	12.08	9.62	5.08	1.25	2.23	0.062	0.08	0.009	70.33	0.017
	LAW 469 microlow									
10	9.97	1.28	3.14	0.71	0.74	0.072	0.02	0.008	73.00	0.007
20	10.68	1.24	3.40	0.67	0.85	0.086	<dl	0.007	73.65	0.007
30	11.29	1.33	3.54	0.66	1.08	0.067	<dl	0.007	74.34	0.007
40	11.32	1.34	3.54	0.65	1.07	0.063	<dl	0.008	74.47	0.008
50	11.23	1.33	3.50	0.65	1.10	0.044	<dl	0.007	74.07	0.008

	LAW 469 microlow									
	Element									
Depth	Al_2O_3	CaO	Fe_2O_3	K_2O	MgO	MnO	P_2O_5	Rb	SiO_2	Sr
cm	Wt%									
60	11.84	1.39	3.50	0.68	1.14	0.050	<dl	0.008	72.08	0.008
70	11.27	1.35	3.50	0.69	1.09	0.069	<dl	0.008	74.35	0.008
80	11.60	1.40	3.62	0.70	1.20	0.064	<dl	0.008	75.09	0.009
90	11.73	1.47	3.67	0.73	1.22	0.068	<dl	0.008	75.67	0.009
100	11.85	1.50	3.74	0.74	1.34	0.065	<dl	0.008	76.21	0.010
110	11.77	1.48	3.74	0.75	1.30	0.050	<dl	0.009	75.43	0.010
120	11.71	1.46	3.73	0.77	1.36	0.050	<dl	0.009	76.20	0.010
130	11.67	1.39	3.70	0.78	1.40	0.052	<dl	0.009	76.05	0.010
140	10.75	5.40	3.75	0.86	1.56	0.065	0.05	0.008	75.58	0.012
150	11.54	2.23	3.68	0.81	1.43	0.060	0.01	0.008	75.30	0.011
160	11.00	5.61	3.80	0.87	1.59	0.080	0.04	0.008	75.42	0.014
170	11.55	6.33	4.21	1.00	1.69	0.061	0.05	0.009	74.60	0.015
180	11.35	11.88	4.82	1.21	2.08	0.057	0.10	0.008	72.70	0.016
190	12.21	13.06	5.57	1.44	2.38	0.060	0.11	0.009	68.62	0.017
200	12.14	12.64	5.19	1.46	2.33	0.063	0.11	0.009	68.44	0.018
210	11.15	13.74	5.09	1.44	2.43	0.055	0.12	0.009	67.72	0.016
220	10.18	11.92	4.12	1.40	1.97	0.040	0.09	0.008	73.93	0.014
230	10.73	13.10	4.60	1.51	2.06	0.050	0.10	0.008	72.08	0.015
	LAW 391 microhigh									
10						NA				
20						NA				
30						NA				
40						NA				
50	11.37	11.86	4.30	1.71	2.56	0.056	0.10	0.010	68.63	0.010
60	12.15	9.04	4.46	1.73	2.35	0.070	0.09	0.010	69.37	0.010
70	9.14	17.02	3.88	1.65	2.45	0.039	0.09	0.008	67.62	0.011
80	10.20	13.97	4.18	1.68	2.50	0.053	0.10	0.009	68.63	0.011
90	10.39	13.59	4.25	1.70	2.40	0.056	0.10	0.009	67.80	0.012
100	10.56	13.78	4.20	1.71	2.50	0.054	0.11	0.009	66.22	0.012
110	10.32	14.43	4.20	1.73	2.57	0.043	0.10	0.009	67.99	0.013
120	11.20	11.25	4.23	1.75	2.43	0.043	0.10	0.010	68.35	0.012
130	10.10	15.31	4.15	1.71	2.66	0.047	0.10	0.008	67.85	0.013
140	12.03	9.34	4.32	1.81	2.46	0.049	0.09	0.010	70.58	0.013
150	11.71	9.57	4.33	1.79	2.32	0.058	0.08	0.010	70.38	0.012
160	10.03	14.72	4.01	1.71	2.43	0.032	0.10	0.008	66.78	0.014
170	10.96	11.81	4.21	1.76	2.31	0.049	0.09	0.009	68.16	0.013
180	10.10	15.37	4.19	1.75	2.65	0.045	0.10	0.008	67.10	0.014
190	9.87	15.85	4.10	1.74	2.56	0.035	0.11	0.008	65.61	0.013
200	10.09	15.32	4.14	1.75	2.53	0.037	0.10	0.008	66.57	0.014
210	9.68	16.51	4.10	1.72	2.60	0.032	0.11	0.008	66.34	0.017
220	9.69	15.89	4.08	1.71	2.39	0.044	0.10	0.008	64.80	0.014

Depth	Al_2O_3	CaO	Fe_2O_3	K_2O	MgO	MnO	P_2O_5	Rb	SiO_2	Sr
	Element									
cm	Wt%									
LAW 391 microhigh										
230	10.41	12.75	4.03	1.77	2.20	0.044	0.10	0.008	67.37	0.013
240	10.44	10.83	3.70	1.74	1.89	0.042	0.08	0.008	69.21	0.012
370	8.21	16.03	3.03	1.80	1.79	0.027	0.09	0.006	69.36	0.012
LAW 391 microlow										
10	12.53	1.55	4.07	1.61	1.54	0.076	0.05	0.011	67.55	0.007
20	14.26	1.70	4.57	1.62	1.87	0.087	0.03	0.001	68.17	0.008
30	13.55	1.62	4.26	1.63	1.72	0.066	0.03	0.011	69.31	0.008
40	13.77	1.65	4.22	1.61	1.81	0.064	0.03	0.011	68.10	0.008
50	13.59	1.65	4.26	1.61	1.90	0.079	0.04	0.011	69.89	0.009
60	14.12	1.69	4.29	1.65	2.03	0.078	<dl	0.012	70.71	0.009
70	13.64	1.76	4.27	1.66	1.88	0.077	0.02	0.011	69.92	0.009
80	13.87	1.77	4.41	1.69	1.97	0.097	0.02	0.012	71.82	0.010
90	13.79	1.58	4.38	1.66	1.88	0.096	0.02	0.012	70.37	0.010
100	13.74	2.36	4.36	1.70	2.06	0.073	0.03	0.012	71.63	0.010
110	13.62	3.45	4.31	1.73	2.09	0.063	0.05	0.011	69.22	0.011
120	13.48	3.89	4.23	1.73	2.05	0.048	0.05	0.011	66.11	0.011
130	12.21	6.84	4.18	1.71	2.10	0.046	0.07	0.010	67.12	0.011
140	11.01	12.01	4.19	1.73	2.40	0.061	0.09	0.009	65.40	0.012
150	14.50	3.00	4.62	1.84	2.24	0.066	0.05	0.012	68.37	0.011
160	13.80	4.98	4.58	1.86	2.40	0.063	0.06	0.011	69.37	0.012
170	13.42	5.75	4.53	1.88	2.28	0.058	0.07	0.011	69.47	0.012
180	13.18	6.39	4.50	1.86	2.33	0.064	0.07	0.011	69.52	0.013
190	12.25	8.84	4.41	1.87	2.40	0.054	0.08	0.010	69.72	0.012
200	12.15	8.63	4.44	1.88	2.34	0.046	0.08	0.010	69.10	0.013
210	12.53	7.62	4.43	1.90	2.25	0.049	0.08	0.011	69.47	0.012
220	9.48	17.12	4.24	1.76	2.55	0.032	0.10	0.008	65.94	0.016
230	9.88	15.55	4.20	1.79	2.53	0.040	0.10	0.008	66.33	0.014
240	10.01	14.41	4.28	1.80	2.48	0.034	0.10	0.009	65.61	0.014
VIC 409 microhigh										
10	9.51	6.63	3.19	1.47	1.69	0.084	0.05	0.008	77.30	0.013
20	9.52	7.93	3.13	1.49	1.76	0.089	0.04	0.007	78.46	0.014
30	9.33	7.77	3.22	1.40	1.65	0.077	0.05	0.007	76.82	0.015
40	9.37	8.50	3.29	1.47	1.82	0.079	0.05	0.008	77.43	0.017
50	9.77	7.62	3.16	1.55	1.91	0.069	0.03	0.007	77.48	0.017
60	9.61	7.97	3.28	1.53	1.86	0.090	0.04	0.007	77.00	0.018
70	9.98	7.21	3.16	1.61	1.94	0.079	0.03	0.007	77.63	0.017
80	9.72	7.32	3.31	1.56	1.79	0.069	0.04	0.008	76.16	0.019
90	9.72	7.41	3.38	1.57	1.86	0.087	0.05	0.008	76.24	0.020
100	9.78	7.34	3.40	1.60	1.85	0.085	0.04	0.008	75.88	0.022
110	10.42	6.36	3.43	1.65	1.93	0.078	0.04	0.008	75.24	0.019

VIC 409 microhigh										
	Element									
Depth	Al_2O_3	CaO	Fe_2O_3	K_2O	MgO	MnO	P_2O_5	Rb	SiO_2	Sr
cm	Wt%									
120	10.20	6.26	3.44	1.62	1.87	0.094	0.04	0.008	76.37	0.019
130	10.02	6.29	3.39	1.62	1.69	0.066	0.03	0.008	75.09	0.019
140	10.09	6.54	3.41	1.69	1.88	0.073	0.04	0.008	76.66	0.019
150	9.86	6.35	3.32	1.62	1.68	0.063	0.04	0.007	76.63	0.018
160	10.10	5.56	3.32	1.66	1.65	0.083	0.04	0.008	77.53	0.017
170						NA				
180	7.88	5.80	2.76	1.08	1.43	0.052	0.08	0.006	73.35	0.016
190	7.27	8.66	2.81	0.96	1.71	0.044	0.09	0.006	68.72	0.018
200	5.15	9.95	2.36	0.43	2.32	0.030	<dl	0.004	61.24	0.018
210	7.17	8.21	2.74	0.95	1.63	0.038	0.08	0.006	69.53	0.017
220	8.40	9.01	3.05	1.43	1.37	0.049	0.06	0.006	71.73	0.016
VIC 409 microlow										
10	9.75	0.96	2.78	1.55	1.11	0.072	<dl	0.008	77.26	0.008
20	10.20	1.17	3.06	1.44	1.26	0.090	<dl	0.008	78.65	0.009
30	10.13	1.17	3.01	1.42	1.22	0.074	<dl	0.008	77.69	0.009
40	10.29	1.27	3.04	1.41	1.32	0.072	<dl	0.008	77.53	0.010
50	10.15	1.77	2.98	1.39	1.39	0.078	<dl	0.008	77.89	0.010
60	9.62	1.80	2.92	1.35	1.28	0.076	<dl	0.008	78.78	0.011
70	9.51	3.79	2.88	1.40	1.42	0.070	<dl	0.007	75.48	0.013
80	9.90	2.88	2.78	1.44	1.46	0.067	<dl	0.007	76.84	0.011
90	10.05	2.62	2.96	1.44	1.45	0.070	<dl	0.008	75.09	0.012
100	8.73	5.67	2.74	1.36	1.44	0.071	0.02	0.007	76.09	0.014
110	9.42	4.07	2.93	1.47	1.41	0.073	0.02	0.007	76.51	0.014
120	9.38	5.09	3.00	1.53	1.47	0.073	0.02	0.007	74.37	0.015
130	8.95	6.30	2.93	1.52	1.49	0.062	0.03	0.007	73.84	0.016
140	9.34	4.99	3.02	1.55	1.41	0.067	0.01	0.007	75.02	0.015
150	9.19	5.85	2.96	1.55	1.49	0.062	0.02	0.007	75.28	0.015
160	9.31	5.74	2.87	1.55	1.41	0.070	0.02	0.007	71.21	0.015
170	9.09	6.06	2.89	1.52	1.47	0.055	0.03	0.007	74.49	0.016
180	8.02	13.76	3.91	1.34	2.11	0.088	0.10	0.006	58.35	0.018
190	8.98	6.83	2.93	1.52	1.53	0.065	0.03	0.007	73.26	0.016
200	9.60	5.20	3.04	1.59	1.44	0.064	0.02	0.007	75.20	0.015
210	9.07	6.77	3.02	1.53	1.51	0.058	0.04	0.007	73.46	0.017
220	9.86	4.01	2.96	1.56	1.41	0.058	0.03	0.007	73.13	0.014
230	9.87	4.25	3.04	1.58	1.51	0.059	0.03	0.007	75.97	0.015
240	9.92	4.44	3.07	1.58	1.42	0.061	0.04	0.007	73.82	0.015
250	9.93	3.23	3.15	1.55	1.45	0.066	0.06	0.008	77.31	0.014
260	9.18	10.06	3.66	1.55	1.73	0.064	0.12	0.007	64.91	0.020
270	8.29	12.66	3.92	1.31	2.21	0.061	0.10	0.007	57.76	0.017

Appendix 4: Data and Statistical Tables for Chapter 4.

Table A4-1. Elemental contents of bulk iron-manganese nodules isolated from modern Texas Vertisols.

Profile designation	Depth	Element						
		Al	Ca	Fe	K	Mn	Si	Ti
	cm	wt %						
LEG 245A L	10	3.41[a]	0.43	19.10	0.32	6.23	12.89	0.17
	50	3.50	0.35	23.86	0.24	3.57	11.63	0.16
	70	3.40	0.23	27.23	0.28	1.16	11.48	0.16
	90	4.22	0.55	15.66	0.35	2.72	17.49	0.22
	110	4.30	0.48	21.10	0.34	1.66	14.23	0.19
	130	3.91	0.49	24.17	0.31	2.46	14.07	0.16
	150	3.85	0.39	25.25	0.21	1.77	13.39	0.17
	170	3.61	0.43	24.57	0.29	1.95	13.17	0.18
	190A	3.70	0.63	22.05	0.34	4.49	13.94	0.17
	190B	3.95	0.66	23.21	0.38	4.78	14.72	0.19
	210	4.23	1.66	21.19	0.50	4.34	14.49	0.22
	230	4.02	3.08	15.85	0.38	4.92	14.33	0.21
	250	4.39	3.56	14.30	0.51	5.44	14.55	0.22
LEG 245A H	10	3.62	0.37	23.89	0.28	2.87	13.90	0.18
	30	3.77	0.60	24.71	0.31	3.72	13.52	0.17
	50	3.65	0.51	23.74	0.31	3.32	15.72	0.19
	70	4.04	0.62	26.31	0.30	2.70	11.94	0.19
	90	4.26	0.34	28.45	0.31	0.84	12.69	0.17
	110	4.18	0.38	27.76	0.31	1.80	13.47	0.17
	130	3.93	0.41	26.84	0.26	1.49	12.90	0.18
	150	3.65	0.53	22.14	0.28	3.25	14.71	0.17
	170	3.79	0.97	26.14	0.28	1.19	14.55	0.17
	190	3.86	0.43	23.76	0.26	1.44	14.86	0.16
	210	3.81	2.03	16.70	0.37	3.73	15.24	0.18
	230	4.07	4.62	12.97	0.54	5.91	14.78	0.20
	250	4.39	1.82	12.30	0.58	9.49	17.00	0.23
LAC 201 L	10	4.14	0.16	20.62	0.57	4.48	16.42	0.18
	30	3.98	0.06	25.01	0.48	1.69	15.90	0.15

[a] Each value represents the composite value of three sub-samplings and extractions.

Profile designation	Depth	Element						
		Al	Ca	Fe	K	Mn	Si	Ti
	cm	wt %						
LAC 201 L	50	4.18	0.14	19.06	0.60	5.33	17.74	0.16
	70	4.23	0.12	22.49	0.58	3.65	16.56	0.15
	90	4.36	0.32	17.81	0.64	6.35	16.89	0.16
	110	4.31	0.31	18.34	0.64	5.88	17.89	0.16
	130	4.65	0.43	16.39	0.69	6.78	19.04	0.19
	150	4.36	0.33	18.92	0.64	3.91	18.67	0.18
	160	4.36	0.23	24.17	0.58	1.30	18.18	0.13
	170	4.11	2.86	14.46	0.64	5.47	17.09	0.15
LAC 201 H	10	4.45	0.37	21.68	0.54	3.05	15.63	0.16
	30	4.55	0.55	16.88	0.56	5.67	16.34	0.19
	50A	4.25	0.28	21.83	0.50	1.43	15.73	0.14
	50B	4.28	1.21	17.62	0.58	5.56	16.73	0.15
	70	4.35	0.44	17.37	0.58	6.03	17.43	0.17
	90	4.67	0.49	16.48	0.62	5.33	17.31	0.18
	100	4.52	0.34	21.90	0.66	2.08	15.85	0.18
	130	4.38	0.33	18.05	0.70	3.77	18.33	0.17
	165	4.39	0.32	18.74	0.67	4.33	16.86	0.16
	180	4.46	0.49	19.44	0.76	1.67	17.93	0.17
	30	5.06	0.58	16.23	0.64	11.26	14.70	0.19
	50	5.56	0.78	13.77	0.72	13.07	17.66	0.23
	60	5.12	0.67	16.01	0.71	10.89	14.55	0.16
LAC 481 L	70	5.28	0.74	13.76	0.74	12.12	15.21	0.19
	90A	5.39	1.01	15.09	0.77	9.89	15.16	0.18
	90B	4.82	0.67	16.81	0.64	10.04	11.93	0.15
	110	4.89	1.71	14.41	0.62	10.55	12.00	0.15
	120	4.57	1.44	12.19	0.67	10.60	11.39	0.18
	130	4.85	2.05	11.03	0.70	10.98	12.79	0.17
	150	4.88	0.97	11.30	0.67	11.05	12.69	0.15
	160	5.00	0.99	10.50	0.74	10.51	13.26	0.19

Profile designation	Depth	Element						
		Al	Ca	Fe	K	Mn	Si	Ti
	cm	wt %						
LAC 481 L	170	5.18	0.97	10.59	0.77	13.00	13.15	0.18
	180	4.30	3.06	17.69	0.46	5.44	12.02	0.18
	200	4.97	1.88	12.09	0.75	8.58	12.55	0.21
	210	4.99	5.37	11.27	0.94	5.47	12.21	0.19
	220	4.99	10.28	8.40	1.04	2.43	12.52	0.19
LAC 481 H	10	5.46	2.20	12.32	0.78	6.29	17.30	0.21
	30	5.26	0.76	15.80	0.65	9.17	14.04	0.18
	50	5.32	0.86	15.89	0.71	10.10	14.24	0.18
	70	5.19	0.72	18.79	0.75	6.17	14.61	0.17
	90	5.49	1.84	15.44	0.85	8.31	13.74	0.18
	110	6.12	1.01	13.36	0.87	9.10	16.33	0.22
	130A	5.57	0.83	18.78	0.78	5.45	14.08	0.19
	130B	5.68	0.96	14.00	0.84	11.16	15.17	0.19
	150	5.90	0.95	13.38	0.91	9.74	16.11	0.23
	170	5.33	2.11	13.03	0.77	10.31	13.40	0.20
	180	5.94	0.81	18.19	0.87	5.63	16.00	0.20
	190	4.54	4.32	10.80	0.85	6.49	12.72	0.17
LAW 239 L	10	4.42	0.70	12.90	0.55	10.72	11.88	0.21
	30	4.61	0.74	12.52	0.57	11.62	13.40	0.22
	70	4.52	0.75	14.73	0.50	8.42	12.71	0.23
	90	4.45	0.97	12.27	0.49	9.80	12.26	0.21
	110	4.15	0.81	13.72	0.48	9.35	11.94	0.20
	120A	4.22	0.78	15.78	0.56	9.56	11.15	0.20
	120B	4.62	6.76	13.95	0.55	4.07	9.61	0.18
	130	3.86	2.56	11.21	0.48	9.64	10.20	0.20
	160	4.05	3.01	11.44	0.56	8.66	11.01	0.21
LAW 239 H	20	4.29	1.44	12.29	0.59	9.94	12.32	0.19
	40	4.32	1.11	10.08	0.55	12.11	12.89	0.22
	50	3.94	3.99	10.55	0.43	9.90	11.52	0.19

Profile designation	Depth	Element						
		Al	Ca	Fe	K	Mn	Si	Ti
	cm	wt %						
LAW 239 H	70	4.50	1.31	16.35	0.59	5.73	11.98	0.21
	90	4.56	5.19	11.91	0.74	6.18	11.55	0.20
	110	4.55	3.83	11.84	0.67	6.10	11.72	0.21
	130	4.80	4.72	11.60	0.70	6.57	12.19	0.21
	150	4.73	1.18	11.70	0.67	9.48	12.68	0.21
	160	4.70	1.57	16.02	0.65	4.78	11.83	0.18
	190	4.11	6.29	9.30	0.59	3.69	9.79	0.16
VIC 409 L	190	1.62	19.92	2.29	0.41	5.39	5.47	0.11
	210	2.45	16.48	3.24	0.39	7.39	7.51	0.15
VIC 409 H	10	0.39	12.47	1.14	<0.05	1.59	2.31	0.04
	30	0.52	33.73	0.97	<0.05	0.55	3.23	0.03
	50	0.91	30.08	1.64	<0.05	2.35	4.02	0.05
	60	3.65	2.19	6.31	0.75	16.49	12.52	0.22
	70	1.23	25.70	2.38	<0.05	4.01	5.07	0.07
	90	2.99	10.20	7.27	<0.05	9.71	9.10	0.17
	180	2.52	18.18	3.52	0.37	6.47	7.52	0.14
LAC 157 L	30	3.81	0.92	12.27	0.66	8.72	6.70	0.14
	130	3.76	0.42	12.31	0.53	8.33	6.76	0.15
	150	0.86	5.34	12.51	0.24	4.65	10.23	0.03
	230	0.18	1.48	12.37	0.37	4.49	4.03	0.04
LAW 469 L	30	3.52	0.95	9.89	0.42	6.17	8.90	0.17
	130	3.55	0.72	10.35	0.38	11.72	8.80	0.17
	150	2.71	0.78	12.45	0.45	8.46	8.00	0.13
	230	2.98	1.41	13.03	0.60	10.57	12.43	0.14
LAW 391 L	30	3.85	1.03	9.56	0.89	4.15	10.67	0.22
	130	3.86	0.51	9.32	0.73	6.93	8.67	0.21
	150	2.65	1.94	9.16	0.76	8.16	8.63	0.18
	220	2.60	2.15	8.85	0.85	8.68	9.89	0.17

Table A4-2. Descriptive statistics for iron and manganese in nodules isolated from modern Texas Vertisols.

Profile	Element	Statistical Value				
		Mean	Standard Deviation	Maximum	Minimum	Confidence Interval (99%)
		wt %				
LEG 245A	Fe	22.05	4.72	28.45	12.30	2.38
LAC 201		19.36	2.75	25.01	14.46	1.59
LAC 157		12.36	0.11	12.51	12.27	0.14
LAC 481		13.96	2.75	18.79	8.40	1.34
LAW 239		12.73	1.98	16.35	9.30	1.14
LAW 469		10.18	0.26	10.45	9.89	0.34
LAW 391		9.22	0.30	9.56	8.85	0.39
VIC 409		3.20	2.22	7.27	0.96	1.91
LEG 245A	Mn	3.36	1.99	9.49	0.84	1.00
LAC 201		4.19	1.79	6.78	1.30	1.03
LAC 157		6.57	2.29	8.72	4.49	2.95
LAC 481		9.08	2.66	13.07	2.43	1.29
LAW 239		8.39	2.56	12.11	3.69	1.48
LAW 469		9.23	2.45	11.72	6.17	3.15
LAW 391		6.98	2.02	8.68	4.15	2.61
VIC 409		6.00	4.91	16.49	0.55	4.22

Table A4-3. Elemental contents of bulk iron-manganese nodules isolated from paleo-Vertisols.

Profile designation	Element						
	Al	Ca	Fe	K	Mn	Si	Ti
	wt %						
Maccrady	5.10	0.25	20.90	1.92	0.01	18.69	0.26
	4.93	0.39	22.14	1.34	0.02	19.78	0.25
	5.74	0.13	19.57	2.02	0.01	17.76	0.27
Pennington I	5.34	2.60	15.81	2.19	0.11	32.69	0.34
	5.20	2.36	13.52	2.89	0.13	33.05	0.28
	4.36	3.10	14.66	1.96	0.12	31.96	0.31
Pennington II	0.20	2.91	7.50	1.01	0.76	4.66	0.21
	0.19	2.09	7.21	0.97	0.80	5.03	0.22
	0.26	2.74	7.51	1.01	0.78	5.95	0.22
Dunkard	3.74	8.73	6.06	2.22	0.31	38.92	0.24
	2.35	8.96	6.32	2.54	0.34	35.64	0.24
	4.50	9.72	5.78	2.34	0.29	37.56	0.21

Vita

Cynthia Ann (French) Stiles was born in Fargo, North Dakota. She spent her youth on the high prairies of western North Dakota, in the Williston Basin, where her early love for soils, rocks, and chemistry was fostered by her parents and the abundant reading material available in the local library. Experiences in an eighth-grade Earth Science class solidified this interest. After completing a Bachelors Degree in Agronomy, with emphasis on pesticide chemistry, she worked in several environmental testing facilities as a technician, then returned to her alma mater, North Dakota State University in Fargo, for a masters degree in Soil Science. From there, she moved to the University of Tennessee in Knoxville to take up a full-time position in the Plant and Soil Science Department as a soil chemist. She started her Ph.D. program in Geology in 1997 under the guidance of Dr. Steven Driese and Dr. Claudia Mora, where she was able to apply her knowledge of the complex interactive soil system to geological studies, and to further her understanding of pedological processes in relatively undisturbed settings. She has had experiences working in Alaska with her mentor, Dr. Chien-Lu Ping, of the University of Alaska-Fairbanks, and on numerous archaeological sites with Dr. John Foss, formerly of the University of Tennessee. She enjoys professional involvement with colleagues whom she has met at various conventions and workshops, and plans to continue to work in the academic field, with emphasis on applied field research of natural soil systems and biogeochemistry. She will taking be a post-doctoral research position at the University of Tennessee within the Initiative for Interdisciplinary Study of Global Environmental Change.